A Combined Optical-Thermal Model for Laser-Assisted Fibre Placement of Thermoplastic Composite Materials

Christopher M. Stokes-Griffin

A thesis submitted for the degree of
Doctor of Philosophy of
The Australian National University

May 2015

Except where otherwise indicated, this thesis is my own original work.



Christopher M. Stokes-Griffin
1 May 2015

Dedicated to Norman Stokes

Acknowledgements

I would like express my deepest gratitude to all of the people involved in making the completion of this thesis possible.

First of all, I would like to thank my primary supervisor, Paul Compston. His generosity in terms of time, resources and opportunities made the PhD experience enjoyable and extend far beyond my expectations. He always made himself available, and showed a high level of commitment to my work. His patience, mentoring and friendship are also greatly appreciated.

I would also like to thank my secondary supervisor for the first half of my candidature, Tim Matuszyk. It was a pleasure working with him, and he always made himself available. He also provided a large amount of assistance in sourcing of experimental equipment and materials to support my work. I must also credit him for making the initial contact with *AFPT*.

Thank you to *AFPT* for generously providing the experimental facilities for my work. Furthermore, it was a pleasure visiting the facilities in Dörth on multiple occasions, which was both an interesting and enjoyable experience. I would like to thank all of the staff for their hospitality and assistance.

I would like to thank the staff from the engineering workshop, in particular David Tychsen-Smith and Benjamin Nash, for providing assistance, advice and facilities that supported my experimental work.

Thank you Zbigniew Stachurski for your support, in particular for your detailed knowledge of polymers and provision of equipment that assisted sample preparation.

I would like to thank Andrew Wilson and the staff from the workshop at the Research School of Earth Sciences for providing training and access to equipment that was required for sample preparation.

Thank you to Andrew Thomson who generously gave up his time for training and providing access to the spectrophotometer that played a vital role in the optical characterisation performed in this work.

Thanks to Mum and Greg for providing support, encouragement and accommodation as I have needed in over the last few years. Thanks to Dad for your support, encouragement and fantastic holidays together. Also thanks for the hospitality–

we were lucky the PhD experience also allowed us to spend more time together in Switzerland. Thank you Laura for the good times we had living together, the meals you cooked and the much needed weekend breaks visiting you in Sydney. I would also like to thank my extended family for their support, in particular my two grandmothers as well as auntie Fiona for having me around for dinner on a regular basis.

Thanks to my office mates– Charles, Chris, Eric, Hamza, Jin, Jun, Oday and Peter for putting up with me, as well as the comic relief and friendship. Thanks to Dave and Adam for the many cups of tea, as well as Lachlan when he joined us for lunch. Thanks to Alex for the runs, bike rides and being there for me in general. Also thanks to the lunch group– Alice, Brendan, Ceilidh, Eddy and Luke.

Finally, I would like to thank Alice. I can't thank you enough for your support and encouragement in the final stages of my thesis. Taking breaks with you in the form of runs, walks, coffees and lunches greatly improved my mood and productivity. I would also like to express my deepest gratitude for the incredibly generous gesture of proof reading my work. I look forward to spending more time together in the future.

Abstract

Automated fibre placement of thermoplastic composites has potential to produce high performance composite structures in a fast, clean, automated, out-of-autoclave process. Structures are built up in an additive fashion by placement of pre-impregnated thermoplastic composite plies layer-by-layer, using a placement head attached to an articulated robot for example. During placement, the plies are welded together in situ, which is achieved by melting the surfaces of the plies to be bonded with application of heat. Previously investigated heat sources include convective approaches such as hot gas torches and direct flames, conductive approaches in the form of hot shoes and rollers, or radiative approaches in the case of a lasers and infra-red lamps. In order to maximise the placement rate for productivity, the heat input must be increased correspondingly so as to maintain the temperatures necessary for bond development. Recent developments in near-infrared diode laser technology have resulted in new heat sources for the process with unsurpassed output power, efficiency, reliability and uniformity. Remotely mounted sources deliver the laser via light cable to compact optics mounted on the placement head. The optics can produce large rectangular spots, ideal for uniform and progressive heating of the composite.

This thesis investigates the near-infrared laser-assisted thermoplastic fibre placement process in detail for carbon fibre/PEEK composites. Topics covered include detailed studies of the optical interaction between the laser and the composite, development of a combined optical-thermal model which provides robust predictive capability for the temperature history, as well as investigation of the evolution of inter-laminar bonding, void dynamics and crystallinity throughout the manufacturing process of a laminate.

Initial thermal modelling accompanied by experimental validations strongly suggested the presence of a shadow prior to the nip point that results in a large temperature drop prior to consolidation, and also the possibility that significant bond development was occurring for temperatures lower than the melting point of the PEEK matrix. The presence of the shadow and the behaviour of the light in the wedge-shaped cavity formed between the tape and substrate was further investigated using a 3D ray tracing optical model. Formulation of such a model required optical characterisation of the composite material in terms of scattering and angular dependent absorption, as well as measurement of the laser beam profile and propagation. The scattering behaviour of the carbon/PEEK tape was found to be highly anisotropic, dominated by specular reflections from the surfaces of the embedded cylindrical carbon fibres. A micro-half-cylinder surface model was found to provide an excellent approximation of the scattering behaviour on the macroscopic level, removing the requirement to model the composite microstructure in 3D. Fresnel's equations were found to provide an accurate estimation of the angular dependent absorption.

The laser beam profile and propagation were measured using a thermographic technique and the source was found to have significant divergence. The source was modelled using beam profile measurements as a spatial emittance function, which is then passed through a paraxial lens to achieve a close approximation of the source divergence. A full optical model of the tape placement system was subsequently formulated and used to determine the heat flux distributions on the surfaces of the composite. The model was then coupled with the thermal model for accurate prediction of the temperature distributions. The results of the combined optical-thermal model were found to be in strong agreement with experimental measurements.

Experimentally validated bonding models from literature were implemented and predictions compared and contrasted using temperature and pressure histories determined by in situ measurements using thermocouples and active pressure sensor arrays. Large differences in the predictions were observed. Three bonding model parameter sets were also proposed based on more recent material property data, with one model found to provide robust predictions over a large range of process parameters.

Placement trials were performed with samples manufactured under conditions that reflect those encountered in a practical manufacturing process. The effects of placement rate and process temperature were investigated. For a given process temperature, increasing the placement rate was found to result in higher cooling rates due to reduced heat soak, leading to decreased levels of bonding and crystallinity. High process temperatures in excess of 500 °C were found to produce the highest mechanical strengths, explained by higher rates of intimate contact development and molecular healing at elevated temperature. Void content and crystallinity predictions also suggest the best properties at high process temperatures to the order of 600 °C. The rapid nature of the process avoids significant degradation when processing at such high temperatures as the dwell time is extremely short. Extremely high cooling rates result from the rapid dissipation of heat into the substrate and cause a highly amorphous bond interface during the initial placement pass. Experimental results from this work show that bond development can in fact occur for interface temperatures lower than 250 °C, explained by the fact the PEEK remains in a highly amorphous state within the consolidation zone. The final crystallinity of the laminates is however predicted to be within the recommended range (20-35 %) due to recrystallisation that occurs as the laminate is reheated during placement of subsequent layers.

The resulting strength of the samples was also compared with those reported in literature for other heat sources. Results show that the near-infrared laser-assisted thermoplastic fibre placement process is capable of producing laminates on unheated tooling with short beam strengths equivalent to samples processed using conventional methods, at placement rates as high as 400 mm/s, four times higher than achieved by other heat sources previously reported in the literature.

Publications

The following publications, developed during my PhD candidature, constitute a large portion of this thesis.

Stokes-Griffin, C. M. and Compston, P. Optical characterisation and modelling for oblique near-infrared laser heating of carbon fibre reinforced thermoplastic composites. *Optics and Lasers in Engineering*, 72 (Sep. 2015), 1–11. doi:10.1016/j.optlaseng.2015.03.016.

Stokes-Griffin, C. M. and Compston, P. A combined Optical-Thermal model for near-infrared laser heating of thermoplastic composites in an automated tape placement process. *Composites Part A: Applied Science and Manufacturing*, Article in press (Aug. 2014). doi:10.1016/j.compositesa.2014.08.006.

Stokes-Griffin, C. M. and Compston, P. Laser-Assisted tape placement of thermoplastic composites: The effect of process parameters on bond strength. In *Proceedings of the 5th International Conference ICSAT 2013*, 133–141. Springer International Publishing, Switzerland. doi:10.1007/978-3-319-01884-3_13.

Stokes-Griffin, C. M.; Compston, P.; Matuszyk, T. I.; and Cardew-Hall, M. J. Thermal modelling of the laser-assisted thermoplastic tape placement process. *Journal of Thermoplastic Composite Materials*, Article in press (Nov. 2013). doi:10.1177/0892705713513285. (cited on pages 88 and 198)

Stokes-Griffin, C. M.; Matuszyk, T. I.; Compston, P.; and Cardew-Hall, M. J. Modelling the automated tape placement of thermoplastic composites with in-situ consolidation. In *Sustainable Automotive Technologies 2012*, 61–68. Springer Berlin Heidelberg. doi:10.1007/978-3-642-24145-1_9.

Contents

Acknowledgments vii

Abstract ix

Publications xi

List of Figures xxii

List of Tables xxiii

Nomenclature xxv

1 Introduction 1
- 1.1 Background and motivation . . . 1
- 1.2 Fibre-reinforced polymer matrix composites . . . 5
  - 1.2.1 Fibres . . . 5
  - 1.2.2 Matrix . . . 5
  - 1.2.3 Thermoplastic prepregs . . . 6
- 1.3 Fundamentals of composite processing . . . 6
  - 1.3.1 Processing of thermoset composites . . . 6
  - 1.3.2 Processing of thermoplastic composites . . . 7
    - 1.3.2.1 Bond development . . . 8
      - Healing/autohesion . . . 8
      - Intimate contact . . . 10
      - Full bond development . . . 10
    - 1.3.2.2 Crystallinity . . . 11
    - 1.3.2.3 Void dynamics . . . 13
    - 1.3.2.4 Residual stress . . . 14
    - 1.3.2.5 Degradation . . . 14
    - 1.3.2.6 Summary . . . 16
- 1.4 The in situ thermoplastic AFP process . . . 16
- 1.5 Aim and scope . . . 18
- 1.6 Thesis outline . . . 19

2 Literature review 23
- 2.1 Experimental AFP studies . . . 24
  - 2.1.1 Summary of experimental studies . . . 42
    - 2.1.1.1 Temperature . . . 42

2.1.1.2 Mechanical properties . . . 43
2.1.1.3 Void content . . . 46
2.1.1.4 Consolidation pressure . . . 47
2.1.1.5 Crystallinity . . . 47
2.1.1.6 Degradation . . . 48
2.2 Modelling of the process . . . 50
2.2.1 Intimate contact . . . 50
2.2.1.1 Effective viscosity . . . 61
2.2.1.2 Summary of intimate contact models . . . 62
2.2.2 Healing . . . 65
2.2.2.1 Welding time . . . 68
2.2.2.2 Differential interface temperature . . . 69
2.2.3 Experimental validations of bonding models . . . 71
2.2.4 Void growth and reduction . . . 75
2.2.5 Thermal degradation . . . 77
2.2.6 Non-isothermal crystallisation kinetics models . . . 78
2.2.7 Effect of crystallinity on healing . . . 79
2.2.8 Thermal modelling . . . 81
2.2.8.1 Approach . . . 82
2.2.8.2 Modelling of consolidation rollers . . . 83
2.2.8.3 Modelling of tooling . . . 84
2.2.8.4 Thermal contact resistance . . . 85
2.2.8.5 Material properties . . . 86
2.2.8.6 Laser source models . . . 86
2.3 Process simulation . . . 89
2.3.1 Parametric studies . . . 90
2.3.2 Process optimisations . . . 93
2.4 Conclusions . . . 95

3 Thermal Model **99**
3.1 Introduction . . . 100
3.1.1 Methodology . . . 101
3.1.2 Model geometry . . . 103
3.1.3 Mass transport . . . 104
3.1.4 Laser heat flux . . . 105
3.1.5 Radiation . . . 106
3.1.6 Convection . . . 106
3.1.7 Contacts and boundary conditions . . . 107
3.1.8 Material properties . . . 109
3.1.9 Sensitivity analysis . . . 109
3.2 Experimental work . . . 111
3.2.1 Laser AFP cell . . . 111
3.2.2 Experimental method . . . 112
3.3 Results and discussion . . . 114

3.3.1 Sensitivity analysis . . . 116
3.4 Conclusions . . . 119

4 Bonding: comparison of model predictions and lap shear strength 121
4.1 Introduction . . . 122
4.2 Process model implementation . . . 125
4.2.1 Intimate contact . . . 125
4.2.1.1 Simplified rectangular wave implementation . . . 126
4.2.1.2 Fractal cantor set implementation . . . 126
4.2.2 Healing . . . 129
4.2.3 Coupled bonding model . . . 129
4.2.3.1 Bonding temperature threshold . . . 130
4.2.3.2 Input parameters . . . 130
4.2.3.3 Relation between bonding and lap shear strength . . . 132
4.3 Experimental method . . . 132
4.3.1 Temperature measurement . . . 133
4.3.2 Pressure measurements . . . 133
4.3.3 Sample preparation . . . 134
4.3.4 Sample testing . . . 135
4.4 Results of preliminary trials . . . 138
4.4.1 Temperature histories . . . 138
4.4.2 Pressure distributions . . . 139
4.4.3 Comparison of predicted and experimental strengths assuming model parameters from the literature . . . 140
4.4.3.1 Bond development history predictions . . . 140
4.4.3.2 Predicted vs. experimental lap shear strength . . . 142
4.4.4 Comparison of predicted and experimental strengths assuming the current model parameters . . . 145
4.4.4.1 Bond development history predictions . . . 145
4.4.4.2 Predicted vs. experimental lap shear strength . . . 146
4.5 Extended placement trials . . . 151
4.5.1 Updated laser AFP head . . . 152
4.5.2 Process parameters . . . 153
4.5.3 Temperature and pressure histories . . . 153
4.5.4 Comparison of predicted and experimental strength . . . 157
4.5.4.1 Rigid brass roller . . . 157
4.5.4.2 Conformable silicone roller . . . 161
4.5.5 Effect of placement rate . . . 164
4.5.6 Effect of consolidation force . . . 166
4.6 Conclusions . . . 166

5 Optical characterisation 171
5.1 Introduction . . . 172
5.2 Optical property characterisation . . . 172

5.2.1 Optical properties of PEEK . . . 173
5.2.2 Optical properties of AS4/PEEK composite . . . 176
5.3 Optical model formulation . . . 179
5.3.1 Scattering . . . 181
5.3.2 Angular dependent reflectance . . . 183
5.3.3 Laser source model . . . 186
5.3.3.1 Beam profiling . . . 187
5.3.3.2 Source model formulation . . . 188
5.4 Conclusions . . . 192

6 Combined optical-thermal model **197**
6.1 Introduction . . . 198
6.2 Optical tape placement model . . . 199
6.3 Thermal model . . . 201
6.3.1 Model geometry and meshing . . . 202
6.3.2 Material properties boundary conditions . . . 202
6.4 Experimental . . . 205
6.5 Results and discussion . . . 206
6.5.1 Optical model . . . 206
6.5.1.1 Laser interaction with the composite . . . 206
6.5.1.2 Analysis of full model . . . 207
6.5.2 Thermal model . . . 212
6.5.2.1 Experimental validation . . . 214
6.5.2.2 Effect of surface model . . . 217
6.5.2.3 Effect of source model . . . 217
6.5.2.4 Effect of fibre orientation . . . 219
6.6 Conclusions . . . 222

7 Short beam strength: predicted vs. experimental **225**
7.1 Introduction . . . 226
7.2 Process model implementation . . . 228
7.2.1 Bonding model . . . 228
7.2.2 Crystallisation . . . 228
7.2.3 Void dynamics . . . 230
7.2.4 Temperature history . . . 233
7.2.5 Pressure history . . . 234
7.3 Experimental . . . 235
7.3.1 Placement trials . . . 235
7.3.2 Short beam strength tests . . . 237
7.3.2.1 Sample preparation . . . 237
7.3.2.2 Test procedure . . . 238
7.4 Results and discussion . . . 238
7.4.1 Temperature and pressure history . . . 238
7.4.2 Bond Development . . . 241

7.4.2.1 100 mm/s placement rate 241
7.4.2.2 400 mm/s placement rate 244
7.4.3 Short beam strength: experimental vs. predictions 249
7.4.3.1 100 mm/s placement rate 249
7.4.3.2 400 mm/s placement rate 250
7.4.4 Crystallinity and void content 252
7.4.4.1 100 mm/s placement rate 252
7.4.4.2 400 mm/s placement rate 255
7.5 Conclusions 257

8 Conclusion **263**
8.1 Thermal Model 263
8.2 Bond Strength Development 264
8.3 Optical characterisation 267
8.4 Combined optical-thermal model 268
8.5 Process simulation and short beam strength 269
8.6 Future Work 271

References **287**

List of Figures

1.1 PEEK molecule repeat unit. 6
1.2 Healing of a thermoplastic interface. 9
1.3 Intimate contact development of a thermoplastic interface. 10
1.4 Diagram of a typical laser-assisted in situ TP-AFP process. 17

2.1 Relative SBS vs. placement rate from the literature. 44
2.2 Dara and Loos [1985] intimate contact (D_{ic}) model. 51
2.3 Flattening of tows in the Dara and Loos [1985] D_{ic} model. 52
2.4 Flattening of tows in the Lee and Springer [1987] D_{ic} model. 53
2.5 Flattening of asperities in the Yang and Pitchumani [2001a] D_{ic} model. . 59
2.6 Temperature dependent viscosity for PEEK and CF/PEEK. 63
2.7 Reptation model. 66
2.8 Temperature dependence of welding time for PEEK from literature. . . 70
2.9 Microscopic void model of Ranganathan et al. [1995]. 76

3.1 Laser-assisted TP-AFP process showing typical laser propagation. . . . 101
3.2 Nip point shadow and mass flows. 102
3.3 Dimensions of the reduced model geometry. 104
3.4 Detail of the roller, tape and substrate mesh at the nip point. 105
3.5 Thermal model boundary locations. 107
3.6 Photograph of a laser placement head used in the experimental studies. 112
3.7 Foil type thermocouple installed on the surface of the 25 ply laminate. . 114
3.8 Temperature distribution for the default model parameters. 115
3.9 Temperature plot for the default model parameters compared with experimental thermocouple measurements. 116
3.10 Temperature plots for roller temperatures of 40 °C and 200 °C. 117
3.11 Effect of roller temperature. 118
3.12 Effect of contact resistance. 119
3.13 Effect of corner radius. 120

4.1 Geometry of the fractal cantor set intimate contact model. 126
4.2 Measurement of the pressure distribution under a conformable roller. . 134
4.3 Preparation of the substrates for lap shear placement trials. 136
4.4 Substrates affixed to the tooling plate prior to placement. 137
4.5 Prepared lap shear samples. 137
4.6 Preliminary lap shear trials: thermocouple and pressure measurements relative to the nip point. 139

4.7 Bond development history predictions based on the parameters assumed in the work of Mantell et al. [1992]. 141
4.8 Bond development history predictions based on the parameters assumed in the work of Tierney and Gillespie [2006]. 143
4.9 Bond development history predictions based on the parameters assumed in the work of Khan et al. [2010]. 144
4.10 Preliminary lap shear trials: Experimental vs. predicted strength assuming parameters from the literature. 145
4.11 Bond development history predictions based on the current study parameters assuming t_w from Khan et al. [2013]. 147
4.12 Bond development history predictions based on the current study parameters assuming t_w from Lee and Springer [1987]. 148
4.13 Bond development history predictions based on the current study parameters assuming t_w from Sonmez and Hahn [1997a]. 149
4.14 Preliminary lap shear trials: Experimental vs. predicted strength assuming parameters from the current work. 150
4.15 Example of the production model laser AFP head. 152
4.16 Extended lap shear trials: example of the process instrumentation. . . . 154
4.17 Extended lap shear trials: thermocouple and pressure measurements relative to the nip point. 156
4.18 Bond development history prediction for an 80 mm brass roller. 158
4.19 Extended lap shear trials: experimental vs. predicted strength for the 80 mm rigid brass roller. 160
4.20 Extended lap shear trials: Example bond development history for an 80 mm conformable roller (ET-1). 163
4.21 Extended lap shear trials: experimental vs. predicted strength for the 80 mm rigid brass roller. 165

5.1 3D surface profile of the composite produced by a confocal microscope at 50x magnification. 173
5.2 Absorption coefficient vs. wavelength for amorphous and semicrystalline PEEK films. 174
5.3 Transmitted intensity vs. path length for amorphous and semicrystalline PEEK at the wavelength of the laser. 175
5.4 Refractive index vs. wavelength for the amorphous PEEK film. 176
5.5 Experimental setup for qualitative scattering observation. 177
5.6 Experimental observations of scattering patterns from the composite tape at various orientations. 178
5.7 Diagrams of integrating sphere centre mount measurements at angles of 10° and 60°. 179
5.8 AS4/PEEK reflectance vs. angle of incidence at various wavelengths. . . 180
5.9 Interaction of light with the composite and also a specular surface model with absorbing radiometric film behind surface. 181
5.10 Scattering from a cylindrical object for 0° and 90° orientations. 182

5.11 MHC surface model with absorbing radiometric film behind surface. . 183
5.12 Scattering patterns from the MHC surface model. 184
5.13 Angular dependence of reflection for AS4/PEEK at λ = 980 nm compared with surface models. 185
5.14 Irradiance profile measurement technique. 189
5.15 Measurements of the irradiance profile at z = 200 mm. 190
5.16 Dimensions of irradiated spot vs. distance. 191
5.17 Visualisation of beam propagation with comparison to experimental measurement. 193

6.1 Combined optical-thermal model geometry. 200
6.2 Thermal model boundary locations. 203
6.3 A linear array of beamlets demonstrating first order reflections from the substrate onto the tape and roller. 207
6.4 A linear array of beamlets demonstrating first order reflections from the tape onto the substrate. 207
6.5 Irradiance maps of first order reflections on tape and substrate from a linear array of 40 beamlets. 208
6.6 Irradiance maps for various source and surface approximations. 210
6.7 LWIR image showing thermocouple at higher temperature. 213
6.8 Experimental measurements compared with the best approximation for laser powers of 1130 and 1056 W. 215
6.9 Comparison of temperature profiles for different surface approximations in optical model. 218
6.10 Comparison of temperature profiles for different source approximations in optical model. 220
6.11 The effect of the substrate fibre orientation on the surface temperature profiles. 221

7.1 Microscopic void model of Ranganathan et al. [1995]. 232
7.2 Example showing the *ASTM D 2344* short beam strength test method. . 239
7.3 Temperature and pressure histories for different process temperatures at a placement rate of 100 mm/s. 242
7.4 Temperature and pressure histories for different process temperatures at a placement rate of 400 mm/s. 243
7.5 Bonding development for different process temperatures for a placement rate of 100 mm/s. 246
7.6 Bonding development for different process temperatures for a placement rate of 400 mm/s. 247
7.7 Comparison of the experimental SBS with model predictions for a placement rate of 100 mm/s. 251
7.8 Comparison of the experimental SBS with model predictions for a placement rate of 400 mm/s. 253

7.9 Crystallinity and void content predictions for different process temperatures at a placement rate of 100 mm/s. 256
7.10 Crystallinity and void content predictions for different process temperatures at a placement rate of 400 mm/s. 258
7.11 Relative SBS vs. placement rate for different heat sources in the literature compared with current NIR laser results. 260

List of Tables

1.1 Maximum exposure time vs. temperature for carbon/PEEK composites. 15

2.1 Survery of SBS vs. placement rate for CF/PEEK. 45
2.2 Temperature dependent viscosity relations for PEEK and CF/PEEK from literature. 62
2.3 Temperature dependent welding time relations for PEEK from literature. 69

3.1 Maximum element dimensions in direction of flow for $v = 133\,\mathrm{mm/s}$. . 103
3.2 Temperature dependent convective heat transfer coefficients. 106
3.3 Temperature dependent material properties. 110
3.4 Parameters for thermal model sensitivity studies. 110

4.1 Parameters for the fractal cantor set intimate contact model. 127
4.2 Crystallisation half-times for PEEK-150G. 131
4.3 Bonding model parameters from experimental validations in the literature. 131
4.4 Bonding model parameters for the current study. 132
4.5 Process parameter sets for the preliminary lap shear trials. 133
4.6 Process parameter sets for the extended lap shear trials. 153
4.7 Approximate period of shadow vs. placement rate. 155

5.1 Optical source models considered for the study. 192

6.1 Combined optical-thermal model geometry. 200
6.2 Maximum element dimensions in direction of flow for $v = 133\,\mathrm{mm/s}$. . 202
6.3 Temperature dependent material properties. 203
6.4 Process control settings. 205

7.1 Parameters applied to the crystallisation model for a carbon/PEEK composite. 231
7.2 Parameters applied to the void dynamics model for a carbon/PEEK composite. 233
7.3 Process parameters for the SBS trials. 236

Nomenclature

Acronyms and Abbreviations

ACP	automated composite placement
AFP	automated fibre placement
ANN	artificial neural network
APC-2	a type of AS4/PEEK composite
AS4	a type of high strength carbon fibre
ASTM	American Society for Testing and Materials
ATP	automated tape placement
BPS	bonding model parameter set
BRDF	bidirectional reflectance distribution function
CF	carbon fibre
CO_2	carbon dioxide
coll.	collimated
DCB	double cantilever beam
DCCB	double cantilever curved beam
DIN	Deutsches Institut für Normung (German Institute for Standardisation)
div.	divergent
DSC	differential scanning calorimetry
emf.	spatial emittance function
FFT	fast Fourier transform
FTIR	Fourier transform infra-red spectroscopy
HPDDL	high power direct diode laser
ILSS	inter-laminar shear strength

IM-7	a type of intermediate modulus carbon fibre
ISD	interlaminar shear device
LWIR	long wave infra-red
MDSC	modulated differential scanning calorimetry
MHC	microscopic half cylinder
NIR	near infra-red
PEEK	poly(ether ether ketone) thermoplastic polymer
PEKK	poly(ether ketone ketone) thermoplastic polymer
PIXA-M	a type of polyimide thermoplastic polymer
PMC	polymer matrix composite
PPS	poly(phenylene sulfide) thermoplastic polymer
RF	rectangular fractal cantor intimate contact model
RFP	robotic fibre placement
RWS	simplified rectangular wave intimate contact model
SBS	short beam strength
TGA	thermogravimetric analysis
TP	thermoplastic
W-M	Weierstrass-Mandelbrot
WLF	Williams, Landel and Ferry time-temperature relation

Greek Symbols

α	absorption coefficient (optics)
α	thermal diffusivity
χ	polymer chain penetration depth across a plane
λ	wavelength
μ_{mf}	temperature dependent matrix-fibre viscosity (effective)
ρ	density
ρ_a	density of amorphous PEEK

ρ_c	density of equilibrium crystalline PEEK
θ_i	angle of incidence
θ_t	angle of refraction
σ	standard deviation (sample)

Roman Symbols

$\ddot{q}$	heat generation per unit area
A	absorptance
a	rectangular wave D_{ic} model: instantaneous height of rectangular elements
a^*	rectangular wave D_{ic} model: lumped geometric parameter related to w^*, a_0 and b_0
a_0	rectangular wave D_{ic} model: initial height of rectangular elements
b	rectangular wave D_{ic} model: instantaneous width of rectangular elements
b_0	rectangular wave D_{ic} model: initial width of rectangular elements
c	specific heat
$C_{1(e)}$	constant coefficient of the temperature dependent pre-exponential factor (epitaxial)
$C_{1(s)}$	constant coefficient of the temperature dependent pre-exponential factor (spherulitic)
$C_{2(e)}$	empirical parameter, associated with the temperature dependence of viscosity (epitaxial)
$C_{2(s)}$	empirical parameter, associated with the temperature dependence of viscosity (spherulitic)
$C_{3(e)}$	parameter associated with the free energy of nucleation (epitaxial)
$C_{3(s)}$	parameter associated with the free energy of nucleation (spherulitic)
D	fractal dimension
D_b	degree of bonding
D_h	degree of healing
D_{ic}	degree of intimate contact
f	fractal scaling factor

$F_{vc(e)}$	normalised epitaxial crystal volume fraction
$F_{vc(s)}$	normalised spherulitic crystal volume fraction
g^*	rectangular wave D_{ic} model: lumped geometric parameter related to a^* and w^*
h	convective heat transfer coefficient
h_0	fractal zeroth generation trough height
K_x	thermal conductivity along x axis
K_y	thermal conductivity along y axis
L	characteristic length for convection
l	maximum element dimension along direction of mass flow
L_0	fractal zeroth generation rectangle length
M	polymer molecular weight
M_c	polymer molecular weight of critical entanglement
n	fractal generation number
n	refractive index (optics)
n_e	Avrami constant (epitaxial)
n_s	Avrami constant (spherulitic)
p	parallel component of polarisation
P_{app}	pressure applied to the bond interface
R	reflectance
s	perpendicular component of polarisation
T	transmittance
t	thickness (optics)
t_h	elapsed healing time
$T_{m(e)}$	melting point (epitaxial)
$T_{m(s)}$	melting point (spherulitic)
t_r	reptation time
t_w	welding time

v	magnitude of the mass flow velocity
v_x	mass flow velocity x component
v_y	mass flow velocity y component
w	rectangular wave D_{ic} model: instantaneous distance between rectangular elements
w^*	rectangular wave D_{ic} model: lumped geometric parameter related to w_0 and b_0
w_0	rectangular wave D_{ic} model: initial distance between rectangular elements
w_e	epitaxial crystal growth weight factor
w_s	spherulitic crystal growth weight factor
x_f	effective laser focal point (x-axis)
x_{hw}	laser spot half-width (x-axis)
$X_{vc\infty}$	equilibrium crystalline volume fraction
X_{vc_i}	initial crystalline volume fraction
X_{vc}	crystalline volume fraction
y_f	effective laser focal point (y-axis)
y_{hw}	laser spot half-width (y-axis)
z	distance from the laser optics
T	temperature
t	time

Chapter 1

Introduction

1.1 Background and motivation

The high specific strength and stiffness of fibre-reinforced polymer matrix composites (PMC) makes them an attractive choice of material for use in lightweight and high performance structures. Additional benefits include the ability to produce complex geometries which result in lower part counts with fewer assembly and joining operations. Despite the advantages of composite materials, their use is typically limited due to factors such as the slow manufacturing process, cost and end of life credentials/recyclability.

Manufacturing process The manufacturing process for high performance composite materials is typically slow due to labour intensive lay-up processes followed by long cure cycles of thermosetting resins. Autoclave processing remains dominant in the manufacture of high performance thermoset-based polymer composites throughout a range of industries, particularly aerospace, having long been established as reliable and capable of meeting stringent quality requirements. Although widely adopted, autoclave processing requires significant capital investment, an issue which is compounded when seeking to process increasingly large composite structures as required by the aerospace industry [Vincent, 2009], and increased productivity. Thermal cure via bulk heating is inefficient due to poor thermal conductivity of the composites. Heating rates must also be limited to avoid quality issues related to excessive rates of exothermic release (leading to thermal runaway), enforcing long and energy

intensive processing cycles. Limitations of autoclave processing have therefore led to research efforts to develop alternative out-of-autoclave manufacturing methods targeted at greater processing efficiency, whilst achieving comparable quality levels [Sakota et al., 2006].

Automated composite placement (ACP) technology has the potential to reduce manual labour costs, improve the precision and accuracy of ply lay-up and fibre orientation, and ultimately lead to increased productivity [McAfee, 1990; Gruber et al., 2001]. Example systems include filament winding, automated fibre and tape placement (AFP & ATP) [Beckwith, 2008], and robotic fibre placement (RFP) [Felderhoff and Steiner, 1993]. A typical ACP system consists of a composite placement head, a material delivery system for composite prepreg tapes or separate fibre and resin constituents, and tooling on which the composite is placed. A placement head, which is mounted to an articulation device such as a gantry or industrial robot arm, consists of a material feed mechanism, and a compaction/consolidation device. The head places the composite ply-by-ply in an additive manufacturing process to produce the desired composite part or structure.

In a typical ACP process for thermoset-based composites, the part would require thermal treatment in an oven or autoclave after placement in order to attain full cure. A manufacturing process involving an oven or autoclave separates the material placement and curing processes. The use of rapid cure thermoset polymer technology as part of an automated placement system could combine these steps by enabling the composite to be cured in situ at, or close to, the point of placement (nip point). Examples of such technologies include electron-beam [Beziers et al., 1990; Cirri, 1993; Crivello et al., 1997; Lopata et al., 1999; Crivello, 1999a; Goodman et al., 1999, 2000; Cano et al., 2001; Burgess et al., 2001; Bykanov et al., 2001; Boey et al., 2002] and ultraviolet cure [Beziers et al., 1996; Crivello, 1999b; Endruweit et al., 2006; Hay and Gara, 2006; Endruweit et al., 2008]. Hence, manufacturing cycle times could be reduced. Alternatively, cure processes can be avoided altogether by using ther-

moplastic composites which can be bonded/welded in situ. Thermoplastic materials can be processed by fusion bonding, a welding process based on the diffusion of polymer molecules across the bond interface at elevated temperatures. This process can be orders of magnitude faster than a typical thermoset cure.

Environmental impact/recyclability Manufacturers are under pressure to use materials and manufacturing processes with minimal environmental impact. Composites are traditionally made using thermoset resins which produce a significant amount of volatile organic compound emissions during the manufacturing process. Recycling of thermoset composites is difficult and commercially viable solutions are still under development [Pimenta and Pinho, 2011].

Thermoplastic composites have the potential ability to address both of these issues. The thermoplastic fusion bonding process involves only the use of heat and pressure– no solvents are involved and negligible emissions are produced making it a very clean process. Furthermore, when coupled with a placement technology such as ATP or AFP, the composite can be bonded in situ as it is placed. This means that once the placement has finished the component is ready for use– the cure cycle is eliminated making the process time much shorter. This process shows a lot of potential for mass production of composite materials. Thermoplastic composites are more easily recycled and have increased potential for repair as they can be re-melted.

In situ thermoplastic AFP (TP-AFP) is an attractive manufacturing process as it is fast, clean, automated and applies to materials with greater end-of-life potential. It also opens the possibility of fully automated composite production. Other advantages of TP-AFP include the relatively small footprint and capital investment requirement when compared with the equivalent thermoset alternative. A thermoset tape placement setup occupies the same area, however the autoclave requirement greatly increases the footprint and capital investment. Cold storage facilities are also required for limited shelf life thermoset prepregs.

While extensive research has been conducted in the area of TP-AFP, the process

has not yet reached maturity. A complete understanding of the process and ability to accurately predict material quality in real processes is required in order for industry to adopt the technology.

Recent advances in near infra-red (NIR) high power direct diode laser (HPDDL) technology has opened new opportunities for TP-AFP process. Traditional heat sources such as hot gas torches and direct flame heating are limited by the convective mode of heat transfer, as well as high running costs [Funck and Neitzel, 1995]. The efficiencies of these systems are also low with 30-40 % of the energy from the hot gas delivered to the material [Tierney and Gillespie, 2003]. Other issues such as gas stagnation [Guan and Pitchumani, 2004] result in non-uniform heat input, and limited heating in the cavity between the tape and substrate near the nip point. Furthermore, process control is difficult due to delayed response of such heat sources. Radiative sources such as laser are more efficient as the radiation is absorbed directly by the surface of the composite. HPDDL lasers have high plug-in efficiencies, high reliability and near instantaneous response time that is ideal for process control [Khan et al., 2010; Grouve et al., 2010]. The laser source can be placed outside of the work-cell as the NIR radiation can be delivered via fibre-optic light cables to the placement head. Compact, lightweight optical modules can produce relatively large rectangular spots of homogeneous intensity, ideal for uniform heating of the composite material over generous heated lengths. HPDDL's are relatively low cost compared with other types of laser, and the output power levels are seemingly unlimited- currently available units have output powers of 20 kW or more.

Thermoplastic composites are emerging as an attractive alternative to thermosets in AFP as they have potential to be rapidly processed in situ. Current quality concerns mean that in situ TP-AFP is often utilised for preforming which is then followed by an autoclave post consolidation [August et al., 2014]. Further research is required to develop confidence and achieve high quality for a true out-of-autoclave in situ TP-ATP process.

1.2 Fibre-reinforced polymer matrix composites

The following section provides a background on fibre-reinforced polymer matrix composites. The structure, composition, available forms and fundamental processing behaviour will be described.

1.2.1 Fibres

The fibres in a composite material are typically very high in stiffness, particularly in the case of carbon fibres. Despite being extremely stiff, bundles of fibres alone are soft and flexible due to their small diameter which is typically 7 µm. However when combined with a matrix, the fibres are held in place giving dimensional stability, and load is transferred between the fibres and matrix. Synergistic effects result in high stiffness, lightweight materials with properties better than both the constituent fibres and matrix.

1.2.2 Matrix

In this work the focus is on high performance thermoplastic composite materials. One class of polymers known as poly(aryl ether ketones) have a particularly attractive combination of properties. They are known for their outstanding qualities in terms of strength, toughness, temperature stability as well as creep and chemical resistance. Poly(oxy-1,4-phenyleneoxy-1,4-phenylenecarbonyl-1,4-phenylene) or poly(ether ether ketone) (PEEK) in abbreviated form is perhaps the most common resin in this family of polymers. The molecular repeat unit is shown in Figure 1.1. Carbon fibre reinforced PEEK composites have excellent mechanical properties in terms of strength and stiffness that are equivalent to a high perfomance carbon/epoxy thermoset composite, however they also have much higher damage tolerance due to the inherent toughness of a thermoplastic matrix. Other added advantages such as low moisture absorption and the possibility of reprocessing and repair make carbon/PEEK a very attractive material. Because of these outstanding properties, the

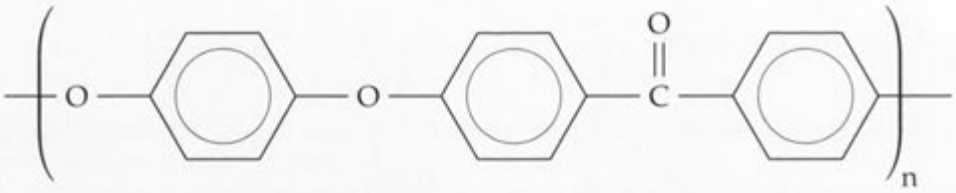


Figure 1.1 – PEEK molecule repeat unit.

majority of thermoplastic AFP literature has been based on carbon/PEEK composites. For this reason, carbon/PEEK is chosen as the candidate material in this body of work.

1.2.3 Thermoplastic prepregs

Thermoplastic prepregs are available in various forms such as commingled tows, powder coated, and fully impregnated forms. For TP-AFP the time for processing is very limited and thus fully consolidated prepregs are only considered in this work. Fully consolidated prepregs come in the form of unidirectional tapes (wide) or towpregs (narrow). Tapes can be slit into narrow tapes for AFP processes, however poor quality edges typically result from the slitting process. Thermoplastic towpregs are high quality narrow tapes that are manufactured to width with smooth, square edges and dimensional tolerances superior to slit tape.

1.3 Fundamentals of composite processing

In this section, the fundamental processing behaviours of high performance composites will be discussed. First, the typical processing behaviour of a thermoset resin will be briefly discussed, and then the fundamentals of thermoplastic composite processing will be discussed in further detail.

1.3.1 Processing of thermoset composites

Strength development for a thermoset based composite is the formation of a three dimensional covalently bonded network of polymer chains. The resin is in the form

of low molecular weight chains known as oligimers. The first step of a thermoset cure is polymerisation, a process whereby the oligimers join end to end forming a strong polymer chain. This typically occurs over a period of time to the order of tens of minutes and results in a rapid increase in the resin viscosity. A cross-linking process then ties these long chains together forming a three dimensional covalently bonded network. Cross-linking causes the material to transition from a soft rubbery state to a stronger, yet more brittle glassy state. This final stage of polymerisation is much slower as diffusion of the reactive species is greatly impeded by the increased viscosity. Because of this, the total cure process takes a long period of time, in the order of hours, to reach completion. This makes the cycle time in the production of thermoset composite components extremely long.

In a thermoset composite manufacturing process, the thermosetting resins begin as relatively low viscosity liquids that are able to flow freely, allowing for good fibre wetout and consolidation between layers. The reason for this low viscosity is the matrix system is in an uncured or b-staged state and consists of oligimers or short polymer chains. The majority of the polymerisation process occurs during the final cure of the complete composite structure as whole.

1.3.2 Processing of thermoplastic composites

High performance thermoplastic composites have quite different processing behaviour to their high performance thermoset counterpart. Thermoplastic composites are fundamentally different as the thermoplastic matrix has already undergone polymerisation prior to the manufacturing process. Unlike thermoset resins, the molecules are not cross-linked. This adds an extra advantage as unlike a thermoset polymer, a thermoplastic can be melted and reprocessed. The time consuming polymerisation step is also removed from the composite manfacturing process. This opens opportunities for high speed processing by means of welding, and also increased repairablity of a composite structure. Processing is achieved by diffusion of the long polymer chains

across the interfaces of the materials being bonded. At ambient conditions, the length and entanglement of the polymer chains is sufficient to cause the material to act as a glassy solid. However, as the polymer is heated beyond its glass transition point, it begins to behave as a rubbery solid due to increased chain mobility. At temperatures above the melting point, the material behaves as a viscous liquid. In the case of a high performance thermoplastic, it behaves more like a soft deformable solid, rather than a liquid as the viscosity remains high due to the length of the polymer chains as well as large functional groups that can act as motion restricting obstacles that prevent the polymer chains from moving freely over one another. The melt viscosity of a high performance thermoplastic typically exceeds that of a conventional epoxy at its gel point [Dara and Loos, 1985].

Compared with a traditional composite process, thermoplastics have the advantage that the lengthy cure process is replaced by a welding process that can be orders of magnitude faster. The processing nature of thermoplastics is fundamentally different to thermosets and thus different manufacturing methods are required. The following sections describe the fundamental processes which occur during the processing of thermoplastic composite materials, and the unique challenges faced when processing such a material.

1.3.2.1 Bond development

Healing/autohesion The fundamental mechanism of strength development between two thermoplastic bodies is the diffusion of polymer molecules across the bond interface. de Gennes [1971] first coined the term of diffusive motion of long polymer chains as reptation, a descriptive name that originated from the snake-like motion of the polymer molecules as they diffuse around one another. When two separate polymer bodies of the same material are brought in contact at high temperature, the molecules will begin to reptate across the contact boundary Figure 1.2, a process referred to in the literature as healing or autohesion. The strength of the interface

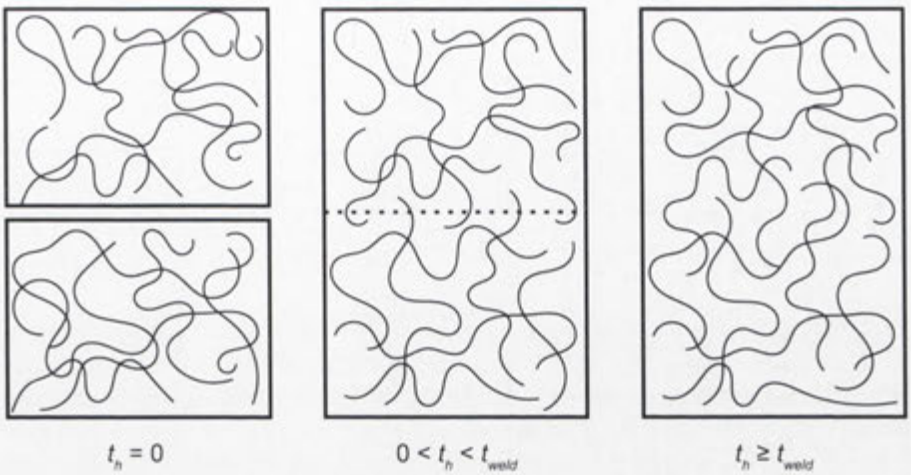


Figure 1.2 – Healing of a thermoplastic interface. Initially the contact is zero (left). After contact at elevated temperature the molecules begin to repatate over the contact boundary (centre). Given sufficient healing time t_h, the interface is no longer detectable and full strength is achieved (right).

depends on the level of interpenetration. For low levels of interpenetration, mechanical failure occurs as chain pull-out. If the chain has migrated far enough and become sufficiently entangled, the interface is much stronger and failure occurs as chain scission. As reptation is a diffusion process, it is highly temperature dependent with greatly enhanced rates at high temperatures.

The process is typically characterised by an isothermal reptation time t_r, which is defined as the amount of time at a given temperature for the molecule to reptate entirely out of the initial space it occupied. This is often visualised as the polymer chain being initially encased in a fixed imaginary tube of the same size, and after the reptation time it will have completely escaped that tube. The bond interface is said to have achieved full strength after the reptation time has elapsed, in which case the bond interface is no longer discernible. For high molecular weight polymers, reptation is slower due to the increased chain length. However due to the increased length, it is not necessary for the chains to undergo complete reptation to develop full strength at the interface, rather an intermediate penetration length is sufficient to obtain the level of entanglement necessary for the interface strength to equal the bulk strength of the polymer. The length of time required to achieve the bulk strength at

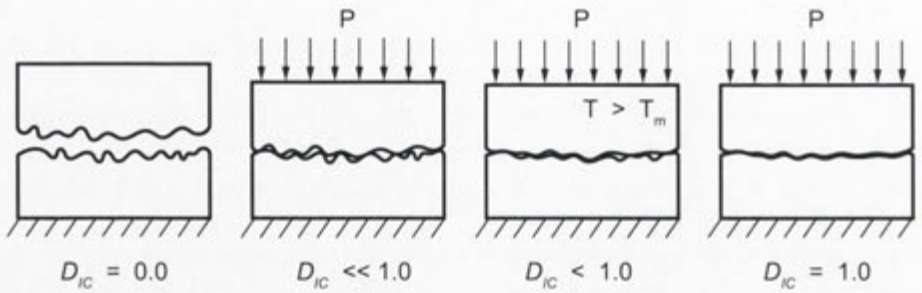


Figure 1.3 – Initially the contact is zero (far left). After applying pressure, the intimate contact is limited to asperities (left). Deformation occurs at high temperatures, increasing the level of intimate contact (right). Sufficient time and pressure application results in complete intimate contact (far right).

the interface is known as the welding time t_w.

Intimate contact In order for reptation of the molecules to occur, the two bodies being joined must first be in contact. As no real surface is truly flat, the initial contact is limited to surface asperities. Given a high enough temperature and applied pressure, the surfaces will begin to plastically deform into one another, increasing the levels of intimate contact. Given sufficient time, temperature and pressure application, full intimate contact will be developed. This process is depicted in Figure 1.3. The degree of intimate contact D_{ic} is defined as the ratio of the area in intimate contact to the total inter-facial area.

Other effects may also contribute to intimate contact. Butler et al. [1998] discuss a wetting phenomenon that occurs when the surfaces are close enough to establish intermolecular forces. If the asperities are of a small enough scale and the viscosity is sufficiently low, surface tension effects can possibly aid in intimate contact development.

Full bond development Healing occurs progressively as new areas of intimate contact are formed. Full bond strength is only achieved after:

1. The complete interface is in intimate contact.

2. All areas in intimate contact have healed sufficiently to achieve the same strength

at the interface as the bulk material.

The bond strength development process is therefore modelled by combining autohesion and intimate contact development models. Thermoplastic bonding models therefore require an accurate account of the coupled temperature and pressure histories from the nip point onwards.

1.3.2.2 Crystallinity

Polymer chains such as PEEK have the ability to align in a preferred, lower energy configuration. Bulk alignment of the chains leads to the formation of crystalline phases, typically spherulitic or epitaxial structures in the case of a PEEK polymer. The crystalline phases act in a similar way to cross-links, reinforcing the polymer which in turn increases the stiffness and also the high temperature mechanical performance as effects such as creep are reduced. High levels of crystallinity also greatly increase the solvent resistance as the reinforcement of the molecular network by the crystalline phases impede dissolution by solvents [Cogswell, 1992]. While high levels of crystallinity improve the stiffness and high temperature stability, the toughness is reduced and the polymer becomes brittle. The stiffness and strength has been reported to vary by $\pm 10\,\%$ for the extreme cases of over crystallised (~40 %) and amorphous samples, while the fracture toughness can vary by as much as $\pm 20\,\%$ relative to samples processed under the optimal conditions with cooling rates of 0.1-10 °C/s yielding crystallinity of 20-35 % [Cogswell, 1992]. The density of the crystalline phases is 10 % higher than the amorphous phases due to the increased packing efficiency of the aligned molecules. Therefore high levels of crystallinity can cause significant shrinkage leading to residual stress development between the fibres and matrix.

In the case of a semi-crystalline polymer the level of crystallinity can change significantly during processing due to the time spent at elevated temperatures. This is particularly important for polymers such as PEEK which shows fast crystallisa-

tion behaviour. When heated above the glass transition temperature but below the melting point, the mobility of the chains is sufficient for cold crystallisation to occur. When the polymer is heated above the melting point, the molecular mobility increases to the point any alignment is lost and the material becomes completely amorphous. It is also possible to have partial melting when the time and temperature is not sufficient to completely melt the crystalline phases. When cooled from the melt, the molecules will start to recrystallise. Any remaining crystalline phases act as nucleation sites which in turn increase the rate of recrystallisation. The rate of recrystallisation is highly temperature dependent, for example for neat PEEK resin at temperatures between 210-260 °C the crystallisation half time is less than 1 s [Tardif et al., 2014], above and below these temperatures up until the melting point and glass transition respectively, the crystallisation time decreases in an almost logarithmic fashion.

The crystallisation behaviour of PEEK is also influenced by the presence of additives such as carbon fibre reinforcements [Velisaris and Seferis, 1986; Cogswell, 1992; Tierney and Gillespie, 2004]. The surfaces of carbon fibres are known to act as nucleation sites for crystal growth. This effect is particularly strong in the case of high modulus fibres and it has been suggested that the mechanism of this nucleation is templating of the aromatic features of the PEEK molecule with the graphitic structures on the surface of the high modulus carbon fibres. This effect is not as strong in the case of high strength fibres such as AS4. Strong nucleation has been observed where two fibres are in close proximity, and it is thought that this is stress induced crystallisation caused by a mismatch in thermal expansion between the fibre and matrix. As the presence of the fibres has an influence on the crystallisation behaviour of the composite, it is necessary to characterise the crystallisation behaviour of the composite material rather than the neat matrix.

1.3.2.3 Void dynamics

During processing of composite materials, small bubbles of gas (voids) can become entrapped in the matrix during manufacture and processing. If these voids are too large they act as sites for crack initiation, degrading the mechanical performance of the material. In the case of a typical thermosetting resin system, the resin viscosity is initially very low and a low void content can be achieved via methods such as vacuum bagging. The viscosity of high performance thermoplastics is sufficiently high that voids do not float to the surface due to buoyancy and they are not easily drawn out of the melt by vacuum. A certain percentage of voids always remains in the prepreg from when it is initially manufactured. Some possible origins of voids are air becoming entrapped during prepreg manufacture, the condensation of dissolved volatiles during processing, gases entrapped during condolidation of plies, the vaporisation of embedded contaminants, and products produced by degradation [Ranganathan et al., 1995; Ye et al., 2002; Simacek et al., 2013].

As the tape is heated and the matrix softens, the internal pressure of the voids can cause them to grow. If the matrix is softened sufficiently at a high enough temperature, the volume fraction of the void content can be reduced by applying pressure which compresses the voids- the gas inside the voids increases in pressure, and the voids shrink in size. If the matrix is cooled sufficiently before the consolidation pressure is released, the voids will remain in this small compressed state, and the effective void content of the material is reduced. Experimental observations have found that when reheating thermoplastic composites the void content is neither sensitive to the maximum temperature or holding time, however it is sensitive to the applied pressure [Ye et al., 2002]. For example one study [Henninger et al., 1998] found a void content of 10 % for an applied pressure of 0.1 MPa, yet increasing the pressure to 0.5 MPa decreased the void content to approximately 3 %. No significant reduction was found when the pressure is increased beyond 1.0 MPa.

1.3.2.4 Residual stress

The nature of thermoplastic composite processing requires the material to be heated to elevated temperatures. The carbon fibre reinforcements have a very low (in the case of high strength fibres) if not negative (in the case of high modulus fibres) coefficient of thermal expansion in the fibre axis. The coefficient of thermal expansion for polymeric matrices is generally higher and also positive. When the composite is cooled, there are residual stresses generated between the fibre and matrix. If the residual stresses are unbalanced, significant distortion of the component can result and even internal failure can appear in the form of cracks. The viscoelastic nature of high performance thermoplastics at elevated temperatures leads to dynamic stress generation and relaxation behaviours resulting in a cooling rate dependence for residual stress..

Residual stresses are generated due to the mismatch in thermal properties between the fibre and the matrix and non-uniform cooling rates through the thickness of the material [Lemarchand et al., 2007; Sonmez et al., 2002].

1.3.2.5 Degradation

Thermoplastic composites need to be processed at high temperatures in order to achieve adequate bonding between the plies of the laminate. Due to the high melt viscosity of thermoplastics, higher temperatures are favourable for decreasing the intimate contact development time. Healing rates are also enhanced at high temperatures, however the polymer will start to degrade if exposed to elevated temperatures for extended periods. Degradation therefore sets the upper limit of the process window. The degradation does not occur at a particular temperature, rather it depends on the time elapsed at elevated temperature. The recommended exposure times for a carbon/PEEK composite at various temperatures is given in Table 1.1. In the case of PEEK, if it is exposed to temperatures above 400 °C for extended periods of time, the matrix has been shown to degrade in the form of cross-linking and/or chain

Table 1.1 – Suggested maximum exposure times at various processing temperatures for carbon/PEEK composites [Cogswell, 1992]

Process Temperature [°C]	Suggested Maximum Exposure Time
400	2 h
450	15 min
500	2 min
550	15 s
600	2 s

branching which further increases the viscosity making the material harder to bond, retarding crystallisation and also impeding the reptation of the molecules [Agarwal et al., 1996; Sonmez and Hahn, 1997b]. Rapid mass loss occurs after the temperature exceeds 575-580 °C [Patel et al., 2010]. For high temperatures over short periods, random chain scission occurs on the either the ether and ketone links and volatile products are released. For temperatures of 450 °C and above, the main products are 1,4-diphenoxybenzene and 4-phenoxyphenol. As the temperature increases, lower molecular weight volatiles are released such as diphenyl ether, benzene and methylbenzene. For temperatures of 650 °C or greater the products are predominantly phenol, carbon monoxide and carbon dioxide.

In the case of high intensity surface heating such as experienced in TP-AFP, it is possible that localised vaporisation/ablation occurs resulting in material removal from the surface. This phenomenon was observed by Rosselli et al. [1997] in a laser consolidation process, and no obvious char residue could be detected in photomicrographs.

The presence of atmospheric oxygen is also known to cause cross-linking at the surface. If a carbon/PEEK composite is melted in air for an hour, the cross-linking can be so significant that the material will no longer bond by healing [Cogswell, 1992]. However, most grades of PEEK that are used in thermoplastic composite prepregs are prepared by nucleophilic reaction processes and trace amounts of diphenyl sulphone remain. Interestingly, when heated above the melt temperature, the diphenyl

sulphone sublimes which can form an intrinsic inert atmosphere on the exposed surfaces of the material [Cogswell, 1992].

The degradation process is complex and cannot be attributed to one particular mechanism, rather it depends on the particular temperature and time period of exposure, and also the presence of oxygen in the surrounding environment.

1.3.2.6 Summary

The processing behaviour of a thermoplastic composite is fundamentally different to that of a traditional thermosetting resin, and requires different processing conditions in order to obtain optimal properties. It can be seen that many of the factors affecting the final quality are highly dependent on the complete thermal history experienced during the manufacturing process, as well as the applied pressure history.

1.4 The in situ thermoplastic AFP process

The in situ TP-AFP process is described by Figure 1.4. Unidirectional pre-impregnated tape is fed down to the top surface of the previously placed layers (substrate). A heat source, such as a laser, heats the surfaces of the tape and substrate as they approach the nip point. The melted surfaces of the tape and the substrate are pushed together by the consolidation device, resulting in a bond. Layers are formed by placing multiple tapes side by side. Parts are made by building up laminates layer-by-layer.

Hot gas torches have been traditionally used for TP-AFP [Mantell et al., 1992; Mazumdar and Hoa, 1996; Tierney and Gillespie, 2003]. The convective mode of heat transfer limits the heat input and operation costs are high as inert gases such as nitrogen must be used to prevent oxidation of the composite [Funck and Neitzel, 1995]. Hydrogen flames have also been employed as a heat source [Khan and Schledjewski, 2010; Khan et al., 2010]. Carbon dioxide (CO_2) lasers (λ = 10.6 µm) with beam powers of 65-80 W were investigated for thermoplastic filament winding [Pistor and Güçeri, 1999; Pistor et al., 1999; Rosselli et al., 1997; Agarwal et al., 1992, 1996]. Round spot

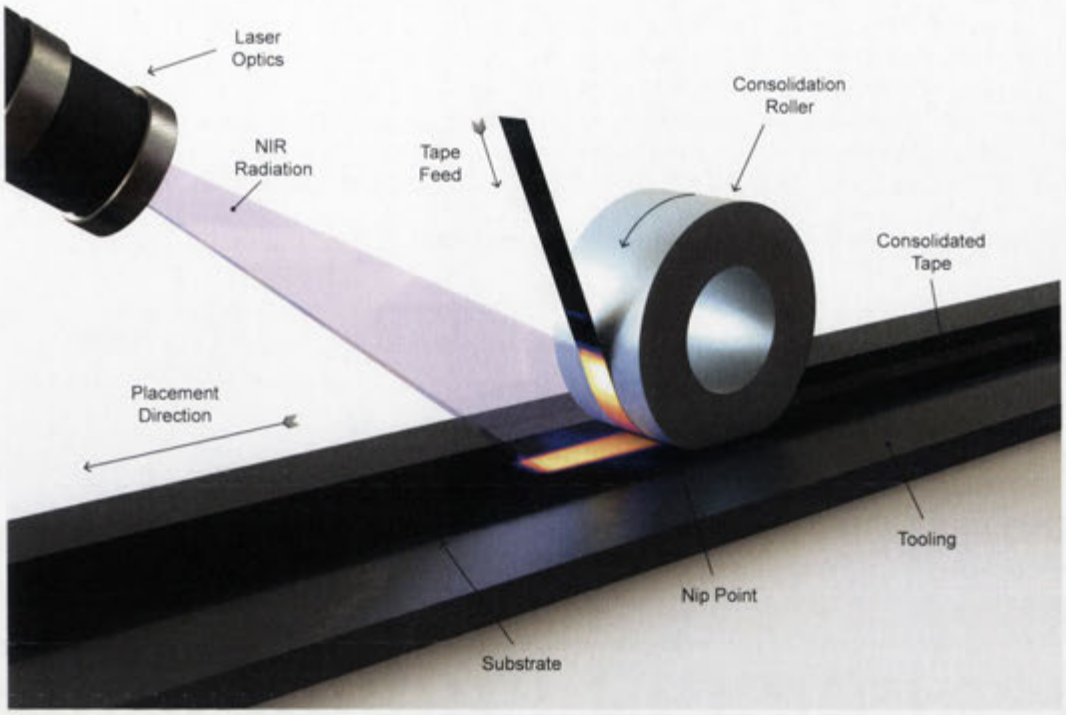


Figure 1.4 – An example of a typical laser-assisted in situ TP-AFP process. It is an additive manufacturing process whereby components are produced by building laminates of thermoplastic composite tape.

outputs were converted into lines (typically 2 mm wide) using ZeSe lenses [Funck and Neitzel, 1995; Pistor and Güçeri, 1999; Rosselli et al., 1997; Agarwal et al., 1992, 1996; Beyeler et al., 1988] or galvanometer scanning [Pistor et al., 1999]. The narrow line width causes high sensitivity to laser position [Beyeler et al., 1988] and poor bonding due to short dwell times [Agarwal et al., 1992, 1996].

More recently, near infra-red (NIR) diode lasers are being investigated due to their high efficiency, near instantaneous response and the ability to deliver higher heat fluxes [Khan et al., 2010]. The lower wavelength (λ = 800-1000 nm) allows delivery of the beam to the placement head via a light cable. Large homogenous rectangular spots (45 mm $\times$ 16 mm) can be produced by compact optical modules, resulting in uniform, progressive heating across the length and width of the tape, increasing the dwell time and therefore bond quality.

The most common consolidation device is a rigid metallic roller, which produces

a very short, intense pressure distribution due to the small contact patch. Other variations have appeared such as conformable rollers which allows for placement on curved surfaces, and also greatly increased length of pressure application. One group used a series of conformable line and area compactors which are used to apply pressure, heat and cooling over large curved areas [Lamontia et al., 2003].

1.5 Aim and scope

The aim of this thesis is to investigate both the capabilities and limitations of a high power diode laser AFP process for the manufacture of high performance carbon/PEEK components in an out-of-autoclave process. Diode lasers are able to produce multi-kilowatt beams with large homogeneous rectangular distributions, opening the possibility of in situ thermoplastic bonding at very high placement rates. The primary aim of this thesis is to determine the quality of laminates that can be produced with the process, particularly for high placement rates, and also to develop a strong understanding of the nature of the process including the interaction of the laser with the composite, the bond development as well as how other qualities such as the crystallinity and void content evolve during processing. A particular emphasis will be placed on how the behaviour changes for increasing placement rate and process temperature.

The bonding behaviour will be investigated with mechanical tests of samples produced in placement trials and also with bonding models implemented from the literature. As the process is highly non-isothermal due to the high laser powers and placement rates, the validity of the bonding models for such conditions are also investigated.

As temperature is the key factor in bond strength development, detailed thermal models are developed for the process. In order to provide accurate predictive capability for the heat flux imparted on the composite by the laser, as well as a deep understanding of the optical interaction within the cavity formed by the tape and

substrate, detailed 3D ray tracing models are formulated for the NIR laser AFP process. This first requires characterisation of the optical properties of the composite and the laser source. A complete optical model for the process is then constructed, and combined with the thermal model in order to provide accurate predictive capability for the temperature history at the bond interface. The laser power is controlled by non-contact temperature measurement of temperatures prior to the nip point. The correlation between this pre-nip point temperature and the consolidation temperature history is not well known and will be investigated with combined optical-thermal model predictions, as well as in situ temperature measurements.

Lastly, the combined optical-thermal model is combined with bonding, crystallisation and void dynamics models to predict the resulting quality of the composite, and develop an understanding of how these quality factors evolve during the process. Such an understanding can provide the insight into the process necessary for understanding the limitations for the process and how it may be improved. Predictions are then compared with results of experimental trials.

1.6 Thesis outline

The research addressing the aims of this thesis is broken down into the chapters as follows. Chapter 2 presents a literature review of TP-AFP processes. The experimental work to date for TP-AFP and closely related in situ processes such as TP filament winding are also considered. The properties of composites produced with TP-AFP compared with conventional methods is of particular interest. The characteristic behaviours of the TP-AFP process are also identified. Models presented in the literature for predicting the various aspects of quality such as intimate contact, healing, crystallinity, void content and degradation are investigated and their appropriateness for the TP-AFP process considered. Process simulations and parametric studies for the TP-AFP process are also reviewed and limitations identified. Areas of interest are then identified for the current study.

In order to first develop an understanding of the nature of the laser AFP process, a thermal model is developed in Chapter 3. The effect of the consolidation roller on the consolidation temperature is investigated, as well as the effect that a shadow would have on the temperature history. The results of the model are compared with experimental temperature measurements. Results strongly imply that a shadow is present in the process, causing significant decreases in temperature prior to consolidation. The laser heat flux was assumed to be a uniform boundary condition, however results suggest that a more detailed model is required. This was realised in later chapters with optical characterisation (Chapter 5) and modelling of the laser flux with 3D ray-tracing calculations (Chapter 6). Results of thermocouple measurements suggest that bonding is occurring below the melting point of the polymer.

The bonding behaviour is investigated in detail in Chapter 4. Bonding models from the literature are implemented and the process instrumented with thermocouples and pressure sensors. Lap shear samples manufactured. Bonding predictions are made using experimentally measured temperature and pressure histories. Bond predictions are compared with lap shear strengths, and results confirm that bonding can occur for temperatures well below the melting point down to temperatures of 200 °C as the rapid cooling history in laser AFP maintains the amorphous state of the PEEK matrix. Strength predictions based on experimentally validated parameters from the literature are compared and contrasted, as well as bonding parameters proposed in the current work. The differences in bond strengths for rigid and conformable rollers are also studied.

Chapter 5 focuses on optical characterisation of composite and laser. A surface model is formulated to capture unique anisotropic scattering behaviour of the composite. Laser source profile and propagation characterised, and an appropriate model formulated. These models are to be used as the building blocks for a full optical model of the laser AFP system that is developed in Chapter 6.

A 3D ray-tracing model of the laser AFP system is constructed in Chapter 6.

The interaction of the laser with the cavity formed between the tape and substrate is investigated in detail. Heat flux distributions are predicted using the ray-tracing are combined with the thermal model developed earlier in Chapter 3. The effects of various optical model simplifications are investigated, as well as a comparison of the current model to the assumptions made previously in the literature.

The final chapter combines the work from Chapters 3–6 to form a process simulator. Experimentally validated void dynamics and crystallisation models from the literature are additionally implemented. The capability of the laser AFP process was investigated with short beam strength tests of samples that were manufactured under conditions that reflect those experienced during the manufacture of components. Experiments were performed to determine the response of the process to increasing process temperature and placement rate. Process simulations were performed taking the effect of subsequent consolidation passes into consideration. Predictions of the strength are then compared with the experimental results. The evolution of void content and crystallinity are also investigated. The strength of samples produced with laser AFP in this work is then contrasted with the values reported for other experimental TP-AFP studies in the literature.

Chapter 2

Literature review

Abstract

The focus of this work is the thermoplastic automated fibre placement process. The following chapter provides an overview of the literature to date concerning the TP-AFP process in terms of experimental studies, process modelling and process optimisation. While the focus is TP-AFP, closely related processes such as thermoplastic filament winding are also considered. This review will be used to identify limitations in the current work and identify areas for further research in this thesis.

2.1 Experimental AFP studies

This section provides a chronological literature review for in situ thermoplastic AFP processing studies which include experimental trials with accompanying property characterisation. The resulting mechanical strength achievable with in situ processes relative to those obtained with conventional processing such as in an autoclave or heat press is of most interest. The placement rate is also an important factor as the process must be fast enough in order to be a competitive manufacturing process. Many of the early experimental trials for in situ thermoplastic processing were performed on simple ring winding apparatuses. While these are not strictly tape placement, they are also included as they are very closely related processes. Characteristic behaviours of the process will also be investigated such as the void dynamics, degradation and crystallinity. The materials of interest in this work are carbon-reinforced aromatic thermoplastic composites such as carbon/PEEK, thus the literature review will focus on such materials.

Beyeler et al. [1988] investigated the possibility of using an 80 W CO_2 laser as a heat source for in situ thermoplastic tape processing. A planar beam 7.5 mm wide was formed using lenses. The positioning of the laser proved difficult due to its narrow width and also by the fact the 10.6 µm radiation is invisible. The process was very sensitive to the laser positioning because of the very narrow width of the beam. Carbon/PPS samples were produced at winding speeds of up to 46 mm/s with good consolidation observed on photomicrographs for a laser power of 70 W. The temperatures experienced during the process are unknown and mechanical characterisation was not performed.

Mantell et al. [1992] performed experiments to validate their previously developed tape placement process model [Mantell and Springer, 1992] which included thermal, bonding and residual stress models. An experimental tape placement apparatus consisted of a 1.5 kW hot gas torch with a 50.8 mm steel roller with consolidation force applied via pneumatic cylinder. 12.7 mm wide APC-2 carbon/PEEK short

beam strength (SBS) and lap shear samples were manufactured in a groove of the same width on a ceramic tool plate. Nitrogen was used as the heating gas to minimise oxidation. The gas temperature was measured in the range of 430 °C. Temperature measurements were performed in situ with K-type thermocouples, the thickness of which was not specified. Samples were tested following the ASTM D 2344 and ASTM D 3165 standards for the SBS and lap shear tests respectively. Reference samples were prepared in a heat press and strengths were found to be 72.4 MPa and 65.5 MPa for the SBS and lap shear samples respectively. The lap shear samples were made by inserting transverse cuts on each side of tape, however it is unclear how precisely the cuts were made and if they completely separated the two layers. Results of the lap shear tests for samples produced at speeds of 11.7 mm/s suggest 50 % of the reference strength was achieved for interface temperatures as low as 260 °C, while 70 % of reference strength was achieved at interface temperatures in the region of 370 °C. In the case of the SBS samples, it was found that the strengths were much lower. The strength relative to the reference samples decreased from 40 % to 15 % as the process velocity was increased from 2.54 mm/s to 5.84 mm/s. The relative strength of a lap shear sample produced under the same conditions was 70 %. The reason for this large discrepancy is unclear. The level of intimate contact was characterised using c-scan measurements and found to be relatively high in the range of 70-80 % for both the lap shear and SBS samples. This would suggest that the large difference in strengths between the lap shear and SBS samples could be due to insufficient healing, however one would expect higher levels healing in the SBS samples due to reheating as the 16 plies are placed on top of each other. It is likely that the much higher strength observed for the lap shear samples is due to insufficient slit depth in the sample preparation, enabling the load to be supported through a thin layer of fibres rather than pure shear loading at the interface. Furthermore, in the case of the lap shear samples that were processed with interface temperatures of 260 °C it is surprising that such high bond strengths could be achieved when the

interface temperature is 80 °C below the melting point of PEEK at 343 °C.

Mazumdar and Hoa [1995] applied the Taguchi method to a laser winding process. The winding apparatus consisted of a 65 W CO_2 laser was combined with a 146 mm mandrel. APC-2 carbon/PEEK rings were manufactured for laser powers of 40, 50 and 60 W, consolidation pressures of 50.4, 100.8 and 151.3 kN/m and placement rates of 6.42, 13 and 27 mm/s, resulting in a total of nine different experiments. The quality characteristic was chosen to be the SBS and results ranged from 20.65-39.57 MPa. No reference samples were produced however a press or autoclaved sample typically has an SBS of 100 MPa, suggesting suboptimal material performance from the laser consolidated samples. The results of the Taguchi analysis found that the relative contributions of laser power, consolidation pressure and tape speed were 79, 2.7 and 17 %, suggesting that the process is most sensitive to the laser power.

Mazumdar and Hoa [1996] studied the effect of process parameters on the temperature history, process induced deformation, crystallinity and fracture load for a hot gas tape winding process. APC-2 carbon/PEEK rings were manufactured on a 146 mm steel mandrel. A pneumatic cylinder was used to apply consolidation load to a 60 mm steel roller. Temperature measurements were performed with thermocouples with a variety of diameters. It was found that the larger diameter thermocouples recorded lower peak temperatures due to the higher thermal mass, therefore thin 0.125 mm were selected for the experimental measurements. Temperatures were logged at a sample rate of 2Hz. The thermocouples were inserted during placement, with temperatures initially reaching around 1000 °C as the thermocouples were heated while suspended in the nitrogen gas stream. It was only after the initial consolidation pass that the thermocouples would become embedded in the composite and give a reading representative of the composite temperature. Heating and cooling rates were as high as 750 °C/s and 100 °C/s respectively.

For a placement rate of 28 mm/s with a hot gas temperature of 905 °C and flow rate of 69 l/min, the interface temperatures during the first and second subsequent

passes was 580 °C and 490 °C respectively. The resulting ring was easily peeled apart indicating poor bonding. The authors state that the peak temperatures may have been higher than this but not captured due to the low sampling rate. After decreasing the placement rate to 13.3 mm/s, temperatures on the subsequent passes increased to 680 °C and 580 °C respectively. The ring could no longer be peeled apart, instead the tape broke indicating good interlaminar bonding. It was concluded that much higher temperatures are required to achieve good bonding during tape placement due to the very short residence times. Elevated temperatures result in much higher rates of molecular diffusion leading to faster healing, as well as reduced resin viscosity resulting in rapid intimate contact development. These results also show that the molten region extends through multiple layers and bond development continues during subsequent passes.

No visible degradation was observed on photomicrographs even when peak thermocouple temperatures exceeded 650 °C. However, it was noted that as the placement rate was decreased from 13.3 mm/s to 3.6 mm/s, the resin rich surface of the tape in the interlaminar region decreased almost to the point it was undetectable. This was attributed to vaporisation of the matrix and/or squeeze out of the resin at lower speed. No significant smoke generation was observed, however it was suggested that it may have been masked/diluted by the flow of hot nitrogen gas. This also led to fibre bridging at the bond interface, which caused double cantilever curved beam (DCCB) fracture tougness tests to no longer represent the toughness of the resin alone. It was therefore suggested that SBS tests are more appropriate for interface bond strength characterisation.

For the parameters studied, the highest SBS was reported to be 54.2 MPa, acheived at a placement rate of 13.3 mm/s. To put this in context, SBSs for autoclaved APC-2 are in the range of 100 MPa. The level of crystallinity was studied using DSC of samples taken from different layers. The experimental temperature history suggested that the remelting near the nip point would destroy any traces of crystallinity,

however during the cooling phase recrystallisation would occur when the material is in the range of 200-300 °C. When the material is at a sufficient depth where the temperature peak is in the range of 200-300 °C, it would no longer melt but recrystallise. DSC measurements support this hypothesis with crystallinity of 36.6 % for the deepest layers and a lower 29 % on the outermost layer.

Agarwal et al. [1996] manufactured APC-2 carbon/PEEK samples using an experimental CO_2 laser filament winding rig. ZeSe lenses were used to shape the laser beam into a 6 mm × 0.5 mm line. Rings were manufactured from 6.35 mm tape at a constant winding speed of 15 mm/s for laser powers between 20-75 W on a 146 mm diameter mandrel. Consolidation pressure was applied with a 25 mm metallic roller with an applied load of 310 N. They estimated the consolidation pressure to be 14 MPa.

The interlaminar properties of curved specimens were assessed by ASTM D 2344 (SBS), double cantilever beam (DCB) and blocking force measurements. The strength and toughness was found to increase with the laser power from 30-50 W which corresponded to consolidation temperatures of 400-475 °C. Properties dropped off for a power of 75 W which resulted in a consolidation temperature of 740 °C. The decrease in properties were attributed to degradation of the polymer at the interface. Earlier work by the authors [Agarwal et al., 1992] show that the tape and substrate temperatures prior to the consolidation temperature are much higher. In the case of the 475 °C consolidation temperature which resulted in the best properties, it would appear that the peak temperature on the surface of the tape prior to consolidation was in the range of 600 °C. For the sample prepared at 75 W which displayed significant degradation, the surface of the feed tape was in excess of 900 °C. The SBS of the best samples was 50 MPa, however no autoclave or heat press reference samples were produced for comparison. Typical SBSs for APC-2 are in the range of 100 MPa suggesting only 50 % of the ultimate strength was achieved with the laser winding rig. No interlaminar voids were observed on photomicrograph cross-sections, sug-

gesting high levels of intimate contact were achieved. The discrepancy in strength was therefore attributed to the short dwell times which result in insufficient healing. Dwell times therefore need to be increased which could be achieved by enlarging the laser spot which would decrease the heating and cooling rates.

Surface crystallinity measurements were performed by means of grazing angle Fourier transform infra-red spectroscopy (FTIR), with the crystallinity determined by the ratio of the peaks at 952 and 966 cm^{-1}. Bulk crystallinity measurements were made using differential scanning calorimetry (DSC). The bulk crystallinity was found to not change significantly with the laser power with values of approximately 28 %. This was explained by annealing effects from the subsequent passes of the laser above. Surface crystallinity measurement was performed on tape and substrate samples after a single winding revolution. The crystallinity was found to significantly decrease with increasing laser power. This reinforces the idea that the crystallinity increases due to reheating by subsequent passes of the laser as there is little difference in the final bulk crystallinity.

The void content was quantified using photomicrography. The presence of interlaminar voids was not detected, indicating high levels of intimate contact. The void content of the unprocessed tape was measured to be 3.9 % ±0.8 %, however the processed samples were found to have void content in the range of 1.5 % with marginally lower values for higher laser powers.

Discoloured regions were observed on photomicrograph cross-sections for samples processed at laser powers resulting in consolidation temperatures of 740 °C. The melting temperature of the sample was also found to be 10 °C lower, suggesting significant degradation. Furthermore, grazing angle FTIR used for surface crystallinity measurements found that no characteristic peaks at 952 and 966 cm^{-1} could be detected for these degraded samples. For lower laser powers with consolidation temperatures of 540 °C or less, degradation was not observed.

Rosselli and Santare [1997] compared short beam strength (SBS) and interlaminar

shear device (ISD) tests for curved samples produced on a laser winding apparatus. An 80 W CO_2 laser ($\lambda = 10.6\,\mu m$) was used with ZeSe lenses converting the beam to an 11 mm × 2 mm spot. 40 ply thick, 5.9 mm wide APC-2 carbon/PEEK rings were wound on a 146 mm diameter mandrel at a rate of 20 mm/s for laser powers ranging from 55-80 W. The strengths determined by the SBS test method were consistently higher than the ISD method by approximately 45 %. They stated the consistency of the relative measurements suggest that both methods are equally suitable for screening of the relative quality of samples made under various process conditions, however the ISD test gives values more suitable for design calculations. Finite element analysis was used to compare the internal stress states within the sample. Results demonstrated a significant difference in the stress states and the SBS test does not produce pure shear. The failure of an ISD test is very distinct and thus it is straightforward to determine the peak load, whereas the SBS shows a plateau behaviour and determination of peak load is less certain. The highest strength corresponded with a laser power of 70 W which had a mean strengths of 46 MPa and 35 MPa for SBS and ISD tests respectively. For comparison, conventionally prepared samples of APC-2 have SBSs in the range of 100 MPa. Error bars were not given in this study, however the same ISD results presented in another study Rosselli et al. [1997] show error bars in the range of $\pm 20 - 35\,\%$.

Continuing from their earlier work [Rosselli and Santare, 1997], Rosselli et al. [1997] investigated the effects of laser angular and positional misalignment. Trials were performed based on default parameters of 70 W laser power for a placement rate of 20 mm/s, which were found to give the highest strength in their previous study. Consolidation load of 838 N was applied pneumatically to a 50.8 mm metallic roller. For the angular offset trials, the laser was consistently aimed at the nip point but from increasing angles biased towards the feed tape. Positional misalignment was varied by offsetting the beam parallel to the default position in both the direction towards the tape and towards the substrate.

Angular offsets of up to 8° had an insignificant effect on ISD strength. The strength was found to decrease by up to 37 % when offsetting the beam towards the substrate by as little as −0.25 mm, however offsets in the tape direction up to 0.5 mm caused no significant difference in ISD strength. This was explained by the offset preheating the incoming tape, but conversely this does not explain the decrease in strength for the case of preheating the substrate. A reference specimen was prepared by first laser winding a ring and then post-consolidating the sample in an autoclave at 380 °C with a pressure of 0.6 MPa for 20 min. ISD tests determined a mean strength of 74.25 MPa. The maximum average ISD strength of the laser processed samples was 46 MPa. Photomicrographs of samples prepared at low laser powers exhibited interlaminar failure indicating insufficient bond development between the plies. For the highest strength samples, intralaminar failure was observed with the crack following a path along the voids in the ply. Void content measurements found the unprocessed prepreg contained high void content in the range of 8-10 %. Laser processing was found to decrease the void content to values in the range of 2.6-5.2 % depending on the process parameters. The minimum void content of 2.6 % was found for a laser power of 70 W, which also corresponded to the highest ISD strength value. This suggests that the final void content of the processed samples plays a significant role in the resulting quality of thermoplastic composites. The void content of the autoclave post-processed sample was found to be further reduced. The strength decrease above 70 W was attributed to matrix degradation, however the strengths appear to correlate well with the reported void content. Smoke was observed when processing at 80 W, however no charring was visible in the photomicrographs. This is suggestive of ablation of the PEEK matrix on the surface of the composite.

The laser consolidation studies up until this point used fixed optics to produce small planar beams only suitable for processing narrow tapes no wider than 6.35 mm. This narrow width is inefficient for the timely production of larger composite structures. Pistor et al. [1999] investigated the used of galvanometer scanning to increase

the processing width while maintaining relatively uniform power across the width of the tape. Scanning also allows for simple adjustment of the width for different tapes. A 6.35 mm wide carbon/PEKK prepreg was chosen for placement trials. It is closely related to the more commonly used carbon/PEEK in terms of performance and processing behaviour. Poly(ether ketone ketone) (PEKK) polymers are part of the same poly(aryl ether ketone) family as PEEK. The repeat unit is identical to PEEK with one ketone linkage in place of an ether linkage. The T_g and T_m are equal, but PEEK crystallises to a greater extent. PEKK is stiffer than PEEK and has a lower toughness. Samples were produced with both fixed optics and scanning optics. The fixed optics produced an elliptical spot with major and minor diameters of 7 mm and 3 mm respectively. In the case of the scanning optics, a 3 mm beam was scanned over a width of 6.3 mm. The geometry of the irradiated areas was therefore closely matched to give a fair comparison.

Samples were manufactured at a fixed velocity of 15 mm/s with laser powers of 65, 70, 75 and 80 W with the fixed optics, corresponding to laser irradiances of 3.94, 4.24, 4.55 and 4.85 MW/m^2. Another sample was prepared with the scanning optics with the laser power set at 45 W, resulting in a laser irradiance of 6.37 MW/m^2 over the 3 mm spot. However as the spot is scanned over a length of 6.3 mm, the time averaged irradiance over the scanned area would be lower at approximately 1.8 MW/m^2. This is less than half the value used for the fixed optics and an important fact not discussed by the authors. SBS tests found the maximum strength to be 29 MPa which was obtained with the fixed optics and a laser power of 70 W. This is approximately 25 % of conventionally prepared samples. The strength of the sample produced with laser scanning had an even lower strength of 18 MPa. The lower strength was attributed to the increased irradiance of the laser which could cause degradation of the polymer. It would however seem more likely that the time averaged irradiance over the scanned area was too low. Nonetheless, when using a laser scanning strategy the material is exposed to much higher peak irradiances to acheive the same temperature

as a non-scanned equivalent. For this reason it therefore likely that higher levels of degradation would be observed for scanned laser.

Density measurements were also performed to estimate the void content. The material is however semi-crystalline, and would also induce a change in density. The density of the samples decreased for laser powers above 70 W for the fixed optics. This correlated well with the decrease in SBS, which was also observed in the study by Rosselli et al. [1997]. Estimated final void contents were in the range of 5-7 %. The scanning system was also shown to be able to fabricate 25.4 mm wide carbon/PPS rings, however a laser source with higher power would be required for processing carbon/PEKK which requires higher process temperatures.

Pistor and Güçeri [1999] investigated the crystallinity of 6.4 mm wide APC-2 carbon/PEEK composite rings that were manufactured using a CO_2 laser filament winding system. The laser spot size was in the form of a small line measuring 2 mm in height by 13.3 mm in width. Samples were prepared at a range of laser powers for a constant winding speed of 20 mm/s. Modulated differential scanning calorimetry (MDSC) was performed on the samples to determine the level of crystallinity, the melting point and cold crystallisation temperatures. It was found that with increasing laser power there is a small but statistically significant decrease in cold crystallisation temperature. The crystallinity was found to increase significantly from 21 % to 40 % when increasing the laser power from 55 W to 80 W, which was explained by slower cooling rates in regions surrounding the melt pool. It is however more likely that the higher laser powers result in larger thermal penetration through the thickness, reheating the lower layers to a more significant degree as seen in Guan and Pitchumani [2004]. The melting temperature was found to drop slightly but suddenly for a laser power of 80W which corresponded with observations of smoke generation. This was attributed to degradation in the form of molecular weight reduction.

Sun et al. [2001] performed tape placement experiments with a hot shoe tape

placement head. Heat is applied to the rear side of the tape via hot shoe, and therefore is a conductive mode of heat transfer. Lap shear samples were produced with APC-2 carbon/PEEK prepregs in the same manner as Mantell et al. [1992], for estimated inter-laminar bonding temperatures of temperatures of 300, 340, 360, 380 and 390 °C under 0.57 MPa shoe pressure at a placement rate of 25 mm/s. The lap joint was made by manually cutting a notch of uniform depth on each side of the sample, spaced at a distance of 6.35 mm. This would likely induce large variations in the result as it is difficult to cut the depth accurately to ensure it is only the inter-laminar region in shear. It is likely that some fibres may be continuous through the length of the sample, increasing the failure load. Only one quarter of the samples were found to fail between the plies, and three other failure modes were observed relating to damage caused by cutting the notches. This led to extremely large amounts of scatter in the results, with scatter to the order of ±50 %. When isolating those samples that failed in the inter-laminar region, the scatter was greatly reduced. The bond strength was found to increase with increasing process temperature. At a process temperature of 380 °C the bond strength was found to be the highest at 72 % of the heat press consolidated reference.

Yousefpour and Nejhad [2001] manufactured 6.35 mm wide APC-2 carbon/PEEK rings using a winding apparatus which used infra-red heaters for heating the incoming tape, the mandrel and also the nip point. Samples were manufactured at 30 mm/s for two different tape preheat temperatures, one above and one below the glass transition at 170 °C and 110 °C respectively, with consolidation forces of 5.5, 12.6, 19.4, 26.0 and 32.4 kN/m. The samples were characterised with a C-ring test. The performance of the samples prepared below the glass transition were found to be superior. The decrease in the performance for the samples prepared above the glass transition was attributed to twisting of the filaments within the tape during preheating. The consolidation pressures which resulted in the best properties were 12.6 and 19.4 kN/m. A finite element model was also formulated to simulate the

C-ring test. Load-displacement values were in good agreement.

Tierney and Gillespie [2003] manufactured AS4/PEEK panels using a thermoplastic tape placement head. The head consisted of two pneumatically actuated consolidation rollers and two nitrogen hot gas torches. The first torch was aimed into the nip point, directly heating the surfaces to be bonded. The first roller is intended to tack the composite to the surface. The second hot gas torch then heats the interface through the thickness of the tape, increasing the level of healing/autohesion. The final roller then compresses any remaining voids and further develops the intimate contact at the bond interface. The torches expel hot nitrogen gas with a temperature greater than 850 °C at a flow rate of 50 l/min.

A thermal model as well as a void dynamics model were formulated for process simulation. Surface temperature predictions were compared with thermal camera measurements, however the emissivity of the material is not stated and reflections of the main heater can be seen on the surface of the composite. There are also periods to the order of 1 s where the model over-predicts the temperature by at least 100 °C. The thermal model is used to determine the through-thickness temperature history, however validations of the through thickness temperature predictions were not performed. The predictions are subsequently used as inputs to the void dynamics model to estimate the total void evolution through the thickness of the composite.

16 ply Carbon/PEEK panels were manufactured at various placement velocities of 30, 40, 50 and 60 mm/s, compaction forces of 190, 230, 270, 310 and 350 N and also torch heights of 3, 6, 9 and 12 mm. Photomicrographs revealed void content gradients through the thickness of the samples. Higher void content was present for the layers close to the tooling as the tooling acted as a heat sink, 'freezing' the voids before they could be compressed by the consolidation roller. The layers near the top of the sample also had high void fractions due to the high temperatures which lead to significant void expansion. The layers in the central region of the sample show much lower void content, as the multiple reheating cycles at lower temperatures allows sufficient

reduction of the viscosity for void compaction, yet cool enough to prevent significant re-expansion of the voids after the roller has passed. Predictions show an increase in void content with process velocity, as well as a larger region of higher void content near the tooling. Interestingly, at lower process velocities there are larger variations in void content during processing compared with higher velocities. At low velocity the void content reaches high values of up to 10 % during the initial heating phase, however there is a longer period under the roller resulting in higher levels of void compaction. The void content in the first 0.5 mm from the tooling was in the range of 6-9 % and 2-7 % in the top 0.5 mm. In the central region of the sample, the void content was around 1-2 %, with the exception of the sample prepared at 60 mm/s which had an almost constant void content of 6 % throughout the thickness.

In this study the gas temperature and flow rates remained fixed so the temperatures decrease with process speed. This makes it unclear if the increase in void content is mostly attributed to the lower temperatures at higher speed or the decrease in time under the consolidation roller. The torch height was varied with a fixed placement rate of 40 mm/s. An increase in torch height should result in a decrease in heat input and therefore also the temperature. Results found that increasing the torch height has an effect very similar to increasing the process velocity. For the lowest torch height, greater levels of void expansion were present leading to high void content near the tool and also the top surface, however the void content in the central region was the lowest of all process conditions. This implies that the heat input/temperature field has strong impact on the final void content. The final average void content responded favourably to increasing consolidation forces, dropping from 4 % to 1.5 % when increasing the force from 190 N to 350 N.

Good agreement was found between the experimental and modelled void contents for the top, centre and bottom regions of the composite, for all process speeds and torch heights. The process setting of 40 mm/s with both torch heights at 6 mm and a consolidation load of 270 N was common to three separate results plots, how-

ever inexplicably different model predictions were presented on each. Unfortunately, mechanical tests were not performed on the samples so it is not apparent whether the conditions necessary for low void content correlate with good bonding. The main conclusion of this study was that re-expansion of the voids trapped within the prepreg material has a large impact on the final void content. The complete temperature and pressure history during processing also plays a large role, with subsequent passes given an appropriate process history leading to significant void reduction for the previously placed layers within the laminate.

Tierney and Gillespie [2006] continued studies using the same placement head as utilised in their earlier work [Tierney and Gillespie, 2003]. A consolidation model was formulated, with temperature predictions based on their previous thermal model. In their earlier work the model was shown to be in reasonable agreement, however there were periods to the order of 1 s where the model over-predicts the surface temperature by at least 100 °C. Validation of the temperature through the thickness of the substrate was not performed. Samples were manufactured out of a carbon/PEEK composite for various placement rates (30, 40, 50 and 60 mm/s) and torch heights (3, 6, 9 and 12 mm). ASTM D 2344 SBS tests were performed to characterise the interlaminar strength of the sample. The sample width was 6.4 mm and the midpoint thickness not given. While not specifically stated, the models imply a 16 ply laminate as was manufactured in their previous study [Tierney and Gillespie, 2003]. Given the 0.1778 mm tape thickness, this would imply a midpoint thickness of 2.85 mm discounting any significant density change due to void dynamics or crystallisation. Samples were reconsolidated in an autoclave to provide a reference for the ultimate SBS. The ultimate strength was taken as the average of the reconsolidated samples. The value exact value was not given, however interpretation of the results suggests that the value was in the range of 80 MPa. It is possible that the samples would have experienced degradation during placement, therefore this value is potentially lower than would be obtained from an autoclave sample prepared using virgin material.

The SBS of the in situ consolidated samples decreased from approximately 50 MPa to 30 MPa when increasing the torch height, for a process speed of 40 mm/s. The decrease was explained by inadequate heating of the material. The strength was found to decease from approximately 60 MPa to 35 MPa when increasing the process velocity from 30 mm/s to 60 mm/s. In this work the hot nitrogen gas temperature and flow rate is maintained at a constant rate, therefore lower temperatures are obtained at higher process rates, as shown by measurements in their previous study [Tierney and Gillespie, 2003]. Therefore it is likely that the decrease in properties is due to both the decreased interface temperatures, as well as shorter residence times due to the higher placement rate.

The samples reconsolidated in the autoclave should reveal if the interface has undergone irreversible degradation, identified by a lower strength. The samples prepared for various torch heights at 40 mm/s had relatively constant strengths after autoclave re-consolidation with a value of approximately 80 MPa. In the case of the samples prepared at differing process speed, the reconsolidated strength was higher at approximately 90 MPa for the samples prepared at speeds of 50 and 60 mm/s, suggesting lower levels of degradation had occurred. This makes sense as both the peak temperature and the dwell time are lower for higher speeds. This also gives a strong indication that their reference sample was also degraded as it had a lower strength at 90 MPa.

Schledjewski and Miaris [2009] prepared samples to demonstrate the efficiency of near-infrared diode laser tape placement. A 600 W direct diode laser module was attached to the placement head. The 980 nm wavelength beam was shaped using optics, producing a rectangular spot 12 mm $\times$ 2.08 mm at a working distance of 170 mm. This spot is approximately double the size of that previously reported for in situ CO_2 laser processes, and the maximum laser power is greater by almost an order of magnitude. The previously reported CO_2 laser processes were ring winding where the laser can be aimed directly into the nip point. As this is a tape placement process, the

laser has to be mounted above the plane of placement for practical purposes. One consequence of this restriction is a shadow is cast by the feed tape just before the nip point. A lower angle of attack reduces the shadow at the nip point.

The placement head design used a single metallic consolidation roller. Wedge peel samples were initially produced for rapid screening of process parameters. The composite was a 12 mm × 0.13 mm carbon/PEEK tape supplied by *Gurit Suprem*. All tests were performed on a hot tooling plate that was temperature controlled to a high temperature of 276 °C. The best parameters determined by the screening for a process speed of 100 mm/s were a laser power of 200 W with 60 % of the beam incident on the tape and an angle of attack of 16.5° for the laser. A 14 ply unidirectional plate was prepared using the optimised process parameters. Samples were cut from this sheet and the interlaminar strength tested using a 'short 3 point bending test'. Details of the test method were not given but appears to be similar to the ASTM D 2344 SBS test. Reference samples were prepared in an autoclave with a 2 h heating ramp to 380 °C and a hold time of 30 min. The consolidation pressure of 0.7 MPa was applied with a vacuum bag. Processing was finalised with a 5 h cooling period.

The strength of the laser placed sample at 100 mm/s was found to be 89.16 MPa, which was 94 % of the 94.8 MPa autoclave strength. Photomicrographs revealed a final average void content of 3.5 %. This study provides evidence that very high properties similar to those achieved in an autoclave can be achieved for in situ processes. The very high tool temperature likely had a significant contribution to the strength as the high temperature reduces the cooling rate, thus increasing the dwell time at the temperatures required for bonding to develop.

Khan and Schledjewski [2010] prepared unidirectional composite plates using a hot gas tape placement head. Hot gas was provided by the combustion of a mixture of hydrogen and oxygen. Consolidation pressure was applied with a 50 mm metallic roller. A hot tool plate was used with a temperature of 280 °C. A thermal model was used to predict the through thickness temperature distribution. The model was

validated using thermocouples placed at one layer and seven layers beneath the surface. The authors state that the temperature was not measured at the surface as the thermocouple would be destroyed if directly heated by the gas torch. However, it was not explained how the thermocouples were embedded in the laminate without being exposed to the torch. The thickness of the thermocouples or the measurement sample rate were not given. Good agreement was reported between the modelled and experimental temperature distributions. The peak temperature at one lamina depth ranged between 320-340 °C.

15 ply laminates were manufactured for process speeds of 83.3, 116.7 and 150.0 mm/s and gas flow rates of 4, 6 and 8 l/min. The corresponding gas temperatures were not provided, however the temperatures assumed for the thermal model ranged from 800-1300 °C. For a fixed gas volume of 4 l/min, the void content of the samples was found to increase from 1.5 % to 3 % when increasing the process velocity. This was explained by inadequate heat transfer resulting in lower temperatures at higher process velocities. Increasing the gas flow rate from 4 l/min to 6 l/min for a fixed process velocity of 150 mm/s was found to reduce the final void content from 3 % to 1.75 %, however increasing the gas flow rate to 8 l/min resulted in a slight increase in void content to 2 %. Additional repetitive passes were found to reduce the final void content of the top layers. The consolidation force was found to not have a large effect when sufficient temperatures were achieved as the matrix viscosity is low enough, however it was found to play a larger role when the material is processed at lower temperatures.

It was concluded that an intermediate heat input resulted in the lowest void content, as sufficient softening occurs for re-consolidation of the voids however the temperature is low enough to prevent excessive void expansion after the consolidation roller. Mechanical characterisation was not performed.

Khan et al. [2010] continued hot gas tape placement studies using the same placement head as their previous work [Khan and Schledjewski, 2010]. While not specifi-

cally stated, the hot gas appears to be generated by hydrogen flame as in the earlier study. Hot tooling was used at a temperature of 280 °C. Wedge peel tests were used for rapid screening while DIN EN 2563 inter-laminar shear strength (ILSS) tests were performed for mechanical characterisation. A reference sample for the ultimate ILSS was prepared by tape placement followed by an autoclave post-consolidation using the same processing cycle as [Schledjewski and Miaris, 2009]. The reference strength was found to be 94 MPa.

Experiments were performed at placement rates of 50.0, 83.3, 116.7 and 150.0 mm/s and gas flow rates of 4, 6, 8 and 10 l/min. The gas temperatures corresponding to the flow rates are not given. An example plot reveals a peak temperature prediction of 600 °C for one process setting. The best ILSS was found to be 91 % of the reference sample at 85.5 MPa obtained at a placement rate of 50.0 mm/s. The strength was found to generally decrease with increasing placement rate and hot gas flow rate. The decrease with placement rate was attributed to lower dwell times at the conditions required for polymer healing to occur. The decrease due to increased gas flow rates was attributed to polymer degradation in the form of cross-linking, which would increase the viscosity of the resin reducing intimate contact development and also impeding the rate of molecular healing. The maximum strength achieved at the highest placement rate of 150 mm/s was 68 MPa.

The effect of different tool temperature was also studied. For a placement rate of 50.0 mm/s with a gas flow rate of 8 l/min, the ILSS was 82.9, 85.0 and 85.5 MPa for tool temperatures of 250, 280 and 300 °C respectively, indicating a small but significant increase in properties within the limited range of temperatures studied. It was reported that tool temperatures much lower than 250 °C resulted in significant thermal distortion of the resulting laminates. Up to three extra dry passes were shown to increase the strength of the uppermost layers by approximately 10 %, beyond this number lead to excessive degradation of the top surface.

2.1.1 Summary of experimental studies

A survey of experimental work performed in the field of in situ thermoplastic processing revealed that the resulting quality of laminates is due to complex behaviours, and highly dependent on the complete temperature and pressure history throughout the process. The temperature history is highly dynamic/non-isothermal with heating and cooling rates to the order of 1000 °C/s, of which have a large influence on the resulting quality of the laminates.

2.1.1.1 Temperature

While the temperature is arguably the single most important aspect of the process, experimental studies have typically not measured or reported the process temperature history. Studies have been based on parameter optimisation for particular head designs, and specific temperature and/or pressure histories are not given. Typically the laser powers or hot gas flow rates are provided, but the resulting temperature on the surface of the composite is scarcely provided. This makes it difficult to adapt findings of particular studies to other placement head designs. Bond interface temperature measurement is not straightforward as the highly non-isothermal behaviour requires the use of thermocouples with fast response times, necessitating the use of very fine, delicate thermocouple wires. The sampling rate must also be sufficiently high to capture the rapidly changing temperature history and the thermocouples must also be able to survive the high temperatures when exposed to the heat source. Mantell et al. [1992] reported the interface temperature to be only 260 °C for lap shear samples which achieved 70 % of the ultimate strength. It is unlikely that this was the actual temperature as the PEEK quickly crystallises in this temperature range, significantly impeding bonding [Lamèthe et al., 2005]. It is likely that the thermocouple was too large and the thermal mass would have prevented the peak temperature from being recorded. Agarwal et al. [1996, 1992] measured the consolidation temperature history at 50 Hz using 12.7 µm thick foil thermocouples, and found that consolidation

temperatures of 475 °C resulted in the best properties, however surface temperatures during heating prior to consolidation were in the region of 600 °C. Mazumdar and Hoa [1996] used fine 0.125 mm thermocouples, however they state that the peak temperatures were not necessarily recorded due to an insufficient sampling rate. They reported temperatures of 680 °C and 580 °C at depths of one and two plies respectively for the conditions that resulted in the highest SBS. A study by Khan et al. [2010] shows peak temperature predictions to the order of 600 °C. Compared with conventional processing, the dwell times at high temperature are extremely short for in situ thermoplastic processes. Because of this, much higher temperatures are required in order to achieve the necessary levels of matrix softening for both intimate contact development and void compaction, as well as sufficient rates of molecular diffusion for strength development.

2.1.1.2 Mechanical properties

The relative strength values reported in the literature are plotted against placement rate in Figure 2.1. The relative strengths are based on inter-laminar strength characterisation such as SBS tests compared with conventionally prepared samples, from a survey of SBS values reported in the literature for CF/PEEK ATP as summarised in Table 2.1. This suggests that CO_2 lasers and hot gas torches perform poorly compared with hydrogen flame and NIR laser sources. It is likely that the poor results from CO_2 laser systems implemented in the literature are due to the extremely short heated lengths and limited laser powers, resulting in low heat soak and thus very short dwell times. In the case of the NIR laser, the spot was larger and the maximum output power was an order of magnitude greater, allowing for high placement rates while attaining sufficient temperatures and dwell times for bond development. In the case of the convective heat sources, the hydrogen flame likely produces superior results to the hot nitrogen gas due to the higher gas temperatures. Higher gas temperatures increase the rate of convective heat transfer, enabling higher placement

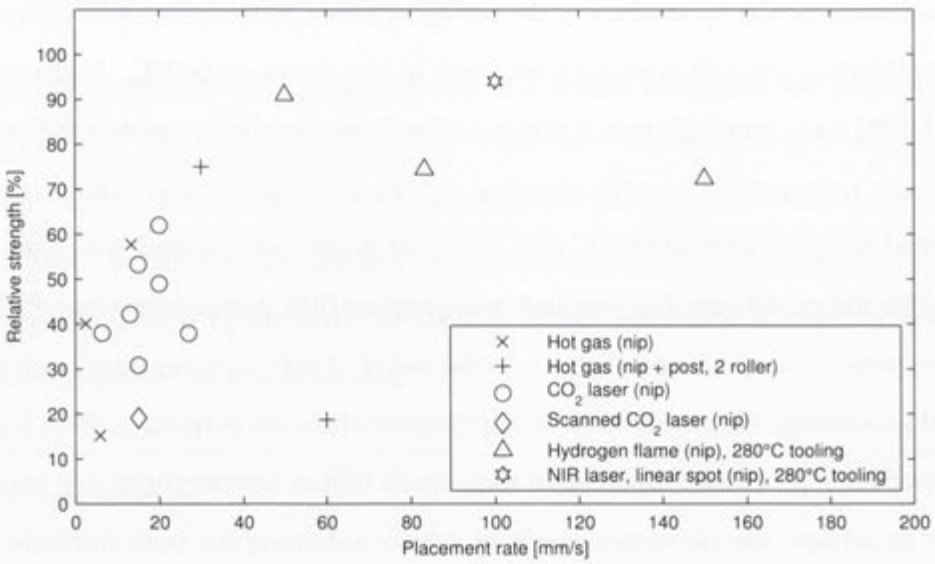


Figure 2.1 – Reported relative strengths vs. placement rate for various heat sources

rates.

The mechanical properties achieved are highly dependent on the processing history. Sufficient time at high temperature combined with ample consolidation pressure is required to achieve full bond development. Not only does the heat source need to supply enough heat to the surface of the composite to achieve a sufficient consolidation temperature, it also must provide enough heat soak to minimise the cooling rate. The amount of heat soak depends on the heated length. Short heated lengths will achieve high temperatures with lower powers, but rapid cooling will occur as there is minimal heat soak. For long heated lengths, greater heat input is required to achieve the same temperature but the heat soak is much higher resulting in lower rates of cooling. The problem is compounded when moving to higher process velocities as the length of time that a specific point on the surface is exposed to the heat source decreases linearly with speed, effectively reducing the heated length in the time domain.

In the CO_2 laser studies, the spot was only 0.5-1 mm high due to the planar beams used, therefore making the heated lengths very small. Studies attributed the poor mechanical properties to insufficient dwell times at the temperatures required

Table 2.1 – A survey of relative SBS vs. placement rate for CF/PEEK composites. Relative values determined by reference samples prepared by heat press (HP), autoclave (A) or autoclave re-consolidation of ATP samples (AR).

Reference	Material	Test Method	Reference Sample		Placement Trial		Rel. Strength
			Prep.	SBS [MPa]	SBS [MPa]	Rate [mm/s]	
Hot gas: N_2 (nip point)							
Mantell et al. [1992]	APC-2	D 2344 - flat	HP	72.4	29	2.54	40%
				72.4	11	5.84	15%
Mazumdar and Hoa [1996]	APC-2	D 2344 - ring	-	90	54.2	13.3	60%
Hot gas: N_2 (nip point & post roller)							
Tierney and Gillespie [2006]	APC-2	D 2344 - flat	AR	90	60	30	67%
				90	35	60	39%
Hot gas: H_2O_2 flame (nip point)							
Khan et al. [2010]	Suprem™	EN 2563 - flat	AR	94	85.5	50	91%
				94	65	150	69%
Laser: CO_2 line (nip point)							
Mazumdar and Hoa [1995]	APC-2	D 2344 - ring	-	90	35.7	6.4	40%
				90	35.7	27	40%
Agarwal et al. [1996]	APC-2	D 2344 - ring	-	90	50	15	56%
Rosselli and Santare [1997]	APC-2	D 2344 - ring	-	90	46	20	51%
Laser: NIR line (nip point)							
Schledjewski and Miaris [2009]	Suprem™	D 2344 - flat	A	89.2	83.8	100	94%

for bonding. The spot size could not be increased significantly due to the limited output power of the CO_2 laser sources studied.

In the case of a hot gas torch, the heated lengths are somewhat larger. However, hot gas torches are fundamentally different to lasers in that the heat transfer is via convection. The rate of heat transfer is proportional to the gas flow rate, and importantly the temperature difference between the gas and the surface of the composite. As the composite surface heats up, the rate of heat transfer can decrease significantly. Thus large volumes of gas at high temperatures are required to achieve high surface heat fluxes. The laser on the other hand acts as a pure heat source where the heat transfer is mostly independent of the surface temperature (for the temperature ranges suitable for in situ thermoplastic processing).

The higher strengths achieved with the hydrogen flame can be explained by the high gas temperatures of up to 1300 °C increasing the rate of convective heat transfer when compared with a nitrogen gas torch which typically supplies gas at 800-900 °C. The NIR laser source that was studied had a source twice the height of earlier CO_2 studies and an output power an order of magnitude higher, allowing for greater heat soak and also the power necessary for higher placement rates. It should be noted that both the hydrogen flame and NIR laser studies used heated tooling at a temperature of 280 °C which would most likely increase the bond strength as the dwell time would be longer due to a lower heat sink effect.

2.1.1.3 Void content

The void content is affected by the total processing history for which the temperature is high enough for softening of the matrix. Cold tooling results in high cooling rates which inhibit void compression in the layers close to the tool resulting in a higher local void content, for the particular head designs studied. The void content in the central region of the laminates is the lowest as multiple re-consolidation passes are experienced as subsequent layers are placed above. The void content in the upper

layers is higher, however dry re-consolidation passes have been shown to greatly reduce the void content. Low void contents in the region of 1 % have been reported for in situ thermoplastic processing, indicating that good quality laminates can be manufactured in an out-of-autoclave process. The void content generally increases for higher process velocities, however this trend appears to be due to insufficient heat input at higher speeds, leading to higher matrix viscosity which impedes void compaction. For example, for the hot nitrogen tape placement head in the work of Tierney and Gillespie [2003], a void content in the centre of the laminate was 1 % for a placement rate of 30 mm/s, yet it increased dramatically to greater than 6 % at a placement rate of 60 mm/s. However in the study by Khan and Schledjewski [2010] where a hydrogen flame is utilised which would likely amount to greater heat input due to the higher gas temperatures, a void content of 1.5 % is reported for a velocity of 83.3 mm/s which increases to 3.4 % at 150 mm/s when processing with the same gas flow rate. Increasing the gas flow rate and therefore the heat input resulted in a final void content of 1.6 % at 150 mm/s. This would suggest that low void content could be achieved for even higher process velocities as long as the heat source can deliver a sufficient heat flux to the surface of the composite.

2.1.1.4 Consolidation pressure

The general consensus for consolidation pressure is that it does not change the properties significantly as long as the material is at a sufficiently high temperature. The consolidation pressure was found to have a greater influence on properties for cases where the material was not heated sufficiently and thus greater force was required for consolidation due to increased matrix viscosity.

2.1.1.5 Crystallinity

The level of crystallinity varies significantly during processing of carbon/PEEK composites. In the regions where the temperature exceeds the melting point, the crys-

talline phases are generally melted. Partial melting may also occur, leaving behind crystallites which act as nucleation points during recrystallisation. Recrystallisation occurs for temperatures between the melting and glass transition temperatures. The rate of recrystallisation is highly temperature dependent, with the maximum rate at a temperature of approximately 240 °C. When the cooling rate is high enough, the material will have little time to crystallise and therefore be highly amorphous. High levels of crystallinity result when significant periods of time are spent in the recrystallisation temperature range. The repeated passes when building a laminate result in reheating of the previously layed layers. The temperature reached in the previous layers decreases with depth. Layers close to the top will typically experience remelting, however those deeper in the composite will be reheated in the re-crystallisation range, increasing the level of crystallinity. Experimental measurements have confirmed this behaviour with high levels of crystallinity measured at 36.6 % for the deepest layers, yet 29 % in the outermost layer [Mazumdar and Hoa, 1996]. Studies have also shown that the bulk crystallinity in laminates does not change significantly with laser power [Agarwal et al., 1996], however another study [Pistor and Güçeri, 1999] found that the crystallinity increased significantly from 21 % to 40 % which was attributed to slower cooling rates at higher power. At much higher placement rates the final bulk crystallinity would most likely be reduced as the heat soak would be reduced leading to lower periods spent at the range of temperatures suitable for recrystallisation.

2.1.1.6 Degradation

Degradation is a complex phenomenon, and the exact mechanisms are not known. Mazumdar and Hoa [1996] found no visible traces of degradation in photomicrographs, however they noted the resin rich layer on the surface of the tape was significantly decreased at low process velocities, which was attributed possible ablation of the matrix or resin squeeze out. No obvious smoke was observed, however it

is likely that the flow of hot nitrogen gas would mask any smoke generated. The work of Agarwal et al. [1992, 1996] found the best mechanical properties when the surface temperature during heating was in the range of 600 °C which corresponded with a peak consolidation temperature of 475 °C. Significant decrease in properties when the peak temperatures for the heating and consolidation were 900 °C and 740 °C respectively. This corresponded with discoloured regions observed in photomicrograph cross-sections, as well as a 10 °C decrease in the melting temperature and a disappearance of the characteristic peaks at 952 and 966 cm^{-1} in FTIR analysis that were used for surface crystallinity determination. They also reported no degradation was observed for samples prepared with consolidation temperatures less than 540 °C. Rosselli et al. [1997] reported decreased mechanical properties for higher laser powers which was accompanied by smoke generation, however photomicrographs did not show any signs of charring, a result that is suggestive of matrix ablation. Pistor and Güçeri [1999] found the melting temperature of samples to drop suddenly at high laser power which also corresponded with observations of smoke generation. They attributed the decrease in melting point to molecular weight reduction of the PEEK matrix. Tierney and Gillespie [2006] reported that the SBS of autoclave reconsolidated samples increased with increasing placement rate, which is likely due to lower degradation due to lower temperatures and dwell times experienced at the higher speed. Khan et al. [2010] attributed strength reduction at higher gas flow rates to cross-linking of the matrix which would impede healing and intimate contact development, while the strength reduction at higher velocities was attributed to decreased high temperature dwell times. From experimental studies, degradation has been suggested to occur as matrix ablation, chain scission leading to molecular weight reduction and also cross-linking.

2.2 Modelling of the process

The placement rate of thermoplastic composite must be maximised for production, however maintaining composite quality is nontrivial due to the highly dynamic behaviours at the nip point. Bonding is governed by intimate contact, autohesion and degradation processes. The quality is a function of the level of bonding, crystallinity, void dynamics and residual stress generation. The behaviour of these processes is dictated by the temperature and/or pressure distributions at the interface. In order to analyse the welding process it is therefore necessary to have models for each of the processes combined with robust pressure and temperature analysis. Process optimisation is a trade-off between the different aspects of quality.

The in situ thermoplastic process is highly non-linear due to the rapid temperature and pressure cycles experienced in the region of the nip point. It involves a number of physical processes that occur simultaneously with each contributing to the the final quality of the composite, therefore robust models for each element of quality are imperative for complete material quality prediction. The modelling work to date for each of these aspects of quality is discussed in the following sections.

2.2.1 Intimate contact

Intimate contact models are used to determine the degree of physical contact between two surfaces when placed together. The degree of intimate contact corresponds to the portion of inter-facial area over which healing can occur. The initial level of intimate contact is limited due to the presence of asperities on the surface. Thermoplastics show viscous behaviour at elevated temperatures, therefore if heat and pressure are applied to the interface, the surfaces will plastically deform over time increasing the level of intimate contact. The amount of intimate contact is therefore dependent on the initial topology of the surface as well as the combined temperature and pressure history. Various models for this process have been presented in literature. They will be discussed from a historical perspective in the following paragraphs.

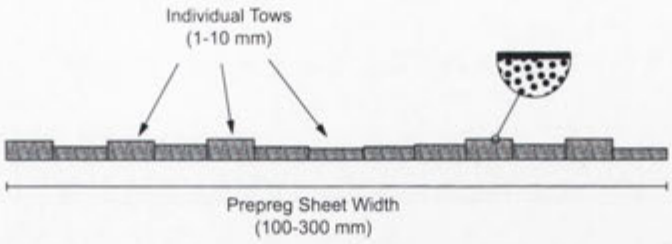


Figure 2.2 – Demonstration of the macroscopic tow height variation in a tape prepreg accounted for by the Dara and Loos [1985] intimate contact model (tow height not to scale).

Dara and Loos [1985] developed a model to simulate the intimate contact development in the compression moulding of carbon/polysulfone thermoplastic composite laminates. The unidirectional prepregs used in the study were manufactured using multiple tows arranged parallel to each other. Each tow had a unique height thus the thickness of the prepreg varied across the width. Micrometer measurements found that the tow height does not vary significantly along the length of the unidirectional prepreg. Figure 2.2 demonstrates the scale of the tow and prepreg used in the model showing that it applies to intimate contact development on the macroscopic level when manufacturing large laminates.

A prepreg geometry sub-model accounts for this macroscopic tow non-uniformity by assuming a series of rectangles of varying heights. The height distribution of the rectangles was described statistically by a two parameter Weibull density function, with the parameters determined from a sample of thickness measurements. A second sub-model captured the viscoelastic response of a single tow as a function of processing time, temperature and pressure. It was assumed that the flow of resin in the fibre direction was negligible and the fibre/matrix distribution remained constant. Time-dependent elastic effects were not considered as the relaxation time of the polymer was small compared to the time for the polymer to flow around the fibres.

The model assumes isothermal and isobaric conditions for the compression moulding process. The tows are assumed to act individually in that they do not contact

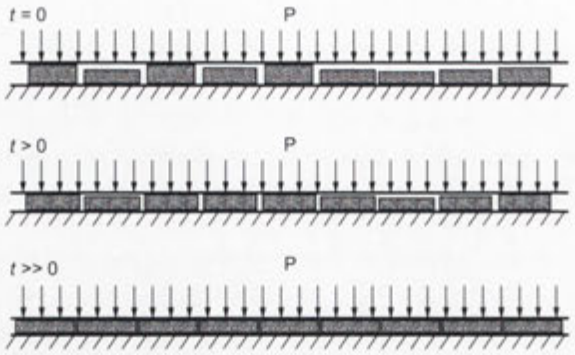


Figure 2.3 – Diagram showing the progressive flattening of tows in the Dara and Loos [1985] intimate contact model. Tow heights are determined statistically by a Weibull density function. The tows act individually in that there is no transverse interaction between tows during deformation, however the tows jointly contribute to supporting the load.

each other in the transverse direction, however they do act together in supporting the applied load Figure 2.3. It is also assumed that both the magnitude and rate of deformation is low. The tows are assumed to deform against a planar boundary, a conservative approximation which is equivalent to the worst case scenario of flattening crossed plies. In the case of a unidirectional laminate, nesting of the tows can occur resulting in more rapid intimate contact development.

The fibre/matrix viscosity was derived by fitting the model to the experimental data. The results of the model were found to predict the intimate contact development behaviour well. The authors state that the model was developed for cross-ply laminates, and it is intuitive that the intimate contact development behaviour of unidirectional laminates will be faster due to nesting of the tows. They anticipate that the model will produce conservative results for unidirectional laminates.

Inspired by the work of Dara and Loos [1985], Lee and Springer [1987] used a similar yet simplified model which assumed a series of uniform rectangles to model the intimate contact development due to macroscopic tow height variation in wide APC-2 carbon/PEEK tape. The deformation behaviour of the rectangular element is captured by calculating the average transverse flow velocity within an element assuming laminar viscous flow of the fibre/matrix. It is not clear for which conditions

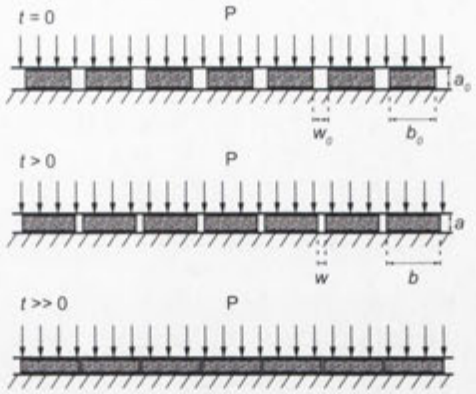


Figure 2.4 – Diagram showing the progressive flattening of tows in the Lee and Springer [1987] uniform rectangular intimate contact model. The tows heights are uniform and act individually in that there is no transverse interaction between tows during deformation, however the tows jointly contribute to supporting the load.

the flow velocity equation is valid. The effective viscosity of the fibre/matrix was determined by fitting the model to experimental data. A diagram of their uniform rectangular model is shown in Figure 2.4.

The degree of intimate contact for the uniform rectangular model was determined from the following expression:

$$D_{ic}(t) = \frac{1}{1+\frac{w_0}{b_0}}\left[1+\frac{5P_{app}}{\mu_{mf}}\left(1+\frac{w_0}{b_0}\right)\left(\frac{a_0}{b_0}\right)^2 t\right]^{1/5} \tag{2.1}$$

The geometric parameters of the rectangles w_0, a_0 and b_0 are measured from photomicrograph cross sections of the unprocessed composite, however it is not explained how the parameters are derived. This detail is important as the tow heights in thermoplastic prepreg are known to vary, for example following a Weibull distribution as found by Dara and Loos [1985]. It is unclear how one would determine the equivalent geometric ratios when assuming the tow height variation is assumed to be uniform. Samples were prepared by placing a single ply of APC-2 in a 76.2 mm × 76.2 mm picture frame mould and processed in a heat press at 350, 360 and 370 °C with consolidation pressures of 0.28, 0.66 and 1.63 MPa. The degree of intimate contact was then determined by measuring the area of the uncompressed

surface. The effective matrix-fibre viscosity μ_{mf} was determined by matching the model to the experimental data. The temperature dependence of the viscosity is based on an Arrhenius relation. The model was shown to fit the experimental data well for the process parameters investigated, providing a predictive capability for the intimate contact development of relatively wide 76.2 mm APC-2 composites in a press consolidation or autoclave process.

The Lee and Springer [1987] model is only suitable for an isothermal, isobaric process with a constant viscosity. The thermoplastic tape placement process is highly dynamic with rapidly changing temperature and pressure conditions therefore the model presented by Lee and Springer [1987] must be modified. Mantell and Springer [1992] adapted this model to a thermoplastic tape placement process. They extended the model to account for time varying temperature, pressure and viscosity:

$$D_{ic}(t) = \frac{1}{1+\frac{w_0}{b_0}}\left[1+5\left(1+\frac{w_0}{b_0}\right)\left(\frac{a_0}{b_0}\right)^2\int_0^t \frac{P_{app}(t)}{\mu_{mf}(T(t))}\mathrm{d}t\right]^{1/5} \tag{2.2}$$

They suggested that the model can be simplified as the second term enclosed within the brackets is generally much larger than unity, therefore the degree of intimate could be then approximated by:

$$D_{ic}(t) \approx \frac{1}{w^*}\left[a^*\int_0^t \frac{P_{app}(t)}{\mu_{mf}(T(t))}\mathrm{d}t\right]^{1/5} \tag{2.3}$$

Where w^* and a^* are defined as:

$$w^* = 1+\frac{w_0}{b_0} \qquad a^* = 5w^*\left(\frac{a_0}{b_0}\right)^2 \tag{2.4}$$

Which can be further simplifed to a lumped geometric parameter:

$$g^* = \frac{a^{*1/5}}{w^*} \tag{2.5}$$

Thus the degree of intimate contact can be approximated by:

$$D_{ic}(t) \approx g^* \left[\int_0^t \frac{P_{app}(t)}{\mu_{mf}(T(t))} dt \right]^{1/5} \tag{2.6}$$

This model was later compared to experimental data in a separate experimental study [Mantell et al., 1992]. Lap shear and short beam strength (SBS) samples were prepared in a heat press and also with at hot gas tape placement apparatus. A narrow 6.35 mm wide APC-2 carbon/PEEK unidirectional tape was chosen for the experiments. It should be noted that this is much narrower than the 76.2 mm tapes used in the heat press experiments of Dara and Loos [1985]; Lee and Springer [1987]. It is most probable that the narrow 6.35 mm wide tape is manufactured from only one or two tows, and therefore much less height variation across the width of the tape, at least on the macroscopic scale. In contrast to the previous studies, unidirectional laminates were manufactured. The original models from which the Mantell and Springer [1992] model extended assume the worst case of crossed plies, and it has been suggested that these models will provide conservative results for unidirectional laminates where tow nesting can occur [Dara and Loos, 1985].

The samples prepared in the heat press were first heated to temperature, and then the consolidation pressure was applied. After a predetermined bonding time (10-30 s), cold water was run through the platens and then the pressure was removed. The tape placed samples were produced at placement rates of 2.54-31 mm/s with hot nitrogen (430-440 °C) provided by gas torch to the nip point. The intimate contact was characterised via ultrasonic c-scan. For the lap shear specimens the intimate contact was determined by the contact between the lap surfaces, whereas the average through thickness value was used in the case of the 16 ply SBS samples. A value of $g^* = 0.29$ was assumed by matching the model to a single data point, however it was not stated whether this data point was for a press or tape placed sample. This is significantly different to the value of $g^* = 0.49$ found by Lee and Springer [1987]. A good agreement was found between the intimate contact predictions and the samples

manufactured in the heat press.

In the case of the tape placed lap shear samples, the intimate contact measurements either agreed with the prediction or was significantly higher, however for the SBS samples the measured intimate contact was approximately 20 % lower than predicted at low speeds (2.54 mm/s), however at a speed of 5.84 mm/s predictions agree well. Multiple passes of the roller on the SBS samples was found to increase the intimate contact closer to the prediction. The authors attribute the higher intimate contact for the lap shear samples to experimental uncertainty, and low values for the SBS samples to insufficient consolidation passes. This is somewhat contradictory as the SBS samples experience multiple passes as the layers above are placed while the lap shear specimens only experience one consolidation pass. The fact that the model has been applied narrow unidirectional laminates rather than larger cross ply laminates is not discussed, however this assumption should lead to conservative predictions. This is most likely compensated for by the lower value they found for the geometric parameter $g^* = 0.29$. It is likely that nesting of the tows would occur, leading to higher levels of intimate contact than predicted. This would explain the results for the lap shear specimens being higher. In the case of the SBS samples it is possible that the c-scan was unable to differentiate between the inter-laminar contact and intra-laminar voids, thus a larger levels of void content were experimentally determined. Further reinforcing this point is the fact that APC-2 prepregs are known to contain significant intra-laminar voids. The most plausible explanation is significant void expansion is occurring during the multiple passes of the placement head and the short amount of pressure application by the consolidation roller is insufficient to compress the voids. For lower speeds, the higher levels of heat soak would lead to greater void expansion. This would also explain why the lap shear specimens had higher contact as they are exposed to only a single pass, thus minimising the time available for void expansion. The heat press consolidated samples are cooled with the pressure applied, therefore there is limited opportunity for void expansion.

It was not made clear as to which temperature and pressure profiles were applied in the model. Temperature predictions were shown to agree with experimental data reasonably well, however there is some doubt in the accuracy of the thermocouple measurements as the temperatures appear to be inadequate for bonding as discussed in Section 2.1. The pressure distributions applied to the tape placement model are not given, only the applied consolidation force despite the pressure distribution being arguably one of the single most important parameters for an intimate contact model. It is therefore hard to verify that this non-isothermal intimate contact model is suitable for the tape placement process given the inconclusive results and unknown input parameters.

Pitchumani et al. [1996] performed simulation based parametric studies for a carbon/PEEK tape placement process. The degree of intimate contact was predicted with the Mantell and Springer [1992] model. They state that the intimate contact model was experimentally validated by another study [Steiner et al., 1995] and shown to predict SBSs within 10 % of the experimental data. This publication is not easily found, and it is not known how the temperature or pressure profiles were determined for the intimate contact model. Other experimental studies which use this intimate contact model such as Dai and Ye [2002a,b]; Tierney and Gillespie [2006]; Schell et al. [2009] use mechanical tests such as lap shear or SBS tests for bond strength characterisation, however the bond strength is determined by a combination of healing and intimate contact, thus intimate contact was not characterised in isolation. Despite the limited and inconclusive validations of the Mantell and Springer [1992] non-isothermal simplified rectangular intimate contact model, it has been implemented for many thermoplastic AFP process simulation and optimisation studies [Pitchumani et al., 1996, 1997; Sonmez and Hahn, 1997a; Sun et al., 2001; Dai and Ye, 2002b,a; Schledjewski and Latrille, 2003; Tierney and Gillespie, 2006; Sonmez and Akbulut, 2007; Lemarchand, 2008; Schell et al., 2009]. Most studies have assumed the lumped geometric parameter to be $g^* = 0.29$ as determined by Mantell et al.

[1992] using the viscosity of the fibre-matrix, however some studies have applied the viscosity of neat PEEK [Tierney and Gillespie, 2006]. Another study [Sun et al., 2001] which assumed the bond strength to correlate with intimate contact (neglecting healing) found $g^* = 0.17$ when curve fitting the model to experimental lap shear data.

The simplified uniform rectangular wave models have been shown to provide good predictions of isothermal intimate contact development for macroscopic tow non-uniformity in wide tape unidirectional prepregs. Non-isothermal adaptations have been made for tape placement however limited validation has been performed. Furthermore, the roughness of a narrow slit tape prepreg or towpreg used in AFP processes is much lower and it is most probable that the bulk of the intimate contact development is in the thin layer of resin at the surface of the tape. The viscosity of the neat polymer should therefore be applied to the intimate contact model rather than the fibre-matrix viscosity [Tierney and Gillespie, 2006; Hinkley et al., 1996]. There is a fundamental problem that the geometric parameters are tuning factors and must determined by fitting the model to experimental data, requiring a significant number of experimental data points.

Yang and Pitchumani [2001a] developed a fractal model for intimate contact development where the input parameters are determined directly from surface profile measurements. They observed that the surface roughness is random and varies over a range of magnitudes. They applied a fast Fourier transform (FFT) to the surface profile data in order to generate a power spectrum of the surface roughness. It was found that the roughness obeys a power-law variation with the spatial frequency, suggesting that a fractal-like structure exists. From this finding they developed a fractal model for the surface profile based on a Cantor ternary set. As the surface roughness is predominantly perpendicular to the fibre direction, a two dimensional model was assumed in the same way as the earlier uniform rectangular models [Lee and Springer, 1987; Mantell and Springer, 1992]. Also as assumed in other models,

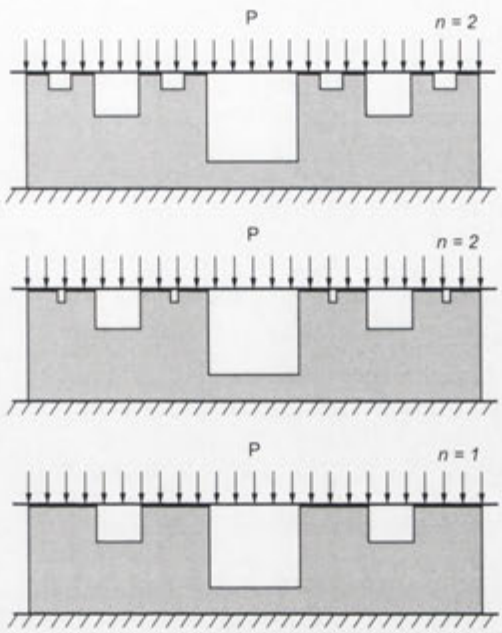


Figure 2.5 – An example of the fractal cantor intimate contact model of Yang and Pitchumani [2001a]. The $n = 2$ asperities flatten towards each other until the gap between them has disappeared, resulting in the formation of the $n = 1$ asperities. The model then progresses to the next generation ($n = 1$), which flattens in the same manner. The process continues until the $n = 0$ gap has closed, resulting in complete intimate contact.

the deformation is against a rigid plane and therefore tow nesting cannot occur. A squeeze flow model was then applied to the asperity elements of the fractal set, resulting in an intimate contact model that accounts for the multi-scale roughness profile of a unidirectional thermoplastic prepreg. The flattening behaviour is assumed to be the compression of n^{th} asperity elements until the gap between them has closed, after which the deformation moves to the next lower generation as shown in Figure 2.5. Full intimate contact is achieved when the gap between the $n = 0$ generation asperities has closed.

APC-2 carbon/PEEK and IM-7/PIXA-M tapes were selected for the experimental validation of the fractal cantor intimate contact model. Surface topology measurements were performed with a profilometer that had a 2.5 µm radius diamond stylus, which is the same order of magnitude as a carbon fibre filament. The authors adopted the fibre-matrix viscosity for an APC-2 carbon/PEEK composite from

Mantell and Springer [1992]. The model was validated against experimental data for APC-2 carbon/PEEK from Lee and Springer [1987], where samples were processed in a heat press under isothermal and isobaric conditions of 350, 360 and 370 °C and 0.28, 0.66 and 1.63 MPa. IM-7/PIXA-M Samples were prepared under isothermal conditions at temperatures of 260, 280 and 300 °C and pressures of 1.125, 2.250 and 3.375 MPa. The experimental degree of intimate contact was determined by 30 MHz ultrasonic c-scans. The predictions were shown to correlate well with the experimental results. This model was not validated for non-isothermal processes, and the periods of time for contact development were in the range of 100-1000 s. A study by Khan et al. [2010] implemented this intimate contact model for a tape placement model. The temperature and pressure fields were simulated and applied to a coupled healing and intimate contact bonding model. The bond strength predictions were shown to agree well with experimental SBSs, however the intimate contact was not characterised in isolation, and validation of the temperature and pressure history is not shown.

Yang and Pitchumani [2001b] considered the same methodology as in their previous study [Yang and Pitchumani, 2001a], however the fractal surface was assumed to be three dimensional, with the asperity elements represented by deformable cylinders of varying heights and radii. An error function and a Weibull function (inspired by the work of Dara and Loos [1985]) were compared for the determination of the cylinder dimensions. Model predictions were compared with the literature in the same manner as their earlier study [Yang and Pitchumani, 2001a], with the Weibull function showing best agreement. This model using either Weibull or error functions was shown to predict the intimate contact behaviour more rapidly compared with the more conservative previously developed fractal cantor model [Yang and Pitchumani, 2001a].

Yang and Pitchumani [2002b] later developed another fractal model based on a Weierstrass-Mandelbrot (W-M) function. The parameters of the W-M function were

determined from surface profile measurements of the composite prepreg. The asperities were modelled as two dimensional stacks of rectangles of varying heights and widths, the dimensions of which were described by the W-M function. The model was validated in the same manner as both of the authors' previous studies [Yang and Pitchumani, 2001a,b]. The predictions were found to agree reasonably well, however it would appear that the Yang and Pitchumani [2001a] model more accurately determines the intimate contact development. This is reinforced by the fact the authors selected the Yang and Pitchumani [2001a] model in a later combined bonding model [Yang and Pitchumani, 2003].

2.2.1.1 Effective viscosity

Rheological measurements of the resin at the temperatures experienced in AFP are out of the typical experimentally measurable range. This is mostly because relatively long periods of time required to perform rheological measurements, and in this time the polymer would undergo significant levels of degradation leading to chain branching or cross-linking which inherently increase the viscosity. As the dwell times in the AFP process are much shorter that those required for rheological measurements, it is possible for the polymer to sustain extreme temperatures without this degradation during AFP.

The viscosity has been determined by various techniques. Lee and Springer [1987] determined the effective fibre-matrix viscosity by fitting their intimate contact model to experimental data for samples processed at temperatures in a narrow range of 350-370 °C. Khan et al. [2010] conducted tow flattening experiments at temperatures from 340-380 °C and determined the viscosity based on thickness change over time. However in a later process simulation study they adopt different values [Khan et al., 2013]. The viscosity of a polymer decreases with increasing temperature. In AFP studies, the viscosity of the polymer has been extrapolated beyond the experimentally measurable range to higher temperatures using Arrhenius temperature depen-

dence relations. A summary of temperature dependent viscosity relations from the literature is presented in Table 2.2. Each of these relations is correspondingly plotted in Figure 2.6 and it can be seen that they differ significantly from one another, with multiple orders of magnitude difference in CF/PEEK viscosity for temperatures above 500 °C. This is significant for the modelling of AFP processes as temperatures will often exceed 500 °C.

Table 2.2 – Temperature dependent viscosity relations for PEEK and CF/PEEK from literature.

Study	Viscosity [Pa · s]
Lee and Springer [1987]:	
PEEK 150P	$\mu_{\text{(PEEK L\&S)}} = 1.13 \times 10^{-10} \left(\exp \frac{19100}{T(\text{K})}\right)$
CF/PEEK	$\mu_{\text{(CFPEEK L\&S)}} = 1.14 \times 10^{-12} \left(\exp \frac{26300}{T(\text{K})}\right)$
Mantell and Springer [1992]:	
CF/PEEK (*APC-2*)	$\mu_{\text{(CFPEEK M\&S)}} = 132.95 \left(\exp \frac{2969}{T(\text{K})}\right)$
Khan et al. [2010]:	
CF/PEEK (*Suprem™ T*)	$\mu_{\text{(CFPEEK K,M\&S)}} = 643 \left(\exp \frac{4367}{T(\text{K})}\right)$
Khan et al. [2013]:	
PEEK	$\mu_{\text{(PEEK K,M\&S)}} = 0.2037 \left(\exp \frac{4871}{T(\text{K})}\right)$
CF/PEEK	$\mu_{\text{(CFPEEK K,M\&S-b)}} = 0.0037 \left(\exp \frac{11115}{T(\text{K})}\right)$

2.2.1.2 Summary of intimate contact models

The rectangular wave models in the literature have been formulated to model the macroscopic deformation of tows in wide tape prepregs. In AFP processes, narrow slit tapes or towpregs are used which are typically very smooth and do not display macroscopic tow non-uniformity. The roughness is on much lower levels, typically less than 10 µm in the case of a modern placement grade towpreg [Khan et al., 2010]. Thus the scale of deformation in a tape placement intimate contact process is much lower and it is more appropriate to consider deformation of a thin layer of neat polymer at the surface of the composite, rather than the macroscopic flattening of a fibre-matrix tow.

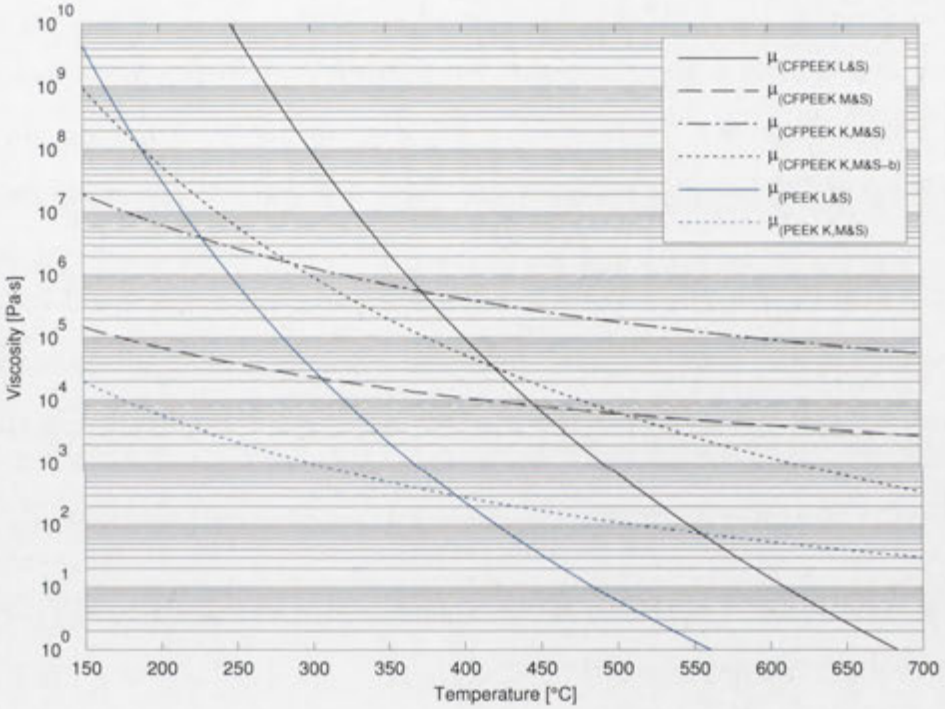


Figure 2.6 – Viscosity vs. temperature for PEEK and CF/PEEK from literature. Relations are typically based on measurements in the range of 340-400 °C. The viscosity below the melting point (343 °C) is generally not valid due to crystallisation effects.

In the studies by Yang and Pitchumani [2001a,b, 2002b] the viscosity is assumed to be the bulk value of the fibre-matrix system, yet features in the fractal models can be smaller than a single fibre. This would result in conservative estimates for the deformation of the smaller fractal elements as the fibre-matrix viscosity is higher. The temperatures that the APC-2 carbon/PEEK samples were processed at were only just above the melting point of PEEK (343 °C), much lower than the typical temperatures used in tape placement processes as reported in experimental studies as found in Section 2.1.1.1.

Limited validations have been performed for intimate contact models under non-isothermal conditions. The time scales in most validations of the intimate contact models are multiple orders of magnitude higher and temperatures much lower than what is experienced in the tape placement process. Various AFP process models have been shown to predict the bond strength using combined healing and intimate contact models, with experimental validations by mechanical test [Dai and Ye, 2002a,b; Tierney and Gillespie, 2006; Schell et al., 2009; Khan et al., 2010] however the intimate contact has not been characterised directly in isolation.

Heat press validations have stationary interfaces under a constant normal pressure field, whereas tape placement has a moving contact development front where the pressure is highly non-isobaric. One possible consequence of this which would not apply for press consolidation is if the resin viscosity is sufficiently low and the consolidation pressure is high enough, a 'bow wave' of resin can be squeezed ahead of the roller at the nip point, possibly aiding in intimate contact development as surface defects may be filled.

The intimate contact models within the literature surveyed assume Newtonian viscous shear flow. Most thermoplastic materials show shear thinning behaviour at elevated shear rates. Narnhofer et al. [2013] investigated the effect of shear thinning in an AFP process. When the tape is applied to a substrate, it flattens to a degree resulting in shear forces at the interface. This effect was modelled and compared to

experimental measurements of tape width change from hydrogen flame placement of carbon/PEEK using a 50 mm metallic consolidation roller. Results suggest average wall shear rates ranging from 80-280 s^{-1}, which equate to a 40-60 % decrease in viscosity. It was also stated that the maximum shear rates would be much higher, leading to even further viscosity reductions. Therefore the shear thinning effect is likely to enhance the rates of intimate contact and the existing assumptions of Newtonian flow in intimate contact models are likely to produce conservative results. Further research is required in this area to establish new models which take into account the shear rate effects during intimate contact development in tape placement processes.

2.2.2 Healing

Healing or autohesion is the process of inter-diffusion of the polymer molecules across the interface two polymer bodies placed in contact at elevated temperature. It is the fundamental process that results in strength development at the interface. The reptation theory developed by de Gennes [1971] is used to describe the diffusive motion of linear random-coil polymer chains throughout an amorphous polymer above the glass transition. In a typical bulk amorphous thermoplastic the high molecular weight results in significant chain entanglement, greatly impeding the diffusive motion of the chains. The motion of an individual chain is confined within an entangled network of chains.

The reptation model assumes that the entanglement of a single chain can be represented by assuming the chain is initially confined to a tube of the same size Figure 2.7. The chain wriggles up and down this tube, with the direction of the head of the chain following a random path as it exits the tube. As time progresses, the ends of the chain gradually escape the initial tube, forming minor chains. After a sufficient period of time, the chain will have escaped the initial tube entirely, and this time is referred to as the reptation time t_r. The reptation time is highly temperature

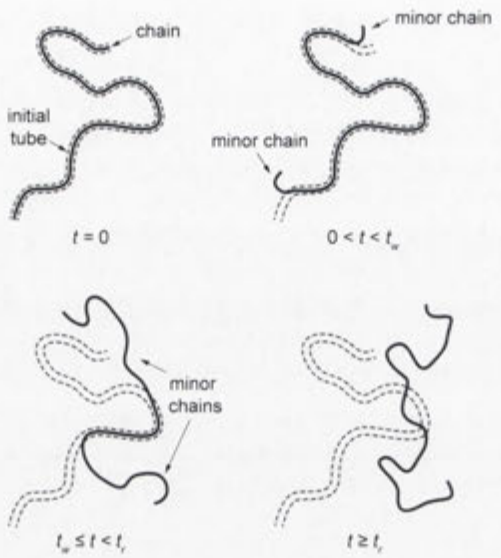


Figure 2.7 – Reptation model.

dependent and has been described by Arrhenius and also Williams, Landel and Ferry (WLF) relations. The depth of penetration of a chain (χ) across a plane in the bulk material was proposed to be related to time by:

$$\chi \sim t^{1/4} \tag{2.7}$$

The reptation theory was extended by Wool and O'Connor [1981]; Wool [1984]; Kim and Wool [1983] to model the strength development due to motion of the chains across a polymer-polymer interface. Healing has been quantified by two main techniques, the most common being mechanical strength tests of the interface as well as a less common technique where radioactively doped polymer chains are traced as they diffuse through the polymer [Dara and Loos, 1985]. The following relation has been used to predict the degree of healing (D_h) at an interface under isothermal conditions:

$$D_h(t) = \frac{\sigma}{\sigma_\infty} = \left(\frac{t}{t_r}\right)^{1/4} \tag{2.8}$$

The degree of healing corresponds with the ratio of the interface strength to the bulk

strength of the polymer. The reptation model is appropriate for linear thermoplastics with molecular weights (M) in the range of $M_c < M < 8M_c$, where M_c is the molecular weight of critical entanglement. In the case of a high performance thermoplastic used in a thermoplastic composite, $M > 8M_c$, and full reptation is not necessary for complete strength development. This is because at higher molecular weights the minor chains are longer, and sufficient interpenetration for full bond strength can be achieved before the chain has completely reptated [Yang and Pitchumani, 2002a]. In such a case it is more appropriate to consider the welding time t_w which is less than the reptation time t_r.

The thermoplastic AFP process is highly non-isothermal therefore a non-isothermal approximation of Eq. (2.8) is required. Based on approximate extensions of the reptation theory, Bastien and Gillespie [1991] and Sonmez and Hahn [1997a] presented various non-isothermal approximations. Yang and Pitchumani [2002a] highlighted the fact that these approximations were only truly valid if applied to an isothermal process, and the relations were mathematical extensions of reptation theory and had no strong physical justification. Despite these facts, these non-isothermal models have been widely implemented for themoplastic AFP processes [Pitchumani et al., 1996, 1997; Sonmez and Hahn, 1997a; Sonmez and Akbulut, 2007; Lemarchand, 2008; Schell et al., 2009]. Yang and Pitchumani [2002a] formulated a non-isothermal model from first principles of the reptation theory. Based on their model, the degree of healing for a non-isothermal process is determined by:

$$D_h(t) = \left[\int_0^t \frac{1}{t_w(T)}\mathrm{d}t\right]^{1/4} \tag{2.9}$$

This non-isothermal approximation has been compared with results from lap shear experiments under non-isothermal conditions. The lap shear samples were manufactured using carbon/PEEK and carbon/PEKK composites. The samples were consolidated in a temperature controlled heat press for heating and cooling ramps between temperatures of 380-420 °C over time periods ranging from 360-5400 s, resulting in

maximum temperature gradients of ~0.1 °C/s. The consolidation pressure was chosen to be high enough to ensure rapid intimate contact development, so as the healing could be effectively tested in isolation. The predictions were compared with the existing models from the literature and shown to give superior results, correlating well with the experimental data. This model was also experimentally validated with lap shear tests of PEEK films [Yang and Pitchumani, 2003]. Films are much smoother and thus intimate contact development is very rapid. The temperature ramps and times used were the same as in the previous study, with temperature gradients no greater than ~0.1 °C/s. The results were again compared with the existing models from the literature and shown to provide good agreement with the experimental data. The previous models underestimate the degree of healing, providing more conservative estimations of strength.

While non-isothermal validations were given for the Yang and Pitchumani [2002a] model, the temperature gradients (~0.1 °C/s) were many orders of magnitude lower than that experienced in a typical in situ thermoplastic AFP process which typically experiences temperature gradients in excess of 1000 °C/s. The validations are also performed at relatively low temperatures no greater than 420 °C compared with tape placement where temperatures can be as high as 600 °C as discussed in Section 2.1.1.1.

2.2.2.1 Welding time

The main input to a healing model is the characteristic welding time t_w. As the welding time is based on a molecular diffusion process, it is highly temperature dependent. Welding time relations have been determined by healing experiments where the interface is brought together for a given time and temperature, and then the strength tested mechanically by means of tensile test [Dara and Loos, 1985; Lee and Springer, 1987] or lap shear test [Yang and Pitchumani, 2002a]. Other studies have assumed the welding time to be the relaxation time of the polymer [Nicodeau,

2005; Khan et al., 2010; Grouve et al., 2013], which can be determined via rheological measurements. The experimental range of measurement for welding time is limited in a similar way to the resin viscosity, and thus the behaviour at high temperatures must be extrapolated. This has been done assuming Arrhenius-type and also WLF relations. The published relations for PEEK found in the literature are presented in Table 2.3. A plot of the values (Figure 2.8) shows large differences in welding time many orders of magnitude apart over a large range of temperatures, which would result in vastly different healing model predictions.

Table 2.3 – Temperature dependent welding time relations for PEEK from literature.

Study	Welding time [s]
Lee and Springer [1987]:	$t_{\text{w (PEEK L\&S)}} = \left(\frac{1}{44.1}\exp\frac{3810}{T(\text{K})}\right)^4$
Sonmez and Hahn [1997a]:	$t_{\text{w (PEEK S\&H)}} = 0.11\exp\left[6892\left(\frac{1}{T(\text{K})}-\frac{1}{673.15}\right)\right]$
Khan et al. [2010]:	$t_{\text{w (PEEK K,M\&S)}} = 2\times10^{-5}\left(\exp\frac{5172}{T(\text{K})}\right)$
Levy et al. [2014a]:	$t_{\text{w (PEEK L,C\&P)}} = 7.6\times10^{-6}\left(\exp\frac{8948}{T(\text{K})}\right)$

2.2.2.2 Differential interface temperature

Smith et al. [2001] studied the effect of differential interface temperature on the healing of neat polypropylene samples. They refer to the differential interface temperature as non-isothermal, which is in the sense that the bodies are not at a common temperature, rather than a time varying temperature history which is the common use of the term. DSC measurements determined the melting point T_m, onset of recrystallisation and peak crystallisation temperatures to be 165, 123 and 110 °C respectively. Square sample plaques (50 mm × 50 mm) were prepared by injection moulding. The healing experiments were performed with the plaques inserted in a matched-die mould. Both halves of the moulds were separately instrumented and temperature controlled with thermocouples. The interface fracture energy was characterised by double cantilever beam tests. The interface temperature T_i for the differential temperature experiments was assumed to the be the mean of the plaque temperatures.

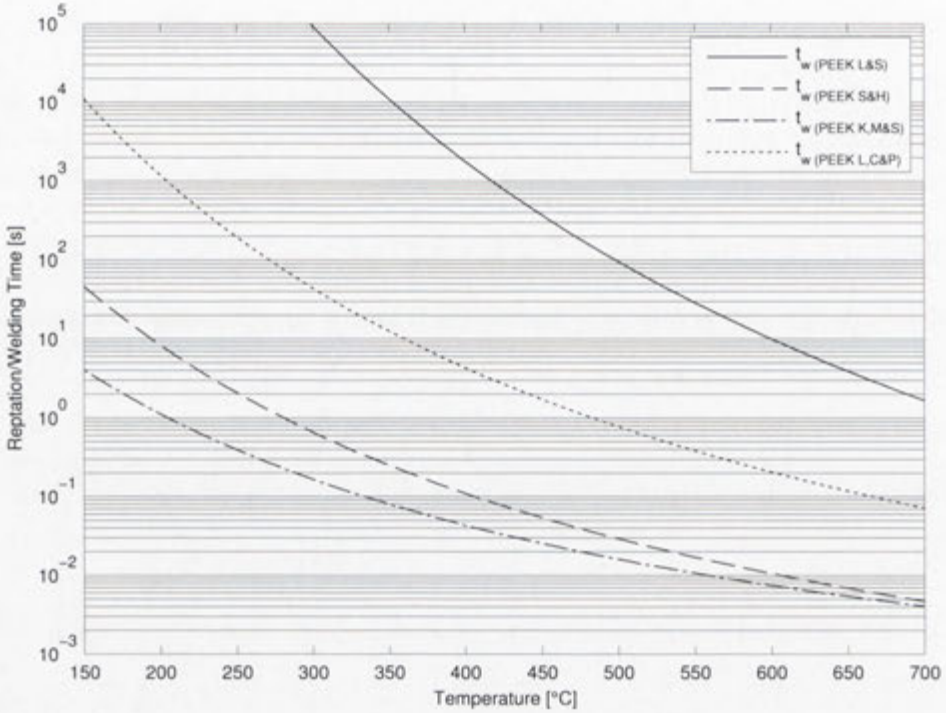


Figure 2.8 – Temperature dependence of welding time for PEEK from literature.

For $T_i < T_m$ with no temperature differential, the fracture energy release rate was negligible, whereas those produced with temperature differentials in the range of 40-100 °C showed energy release rates approximately 4 % of the value achieved for the bulk polymer. When interface temperatures exceeded T_m the fracture energy release rate increased to values close to that of the bulk polymer for both the isothermal an differential cases. It was found that when the temperature differential was sufficiently large, bonding would occur despite one of the interfaces being below T_m. Furthermore, the samples produced with temperature differentials developed stronger interfaces after shorter periods. This was partly explained by the polymer having higher heat capacity at higher temperatures which would lead to initial interface temperatures higher than the mean temperature on initial contact. It was also observed that the samples produced below T_m with differential temperature showed evidence of increased wetting at the interface compared with the isothermal samples. The explanation for this was the viscosity of the high temperature interface is

decreased and allows for rapid wetting, leading to higher bond strengths. The study concluded that polypropylene could be bonded more rapidly for the same mean interface temperature when bonding with differential interface temperatures.

The same research group also investigated the differential interface temperature bonding of polyamide 12 [Zanetto et al., 2001]. It was found that the behaviour of polyamide 12 was very similar to that of polypropylene in their previous studies. For the case of one interface below the melting point, cross-sections suggest that a thin molten layer is created on the surface of the cool interface, which then acts as a nucleation site during recrystallisation. This could then lead to crystallisation back across the original boundary, increasing the bond strength. The group later developed a phenomenological intimate contact model that was used to determine process windows [Plummer et al., 2003].

2.2.3 Experimental validations of bonding models

Various models for intimate contact and healing have appeared in the literature. Non-isothermal formulations are required for AFP processes due to the rapidly changing temperature and pressure conditions. Non-isothermal validations have been performed, however for time periods orders of magnitude larger, and for temperatures much lower than those experienced in AFP. The overall bond strength is determined by coupling both intimate contact and healing models. The following section will investigate the studies where combined bonding models have been formulated for AFP processes and compared with experimental data.

Mantell et al. [1992] implemented their previously developed intimate contact model. Healing was not considered, and effectively assumed to be unity. It was not made clear as to which temperature and pressure profiles were applied in the model. Temperature predictions were shown to agree with experimental data reasonably well, however there is some doubt in the accuracy of the thermocouple measurements as previously discussed in Section 2.1. The pressure distributions applied to

the tape placement model are not given, only the applied consolidation force. Short beam strength tests show experimental strengths much lower than those predicted. This most likely because a healing model was not considered, leading to large over-estimation of the bond strengths.

Butler et al. [1998] compares experimental SBS results with predicted bond strength and found to be in good agreement. The non-isotherml healing model of Bastien and Gillespie [1991] was implemented, however this is known to produce overly conservative results for non-isotherml conditions as shown in Yang and Pitchumani [2002a]. The Mantell and Springer [1992] intimate contact model was coupled with the healing model for bond prediction. A geometric parameter $g^* = 0.13$ was determined by fitting the model to the experimental data. The simulator of Pitchumani et al. [1996] was implemented for determination temperature and pressure profiles, however validation of this simulator was not given. The predictions of the coupled bonding model were found to match the experimental strengths to within 20 %.

Sun et al. [2001] used the Mantell and Springer [1992] model and predicted the bond strength based on the intimate contact model only. Autohesion was assumed to be unity. The lumped geometric parameter was determined by fitting the model to lap shear results, and they determined a value of $g^* = 0.19$, which is much lower than the $g^* = 0.29$ that was reported for the same material in an earlier study [Mantell et al., 1992]. Another difference was the viscosity of the continuum was assumed to be that of the PEEK matrix and not that of the fibre-matrix system as previously assumed. The predictions were shown to fit the experimental data well. The temperature and pressure profiles used as inputs for the intimate contact model were not presented nor discussed.

Tierney and Gillespie [2006] implemented the Yang and Pitchumani [2002a] non-isothermal healing model in combination with the Mantell and Springer [1992] intimate contact model. A value of $g^* = 0.29$ was assumed as found in [Mantell et al., 1992], however the viscosity was assumed to be that of the neat resin, rather than

that of the fibre-matrix. The welding time t_w was assumed to be that used by Sonmez and Hahn [1997a], however the origins of this value for t_w are unknown. The intimate contact was assumed to develop instantaneously under the consolidation roller, as the intimate contact development occurs much over a much shorter time scale than healing. This is likely to be a reasonable assumption as a rigid metallic roller was used and the pressure distribution is effectively instantaneous due to the extremely short contact patch. The temperature history was predicted using a previously developed thermal model [Tierney and Gillespie, 2003], however as discussed in Section 2.1 there are periods to the order of 1 s where the model over-predicts the temperature by at least 100 °C, and through thickness temperature validations were not given. The pressure field was determined using the macroscopic pressure model of Ranganathan et al. [1995]; Pitchumani et al. [1996]. Healing was assumed to occur for temperatures above the melting point of 338 °C. The bond predictions were compared with SBS tests. Samples were reconsolidated in an autoclave to provide a reference for the ultimate SBS. The ultimate strength was taken as the average of the reconsolidated samples. The value exact value was not given, however interpretation of the results suggests that the value was in the range of 80 MPa. It is likely that the samples would have experienced degradation during placement, therefore this value is potentially lower than would be obtained from an autoclave sample prepared using virgin material. Predictions were shown to agree well with the experimental data, however the thermal model is known to overestimate temperatures, and the intimate contact and healing models have not been validated separately for such highly non-isothermal conditions. It is not clear whether the same models implemented for a different head design would yield accurate predictions.

Khan et al. [2010] implemented a bonding model based on the non-isothermal healing model of Yang and Pitchumani [2002a] and the fractal cantor intimate contact model of Yang and Pitchumani [2001a]. *Suprem*™ *T* 60 % v/v AS4/PEEK-150 0.13 mm × 12 mm prepreg was used in the experimental work. The surface rough-

ness was characterised for the fractal model using white light profilometry, resulting in values of $FD = 1.3$ and $f = 1.44$ which imply the prepreg is smoother than the APC-2 studied in Yang and Pitchumani [2001a]. The viscosity for the intimate contact model was determined by monitoring the thickness change during the flattening of unidirectional plies in a heat press. The viscosity was then determined by fitting data to Newtownian flattening model, resulting in an effective fibre-matrix viscosity. The welding time t_w was assumed to be equal to the longest molecular relaxation time of the melt, which was determined by a series of rheological measurements on neat PEEK at temperatures of 340, 360, 380 and 400 °C. The relaxation time was determined using the Carreau model, and the temperature dependence was based on fitting the data to an Arrhenius relation. The temperature thresholds assumed for the calculation of intimate contact or healing were not stated. The degree of bonding is stated as being simply the the product of the degrees of intimate contact and healing, rather than considering an integral style formulation where the healing of each new increment of intimate contact develops separately over time. The thermal model was developed in earlier work [Schledjewski and Latrille, 2003], however no validation of the temperature history is given in either study. Pressure distributions were determined using the model of Ranganathan et al. [1995]. DIN EN 2563 interlaminar shear strength (ILSS) tests were performed for mechanical characterisation. A reference sample for the ultimate ILSS was prepared by tape placement followed by an autoclave post-consolidation. The reference strength was found to be 94 MPa. Bond predictions were shown to agree well with three experimental results.

It can be seen that few studies have compared coupled bonding model predictions with experimental results. Temperature and pressure histories have been estimated using models, rather than direct experimental measurements. Each model has used a simplification of the coupled bond prediction, such as assuming the intimate contact to occur as a step function, or simply considering the product of the degrees of healing and intimate contact rather than the full integral type formulation. It is clear

that further work is required in the validation of coupled bonding models for the AFP process, and is identified as an area of focus in this work.

2.2.4 Void growth and reduction

Ranganathan et al. [1995] developed a void dynamics model for the AFP process. This included a macroscopic squeeze flow model which is used to determine the pressure distribution within the tape while under the load of a rigid cylindrical compaction roller. A microscopic void consolidation model is used to determine the growth and reduction of the voids. It assumes that a typical void within the composite can be represented by a microscopic spherical void (of radius r_v) that is encased by viscoelastic shell of resin (of raduis r_s) as depicted in Figure 2.9. The growth and collapse of the void is determined by the balance of the internal void pressure P_g and the pressure applied to the exterior of the shell P_f, the surface tension σ_v and the resin viscosity μ_s:

$$4\mu_s \left(\frac{r_v^3}{r_s^3} - 1 \right) \frac{\mathrm{d}r_v}{\mathrm{d}t} + \left(P_g - P_f \right) r_v - 2\sigma_v = 0 \tag{2.10}$$

The internal void pressure is determined from the ideal gas law, whereas the pressure applied to the shell is determined by the macroscopic squeeze flow model.

The Ranganathan et al. [1995] model was implemented by Tierney and Gillespie [2003] and Khan and Schledjewski [2010]. Results confirmed this model to give reliable predictions of void content for a range of processing conditions. The pressure field is linked to the temperature distribution due to the temperature dependence of viscosity. The thermal model of Tierney and Gillespie [2003] has been observed to overestimate the temperature by up to 100 °C for periods to the order of 1 s. It is unclear how much of an effect such a discrepancy would have on the predicted pressure distribution, and also the microscopic void compression model. The model implemented by Khan and Schledjewski [2010] was validated against temperature measurements in the second and seventh layers, and shown to be in good agreement.

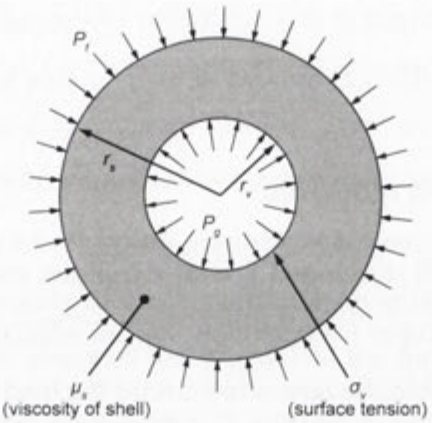


Figure 2.9 – Microscopic void model of Ranganathan et al. [1995]. The model assumes a spherical void encased by a viscoelastic shell. The rate of growth/collapse is determined by the balance of P_f and P_g, and the parameters σ_v and μ_s.

More recently Simacek et al. [2013] developed a non-local void filling model for AFP. The model is suitable for cases where the voids contained within the composite are of a significant diameter (tens of microns) relative to the thickness of the tape and much larger than a fibre diameter (7 µm). This model therefore applies to materials such as older prepregs such as APC-2 carbon/PEEK that is known to contain significant intra-laminar voids. The voids in this case are large enough that they contain a bed of dry fibres. The void consolidation process is therefore modelled as the flow of resin through a bed of fibres using Darcy's impregnation model. No experimental validation was performed, however a model capability demonstration suggests that the void size and spacing are just as important as the initial void content for achieving minimum void content. This is because fewer large voids take longer for the resin to flow through and impregnate compared with many smaller voids.

In the case of a modern AFP grade carbon/PEEK prepreg such as *Suprem*™ *T* the voids are typically much smaller and occur in the spaces between fibres and dry fibre beds are not present (as can be seen in [Khan et al., 2010]). In such a case the Ranganathan et al. [1995] microscopic void dynamics model is more appropriate.

2.2.5 Thermal degradation

High temperatures are required in order to achieve bonding in situ at a reasonable rate. The temperatures are sufficiently high to cause decomposition and cross linking. Degradation in some AFP studies using PEEK composites have assumed degradation to occur above a fixed temperature of 550 °C [Beyeler and Güçeri, 1988; Nejhad et al., 1991; Nejhad, 1993]. As discussed previously in Section 1.3.2.5, the degradation process is however highly complex and is related to cumulative time and temperature history. Nam and Seferis [1992] developed a non-isothermal model for the degradation by weight loss for PEEK in a nitrogen atmosphere. The rate of degradation was related to temperature using an Arrhenius-type relation. This model was implemented for AFP processes by Pitchumani et al. [1997]; Sonmez and Hahn [1997b,a]; Sonmez and Akbulut [2007]. Sonmez and Hahn [1997b] justified the used of this model in air by the fact that the extremely short periods involved in the tape placement process do not allow sufficient time for oxygen to diffuse through the melt. Therefore the model of degradation in nitrogen can be applied to the AFP process.

Nicodeau et al. [2006] assumed the degradation to occur in the form of cross-linking. Rheological measurements were performed on neat PEEK resin at temperatures of 360-460 °C with long measurement periods of up to 6 hours. At the highest temperature of 460 °C, minimal viscosity change appears for a period of a minute. The viscosity was then related to the degree of cross-linking, and a model formulated which relates the cross-linking rate to temperature using an Arrhenius relation. This assumption conflicts with the literature which suggests that degradation occurs in the form of cross-linking for long periods (to the order of tens of minutes to hours) at low temperature, while chain scission leading to release of volatiles occurs for short periods (seconds) at high temperatures. Furthermore, in order for cross-linking to occur, there surely must first be scission events leading to the production of a free radicals which can then in turn form cross-links. Despite these facts, the model has

been implemented for AFP processes by Nicodeau et al. [2006]; Regnier et al. [2007]; Khan et al. [2010, 2013].

A small number of degradation models for PEEK applicable to the AFP process have been presented in the literature. These models are used to infer the time and temperature dependent levels of degradation in the form of either weight loss or cross-linking, however the exact effect of such degradation on the resulting material is not studied. The allowable level of cross-linking or weight loss is simply capped at a fixed value. Thus the models can be used to determine equivalent levels of degradation for different process histories. In the case where the material is ablated from the surface leaving no apparent residue [Rosselli and Santare, 1997], it is possible that minimal adverse effects of degradation would result. However development of char residues, changes in molecular weight distribution, and cross-linking or branching will likely have a significant impact on the resulting inter-laminar bond strength.

2.2.6 Non-isothermal crystallisation kinetics models

Due to the rapidly changing temperature history in the tape placement process, it is necessary to consider a non-isothermal crystallisation kinetics model. Various non-isothermal models have been formulated for PEEK such as that of Velisaris and Seferis [1986] which is based on the Avrami equation, and the Choe and Lee [1989] model which is based on the Ozawa equation. The model of Choe and Lee [1989] was implemented by Sonmez and Hahn [1997b] for a parametric study, however no experimental validation of crystallinity was performed. Seferis et al. [1987] determined the parameters for the Velisaris and Seferis [1986] model for APC-2 carbon/PEEK composite. Tierney and Gillespie [2004] later validated the model with the parameters for carbon/PEEK for highly non-isothermal conditions similar to those experienced in tape placement using a novel experimental apparatus. A good agreement was found between the model and experimental results. This model was then used by Guan and Pitchumani [2004] in a parametric study for a hot gas tape placement process.

2.2.7 Effect of crystallinity on healing

A study by Lamèthe et al. [2005] investigated the healing behaviour of PEEK and APC-2. The first part of the study investigated if healing was possible for semi-crystalline PEEK, as the crystalline phases would significantly hinder chain motion. Long term healing tests of semi-crystalline PEEK were performed at temperatures in the region of the melting temperature 330, 340 and 348 °C in an oven with a controlled argon atmosphere to prevent oxidation. DSC measurements determined the melting temperature to be 345 °C. The strength of the interface was characterised using the Boeing wedge test. For temperatures of 330 and 340 °C, the strength was observed to be developing very slowly over long periods of 1-100 h, proving that healing is possible for semi-crystalline PEEK below the melting temperature. The strength of the samples prepared at 348 °C was found to plateau after healing times of 6 h. It was reported that samples prepared in the same oven from the melt (totally amorphous state) would fully heal in under 1 min. The second part of the study investigated the healing behaviour for short periods using a custom built experimental device. The test device consisted of two temperature controlled copper mounts in which the material samples were affixed using high temperature adhesive. An infra-red element is then placed between the surfaces of the samples for varying times with a computer controlled actuator. Once the heating element is removed, the samples are quickly pressed together at 0.3 MPa. The temperature on the surface during healing therefore depends on the hold time of the heater and the delay between pressure application. A thermal model was used to predict the surface temperature history as experimental measurement was difficult. It was found that the crack would no longer propagate the interface of the wedge test (suggesting complete healing) for a mount temperature of 250 °C and an IR lamp holding time of 5.5 s followed by 0.25 second pressure application and then quenching water. The initial interface healing temperature predicted by the model for this experiment was 375 °C and declines rapidly thereafter. It was also determined that the critical interface temperature above

which bonding could occur (when bonding from the melt where the material would be amorphous) was 290 °C. Below this temperature, it is suggested that formation of crystalline phases would significantly restrict the chain motion.

Until recently, measurements of crystallisation rate at temperatures below 280 °C have not been possible as the crystallisation rates are too high for experimental measurement with standard DSC technology. The reason for this being the thermal mass of the sample prevents rapid cooling to the temperatures required to perform the measurements, with significant levels of crystallisation occurring as the sample is cooled to the measurement temperature. This problem can be overcome by using samples of very low mass to the order of 100 ng, however specialised high sensitivity sensors are required. The recent development of nano-DSC have enabled measurement of the crystallisation rates for PEEK over the complete temperature range. Tardif et al. [2014] characterised neat PEEK 150G resin over the complete temperature range for which crystallisation can occur, that is for $T_g \leq T \leq T_m$. The crystallisation rate was found to be the highest at 230 °C. The crystallisation half-time at this temperature was found to be 0.48 s. The intimate contact development time in a laser AFP process is typically shorter than this value. This would suggest that the composite remains in a highly amorphous state during initial placement and therefore it is likely that healing could occur for temperatures below the typically assumed lower healing threshold of 290 °C.

For carbon/PEEK tape placement processes, the cooling rates can be sufficiently high to result in very low levels of crystallinity at the bond interface during initial placement of a layer [Sonmez and Hahn, 1997b; Guan and Pitchumani, 2004; Quinlan et al., 2010]. When subsequent layers are added above, the interface of the previously added layer undergoes re-heating. If it is re-heated above the melting temperature, all crystallinity is lost and then some minor level of recrystallisation occurs as the material cools from the melt. In the case that the layer is reheated above the glass transition temperature but below the melting point, cold crystallisation will develop

the crystallinity further to more significant levels. This behaviour is highly dependent on the specific heating profile in the process, tape thickness and placement velocity. In the case of a hot gas tape placement process with a placement rate of 10 mm/s and a maximum substrate surface temperature in the range of 600 °C, the majority of the crystalline development typically occurs progressively during the placement of the second through to the fifth layer above [Sonmez and Hahn, 1997b; Guan and Pitchumani, 2004]. Since the level of crystallinity is effectively zero during the placement of the first layer due to the extreme cooling rates experienced in tape placement, it is therefore likely that healing can occur for temperatures lower than 290 °C, in contrast to most other process where the cooling rates are sufficiently low that crystallisation greatly impedes chain motion when temperatures drop below 290 °C. This is fact is supported by the recent measurements of Tardif et al. [2014] as discussed previously. Furthermore, the fact that the chain mobility is high enough for crystalline structures to form during cold crystallisation at temperatures above the glass transition suggests that healing would still occur for the amorphous polymer right down to the glass transition temperature. The level of healing however at these temperatures would be relatively low, nonetheless it adds to the final bond strength. This is a topic of particular interest and will be investigated in this thesis.

2.2.8 Thermal modelling

It has been shown that the thermoplastic AFP process is strongly linked to the temperature history throughout the process. Not only the bonding process, but also the crystallinity, void content, residual stress and degradation processes are highly temperature dependent. An accurate thermal model is therefore required to provide the necessary foundations for predictive process modelling capability. The following sections investigate the various modelling approaches and assumptions that have been made in the literature.

2.2.8.1 Approach

In the TP-AFP process, the material would ideally be heated uniformly across the width so as to achieve uniform properties. Due to the low transverse diffusivity of the composite, heat flow in the transverse direction is low, and losses at the edges are minimal. In this case the thermal model can be assumed to be two dimensional, as a side on cross-section view cut through the width of the material. The motion of the placement head must also be considered. The most straightforward method of modelling the motion is to attach the frame of reference to the placement head. In this case the material moves through the reference frame and therefore is an Eulerian modelling approach. In such a case, the mass flow is accounted for by adding velocity terms to the energy balance partial differential equation.

The most commonly implemented thermal models are 2D with an Eulerian frame of reference attached to the placement head, either employing finite difference [Beyeler and Güçeri, 1988; Nejhad et al., 1991; Agarwal et al., 1992; Nejhad, 1993; Tumkor et al., 2001] or finite element [Grove, 1988; Sarrazin and Springer, 1995; Kim et al., 1996; Sonmez and Hahn, 1997b,a; Sonmez et al., 2002; Sonmez and Akbulut, 2007; Han et al., 2012] methods. Others have considered a 2D control volume approach [Pitchumani et al., 1996, 1997] or a 3D finite element model [Schledjewski and Latrille, 2003]. Various one dimensional simplifications have also been made [Tierney and Gillespie, 2003, 2006; Khan and Schledjewski, 2010] as the heat flow in the process direction is small compared to the mass transport of heat due to the motion, thus a one dimensional element aligned through the thickness of the material is considered. Such a model can be visualised as tracing a slender rod of material as it moves through the process. Kim et al. [1996] suggest a 3D model is required for non-uniform hot gas impingement.

While a significant number of thermal models have been presented, not all have been validated. The models of Grove [1988]; Beyeler and Güçeri [1988] had no validations. Analytical validations were given for the models of Nejhad et al. [1991]; Ne-

jhad [1993]; Sarrazin and Springer [1995]; Sonmez and Hahn [1997b]. Other models were validated experimetally. Mantell et al. [1992]; Khan et al. [2010] used thermocouples of unspecified thickness and the measurement sampling rate was not given. Agarwal et al. [1992] performed measurements at 50 Hz with 12.7 µm foil thermocouples for superior response time. Their model of laser heating was found to require 6 W of power to achieve a temperature of 200 °C, whereas the experiments required 30 W. Assumption of 80-85 % reflectivity resulted in good agreement, however this suggested that reflections were not absorbed on the opposing side of the cavity between the tape and substrate. Kim et al. [1996] compared thermal model predictions with experimental temperature measurements made using 0.076 mm fine wire K-type thermocouples for a hot gas AFP system. Many measurements were performed including those with thermocouples embedded up to 4 layers deep in the composite. The heat transfer coefficients used in the model were the average of the impinged gas heat transfer values. Reasonable agreement was found but the authors suggest development of a 3D model as an avenue of improvement. Tumkor et al. [2001] compared results of their thermal model for a hot gas process to published experimental results in the literature. Tierney and Gillespie [2003] validated their thermal model using a long wave infra-red (LWIR) camera. Qualitative comparisons were favourable, however periods of up to one second showed differences to the order of 100 °C. Details of the emissivity used for the measurement were not given, and the composite shows specular reflectivity at LWIR wavelengths, making accurate measurement somewhat challenging.

2.2.8.2 Modelling of consolidation rollers

The thermal models in AFP literature have been mostly applied to processes using rigid metallic rollers. The rollers have been approximated as a convective boundary condition on the rear side of the tape with vastly differing heat transfer coefficients of 400 $W/(m^2 \cdot K)$ [Sonmez and Hahn, 1997b,a; Han et al., 2012] 500 $W/(m^2 \cdot K)$ [Grove,

1988; Beyeler and Güçeri, 1988; Agarwal et al., 1992], 1000 $W/(m^2 \cdot K)$ [Kim et al., 1996; Tumkor et al., 2001] 1500 $W/(m^2 \cdot K)$ [Khan and Schledjewski, 2010] or simply a fixed boundary temperature [Pitchumani et al., 1996, 1997; Tierney and Gillespie, 2003; Toso et al., 2004; Tierney and Gillespie, 2006]. Important details such as the geometry of the roller and/or the contact length of the tape on the roller is often omitted [Grove, 1988; Beyeler and Güçeri, 1988; Agarwal et al., 1992; Pitchumani et al., 1996, 1997; Sonmez and Hahn, 1997b,a; Tumkor et al., 2001; Tierney and Gillespie, 2003; Toso et al., 2004; Tierney and Gillespie, 2006; Khan and Schledjewski, 2010; Han et al., 2012]. Schledjewski and Latrille [2003] appears to model the roller as a physical body, however no geometry, properties or results are presented. From the literature reviewed, no studies have modelled the roller as a physical body and analysed its relative influence on bond line temperature. Conformable rollers allow for placement on curved surfaces and irregular geometry. They can provide much longer and more uniform pressure distributions (Figure 1.4). The result is an increase in the amount of time available for consolidation for a given process speed, as well as a much larger area of thermal contact with the roller. Since the process is highly dependent on the post nip point temperature history, it is therefore of interest to study the effect of the roller on the thermal history.

2.2.8.3 Modelling of tooling

The tooling has been approximated as a convective boundary condition on the base of the substrate with a broad range of values. 400 $W/(m^2 \cdot K)$ was assumed by Khan and Schledjewski [2010], 500 $W/(m^2 \cdot K)$ by Grove [1988] 1000 $W/(m^2 \cdot K)$ by Beyeler and Güçeri [1988]; Nejhad et al. [1991]; Agarwal et al. [1992]; Kim et al. [1996]. Other studies use a fixed boundary temperature [Mantell et al., 1992; Pitchumani et al., 1996; Tierney and Gillespie, 2003, 2006] or model the tooling as a physical body [Nejhad, 1993; Tumkor et al., 2001; Toso et al., 2004; Han et al., 2012]. Sonmez and Hahn [1997b,a] appears to model the tooling boundary as convection in air. Tierney

and Gillespie [2003] found that the tooling acts as a significant heat sink, particularly at the beginning of the process when the substrate is thin, and thus it is important to include the tooling in thermal models.

2.2.8.4 Thermal contact resistance

In a thermoplastic placement processes, attachment of the first ply to the tooling is an area of ongoing research. The component must be removed from the tooling when placement has finished, and thus it must not be bonded to the tooling. In thermoset placement processes the prepregs have sufficient tack to adhere to the surface of a tool. Thermoplastic composite prepregs are quite different in nature, they are stiff, dry and boardy and possess no tack or adhesive qualities. The first ply may be attached to the tooling using methods such as high temperature adhesives, mechanical clamping or vacuum table style tooling which literally sucks the prepreg to the surface. Since the process is sensitive to the tooling [Tierney and Gillespie, 2003], it is important to consider the thermal contact between the substrate material and the tooling, as it will be vastly different depending on the method of first ply attachment. It is also possible that there will be thermal contact resistance between the roller and the rear side of the tape. Neither of these effects appear to have been investigated in the literature.

The inter-laminar bonding process of the composite itself includes intimate contact development. In the early stages of contact development there is thermal contact resistance between the plies. Levy et al. [2014b] studied this effect and developed relations between the degree of intimate contact and the thermal contact resistance for a carbon/PEEK interface. The experiments were performed at very low pressures (1.34 kPa with *Cytec APC-2* prepreg which is has both high surface roughness and a significant intralaminar void fraction [Mazumdar and Hoa, 1996]. Surface profile measurements found surface asperity depth to be 21.1 µm, which is approximately double of that of the *Suprem™ T* composite used in Khan et al.

[2010]. 76.2 mm × 76.2 mm cross ply laminates were manufactured at 400 °C using an aluminium block to supply the consolidation pressure. Intimate contact was determined with optical micrograph. The inter-laminar regions were easily identified due to the cross-ply orientation. Thermal contact resistance was determined via laser flash analysis. It is likely that processing under these temperature and pressure conditions would have resulted in void expansion which would effect the thermal properties of the plies. The thermal contact resistance was shown to decrease from $5 \times 10^{-4}\,\mathrm{m^2 \cdot K/W}$ to $7 \times 10^{-3}\,\mathrm{m^2 \cdot K/W}$ when increasing the intimate contact from 0.64 to 0.94. It was shown that the effective equivalent thermal conductivity can be 50 % lower in the case of initial intimate contact. The authors flag investigating the effect of intra-laminar void content on the thermal properties as a direction for future studies.

2.2.8.5 Material properties

Unidirectional composites such as carbon/PEEK have anisotropic thermal properties. The conductivity in the fibre axis is typically an order of magnitude higher than the transverse directions. The majority of thermal models applied to AFP assume the composite to be an anisotropic yet homogeneous continuum. A range of studies have assumed temperature dependent non-linear properties [Nejhad, 1993; Sarrazin and Springer, 1995; Kim et al., 1996; Tumkor et al., 2001; Schledjewski and Latrille, 2003]. Many of the early studies included the heat due to crystallisation kinetics. AFP studies have found that this heat release is negligible compared to heat input from the main heat source [Pitchumani et al., 1996; Tierney and Gillespie, 2003; Schledjewski and Latrille, 2003; Toso et al., 2004], hence it can be safely omitted.

2.2.8.6 Laser source models

Carbon dioxide lasers with output powers of 65-80 W have been studied as a heat source for the closely related thermoplastic filament winding process [Pistor and

Güçeri, 1999; Pistor et al., 1999; Rosselli et al., 1997; Agarwal et al., 1992, 1996; Beyeler et al., 1988]. The typical output of such a laser is a small round spot at a wavelength of 10.6 µm. For composite processing, a line or rectangular distribution is preferred so as to produce uniform heating across the width of the tape and substrate. The round spot output of the source has been converted into line sources through the use of ZeSe lenses [Pistor and Güçeri, 1999; Rosselli et al., 1997; Agarwal et al., 1992, 1996; Beyeler et al., 1988; Funck and Neitzel, 1995] or galvanometer scanning [Pistor et al., 1999]. The resulting lines are no more than 2 mm in width, making the process extremely sensitive to the laser position [Beyeler et al., 1988] and the bond quality is adversely affected by short dwell times [Agarwal et al., 1992, 1996].

Filament winding differs from tape placement in that the laser source remains stationary and the laser can be aimed directly into the nip point as the mandrel is curved. In tape placement, the beam must aimed from an angle above the plane placement and therefore cannot be aimed directly into the nip point. A shadow cast by the consolidation roller as consequence of this limitation. Furthermore, high power carbon dioxide laser sources are too bulky for direct mounting on a placement head, and the long wavelength of the radiation is not suited to fibre optic delivery [Beyeler et al., 1988].

In more recent times near infra-red (NIR) diode lasers have been used as they are able to deliver higher heat fluxes, are more efficient and have a near instantaneous response which is ideal for process control [Khan et al., 2010]. Furthermore, the radiation can be delivered to compact, lightweight optics on a placement head via light cable owing to the lower wavelength (800-1000 nm) of the radiation. The laser tape placement system considered in this study uses utilises optics to produce an enlarged rectangular spot of uniform intensity, the size of which is position dependent due to beam divergence. The spot size typically used for a 12 mm tape is 40 mm long and 18 mm wide at a focal length of 127 mm, much larger than the spot sizes reported for carbon dioxide lasers. This allows for progressive and homogenous heating across

the length and width of the tape, as well as longer dwell times which enable higher placement rates. Thermal models for this type of laser tape placement process have not been reported in literature.

The majority of the literature concerning thermal modelling of laser TP-ATP has simply assumed uniform heat fluxes applied to the tape and substrate as a boundary condition [Sonmez and Hahn, 1997a,b; Agarwal et al., 1992; Beyeler and Güçeri, 1988; Nejhad et al., 1991; Nejhad, 1993]. In these studies the presence of a shadow not considered and the uniform heat flux considered to continue up to the nip point. For composite placement systems using a nip point heating strategy, the laser is aimed into a wedge shaped cavity formed by the tape and substrate (Figure 1.4). The laser is aimed at a moderate to high angle of incidence, resulting in potentially significant levels of reflection. In ATP, the laser optics must be mounted above the plane of placement to provide adequate clearance from the tooling. A consequence of this geometry is the curvature of the tape prior to the nip point blocks the laser beam from directly irradiating the substrate and tape immediately before the nip point, potentially creating a shaded region [Stokes-Griffin et al., 2013]. Previous studies suggest that a significant temperature drop would occur, adversely affecting the bond quality [Grouve, 2012; Stokes-Griffin et al., 2013]. It is possible that the high angles of incidence would cause significant reflections that would result in indirect irradiation of the shaded areas. It is of interest to investigate how the light interacts with the cavity and, if shadows exist, what influence do they have on the temperature history.

Grove [1988] attempted to model the reflection and shadowing behaviour for a laser tape placement process using simple geometric calculations in 2D for a laser source in the form of a 1 mm wide line. It was reported that the reflectance varied inconsistently with angle of incidence and position, ranging from 0.14 to 0.42. Details of the measurement wavelength or apparatus were not given. The average of the reflectance values was assumed for the geometric calculations which assume a specular (i.e. mirror-like, non-scattering) surface.

Grouve [2012] modelled NIR laser-assisted TP-ATP for welding Carbon/PPS unidirectional tapes to pre-manufactured woven laminates of the same material. The scattering behaviour from the composite was shown to be anisotropic, and measurements of the reflectance at various angles of incidence were performed using a photometer and a $\lambda = 980\,\text{nm}$ laser pointer. The measurement technique employed appears to measure only the specular component of the reflection. The angular dependence of the reflection was curve fit to Fresnel's equation yielding a refractive index of $n = 1.8$. A 2D ray tracing model was subsequently formulated assuming specular Fresnel reflections and a perfectly uniform, collimated laser source. A flexible compaction roller was used which deforms significantly during the process, however it is assumed to be a perfect cylinder in the optical model. An infrared camera was used to validate the results which were shown to agree well for the tape, however the substrate temperatures were significantly overestimated. This was attributed in part to the 2D simplification of the optical model and also the assumed thermal properties.

Few other experimental validations exist in the literature. Agarwal et al. [1992] modelled a CO_2 laser filament winding process. Experimental validation was performed using 12.7 µm foil thermocouples. It was found that the thermal model required approximately 1/5th of the power used in the experiments. This large discrepancy was partly explained by the reflected energy not being absorbed by the opposing surface, therefore it was suggested a 3D optical model is necessary.

2.3 Process simulation

This section describes the process simulations reported in literature. The simulations are based on implementations of various combinations of models for physical processes that occur during tape placement as reviewed in Section 2.2. Here, the simulations are grouped into parametric studies and process optimisations.

2.3.1 Parametric studies

Pitchumani et al. [1996] implemented an AFP process simulator which included a 2D FD thermal model, a void consolidation model developed in Ranganathan et al. [1995], as well as the intimate contact model of Mantell and Springer [1992] combined with a non-isothermal healing model Bastien and Gillespie [1991]. As discussed in Section 2.2, the healing model was shown in another study to be inaccurate for non-isothermal processes [Yang and Pitchumani, 2002a]. The intimate contact model was implemented with a different viscosity, therefore the validity of this model is uncertain. Validation of the thermal model was also not provided. Despite these facts, the model should still give valuable insight into the response of the process to various parameters. Increasing compaction force was shown to increase degree of bonding and reduces final void content in the composite. Increasing heat input increases bonding, but also increases final void content. Addition of an extra consolidation is predicted to improve the process considerably. Forced cooling may be needed to obtain parts with low void content in order to 'freeze' the voids.

Pitchumani et al. [1997] performed further studies, building on their previous model [Pitchumani et al., 1996] by adding the degradation model of Nam and Seferis [1992]. The degradation limit was chosen to be 0.04 % weight loss. Both time-optimal and strength-optimal parameter sets were determined, and found to be mutually exclusive. The process window was found to become narrower for higher gas torch temperatures. The heat sink effect of the mandrel resulted in very low levels of bonding for the first few layers, however as the thickness of the composite increases the self insulating effect results in higher degrees of bonding. This effect is much more pronounced at low speeds as there is more time for the heat to diffuse into the tooling. For higher speeds, this effect is greatly reduced and relatively uniform levels of bonding are predicted throughout the thickness. Despite this increased uniformity, the overall degree of bonding decreases by from 0.88 to 0.35 when increasing the placement rate from 10 mm/s to 70 mm/s. The degree of bonding plateaus when

the composite was more than 10 layers thick. The degree of degradation was shown to decrease significantly when increasing the placement rate, and increase with the number of layers due to the longer residence time at high temperatures due to the self-insulating effect. The void fraction for the 6th layer and above was found to increase from 0.10 to 0.26 when increasing the speed from 10 mm/s to 70 mm/s. The void fraction in the lower plies was predicted to be very high ranging from 0.2 to 0.55 over the same range of speeds. This is because the material cools faster and compresses more slowly under the consolidation roller. This also implies that longer pressure application is required to achieve acceptable levels of intimate contact.

Sonmez and Hahn [1997b] formulated a process simulator for a hot gas placement process. A 2D FE thermal model was combined with a degradation [Nam and Seferis, 1992] and crystallinity [Choe and Lee, 1989] model. The thermal model was verified against a simple analytical model [Nejhad et al., 1991], but no experimental validations were performed. They concluded that the tape placement process is highly complex with a large number of process variables and continually changing boundary conditions, and no straightforward rules can be used for determining the best process parameters for a given situation. Higher levels of degradation were predicted at low speed due to the increased exposure. Increasing the placement rate for a fixed heated length results in shorter dwell times, reducing the level of bonding. Preheating of the substrate was found to be beneficial due to the decreased cooling rates, and therefore increased dwell time. Low placement rates and preheating of the substrate to temperatures in the region of the glass transition resulted in optimum levels of crystallinity.

Sonmez and Hahn [1997a] added a stress model to their previously developed process simulation [Sonmez and Hahn, 1997b] enabling determination of the combined temperature and pressure histories. The intimate contact model of Mantell and Springer [1992] was combined with their own non-isothermal healing approximation for bond strength prediction. Degradation [Nam and Seferis, 1992] and crystallinity

[Choe and Lee, 1989] models were also included. The effects of preheat temperature, heated length, roller radius, laminate thickness and heated length ratio were studied. A simulations found that a placement head using a single roller could produce good quality laminates at speeds up to 30 mm/s, however addition of a secondary roller allows speeds upwards of 50 mm/s. The process was found to respond positively to preheating of the substrate, however preheating of the roller and tape had little effect. Increasing the heated length was found to be beneficial up until a length of 20 mm, beyond which the benefit was small. Longer heated lengths increased the heat soak and therefore the dwell time at temperatures sufficient for bond development increased. A 5:1 ratio of heat input on the substrate vs. the tape was found to result in the best properties. Larger roller diameters result in longer periods of pressure application, resulting in better consolidation. The optimal placement rate for the first few layers was low (5 mm/s) due to the heat sink of the tooling, however after the 6th layer was placed the rate plateaued at 17.5 mm/s. The quality in each layer is developed over subsequent passes, and thus the final layer must applied at low speed as it does not receive any subsequent thermal history.

Khan et al. [2013] performed parametric studies using their previously developed process simulator [Schledjewski and Latrille, 2003]. The model was updated with the intimate contact of Yang and Pitchumani [2001a], the healing model of Yang and Pitchumani [2002a] and the degradation model of Nicodeau et al. [2006]. As discussed in Section 2.2.5, there is some doubt that the cross-linking degradtion model of Nicodeau et al. [2006] is appropriate for an AFP process due to the very short time periods involved. A variety of process configurations were considered in the study such as the effect of various consolidation devices including single roller, multiple roller and line compactor, the effect of the material properties, and also process parameters such as placement rate, heated length and tool temperature. It was found that parameters which result in greater heat soak would increase the level of bonding, however the void content would also increase. Larger rollers and line

compactors with longer contact lengths increase both the degree of bonding and decrease the void content, however only if the force is correspondingly increased so as to maintain the pressure. High tool temperatures and thick laminates (due to the self-insulating effect) increase the level of bonding due to longer dwell times. Prepregs with low surface roughness improve both bonding and void content.

Various parametric studies have been performed to analyse the process using various combinations of the models for different aspects of quality. The majority of these studies have used simplified 2D thermal models and consider head a head placing PEEK with a single rigid roller and a hot gas gun. Often models are used which have not been experimentally validated, or validated models are adapted yet different input parameters are used. These studies however provide a better understanding of the fundamental behaviours and effects of the process parameters on quality for AFP processes.

2.3.2 Process optimisations

The highly non-linear behaviour and the number of aspects of quality to consider make optimisation of the process difficult. Few studies have appeared in literature. Mazumdar and Hoa [1995] applied the Taguchi method to a CO_2 laser filament winding process for carbon/PEEK composites. Three factors were considered (laser power, consolidation force and placement rate) at three different levels. Short beam strength (SBS) tests were used as the quality characteristic. The relative contributions of the three factors were found to be 79.1, 2.7 and 17.1 % for the laser power, consolidation force and placement rate respectively. While this study shows the sensitivity of the process to various factors, the optimal parameters only relate to the particular manufacturing system. Furthermore this method treats the system as a black box, and it is not known what the limiting factors are in the process and how the design of the system could be further improved. Aized and Shirinzadeh [2011] applied the response surface method to a carbon/PPS AFP process. The material quality char-

acteristics were analysed qualitatively in terms of adhesion of the first ply to the tooling, adhesion of the tows within the laminate and the substrate remaining in contact. Quantitative measurements such as mechanical properties or void content were performed.

Heider et al. [2003] implemented an artificial neural network (ANN) for on-line process optimisation of the AFP process. The ANN was first trained off-line using the bonding and void dynamics models from the literature. This then allowed online predictions of to be executed 100,000 times faster, allowing for rapid determination of optimal process parameters. Virtual panels were then produced with and without the ANN based controller. The resulting quality predictions for the ANN component were shown to be superior.

Sonmez and Akbulut [2007] used a Nelder-Mead zeroth-order approach for optimisation of a hot gas AFP process which considered bonding, degradation and residual stress. Void dynamics and crystallinity were not considered. They implemented the Mantell and Springer [1992] intimate contact model combined with their previously developed non-isothermal healing approximation [Sonmez and Hahn, 1997a]. This combination of models for the bonding process was not experimentally validated, and the intimate contact model [Mantell and Springer, 1992] displayed large discrepancies with experimental results in Mantell et al. [1992]. Based on those experimental results of that study however, it is likely that the strength will be significantly underestimated. Results of the optimisation predicted that with a goal of achieving minimal residual stress, the placement rate had to be very low with speeds in the range of 4 mm/s. Bonding was predicted to be fully developed, and degradation was within acceptable levels. For maximisation of the placement rate, a minimum degree of bonding was imposed with a value of 0.8. The maximum placement rate was found to be 80 mm/s] while maintaining the minimum bonding requirement and keeping the level of degradation weight loss below 0.01 %. This is different to the value of 0.04 % chosen in the study by Pitchumani et al. [1997]. From this study it

is clear that optimisation of the process depends on the particular goals set for each aspect of quality, as well as the required placement rate.

2.4 Conclusions

The fundamental process of bond strength development in thermoplastic composite processing is a combination of intimate contact development and healing. Various models have been presented, including non-isothermal formulations that are required for a highly dynamic process such as thermoplastic AFP. Limited experimental validations of coupled bonding models have been performed, and the temperature and pressure distributions applied to these models have been determined using thermal and pressure models that have not been comprehensively validated. A large number of thermal models have been presented in the literature but few provide a satisfactory validation of their accuracy.

Despite the limited validation of thermal models and coupled bonding models for AFP processes, a large number of parametric simulations have been studied adapting various models from the literature and assuming various non-validated input parameters. While these studies have provided valuable insight into the fundamental behaviours of the process, there is a risk that they have led to gross underestimation of the potential of the thermoplastic AFP process.

In order for the technology to be accepted, the understanding of the process needs to have matured to the point where full quality predictions can be made for real components in real manufacturing processes. Due to the complexity of the process and its strong dependence on thermal history, it is anticipated that process optimisation should be integrated with the path placement planning software. This way the full thermal history of the tape and tooling is captured, and the thermal effects of recently placed tape are taken into consideration.

Although imperative for complete quality prediction, to date there has not been a single study or simulation tool that has encompassed all of the aspects of quality

as described in this chapter. Models exist in the literature to create a process model capable of full material quality prediction, however this is yet to be implemented. Further model validations are also required to confirm the validity of the models for the highly non-isothermal laser AFP process. At the stage when models have been comprehensively validated, a virtual process model can be constructed. Virtual process models can then be used to rapidly optimise the placement head configuration in terms of consolidation devices and heat flux distributions, therefore the placement head can be refined for the process rather than optimising process parameters for a given placement head design as has been done previously.

The first step towards a virtual process model is to first be able to predict the bond strength using input parameters that are independent of a particular head configuration, rather than having a model that is 'tuned' to a particular head design as is the case with most models implemented in literature. It is therefore identified in this work that coupled bonding models need to be formulated and validated using *experimentally* measured temperature and pressure histories as model inputs, rather than pressure and temperature histories predicted by lightly validated models. From this it can be determined whether the current non-isothermal formulations are appropriate for the extremely dynamic thermoplastic AFP process. As the process is highly dependent on the temperature history not only at the bond interface, but also at the interfaces of previous plies, it is also necessary to develop an accurate thermal model and validate not only the surface temperature but also the through-thickness temperature history.

To date, there have been no detailed models for the laser heating of composite materials for a TP-AFP process. The best approaches have been 2D ray tracing calculations assuming specular behaviour. When observing the surface of a carbon fibre composite, no mirror-like reflections can be seen as the fibrous nature of the carbon fibre prepreg causes light to be scattered in all directions, thus a specular surface and 2D calculations are likely to be innaccurate assumptions. Development of a 3D

model for predicting the interaction of the light with the placement cavity is identified as an area to be researched within this thesis. Implementation of such a model should provide a better understanding of the laser heating process in general, and also allow for more accurate predictions of the temperature history in the laser AFP process.

Chapter 3

Thermal Model

Abstract

A 2D finite element thermal model incorporating the mass transport of heat was formulated for laser AFP of carbon/PEEK using a conformable consolidation roller. Previous studies have assumed rollers to be a convective boundary or simply a fixed boundary temperature. Here, the interaction of the consolidation roller will be investigated in detail, with it modelled as a physical body. The positioning of the laser potentially results in a shadow near the nip point. The effect of the consolidation roller shape on the shadow is also a topic of investigation. Effects such as the roller shape on the laser. In situ temperature measurements are performed using a fine wire K-type thermocouples. The model was compared with the thermocouple measurement and found to correlate reasonably well, particularly in terms of timing of the heated, shaded, consolidation and cooling regions with respect to each other, however experimental temperature measurements imply higher tape temperature than modelled. The presence of the shaded region results in significant cooling of the surface prior to the nip point, particularly on the incoming tape. This suggests that significant overheating is required in order to achieve the necessary nip point temperatures for bonding.

3.1 Introduction

The thermal models for other heat sources in the tape placement literature assume rigid metallic rollers. The rollers have been approximated as a convective boundary condition with vastly differing heat transfer coefficients of $400\,W \cdot K/m^2$ [Sonmez and Hahn, 1997b] $500\,W \cdot K/m^2$ [Agarwal et al., 1992; Grove, 1988; Beyeler and Güçeri, 1988], $1000\,W \cdot K/m^2$ [Kim et al., 1996; Tumkor et al., 2001] $1500\,W \cdot K/m^2$ [Khan and Schledjewski, 2010] or simply a fixed boundary temperature [Tierney and Gillespie, 2003]. A search of the literature found no studies that model the roller as a physical body and analyse its relative influence. Conformable rollers allow for placement on curved surfaces and irregular geometry. They can provide much longer and more uniform pressure distributions (Figure 3.1). The result is an increase in the amount of time available for consolidation for a given process speed, as well as a much larger area of thermal contact with the roller. Since the process is highly dependent on the post-nip point temperature history it is therefore of interest to model the effect of this contact on the thermal history. The thermal interface between the roller and composite is likely to be imperfect, resulting in a thermal contact resistance. Published values of contact resistance between thermoplastic composites and elastomeric materials are not readily found, and determination of such values is not straightforward. It is therefore necessary to also investigate the response of the process to variations of the interfacial thermal contact resistance.

This chapter will 1) present a thermal model of the NIR laser-assisted tape placement process utilising a conformable elastomeric roller 2) present an initial experimental validation and 3) investigate the effects of the roller geometry, roller temperature and roller-to-composite contact resistance on the post nip point temperature distributions. In contrast to earlier studies where the roller is modelled as a boundary condition, the roller will be physically modelled.

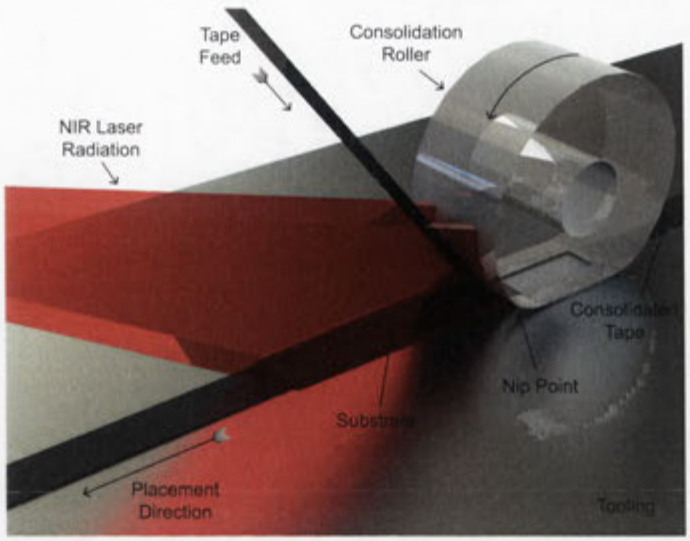


Figure 3.1 – Laser-assisted tape placement process showing typical laser beam propagation and conformable roller.

3.1.1 Methodology

The layout of the placement system in question is shown in Figure 3.1. A rectangular laser spot is aimed at the nip point. The spot overshoots the width of the tape by 2 mm per side to ensure uniform temperature across the width of the consolidation zone. The size of the laser spot is dependent on the position due to beam divergence. The tape is fed at an angle of approximately 50°. Consolidation pressure is applied with a conformable roller which deforms significantly. In this study a single tape is placed at rate of 133 mm/s onto a 25 ply unidirectional laminate. As the rectangular spot of the laser heats the tape evenly across the width, and the transverse thermal diffusivity is low, it is assumed that a 2D model is therefore sufficient to model the system for the purpose of this study.

Various 1D simplifications [Khan and Schledjewski, 2010; Tierney and Gillespie, 2003] have been made in the literature as the heat flow in the process direction is small compared to the mass flows. The most common approach is a 2D model with an Eulerian frame of reference attached to the placement head and this approach has been justified when the tape and substrate are heated uniformly across the width [Sonmez and Hahn, 1997b; Agarwal et al., 1992; Grove, 1988; Nejhad et al., 1991;

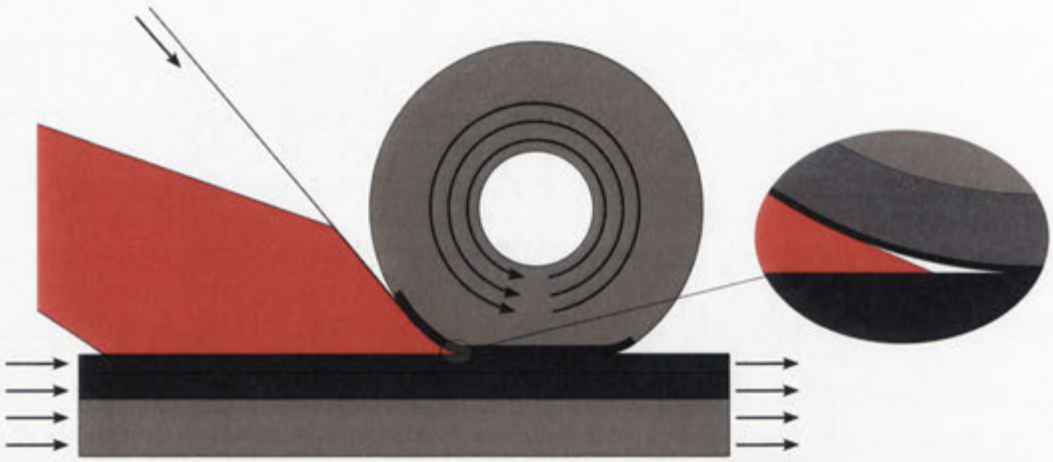


Figure 3.2 – Arrows indicate the mass flows. Reduced geometry (dark grey) overlayed on the original geometry (light grey). The positioning of the laser causes a small shaded region prior to the nip point.

Beyeler and Güçeri, 1988; Sarrazin and Springer, 1995]. Kim et al. [1996] suggest a 3D model for non-uniform hot gas impingement. In this study the tape and substrate are heated uniformly across the width, therefore a nonlinear steady-state 2D finite element approach was implemented in *ANSYS 13.0*. The reference frame for the analysis was fixed to the placement head. Due to the translation of the head during placement, the tooling, tape and substrate pass through the reference frame as indicated by the arrows in Figure 3.2. The roller is also rotating within the reference frame, carrying heat away from the nip point. These mass flows are significant and therefore must be taken into consideration. *ANSYS* thermal element type *PLANE55* is a first order quadrilateral element capable of mass transport heat flow for constant velocity fields. This is taken into account by adding a velocity vector to the thermal energy balance equation so as to include the mass transport of heat. In the case of a 2D analysis the generalised partial differential equation is of the form:

$$\rho c \left(\frac{\partial T}{\partial t} + v_x \frac{\partial T}{\partial x} + v_y \frac{\partial T}{\partial y} \right) = \ddot{q} + \frac{\partial}{\partial x} \left(K_x \frac{\partial T}{\partial x} \right) + \frac{\partial}{\partial y} \left(K_y \frac{\partial T}{\partial y} \right) \tag{3.1}$$

The size of the elements must be sufficiently small to prevent oscillations in the

solution. The solution is valid for Peclet numbers less than unity [Gresho and Lee, 1981]. The Peclet number is defined as follows:

$$Pe = \frac{vl}{2\alpha} \tag{3.2}$$

Thus the maximum element dimension (l) aligned with the flow vector is dependent on the thermal diffusivity (α) of the material and the magnitude of velocity (v). The maximum element dimensions for the materials used in the current model were calculated and are shown in Table 3.1.

Table 3.1 – Maximum element dimensions in direction of flow for $v = 133\,\mathrm{mm/s}$.

	Unit	AS4/PEEK 61 % v/v axial [Cogswell, 1992]	Roller Elastomer	Aluminium (Tooling)
Thermal Diffusivity	$[m^2/s]$	2.70×10^{-6}	1.15×10^{-7}	9.29×10^{-5}
Maximum element dimension	[mm]	4.05×10^{-2}	1.73×10^{-3}	1.39

It can be seen that the mesh must be extremely fine in the direction of the mass flow for the roller. To minimise computational effort, the elements for the roller are meshed with high aspect ratios in the areas away from the contact boundary. The size requirement for the composite is also relatively small.

3.1.2 Model geometry

Due to the small element sizes required, particularly in the case of the roller, a large number of elements are required to achieve a valid solution. Due to the very low thermal diffusivity of the roller elastomer and the relatively fast mass transport it was found that the temperature distribution has a small penetration into the roller. Iterative geometry reductions found that the roller geometry could be modelled as a slender strip of material along the boundary of the tape (Figure 3.2). The tooling could also be reduced in a similar fashion.

The dimensions of the reduced geometry are shown in Figure 3.3. The geometry

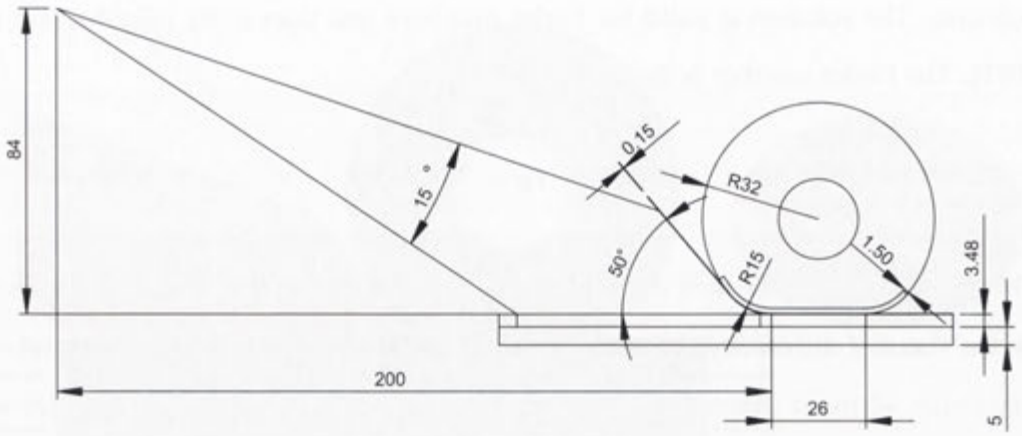


Figure 3.3 – Dimensions of the reduced model geometry [mm].

of the irradiated region was estimated from process monitoring videos recorded by a camera mounted on the placement head. Note the shape of the conformed roller is modelled as a chord of the undeformed roller shape with radiused corners. Detail of the refined mesh is shown in Figure 3.4. A large number of elements was required to meet the required Peclet number as well as a converged result for the through thickness temperature distribution. The roller, composite and tooling contain 1.3, 0.4 and 0.2 million elements respectively.

3.1.3 Mass transport

Mass flow was assumed to be uniform and laminar, therefore the placement velocity was assigned to the elements in regions of linear flow such as the tooling, substrate and tape feed. In the regions where the material moves in a curved path (such as the roller and the tape prior to the nip point), local cylindrical coordinate systems were defined for each respective region of curvature. Velocity is assigned to each elements based on the radial distance from the local origin, so as to maintain a constant angular velocity.

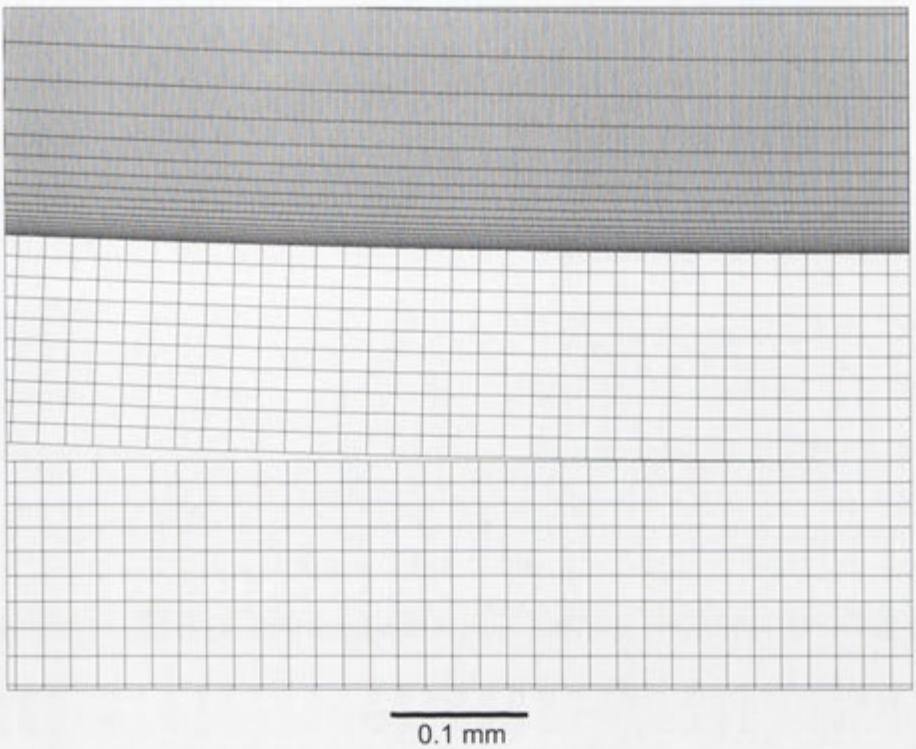


Figure 3.4 – Detail of the roller, tape and substrate mesh at the nip point.

3.1.4 Laser heat flux

The typical mounting location for the laser creates a shaded region just prior to the nip point (Figure 3.2). The literature for in situ laser processing of composites assumes uniform heat flux distributions in the nip point region to approximate the laser heat input, excluding any effects of shadowing. Exceptions are the studies by Grove [1988]; Grouve [2012] where 2D ray tracing calculations were used to predict the heat flux distributions. Agarwal et al. [1992] found large discrepancies between the experimental and modelled laser power requirement, which was attributed to reflections. For this model, radiation was simplified as a uniform heat flux over the illuminated regions, therefore taking the shaded regions into consideration. The degree of overshoot of the laser spot across the width of the tape and the absorptivity of the material was not known; therefore it was not possible to accurately calculate the incident heat flux. The focus of this chapter is to develop a thermal model and

Table 3.2 – Temperature dependent convective heat transfer coefficients.

Surface Temperature °C	Convective heat transfer coefficient (h) W/(m^2 · °C)
20	5.0
50	9.9
100	12.6
150	14.1
200	15.3
300	17.1

investigate the effect of the consolidation roller on the post nip point history. Therefore accurate determination of the laser heat flux is beyond the scope of this chapter, however this topic will be revisited and investigated in great detail in Chapters 5 and 6. In this initial case, the heat flux was adjusted so as to match the nip point temperature recorded in the experimental work.

3.1.5 Radiation

Thermal radiative losses were not considered as the maximum heat flux calculated based on a black-body losses to the ambient environment are less than one percent of the laser flux.

3.1.6 Convection

Convection loads were applied to all surfaces exposed to the ambient environment. Laminar natural convection on a horizontal plate was assumed for calculation. Eq. (3.3) is suitable for such conditions [Holman, 2002].

$$h = 1.32 \left(\frac{\Delta T}{L} \right)^{1/4} \tag{3.3}$$

Convection coefficients were subsequently calculated for a characteristic length $L = 0.01$ m under ambient conditions. The coefficients are listed in Table 3.2.

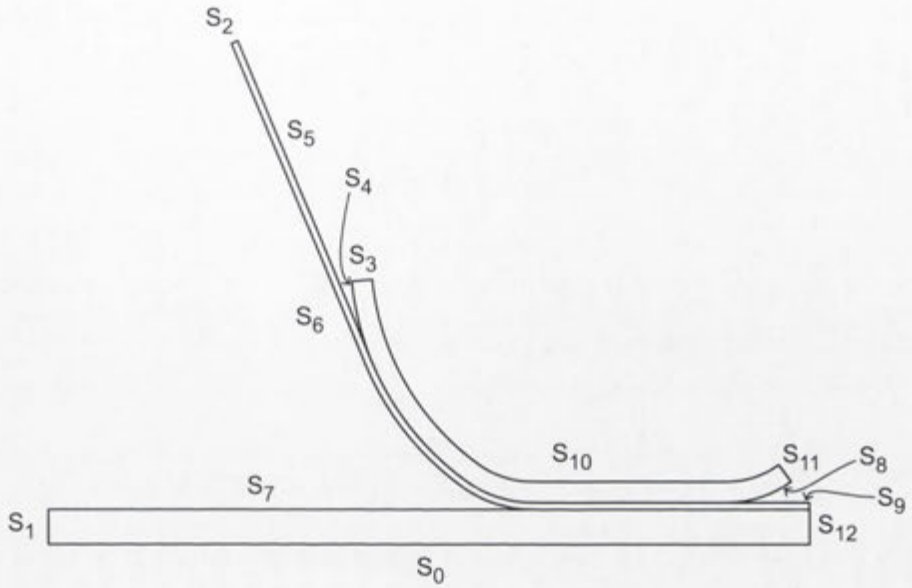


Figure 3.5 – Thermal model boundary locations.

3.1.7 Contacts and boundary conditions

The substrate is assumed to be a perfect 25 ply unidirectional laminate with no interlaminar thermal contact resistances. The heat effects due to crystallisation kinetics were not included as they are insignificant compared with the laser heat flux required for the studied placement rate.

Refering to Figure 3.5, the boundary conditions are described as follows:

The boundary S_0 is the base of the composite substrate in contact with an aluminium tooling plate. Due to the large thermal mass of the tool, a fixed temperature boundary condition was assumed where:

$$T = T_{tool} = 20\,^{\circ}\mathrm{C} \quad \text{on } S_0 \tag{3.4}$$

The mass flow inlet boundaries S_1 and S_2 for the substrate and tape respectively were assumed to be at ambient temperature.

$$T = T_{amb} = 20\,^{\circ}\mathrm{C} \quad \text{on } S_1 \text{ and } S_2 \tag{3.5}$$

The roller mass flow inlet boundary S_3 was assumed to be a fixed temperature boundary condition at 50 °C, approxmiated from LWIR camera images.

$$T = T_{roller} = 50\,^{\circ}\mathrm{C} \quad \text{on } S_3 \tag{3.6}$$

The boundaries exposed to the ambient environment (S_4–S_9) were assumed to have a convective heat transfer boundary condition.

$$k_t \frac{\partial T}{\partial y} = -h(T - T_{amb}) \quad \text{on } S_4\text{–}S_9 \tag{3.7}$$

Where k_t is the transverse thermal conductivity of the material and h is the convective heat transfer coefficient, which was determined in Section 3.1.6.

Select areas of the boundaries S_6 and S_7 are also irradiated by the laser. In this initial study, the laser heat flux is assumed to be uniform. The position dependent irradiance values $q_{(x)}$ were determined geometrically, and include a shadow prior to the nip point on the tape and substrate.

$$k_t \frac{\partial T}{\partial y} = -q_{(x)} \quad \text{on irradiated areas of } S_6 \text{ and } S_7 \tag{3.8}$$

The inside boundary of the roller S_{10} was assumed to have a zero temperature gradient (perfectly insulated) boundary condition, as are the mass flow outlet boundaries S_{11} and S_{12}.

$$\frac{\partial T}{\partial x} = 0 \quad \text{on } S_{10}, S_{11} \text{ and } S_{12} \tag{3.9}$$

Perfect contact was assumed initially for the roller-to-composite interface. The tape and substrate were assumed to be in perfect contact after the nip point, justified by the high surface quality of the prepreg used, the high surface temperatures and the pressure application from the conformable the roller.

3.1.8 Material properties

Suprem™ *T* 60 % v/v AS4/PEEK-150 0.15 mm × 12 mm unidirectional prepreg tape was used in the experimental work. The specific thermal properties of this particular system were not available. The properties for an AS4/PEEK 61 % v/v unidirectional tape were assumed as found in Table 3.3. Levy et al. [2014b] demonstrated that the degree of intimate contact can introduce a thermal contact resistance between the plies of a laminate. The experiments were performed at low pressures (1.34 kPa with *Cytec APC-2* prepreg which is has both high surface roughness and a significant intralaminar void fraction. Furthermore, crossply laminates were manufactured using wide prepreg tapes. The *Suprem* prepreg used in this work typically has a much smoother surface [Khan et al., 2010] and the average consolidation pressure under the roller was measured to be 180 kPa. Unidirectional laminates were manufactured, which would result in tow nesting that would result in more rapid intimate contact development. For the purposes of this study it is therefore assumed that perfect contact exists between the tape and substrate after the nip point.

3.1.9 Sensitivity analysis

The effects of the roller temperature, contact resistance and corner radius were studied individually with respect to the default parameters (indicated in bold, Table V). The roller temperature was adjusted at the mass flow inlet boundary. Contact resistances were applied at the boundary between the roller and the composite. Various corner radii were applied while maintaining the same laser position relative to the nip point. Slight changes in the total irradiated length occur due to the change in size of the shaded region. The heat flux was adjusted accordingly so as the total heat input remained constant between the studies. The studied values are listed in Table 3.4.

Table 3.3 – Temperature dependent material properties.

Temperature °C	Specific Heat J/(kg · °C)	Density kg/m^3	Thermal Conductivity (Axial) W/(m · °C)	Thermal Conductivity (Transverse) W/(m · °C)
AS4/PEEK 61 % v/v composite tape [Cogswell, 1992]:				
0	800	1601	3.5	0.42
50	930	1598	4.6	0.52
100	1040	1593	5.1	0.6
150	1260	1586	5.9	0.7
200	1300	1575	5.9	0.7
250	1400	1563	6.1	0.7
300	1550	1551	6.7	0.75
350	1650	1537	6.8	0.68
400	1700	1524	7.0	0.65
Roller Elastomer:				
–	1255	1250	0.18	0.18
Aluminium Tooling:				
–	951	2689	237.5	237.5

Table 3.4 – Parameters used for each of the three sensitivity studies (default parameters indicated in bold).

Roller corner radius mm	Roller contact resistance m^2 · K/kW	Roller temperature °C
5.0	**0.0**	40
7.5	0.5	**100**
10	1.0	200
12	2.0	300
15	5.0	

3.2 Experimental work

3.2.1 Laser AFP cell

Composite placement experiments for this thesis were performed at AFPT GmbH. at their facility located in Dörth, Germany. The placement head was mounted on an *ABB IRB-6600* series robot as seen in Figure 3.6. The robot is mounted on a linear axis, allowing the robot to traverse the length of the placement cell. A fibre coupled near infra-red diode laser source was located outside the work cell. It has a maximum optical output power of 3.0 kW divided between two wavelengths of (λ = 940 nm and λ = 980 nm). An optical cable connects the source to the placement head within the work cell. Optics on the placement head convert the beam into divergent rectangular geometry. An optical module that is commonly used on the head produces a homogenous rectangular spot 40 mm × 18 mm in size at a working distance of 127 mm. The temperature on the surfaces of the tape and substrate prior to the nip point were monitored by non-contact temperature measurement using a LWIR sensor array. Based on this measurement, a control system regulates the laser power so as to maintain a user set constant surface temperature. The angle of the laser optics is also controlled so as to maintain even temperature between the tape and substrate. Consolidation force is applied to a 64 mm diameter conformable silicone roller using a pair of 40 mm diameter pneumatic cylinders, actuated by a pressure regulated supply so as to maintain a constant consolidation force. The silicone elastomer is transparent to NIR radiation, thus no damage is incurred by the laser even at high power levels.

It should be noted that the temperature measurements for the process control are performed on the surface of the composite prior to the nip point, and the correlation between the pre-nip point surface temperature and the post nip point temperature (in the consolidation zone) is not known. This is identified as a topic to be investigated in this thesis.

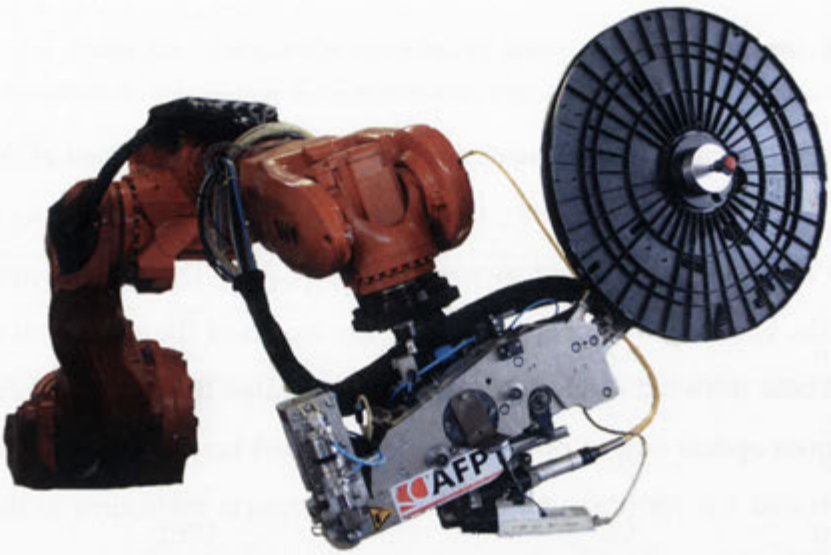


Figure 3.6 – AFPT prototype laser placement head mounted on an *ABB IRB-6600* series robot. The robot was mounted on a linear axis allowing it to traverse the work cell. Note the yellow laser delivery cable.

3.2.2 Experimental method

In this study, the temperature along the bond interface where consolidation takes place is of interest. Non-contact methods such as thermal imaging are not feasible for measurement of the bond line temperature as it is not externally viewable. The temperature must therefore be measured directly in situ. In this study, the temperature measurements were realised by affixing thermocouples directly to the surface of the substrate.

Due to the rapid placement rates and high heat inputs, temperature gradients can exceed 1000 °C/s in laser tape placement. It is therefore necessary to use thermocouples with very short response times, typically achieved by minimising thermal mass. In this work, 12.7 µm foil and 25 µm unsheathed fine wire K-type thermocouples were selected as they have a very short response times. They were sourced from *OMEGA® Engineering Inc.* and the part numbers were *CO2-K* and *CHAL-001* respec-

tively. The maximum service temperatures for the foil and fine wire thermocouples are 650 °C and 890 °C respectively for short periods of time, well above the expected substrate temperatures.

The thermocouple measurements were logged using a *National Instruments cDAQ-9213* 16-channel thermocouple data acquisition module. Shielded thermocouple extension wires were used to connect the thermocouples to the acquisition module which is placed out of sight to prevent stray radiation heating the unit and causing cold junction errors. The system was configured to perform measurements at 100 Hz on each channel.

Initially a single ply of *Suprem*™ *T* 60 % v/v AS4/PEEK-150 0.15 mm × 12 mm tape was affixed to the surface of the tooling at each extremity of the 700 mm × 300 mm × 16 mm aluminium tooling plate using a technical adhesive tape. As discussed in the literature review Section 2.3, the process is known to be sensitive to the tooling for the first few layers. In order to simplify the thermal behaviour for the model and validation, it was decided to perform temperature measurements on a twenty-five ply laminate. Twenty-four plies were then placed at 133 mm/s with a process control temperature of 383 °C. The result is a 25 ply unidirectional laminate. The thickness of the laminate was measured to be 3.48 mm and subsequently applied to the model geometry.

The thermocouples were then welded to the centre of the substrate surface Figure 3.7 of the composite using a soldering iron so as to maximise thermal contact without the use of adhesives that may influence the measurement for reasons such as differing thermal or laser absorption properties. The temperature was logged while a single tape was placed on the substrate with the same process parameters. While the foil type thermocouple has a faster response time, it also has a relatively large surface area in comparison with the fine wire thermocouple and is therefore expected to reflect the laser to some degree. This would locally influence the amount of absorption and therefore the temperature on the surface in the vicinity of the measurement.

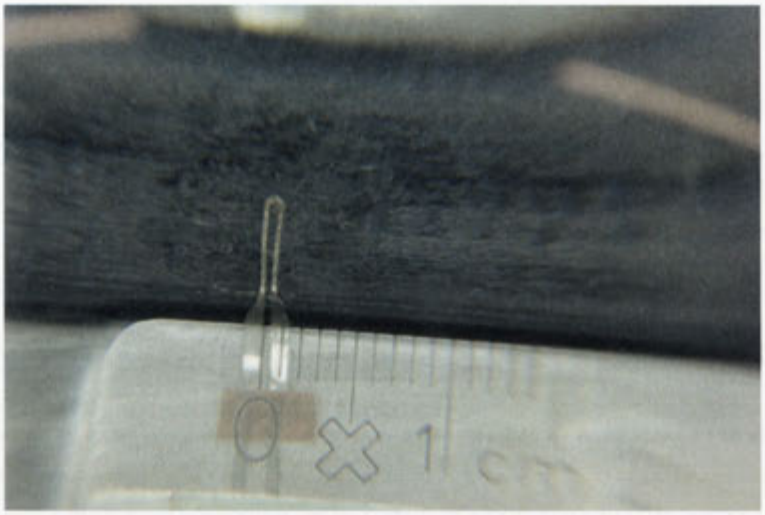


Figure 3.7 – Foil type thermocouple installed on the surface of the 25 ply laminate.

The data acquisition module was connected to a computer outside the work cell via an Ethernet cable. It was allowed to reach stable operating temperature for 30 minutes. Peak-to-peak noise was measured to be 0.5 °C on the connected channels. A single tape was then placed on the substrate at 133 mm/s with a process control temperature of 383 °C.

3.3 Results and discussion

The temperature plot for the default model parameters is shown in Figure 3.8. The model predicts localised surface heating of the composite with shallow penetration of the heat into the substrate and roller at the time of placement. This is due to a combination of the relatively fast motion of the placement head and the low transverse thermal diffusivity of the composite and roller. The incoming tape is heated quite uniformly through thickness prior to contact with the roller as the convective heat losses on both sides of the tape are insignificant compared with the heat input from the laser. When the tape contacts the roller some dissipation of heat occurs although the heat sink effect is small due to the low thermal diffusivity of the roller. Significant cooling of the tape surface is also predicted with the tape reaching maximum

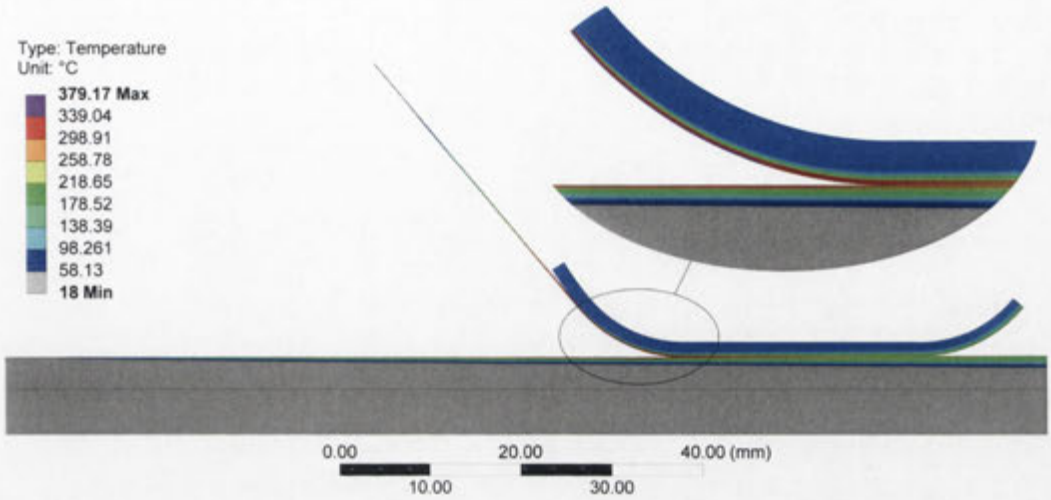


Figure 3.8 – Temperature distribution for the default model parameters.

of 380 °C on the surface during heating yet dropping to 310 °C immediately prior to the nip point. This is due to the dissipation of the heat away from the surface in the shaded region. A similar effect is observed on the substrate, however the shaded region is approximately half the size thus the effect is not as large. This result suggests that significant overheating is required in order to achieve the nip point temperatures necessary for bonding, given the presence of a shaded region.

The measured substrate temperature is plotted in Figure 3.9 along with the model prediction. There is good agreement between the measured data and the prediction in terms of the timing of the events as shown by the notation in Figure 3.9, indicating the validity of the modelled geometry. The step at the start of the consolidation region is due the temperature differential between the tape and substrate. The prediction shows a hotter substrate coming into contact with a colder tape, whereas the measured data shows the opposite. This likely caused by the underestimation of the heated length on the incoming tape. Further experimental work is required to confirm incoming tape temperature profile.

The step in the measured data at the onset of irradiation is most likely due to out of focus radiation, however the model assumes uniform intensity on illuminated areas. It is clear that an optical ray-tracing model is required to predict the flux

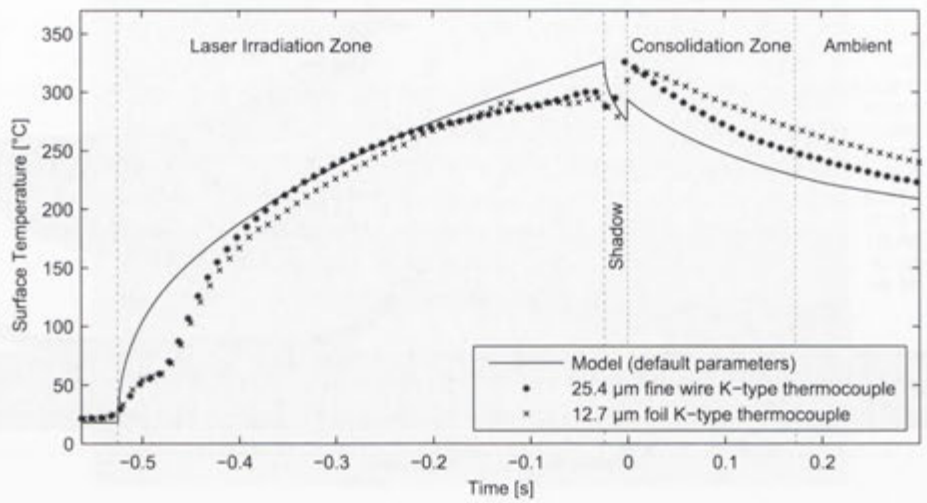


Figure 3.9 – Temperature plot for the default model parameters compared with experimental thermocouple measurements.

distribution of the laser in order to accurately predict the temperature history prior to the nip point. The sudden drop in temperature in the shaded region prior to the nip point is due to dissipation of the heat away from the surface of the substrate as can be seen in Figure 3.10. The measurements suggest that this shadow does exist, however it is hard to confirm given the limited number of data points in the predicted shaded region.

3.3.1 Sensitivity analysis

The effect of the roller temperature is shown in Figure 3.11. It can be seen that higher roller temperatures have two dominant effects. The first is an increase in the incoming tape temperature as there is less heat loss to the roller as the tape approaches the nip point as can also be seen in the temperature plots in Figure 3.10. This is reflected by the larger discontinuity in temperature at the nip point followed by a higher bond line temperature immediately afterwards. The second effect is to lower rates of cooling on the bond line. This is logical as the heat sink effect is reduced. When comparing only the relative slope of the experimental data with the predictions, it would appear that the roller is at a relatively low temperature in the

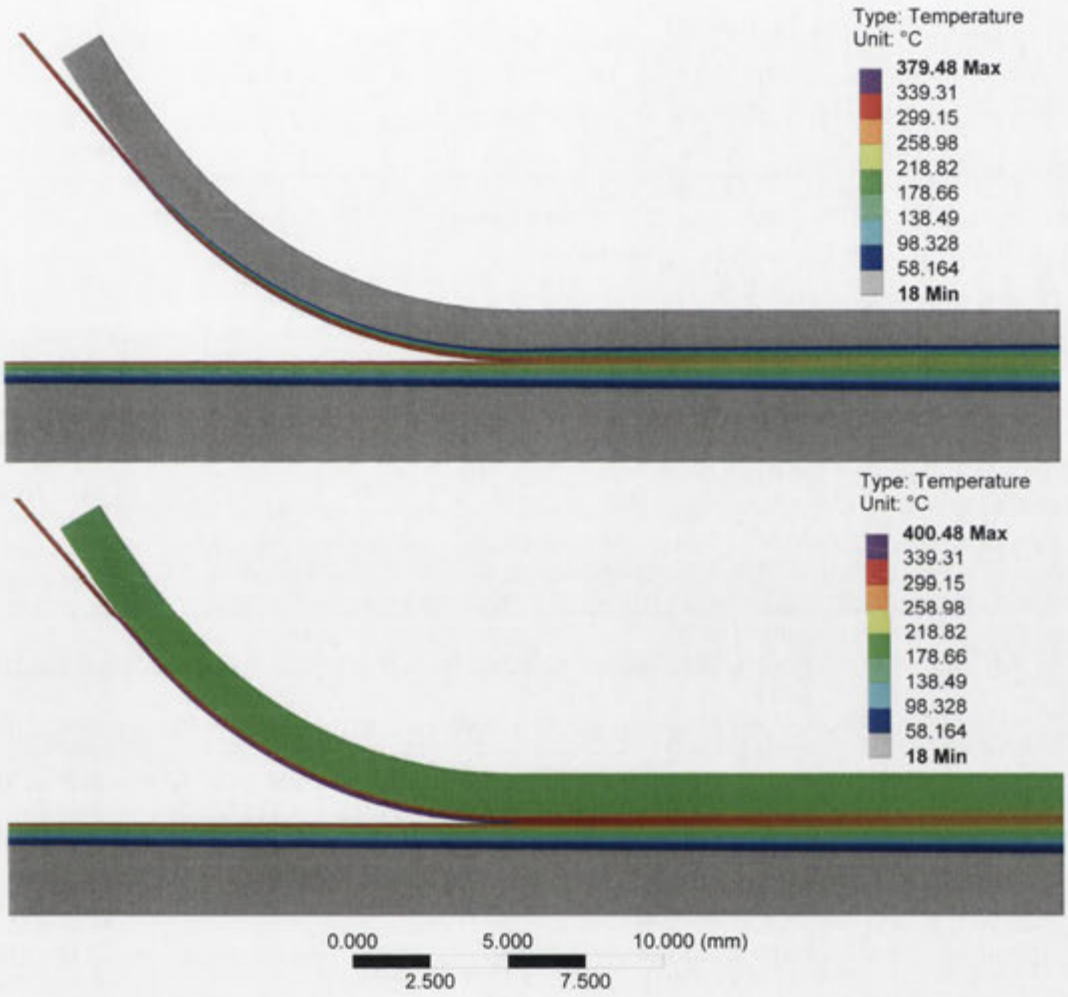


Figure 3.10 – Temperature plots for roller temperatures of 40 °C (above) and 200 °C (below). Note the incoming tape is heated through thickness however the substrate has a large gradient through thickness.

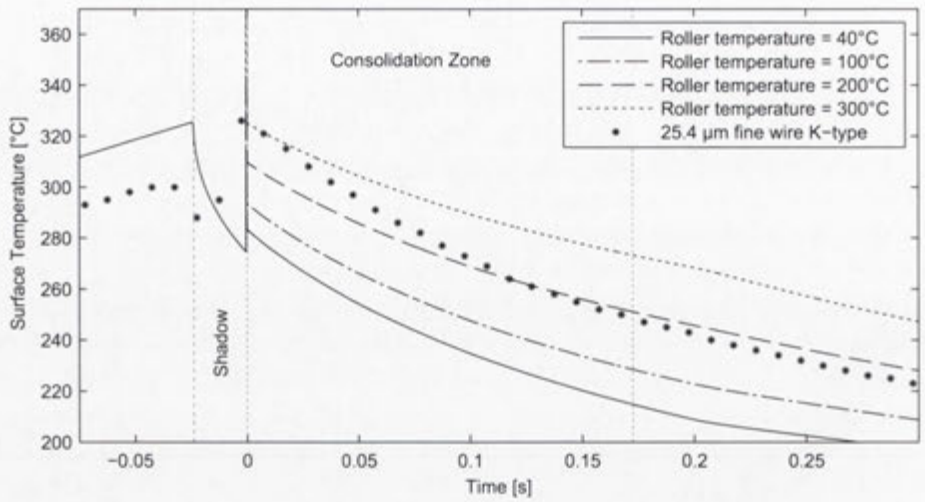


Figure 3.11 – Effect of roller temperature.

range of 40 °C during the experiments. It is of interest to note that the 300 °C roller, while at a higher temperature than half of the consolidation region, it does not impart a heating effect on the bond line. Cooling is dominated by dissipation of heat to the substrate. For every 100 °C of roller temperature, there is a corresponding change of approximately 12 °C in temperature at the start of the consolidation region.

Introducing a contact resistance between the composite and the roller has the effect of offsetting the cooling profile upwards as can be seen in Figure 3.12. The effect of increasing the thermal contact resistance reduces the heat sink effect of the roller, leading to higher tape temperatures. The results show good agreement for a contact resistance in the range of 1.0-2.0 $m^2 \cdot K/kW$. This is to the same order of magnitude of a silicone to stainless steel interface as reported in literature [Parihar and Wright, 1997].

The size of the corner radius has a direct effect on the degree of shaded area near the nip point. Decreasing the corner radius results in a smaller shaded region, thus a smaller temperature drop is expected prior to the nip point. Figure 3.13 shows the modelled effect. It can be seen that a reduction in the corner radius reduces the dip in temperature leading to higher consolidation temperatures. The model predicts that a reduction of the radius from 15 mm to 5 mm will result in a 10 °C increase in

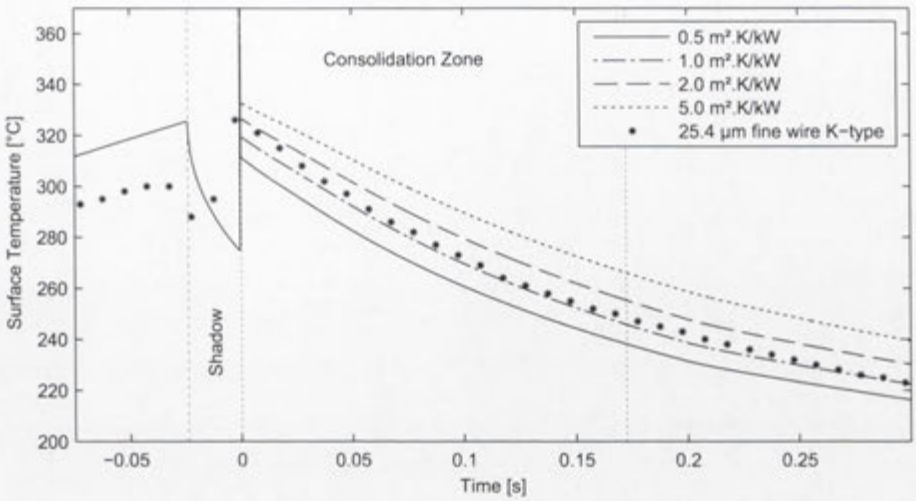


Figure 3.12 – Effect of contact resistance.

temperature at the nip point, given the default model parameters.

3.4 Conclusions

A 2D finite element thermal model incorporating the mass transport of heat was formulated for a laser assisted thermoplastic tape placement system using a conformable consolidation roller. It was found that the roller geometry could be significantly reduced due to a combination of the low thermal diffusivity of the roller elastomer and relatively fast mass flows.

In situ temperature measurement was successfully performed using a fine wire K-type thermocouple. The model was compared with the thermocouple measurement and found to correlate reasonably well, particularly in terms of timing of the heated, shaded, consolidation and cooling regions with respect to each other, however experimental temperature measurements imply higher tape temperature than modelled. The model predicts a relatively uniform temperature distribution through the thickness of the incoming tape, however a significant temperature gradient is present through the thickness of the substrate due to dissipation of the heat. The presence of the shaded region results in significant cooling of the surface prior to the

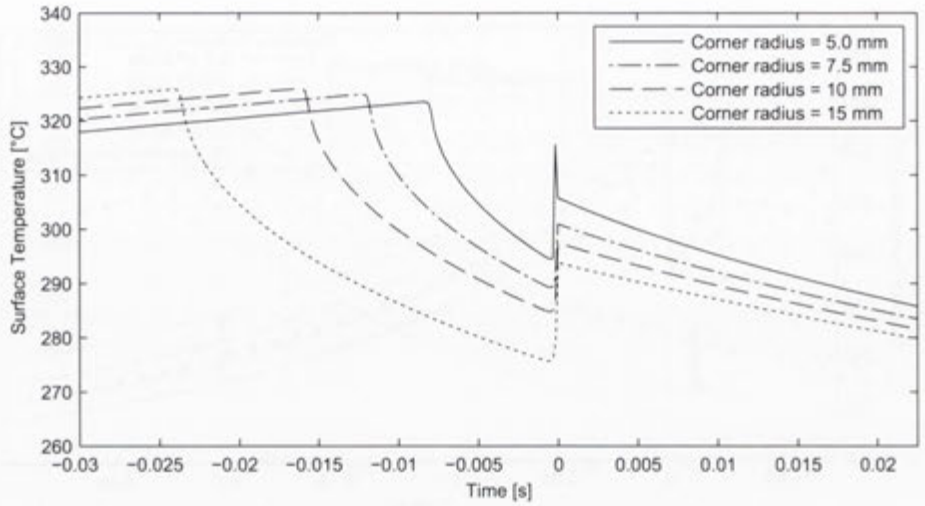


Figure 3.13 – Effect of corner radius.

nip point, particularly on the incoming tape. This suggests that significant overheating is required in order to achieve the necessary nip point temperatures for bonding.

The effects of roller temperature, corner radius and thermal contact were studied using the model. The temperature of the consolidation roller was found to have a significant impact on the cooling rate at the bond line and also the temperature of the incoming tape. Increasing the thermal contact resistance was found to have a reasonable influence with the main effect of raising the incoming tape temperature due to a decreased heat sink effect from the roller. The model assuming $2.0\,\mathrm{m}^2 \cdot \mathrm{K/kW}$ had good agreement with the measured data. Reducing the corner radius of the consolidation roller was found to slightly bias the heat towards the tape, as well as a small increase in the temperature at the nip point.

The temperatures measured during these trials appear to be too low for bonding as the temperature in the consolidation zone (no greater than 330 °C) is lower than the melting point of PEEK (T_m = 343 °C). Results of this thermal model suggest that the feed tape has reached higher temperatures and has melted. Despite the low consolidation temperature, the tape had bonded very well to the substrate. In the the next chapter, the bonding behaviour will be investigated, particularly for the case where the bonding temperature is in fact below the melting point of the polymer.

Investigation of bonding: comparison of model predictions and lap shear strength

Abstract

In this chapter, various bonding models from the literature are implemented and compared with experimental lap shear mechanical tests. Rather than estimating the temperature and pressure histories using models as has been the approach in other studies, the process was instrumented with thermocouples and active pressure sensor arrays. Bond predictions were then performed utilising these process measurements, thus avoiding the cumulative errors from multiple models in series. This should therefore provide a better assessment of the predictive capability of the bonding models. Predictions assuming the values from other validations in the literature are presented and contrasted, as well as predictions using more recent data. In the previous chapter, thermocouple measurements suggested that bonding was occurring at temperatures below the melting point of the polymer. Findings in this chapter suggest that bond development can occur for interface temperatures lower than 250 °C as the extreme cooling rates maintain the amorphous state of the polymer, allowing healing to still occur at low temperatures that would usually be impeded by crystallinity in other manufacturing processes where larger time scales are involved. Good agreement was found between the experimental results and the currently proposed models.

4.1 Introduction

The ability to predict the bond strength in thermoplastic AFP processes is valuable as it can be used as a tool to optimise process parameters for a given placement head design, as well as providing a better understanding of the process overall. When combined with robust temperature and pressure field models, they can be used in the creation of virtual process models. Such models could lead to the development of highly tailored head designs that are optimised for the process, pushing the boundaries of what is truly possible with thermoplastic AFP. The first step towards this goal is to formulate and validate an appropriate bonding model.

Experimental validations of bonding models in AFP processes have used model predictions for temperature and pressure which have not been conclusively validated. Model predictions for bond strength will only be as good as the process history data applied to the bonding model. A range of values in the bonding models are used as tuning factors, with values adjusted so as to achieve a good fit to the experimental data. The issue here is the intimate contact models assume the worst case of crossed plies and therefore effects such as fibre nesting are not taken into account. The models should therefore provide conservative estimates for unidirectional lay-up if using values that are truly representative of the material. The work in the literature has however shown good agreements in the case of unidirectional plies, which should exhibit significant fibre nesting thus higher rates of intimate contact development should occur than the models would otherwise predict. This would suggest that the input parameters of the models have been tuned to correlate with experimental results, however this is misleading as the models do not account for nesting of fibres. Therefore if the same parameters were applied to a process for the manufacture of laminates that were not unidirectional, it is likely that a significant overestimation of intimate contact development would result.

The non-isothermal formulations of intimate contact and healing models in the literature have only been validated in isolation for heating and cooling rates that are

orders of magnitude less than experienced in the laser AFP process (Sections 2.2.1 and 2.2.2). Experimental validations of combined models for AFP processes have been performed for speeds of 30-133 mm/s [Tierney and Gillespie, 2006; Khan et al., 2010]. The laser AFP system considered in this work has been able to produce components at speeds of 1000 mm/s, which is an order of magnitude higher than reported for other experimental thermoplastic AFP studies in the literature. It is therefore unclear how suitable such models are when working at higher placement rates, and therefore it is of interest in this work to study their suitability.

As discussed in Section 2.2.7, recent measurements of the crystallisation behaviour of PEEK using nano-DSC have shown that the fastest crystallisation half-time is to the order of half a second [Tardif et al., 2014], which occurs for temperatures in the range of 220-250 °C. In the case of an AFP process, the time at elevated temperatures (>200 °C) is typically lower than this value to the order of 0.2 s (Figure 4.6), which would suggest that the PEEK matrix remains in a highly amorphous state throughout the consolidation zone. Since there would be minimal or no crystalline phases present to increase the viscosity or inhibit healing, it would suggest that bond development would be possible for temperatures lower than the melting point, and in fact all the way down to the glass transition temperature. Previous AFP model validation studies have either assumed a temperature threshold of 338 °C [Tierney and Gillespie, 2006] for bonding calculations, or otherwise it was not mentioned [Mantell et al., 1992; Khan et al., 2010]. In Section 2.1 the work of Mantell et al. [1992] was discussed, where bond strengths of 50 % were reported despite thermocouple measurements indicating a maximum temperature of 260 °C. This was possibly due to measurement errors from using a thermocouple of high thermal mass that would result in lower measurement temperatures than actual. However it is possible that bonding could occur as long as the PEEK is sufficiently melted prior to consolidation to achieve the amorphous state. This topic of the possibility of bonding well below the melting point is of great interest and will be investigated in this chapter.

In order to validate the bonding model predictions, a suitable test method must be selected. As discussed throughout the literature review (Chapter 2), the bond strength development occurs not only for the initial placement of the layer, but also as the interface experiences repeated thermal and pressure cycles during placement of the subsequent layers above. Validation of a model using multiple repeated passes would result in larger cumulative errors in terms of the pressure and temperature histories applied to the model. It is more straightforward to measure the history for the placement of a single layer. It is also necessary to produce samples that are not completely bonded. If all of the samples were completely bonded then the bonding model cannot be validated as there would be no variations in the results. Therefore it was identified that a test method which tests a single interface in isolation, without any repeated process history would be most suitable for the validation of the bonding model predictions. Test methods such as the short beam strength (SBS) and double cantilever beam (DCB) require multi-layered samples to be manufactured and therefore are not considered in this case. Methods which characterise the strength of a single interface include the wedge peel test and lap shear tests. In this work the strength of the interface was characterised using the *ASTM D 5868* lap shear test method as selected in similar studies [Yang and Pitchumani, 2002b, 2003; Schell et al., 2009; Mantell et al., 1992].

It should be noted here for the sake of clarity, the lap shear tests only experience a single placement history, therefore it is expected that the resulting bond strengths would be lower than the ultimate strength of the material. Furthermore, in this case the samples are manufactured directly on the tooling which results in more rapid cooling history which is known to impede the bonding behaviour [Pitchumani et al., 1997; Sonmez and Hahn, 1997a; Tierney and Gillespie, 2003]. The increased cooling results in more extreme non-isothermal history, making for a better assessment of the performance of the models under highly non-isothermal conditions. The focus of this chapter is to validate bonding models and the result of incomplete bonding is

required to generate the data points necessary for the model validations. During the manufacture of real components, the bond interfaces experience multiple repeated passes which develop the inter-laminar strength to a much higher degree, if not to completion. In Chapter 7, SBS samples will be manufactured which represent the true inter-laminar strength achievable when manufacturing actual components.

4.2 Process model implementation

As discussed previously in Section 1.3.2.1, the bonding process is the source of strength development and is based on the diffusion of polymer molecules across the bond interface, a process known as healing or autohesion. Healing will only occur if the surfaces are in intimate contact. The bond strength development process is therefore modelled by combining healing and intimate contact development models. The laser AFP process has a highly dynamic temperature and pressure history, and therefore it is imperative that models which apply to non-isothermal conditions are considered.

4.2.1 Intimate contact

As real surfaces are not truly flat, the initial contact is limited to asperities. As temperature and pressure are applied the material softens and begins to flow increasing the level of intimate contact between the surfaces. As discussed in Section 2.2.1, various models for intimate contact have been proposed in the literature. In this study the Mantell and Springer [1992] non-isothermal adaptation of the simplified rectangular wave (RWS) model was implemented, as well as the rectangular fractal cantor (RF) model developed by Yang and Pitchumani [2001a].

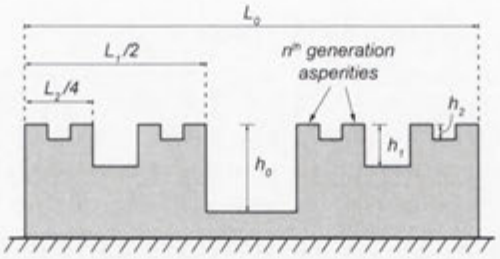


Figure 4.1 – Geometry of the fractal cantor set intimate contact model.

4.2.1.1 Simplified rectangular wave implementation

The Mantell and Springer [1992] model was implemented as follows. Revisiting the simplified rectangular model equation from Section 2.2.1, we have:

$$D_{ic}(t) \approx g^* \left[\int_0^t \frac{P_{app}(t)}{\mu_{mf}(T(t))} dt \right]^{1/5} \tag{4.1}$$

Where t is the bonding time and P_{app} is the pressure applied to the interface. g^* is an empirically determined geometric parameter where 0.29 was the value assumed here as used in similar work [Mantell and Springer, 1992; Tierney and Gillespie, 2006].

4.2.1.2 Fractal cantor set implementation

A fractal cantor set intimate contact model was also implemented following that of Yang and Pitchumani [2001a]. Referring to Figure 4.1, the degree of intimate contact is calculated as follows:

$$D_{ic}^{(n)}(t) = \frac{1}{f^n} \left[\frac{5}{4} \left(\frac{h_0}{L_0} \right)^2 \frac{f^{\frac{2nD}{2-D}+n+4}}{(f+1)^2} \int_{t_{(n+1)}}^{t} \frac{P_{app}(t)}{\mu_{mf}(T(t))} \mathrm{d}t + 1 \right]^{1/5} \tag{4.2}$$

$$\text{for} \quad t_{(n+1)} \leq t \leq t_{(n)}$$

The parameters applied to the model in this study are shown in Table 4.1. The carbon/PEEK composite used in this study was *Suprem*™ *T* 60 % v/v AS4/PEEK-150 0.15 mm × 12 mm . The fractal scaling factor f and the fractal dimension D for this particular prepreg were previously determined by Khan et al. [2010], and therefore

Table 4.1 – Parameters for the fractal cantor set intimate contact model.

Parameter	Value	Source
f	1.44	Khan et al. [2010]
D	1.30	Khan et al. [2010]
h_0/L_0	0.050	Yang and Pitchumani [2001a]
ω_0	$4.8 \times 10^3\,\mathrm{m}^{-1}$	Yang and Pitchumani [2001a]

adopted for this study. The length of the zeroth generation asperity L_0 is calculated from the low frequency limit of the surface profile power spectrum ω_0 as follows:

$$L_0 = \frac{1}{\omega_0} \tag{4.3}$$

The time at which the n^{th} generation asperity has fully compressed is $t_{(n)}$. The compression of the n^{th} generation asperity therefore starts when the next higher generation has fully compressed at $t_{(n+1)}$. In order to solve Eq. (4.2), the times $t_{(n)}$ at which the generations have compressed must first be determined. The process to determine $t_{(n)}$ is as follows. For an asperity of initial height and width of a_0 and b_0 respectively, applying the conservation of volume to the one dimensional squeeze flow, Yang and Pitchumani [2001a] produced the following relation:

$$\int_0^t \frac{\hat{F}}{\mu_{mf}(T(t))}\mathrm{d}t = \frac{4(a_0 b_0)^3}{5}\left(\frac{1}{a_t^5} - \frac{1}{a_0^5}\right) \tag{4.4}$$

Where $\hat{F}$ is the applied force per unit asperity depth and a_t the height of the element at time t. The force can be expressed in terms of the gauge pressure P_{app}, number of asperities N_{asp} and the length of the n^{th} generation L_0:

$$\hat{F} = \frac{L_0 P_{app}(t)}{N_{asp}} \tag{4.5}$$

Where the number of asperities N_{asp} is calculated as:

$$N_{asp} = \left(f^{\frac{D}{2-D}}\right)^n \tag{4.6}$$

Substituting Eq. (4.5) in Eq. (4.4),

$$\frac{L_0}{N_{asp}} \int_{t_{(n+1)}}^{t_{(n)}} \frac{P_{app}(t)}{\mu_{mf}(T(t))} \mathrm{d}t = \frac{4(a_{n(0)}b_{n(0)})^3}{5} \left(\frac{1}{a_{n(t)}^5} - \frac{1}{a_{n(0)}^5} \right) \quad \text{for} \quad t_{(n+1)} \leq t \leq t_{(n)} \tag{4.7}$$

Is then rearranged to give:

$$\int_{t_{(n+1)}}^{t_{(n)}} \frac{P_{app}(t)}{\mu_{mf}(T(t))} \mathrm{d}t = \frac{N_{asp}}{L_0} \frac{4(a_{n(0)}b_{n(0)})^3}{5} \left(\frac{1}{a_{n(t)}^5} - \frac{1}{a_{n(0)}^5} \right) \quad \text{for} \quad t_{(n+1)} \leq t \leq t_{(n)} \tag{4.8}$$

The parameter $a_{n(0)}$ is determined by:

$$a_{n(0)} = h_{n-1} - u_{n+1} \tag{4.9}$$

Where h_{n-1} and u_n are:

$$h_{n-1} = h_0 \left(\frac{1}{f} \right)^{n-1}; \qquad u_n = \frac{h_0}{f^{n-2}(f+1)} \tag{4.10}$$

Furthermore,

$$b_{n(0)} = \left(\frac{L_n}{N_{asp}} \right); \qquad L_n = L_0 \left(\frac{1}{f} \right)^n \tag{4.11}$$

Thus Eq. (4.8) can now be solved. In order to determine the times $t_{(n)}$ at which the n^{th} generations have compressed, Eq. (4.8) is solved for time assuming the asperity has fully compressed, that is $a_{n(t)} = a_{n(f)}$, where $a_{n(f)}$ is the final asperity height, determined by:

$$a_{n(f)} = h_{n-1} - u_n \tag{4.12}$$

After the asperity generation compression times have been determined, the intimate contact is then determined using Eq. (4.2). In this study it was found that 10 asperity generations was sufficient to describe the intimate contact process which is consistent

with the findings of Yang and Pitchumani [2001a]. This is because any higher order generations become extremely small and the compression process diminishes in time rapidly, therefore having an insignificant effect.

4.2.2 Healing

Healing is the inter-diffusion/reptation of the polymer chains across regions of the bond interface that are in intimate contact. The rate of healing is highly temperature dependent. Yang and Pitchumani [2002b] formulated a non-isothermal model of reptation theory from first principles. The non-isothermal degree of healing D_h is related to the time t, temperature T and characteristic welding time of the polymer t_w by the following relation:

$$D_h = \left[\int_0^t \frac{1}{t_w(T)} dt\right]^{1/4} \tag{4.13}$$

4.2.3 Coupled bonding model

Healing only occurs on areas in contact. For each increment of newly formed intimate contact, a separate healing process starts. Full bond strength occurs when the last increment of intimate contact has formed and has subsequently healed completely. Mathematically the degree of bonding D_b can be represented by:

$$D_b(t_b) = \int_0^{t_b} D_h[t, t_b] \frac{\mathrm{d}D_{ic}}{\mathrm{d}t} \mathrm{d}t \tag{4.14}$$

Where t_b is the final time for the bond calculation. The degree of healing D_h is calculated for the time interval of $[t, t_b]$, where t is the time of formation of a new increment of intimate contact.

As discussed in Section 2.2.3, previous studies that have compared bonding predictions with experimental results have used some form of simplification in the calculation of the degree of bonding, such as assuming healing to occur instantaneously or intimate contact to occur in the form of a Heaviside step function. In this work

Eq. (4.14) is calculated in its complete form, with no simplifications made. This is important as the conformable consolidation rollers have a much longer pressure distribution, resulting in intimate contact development over a much longer period. Furthermore, the temperature history at the interface changes significantly while under the pressure of the consolidation roller. Eq. (4.14) is solved numerically and it was found that calculation over a time increment of 0.001 s was sufficient for convergence of the degree of bonding predictions.

4.2.3.1 Bonding temperature threshold

The model implemented by Tierney and Gillespie [2006] assumes that bonding can only occur for temperatures above the melting point of PEEK, which was taken to be $T_m = 338\,°C$. The temperature thresholds used in other bonding validation studies have not been reported [Mantell et al., 1992; Khan et al., 2010]. In this work, it was assumed that bonding can occur for temperatures right down to the glass transition $T_g = 143\,°C$. This is justified by the fact that the minimum crystallisation half-time for PEEK (Table 4.2) even at the temperature of peak crystallisation rate, is at least twice as long as the typical time period available for intimate contact development (0.2 s) as can be seen in Figure 3.9. For this reason it is assumed that as the PEEK will remain effectively amorphous during the consolidation zone even for temperatures as low as 200 °C. The Arrhenius relations used to extrapolate the properties of polymers in the amorphous state to temperatures outside of the experimental range should therefore still remain valid at even temperatures well below the melting point. Therefore in this work it is assumed that both healing and intimate contact can still occur for temperatures as low as the glass transition, within short periods after the nip point.

4.2.3.2 Input parameters

The predictions of the bonding model are highly dependent on the input parameters such as the temperature-dependent viscosity and welding times, as well as the in-

Table 4.2 – Crystallisation half-times for PEEK-150G as reported by Tardif et al. [2014].

Temperature [°C]	Crystallisation half-time [s]
200	1.36
210	1.10
220	0.51
230	0.48
240	0.50
250	0.62
260	0.78
270	1.40
280	2.32

timate contact model that is used. Here, the experimental results will be compared with predictions based on the model parameters applied to experimental bonding model validations from the literature for thermoplastic AFP processes. The models and relations applied for calculation of D_b based on the previous studies in the literature are summarised in Table 4.3.

Table 4.3 – Bonding model parameters from experimental validations in the literature. Naming conventions for viscosity and welding time follow those from Tables 2.2 and 2.3 respectively.

Study	Intimate Contact	Viscosity	Welding time
Mantell et al. [1992]:	Eq. (4.1) (RWS)	$\mu_{\text{(CFPEEK M&S)}}$	$t_w = 0$, $(D_h = 1)$
Tierney and Gillespie [2006]:	Eq. (4.1) (RWS)	$\mu_{\text{(PEEK L&S)}}$	$t_{w\ \text{(PEEK S\&H)}}$
Khan et al. [2010]:	Eq. (4.2) (RF)	$\mu_{\text{(CFPEEK K,M&S)}}$	$t_{w\ \text{(PEEK K,M&S)}}$

In this work, the *Suprem*™ *T* composite has a very smooth surface. In the case where the scale of deformation is smaller than the diameter of an individual fibre, it can be assumed that the local viscosity at the surface is that of the neat polymer [Tierney and Gillespie, 2006]. The same assumption was made in this work and the viscosity applied to the intimate contact model will be that of neat PEEK polymer, the value of which for the particular grade of PEEK used in the composite considered in this study was adapted from Khan et al. [2013]. The values reported in the literature

for the welding time t_w of PEEK are vastly different, with each separated by at least one order of magnitude as shown in Figure 2.8 of Chapter 2. Therefore in the current study, the focus will be on the most appropriate value to be used for t_w. The intimate contact model and the viscosity thus remain fixed. The input parameters for the current study are listed in Table 4.4

Table 4.4 – Currently investigated combined bonding model parameters. Naming conventions for viscosity and welding time follow those from Tables 2.2 and 2.3 respectively.

Bonding parameter set	Intimate contact	Viscosity	Welding time
BPS-1	Eq. (4.2) (RF)	$\mu_{\text{(PEEK K,M\&S)}}$	$t_{\text{w (PEEK K,M\&S)}}$
BPS-2	Eq. (4.2) (RF)	$\mu_{\text{(PEEK K,M\&S)}}$	$t_{\text{w (PEEK L\&S)}}$
BPS-3	Eq. (4.2) (RF)	$\mu_{\text{(PEEK K,M\&S)}}$	$t_{\text{w (PEEK S\&H)}}$

4.2.3.3 Relation between degree of bonding and lap shear strength

As assumed by other studies in the literature, the lap shear strength was considered to be directly proportional to the degree of bonding D_b. Strength predictions were calculated by multiplying the degree of bonding by the ultimate lap shear strength. The ultimate lap shear strength of a carbon/PEEK composite has been reported as 65.5 MPa [Mantell et al., 1992] and also 64 MPa [Yang and Pitchumani, 2002a], which was the value assumed in this work.

4.3 Experimental method

Suprem™ *T* 60 % v/v AS4/PEEK-150 0.15 mm × 12 mm unidirectional prepreg tape was used in the experimental work. In the preliminary lap shear study, the experimental placement head described in Section 3.2 was used. A single tape was placed onto another on top of aluminium tool at room temperature, forming a 2 ply unidirectional laminate. The substrate ply was affixed to the tooling at each extremity using a technical adhesive tape. Process parameters were chosen to investigate the

Table 4.5 – Process parameter sets for the preliminary lap shear trials. Note: the process temperature is based on non-contact process control measurements and may not be representative of the true temperature.

Placement trial	Placement rate [mm/s]	Process temperature [°C]	Consolidation force [N]	Laser power [W]
A	200	350	300	1000
B	200	400	300	1200
C	200	450	300	1400
D	100	400	300	700
E	200	400	150	1200

effects of laser power and consolidation force. The process parameters studied are shown in Table 4.5.

4.3.1 Temperature measurement

Due to the rapid placement rates and high heat inputs, temperature gradients can exceed 1000 °C/s in laser tape placement. It is therefore important to use thermocouples with a very fast response time/low thermal mass. 25.4 µm fine wire K-type thermocouples were attached to the surface of the substrates using a soldering iron and a minimal amount of PEEK shavings. Temperature was logged during the process at 100 Hz using a *National Instruments cDAQ-9213* thermocouple module. The response of the thermocouples was tested by quickly alternating the thermocouples in pots of 20 °C and 90 °C water. Results of the tests found that the thermocouples had a response much faster than the sampling rate of the data acquisition module, indicated by an instantaneous change in the measured temperature.

4.3.2 Pressure measurements

Pressure was measured with a *Tekscan I-Scan* system using a type 5051 sensor which consists of a 44 × 44 sensel array with a pitch of 1.27 mm. The consolidation roller is attached to the placement head with a pair of linear bearings which allow the roller to move in the vertical direction. Consolidation force is applied with a pair of 40 mm

pneumatic cylinders. The pressure applied to the cylinders is controlled by adjusting a pressure regulator. Calibration of the pressure sensor was performed by applying pressure to the consolidation roller on top of a *Kern DE 35K5D* certified mass balance. Static pressure measurements were performed for consolidation forces of 150 and 300 N which corresponded to cylinder pressures of 0.6 and 1.2 bar. Figure 4.2 shows the pressure being measured for the 64 mm diameter conformable roller. The pressure values used in the bonding model were taken as the average pressure across the width of the bonding region, that being the pressure in the region between the tape and the substrate. The pressure distribution was converted to the time domain by multiplying the position by the placement rate.

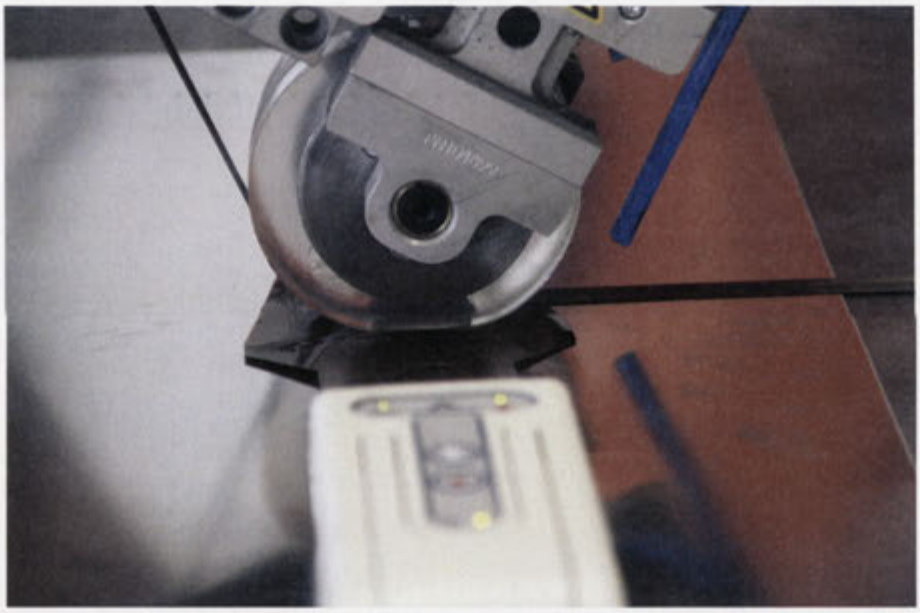


Figure 4.2 – Measurement of the pressure distribution under a conformable roller using a 44 × 44 sensel array.

4.3.3 Sample preparation

For each process setting a total of nine lap shear samples were prepared. The gauge length, width and overlap of the prepared samples were 90, 10 and 6 mm respectively. Due to the continuous nature of the tape placement process, it is not feasible to introduce the breaks in the layers necessary to produce a lap shear sample during

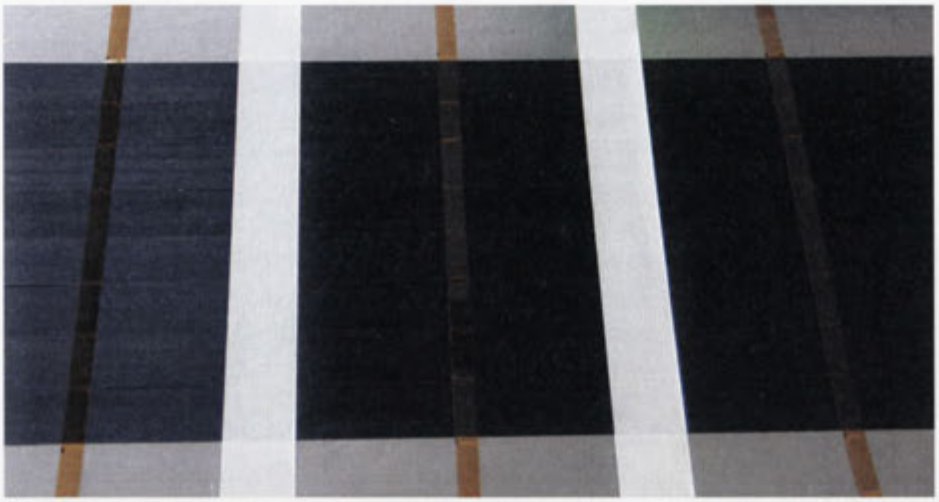
placement. Instead, strips of 3 mm polyimide adhesive tape were attached to the substrate prior to placement, so as to introduce breaks in the bond line precisely isolating a 6 mm long bonded lap region. The polyimide tape is 25.4 µm thick and uses a residue free high temperature silicone based adhesive. PEEK is not miscible with polyimide, therefore no bonding takes place.

The samples were prepared as follows. As it is difficult to ensure exact placement of a 12 mm tape onto a manually aligned substrate of the same width, wider 18 mm substrate samples were selected to ensure bonding across the full width of the placed tape. Multiple substrate samples were then affixed to a preparation surface, placed parallel to each other (Figure 4.3a). In order to ensure a consistent 6 mm spacing of the 3 mm polyimide tape, a 6 mm wide polyimide tape was first placed across the substrates as shown in Figure 4.3a. The 3 mm polyimide tape which is used to form the precisely spaced 6 mm breaks in the bond was then applied either side of the 6 mm spacing tape (Figure 4.3b). Extra care was taken to ensure no gap or overlap was present. The 6 mm spacing tapes were then removed (Figure 4.3c). The remaining 3 mm tapes were then slit between each substrate with a scalpel. The prepared substrates were then placed directly onto the aluminium tooling plate (Figure 4.4). The positioning was maintained during placement using polyimide tape on the edges of the sample outside the bond width.

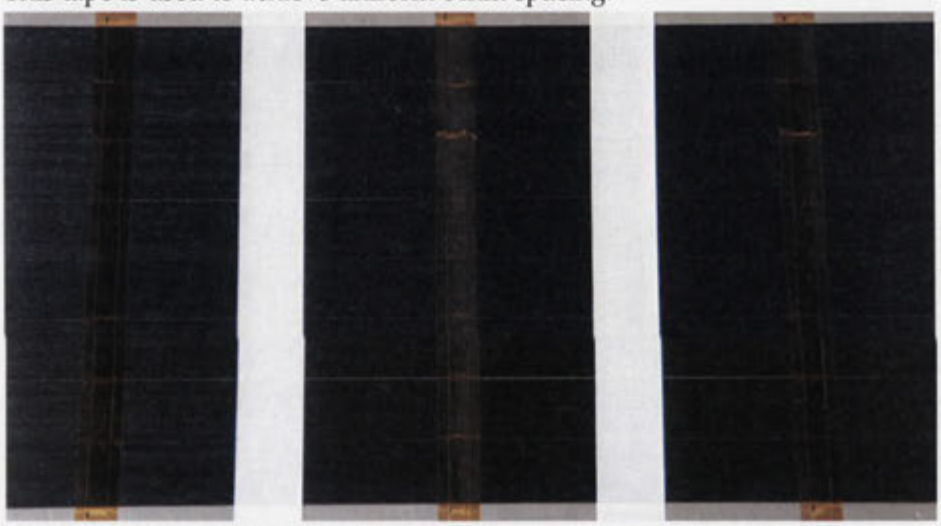
4.3.4 Sample testing

After placement, the nine samples were cut to length and width. Breaks were made above the polyimide tapes on opposing sides of the sample using a 1 mm diamond slitting wheel installed on a surface grinding machine. The surface grinding machine cutting depth can be controlled in 1 µm increments, providing the level of control required for precise cutting of a single ply down to the depth of the polyimide tape. The result is a lap shear specimen as shown in Figure 4.5.

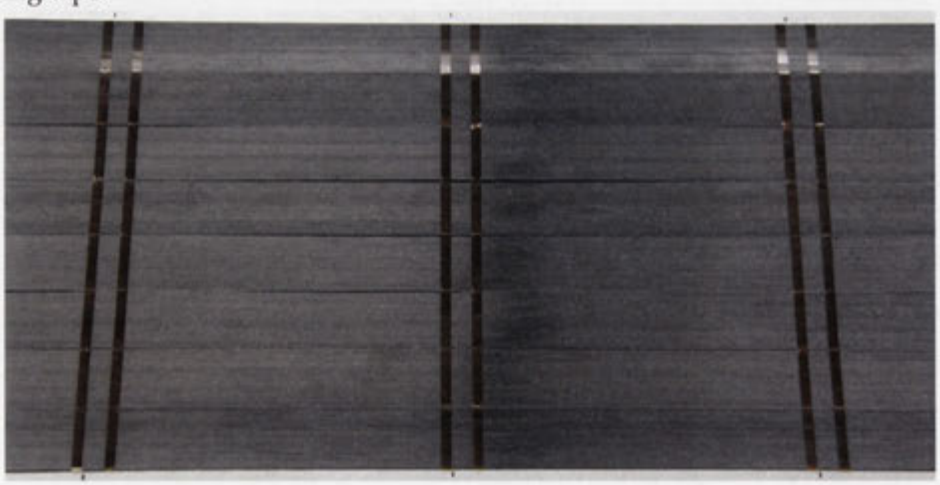
Following *ASTM D 5868*, tensile tests were performed at room temperature on an



(a) Step 1 – Position 6 mm polyimide tape (yellow) across the substrate samples. This tape is used to achieve uniform 6 mm spacing.



(b) Step 2 – Position 3 mm polyimide tapes against the sides of the 6 mm spacing tape.



(c) Step 3 – Remove the 6 mm spacing tapes and cut the 3 mm tapes between each substrate.

Figure 4.3 – Preparation of the substrates for lap shear placement trials.

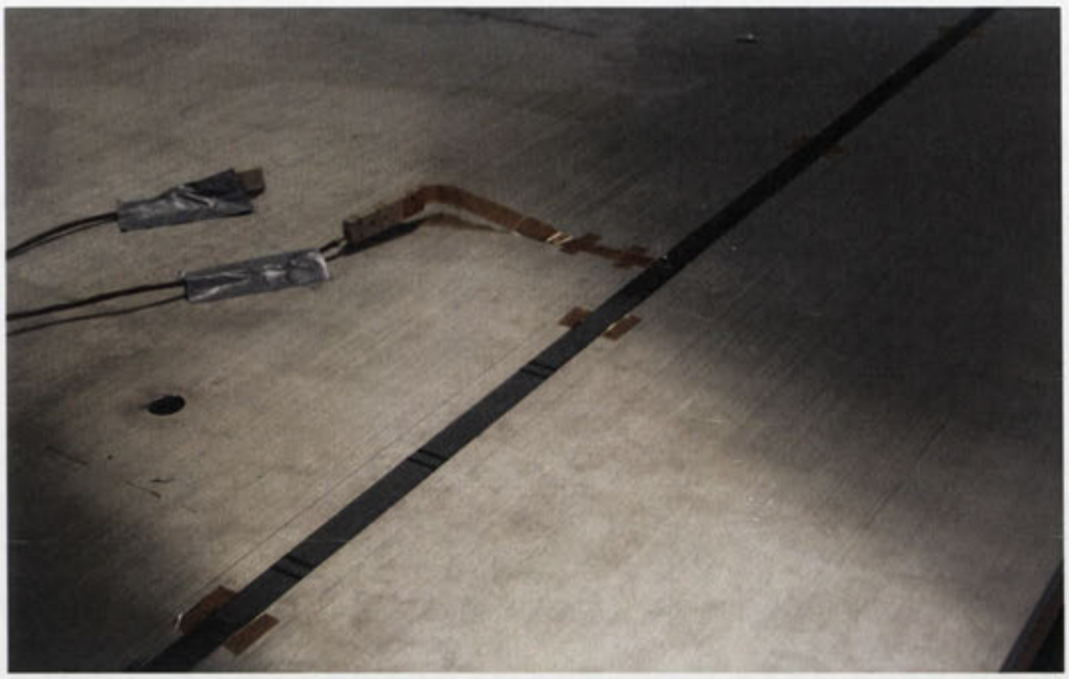


Figure 4.4 – The substrates on the aluminium tooling plate prior to placement. A thermocouple can also be seen attached on the substrate.

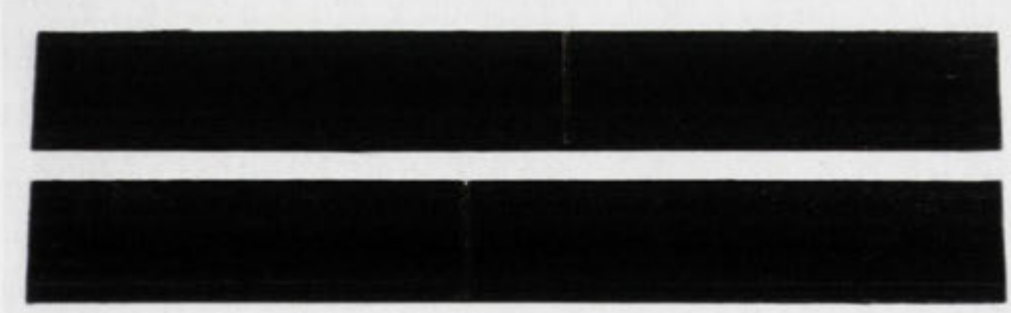


Figure 4.5 – Cuts are made in the upper (top) and lower (bottom) sides of the samples down to the polyimide tape so as to produce a lap shear sample.

Instron testing machine at a loading rate of 13 mm/min. The lap shear strength was calculated as the peak load divided by the area of the fracture surface.

4.4 Results of preliminary trials

4.4.1 Temperature histories

The measured substrate temperature histories are shown in Figure 4.6. As found in Chapter 3, the corner radius of the consolidation roller is approximately 12 mm, which would result in estimated shadows of 14 and 30 ms for placement rates of 100 and 200 mm/s respectively. The nip points were assumed to occur after these shadow periods beyond the peak recorded temperature. The characteristic increase in temperature after the shadow that was observed previously in Figure 3.9 was not observed here as the tape was cooler due to bias of the heating towards the substrate in these trials. Since the laser power and placement rates are the same for trials B and E, the temperature was only logged for test B. While trials A and B are performed at different laser power levels, the measured peak temperatures are almost equal, however the cooling history is quite different. A review of the process data revealed that the laser angle was set with a greater bias towards the substrate for test A, resulting in a higher substrate temperature yet a lower tape temperature prior to the nip point. As shown in Chapter 3, the tape becomes heat soaked and has more of an influence over the cooling history, which also explains the difference in the cooling history between the studies. In the case of a bonding model validation, these discrepancies are not such an issue because it was the resulting interface temperature history that was applied to the bonding model. Therefore the results are still suitable for the purposes of a bonding model validation. The initial consolidation temperatures (at the nip point) were in the range of approximately 450-600 °C.

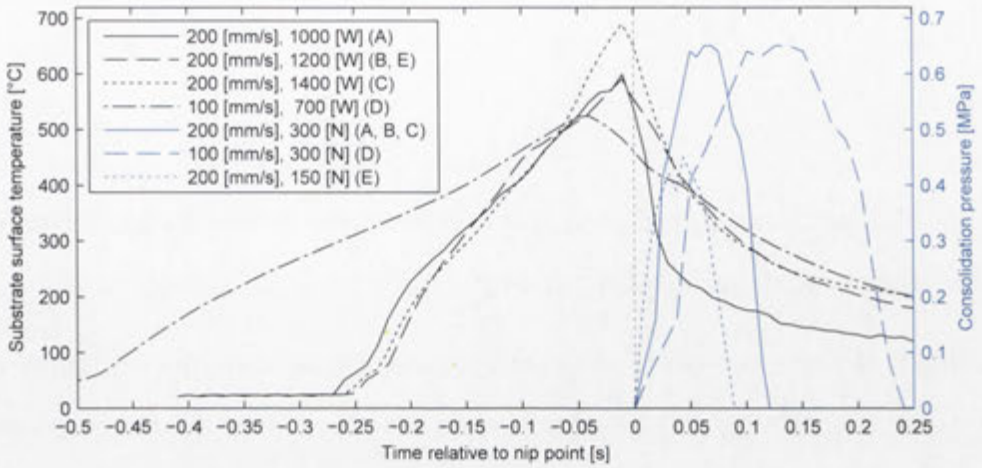


Figure 4.6 – Thermocouple and pressure measurements relative to the nip point for the preliminary placement trials.

4.4.2 Pressure distributions

The pressure distributions for the different consolidation forces are also shown in Figure 4.6. The nip point is assumed to occur where the pressure becomes non-zero as this is where load is first transferred to the substrate. Interestingly, when comparing the forces of 150 and 300 N for the same placement rate of 200 mm/s, it can be seen that the maximum consolidation pressure only increased by 62 %. The reason for this is the conformable roller spreads the pressure over a larger area for higher roller forces. A similar result was predicted by Tierney and Gillespie [2006], they found that increasing the force by 67 % is found to increase the maximum pressure by only 40 %, but is found to broaden the load distribution under the roller. A more important observation is the fact that the pressures immediately after the nip point in the first 0.03 s are almost equal, despite a factor of two difference in the applied load. The applied pressure in the region immediately behind the nip point is more 'valuable' as the corresponding interface temperatures are higher. The resin viscosity has a non-linear temperature dependence and thus the intimate contact development occurs at increased rates at higher temperatures. The earlier the intimate contact develops in the process, the sooner the healing process can start, which in turn will

occur at higher rates the closer it is to the nip point. The overall result would be increased levels of bonding. This topic is identified as a particular area of interest for future work.

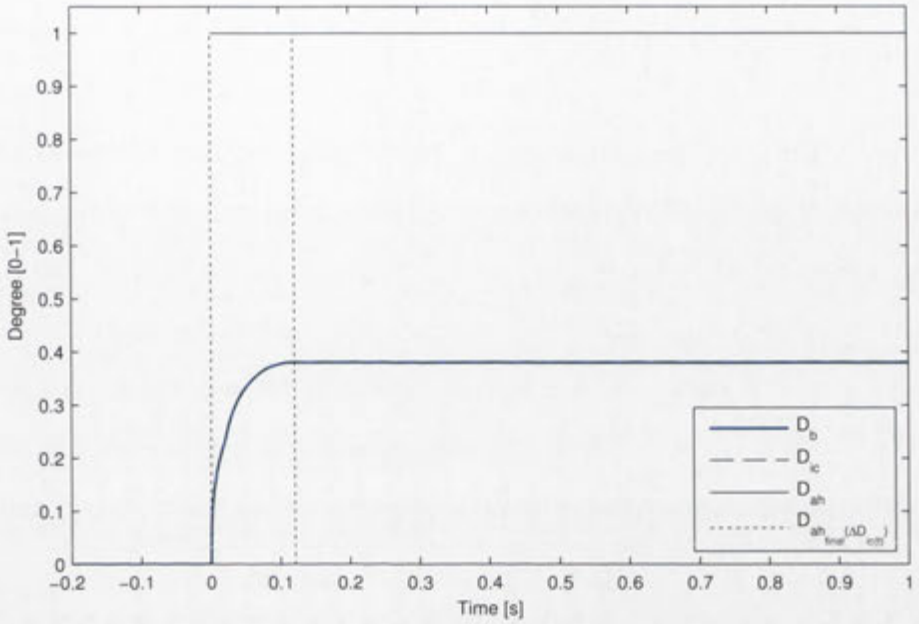
4.4.3 Comparison of predicted and experimental strengths assuming model parameters from the literature

The combined temperature and pressure histories that were experimentally determined were applied to the coupled bonding model. The following sections will investigate the behaviour of the models in the literature. Results of the predictions will then be compared with the lap shear strength results from the preliminary experimental trials.

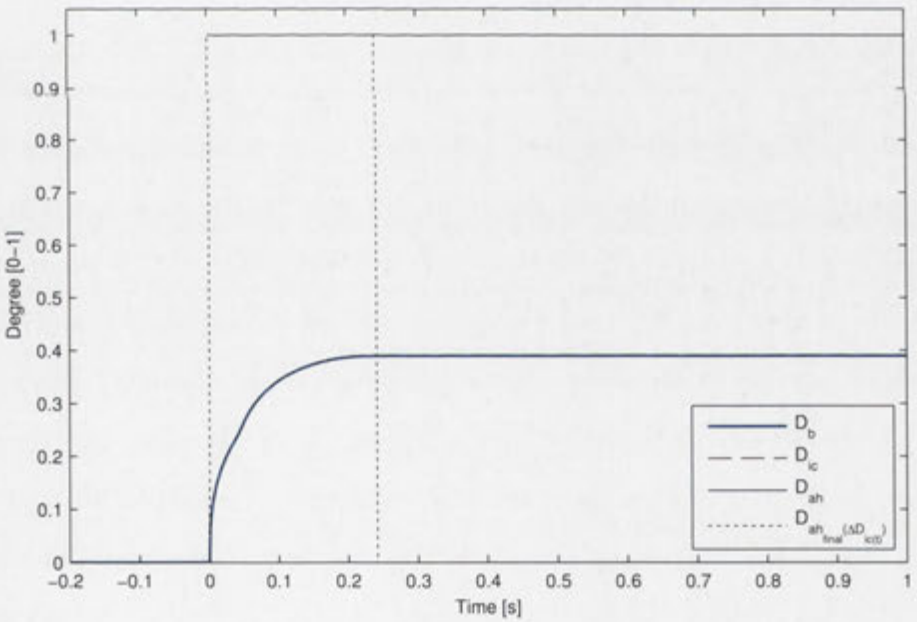
4.4.3.1 Bond development history predictions

First, the model based on the parameters of Mantell et al. [1992] is considered. As it would be both impractical and unnecessary to plot the predictions for all placement trials, the pair showing the most difference (parameter set B and D) were plotted in Figure 4.7. It can be seen that for both cases, the predictions suggest the process to be intimate contact limited, as healing is assumed to occur instantaneously. Both predictions are approximately $D_b = 0.4$, and the majority of intimate contact development occurs in under 0.1 s, conditions of which would definitely result in highly amorphous PEEK based on Table 4.2.

Next, the formulation of Tierney and Gillespie [2006] was investigated. Example predictions are shown in Figure 4.8. The assumption of the viscosity of neat PEEK results in much higher predictions for intimate contact as the viscosity is much lower than that of the fibre-matrix as can be seen in Figure 2.6. Figure 4.8a predicts full bonding to occur in less than 0.1 s. Interestingly, the results for lower placement rate (Figure 4.8b) predict incomplete bonding. The intimate contact develops rapidly at first but stalls at a value of approximately 65 % before 0.1 s has elapsed. The healing



(a) Placement trial B.



(b) Placement trial D.

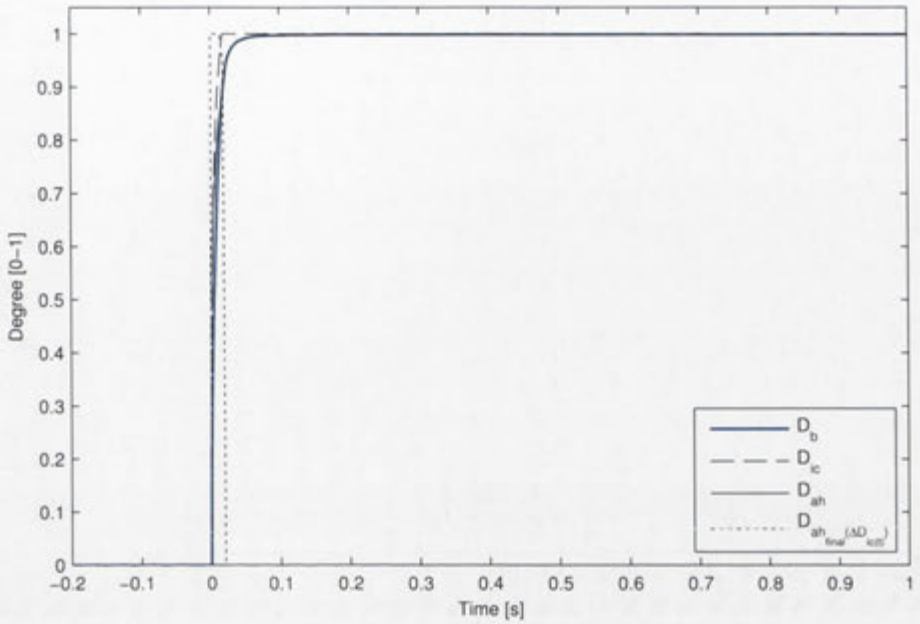
Figure 4.7 – Example predictions based on the Mantell et al. [1992] bonding model parameters ($D_{ic(RWS)}$, $\mu_{(CFPEEK\ M\&S)}$, $D_h = 1$). Autohesion is assumed to occur instantaneously and thus the bonding is predicted to be intimate contact limited.

process can be seen to proceed at a high rate, with close to complete healing for the *initial* increment of intimate contact development (ΔD_{ic}). The overall level of healing is approximately 92 %. In this case the process is predominantly intimate contact limited.

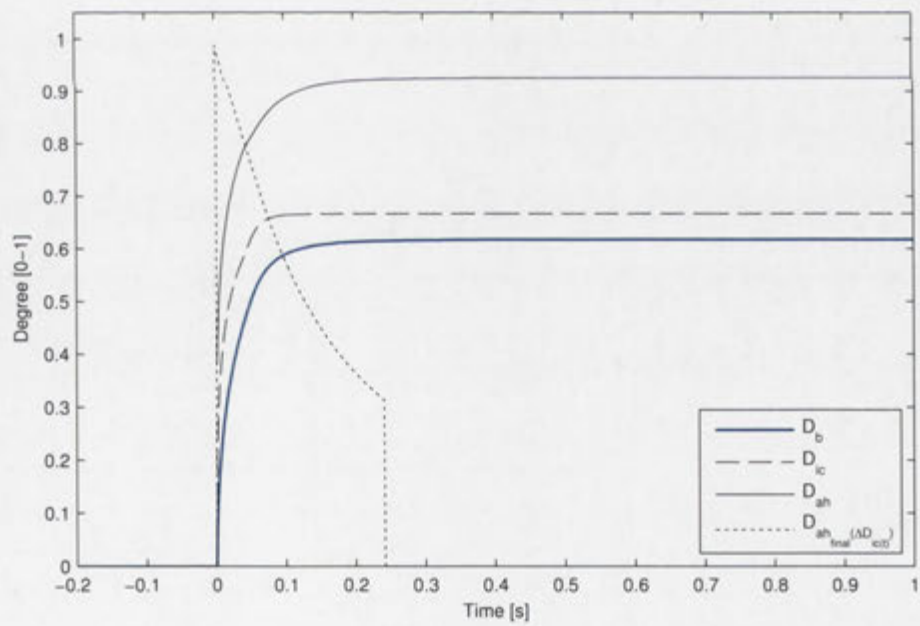
When considering the parameters of Khan et al. [2010] quite different behaviour is predicted by the model. Typical examples in Figures 4.9a and 4.9b suggest that the healing behaviour is extremely fast with final levels in excess of 97 %. The process is predicted to be strongly limited by intimate contact with values less than 0.2, mostly due to the high viscosity assumed for the carbon/PEEK composite. The final bond predictions are remarkably similar despite the factor of two difference in placement rate. The resulting degree of bonding is to the order of 15 % and closely follows the intimate contact due to the high levels of healing.

4.4.3.2 Predicted vs. experimental lap shear strength

The bond predictions assuming the various model parameter sets from the literature are plotted alongside the experimental lap shear strength results in Figure 4.10. The predictions are vastly different. For trials B, C and E, the model of Tierney and Gillespie [2006] predicts complete bonding, while only $D_b = 0.15$ is predicted using the model parameters of Khan et al. [2010]. As previously shown in Figures 4.7, 4.9 and 4.8, all predictions were generally intimate contact limited, with very high levels of healing in excess of 90 % for all cases. The reason for the Tierney and Gillespie [2006] model predicting such high strengths was rapid intimate contact development due to the assumption of the viscosity being that of neat PEEK polymer rather than the effective fibre-matrix viscosity. There is generally a good qualitative agreement in terms of relative differences for each model, with the predictions for trial A consistently low. As discussed in Section 2.2.1.2, for a number of reasons including fibre nesting and shear thinning, it is expected that the bond predictions (in the case of an intimate contact limited bonding) should be if anything conservative

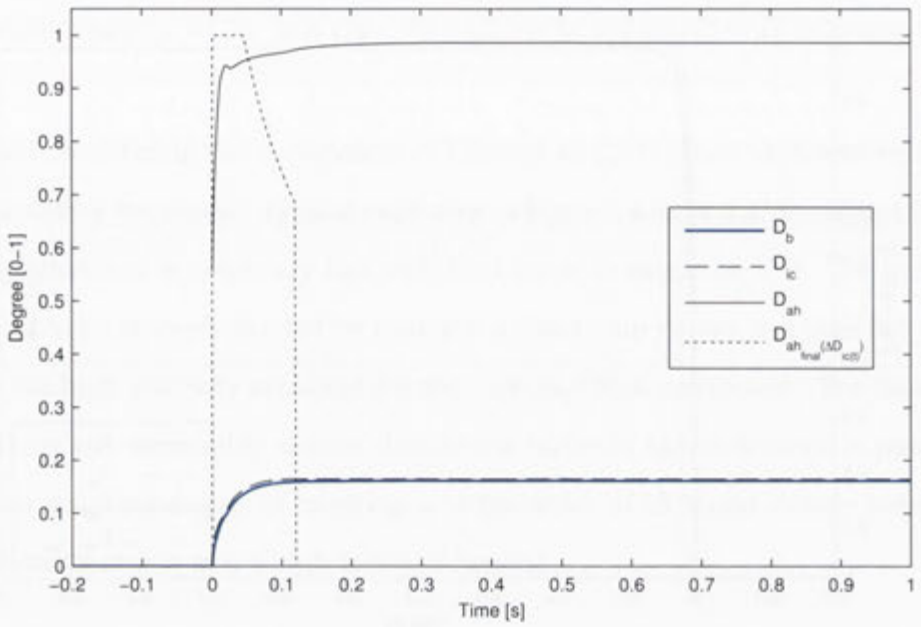


(a) Placement trial B.

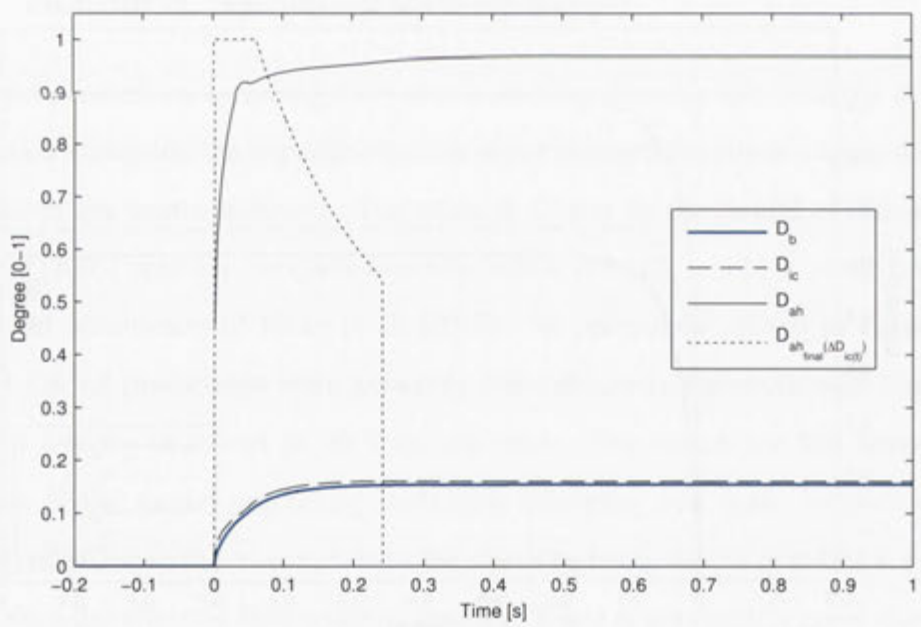


(b) Placement trial D.

Figure 4.8 – Example predictions based on the Tierney and Gillespie [2006] bonding model parameters ($D_{ic(RWS)}$, $\mu_{(PEEK\ L\&S)}$, $t_{w\ (PEEK\ S\&H)}$).



(a) Placement trial B.



(b) Placement trial D.

Figure 4.9 – Example predictions based on the Khan et al. [2010] bonding model parameters ($D_{ic(RF)}$, $\mu_{(CFPEEK\ K,M\&S)}$, $t_{w\ (PEEK\ K,M\&S)}$).

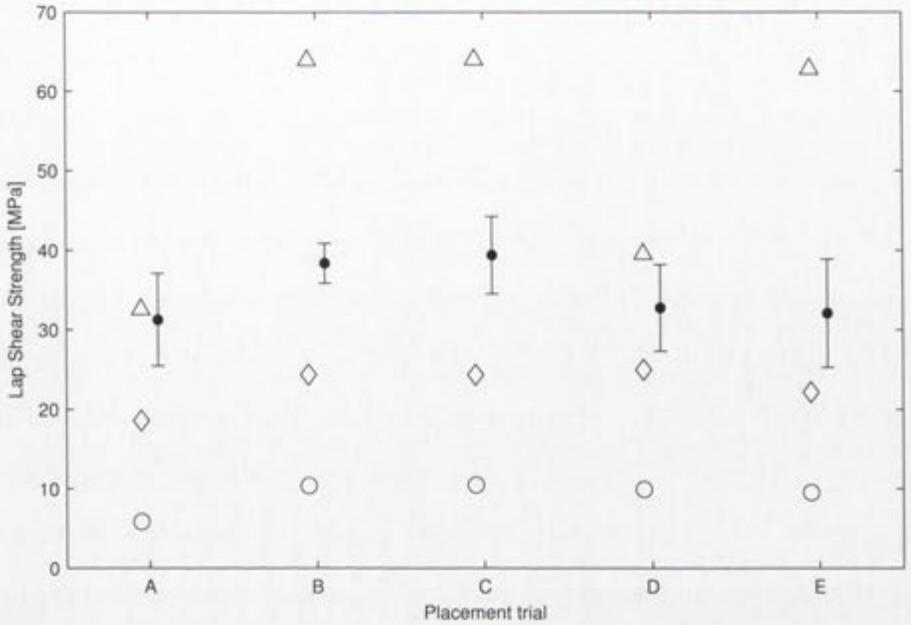


Figure 4.10 – Preliminary lap shear trials: comparison of experimental strengths (•) with bond strength predictions based on models from the literature (Table 4.3). Khan et al. [2010] (○), Mantell et al. [1992] (◊) and Tierney and Gillespie [2006] (△). Error bars represent $\pm\sigma$.

compared with the experimental results, therefore the models of Mantell et al. [1992]; Khan et al. [2010] appear more suitable than that of Tierney and Gillespie [2006].

4.4.4 Comparison of predicted and experimental strengths assuming the current model parameters

4.4.4.1 Bond development history predictions

Here, a comparison is made of predictions based on the current assumptions in this work as per Table 4.4. The main purpose is to investigate the sensitivity of the bonding model to the welding time t_w. First, the welding time of Khan et al. [2013] is considered, the value of which is assumed to be the stress relaxation time of the polymer. Example results for typical predictions are plotted in Figure 4.11. First of all, it can be seen that the assumption of the viscosity of neat PEEK polymer results in relatively high levels of intimate contact development greater than 70 %. Referring to Figure 2.8, it can be seen that the assumed welding time in this case is

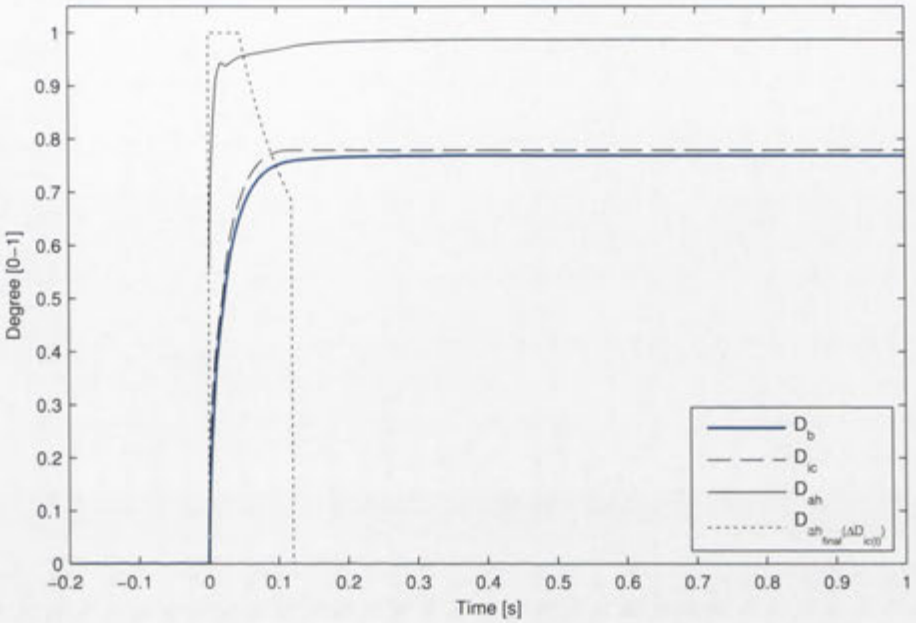
the shortest of the studied values. The result is very rapid healing behaviour with the degree of healing predicted in excess of 95 %. The process is therefore predicted to be predominantly limited by high but incomplete intimate contact levels.

Next, the welding time of Lee and Springer [1987] is considered, which was determined by experimental healing experiments where the degree of healing was characterised by tensile tests. The welding times are many orders of magnitude greater than those of Khan et al. [2013] as shown in Figure 2.8. This is reflected in the bonding predictions (Figure 4.12) where the degree of healing is to the order of 10 %. The parameters of the intimate contact model is the same, therefore no difference is seen between the last model in terms of intimate contact. The bonding prediction in this case is strongly healing limited, with the final degree of bonding predicted to be less than 10 %.

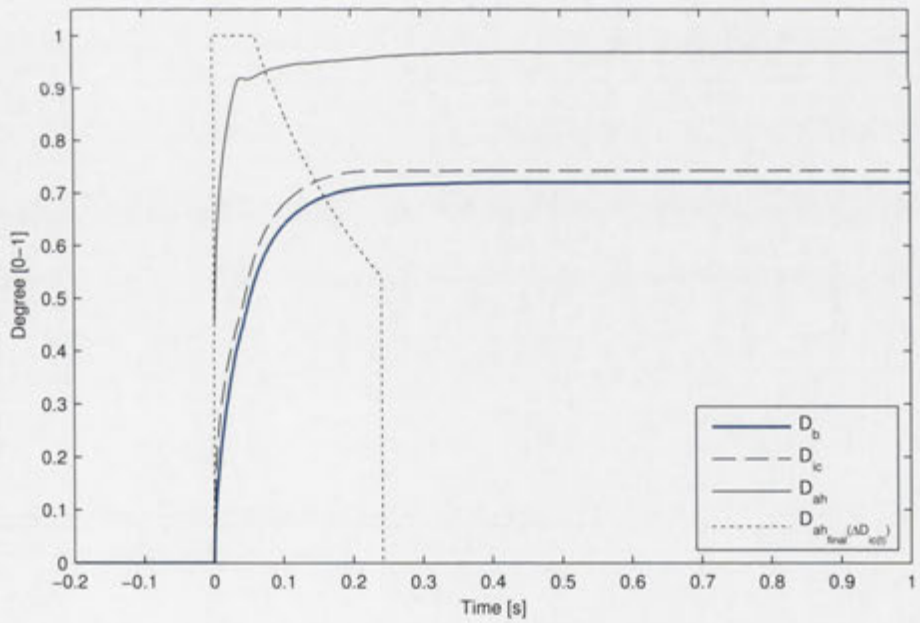
Finally, the welding relation that was published in the work of Sonmez and Hahn [1997a] was considered. The origins of the welding time are unclear, however it appears to be the same relation that was used in the study of Pitchumani et al. [1996]. The value of the welding time in this case is an intermediate value between those already considered above. The results are presented in Figure 4.13. In this case the healing is predicted to be quite high, in excess of 80 %. The result is similar to assuming the value from Khan et al. [2013]. The level of bonding is predicted to be reasonable at 60-70 % and is limited by high yet incomplete levels of both intimate contact and healing.

4.4.4.2 Predicted vs. experimental lap shear strength

A comparison of the predicted lap shear strengths with the experimental results, based on the currently assumed model parameters, is presented in Figure 4.14. The bond predictions appear to be in good agreement with the experimental results for the cases where the welding times of Sonmez and Hahn [1997a] and Khan et al. [2013] are assumed. As the predictions suggest that the degree of healing is very high and

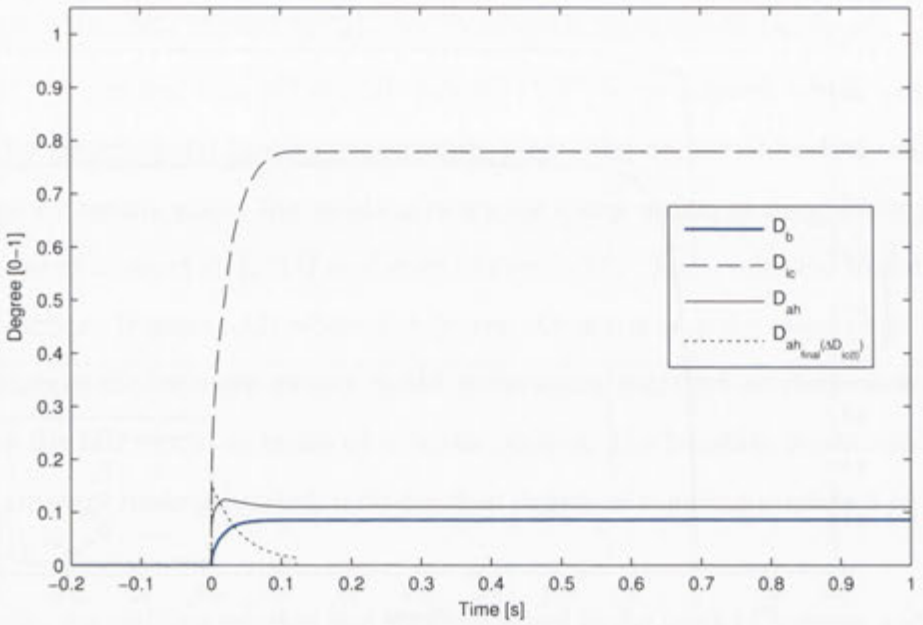


(a) Placement trial B.

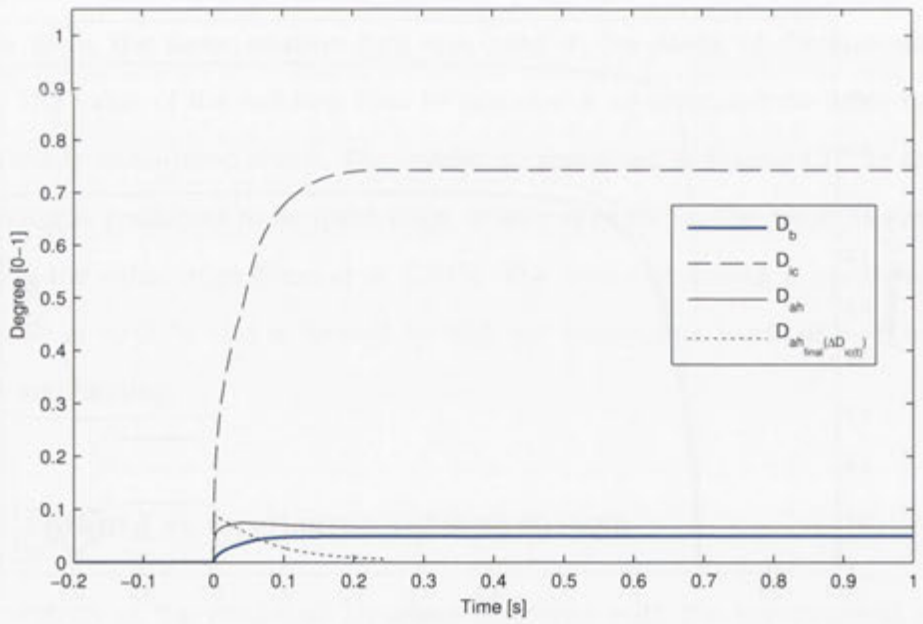


(b) Placement trial D.

Figure 4.11 – Example predictions for the current study assuming the welding time from Khan et al. [2013] ($D_{ic(RF)}$, $\mu_{(PEEK\ K,M\&S)}$, $t_{w\ (PEEK\ K,M\&S)}$).

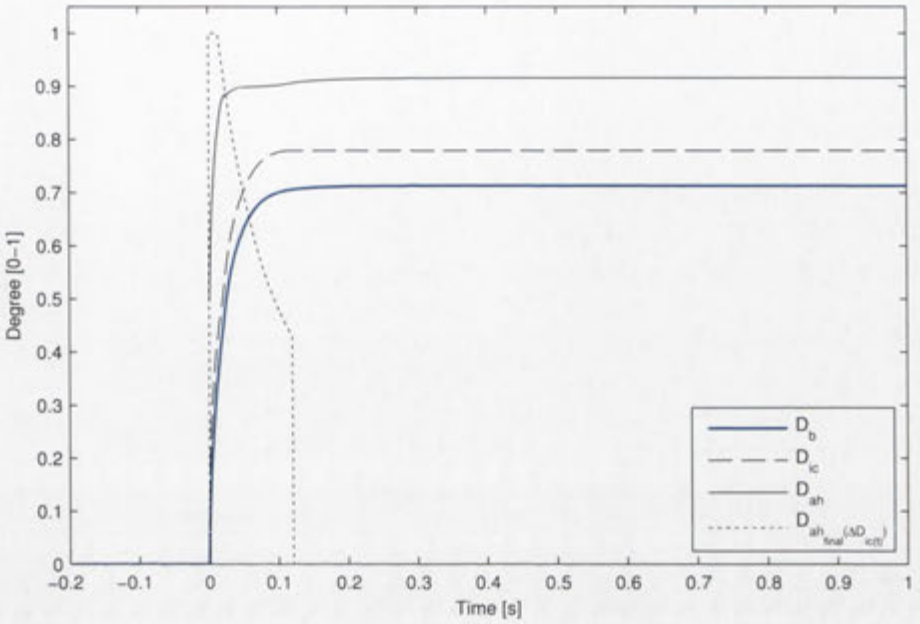


(a) Placement trial B.

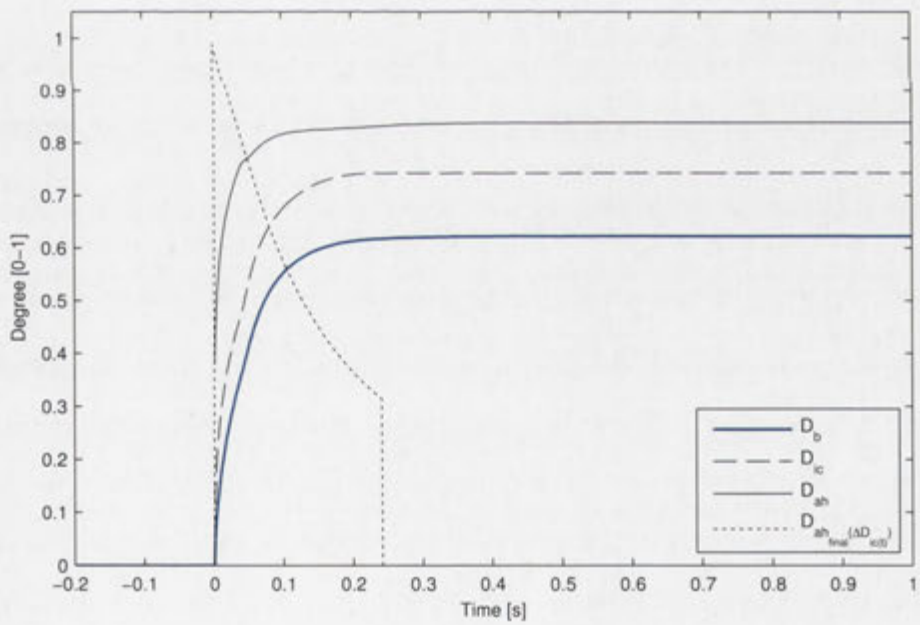


(b) Placement trial D.

Figure 4.12 – Example predictions for the current study assuming the welding time from Lee and Springer [1987] ($D_{ic(RF)}$, $\mu_{(PEEK\ K,M\&S)}$, $t_{w\ (PEEK\ L\&S)}$).



(a) Placement trial B.



(b) Placement trial D.

Figure 4.13 – Example predictions for the current study assuming the welding time from Sonmez and Hahn [1997a] ($D_{ic(RF)}$, $\mu_{(PEEK\ K,M\&S)}$, $t_{w\ (PEEK\ S\&H)}$).

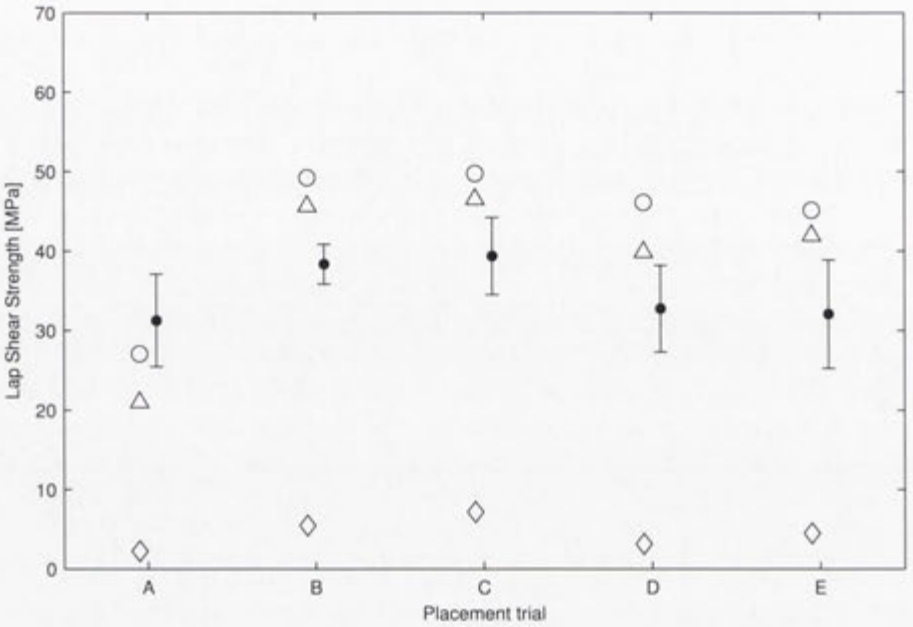


Figure 4.14 – Preliminary lap shear trials: comparison of experimental strengths (•) with bond strength predictions based on the parameters assumed in the current work (Table 4.4). BPS-1 (○), BPS-2 (◇) and BPS-3 (△). Placement trial parameters are presented in Table 4.5. Error bars represent $\pm\sigma$.

the process is predominantly intimate contact limited for those cases, it is expected that the predictions would be if anything conservative as the intimate contact model assumes crossed plies rather than unidirectional plies where nesting can occur. The predicted strengths in the case of the Lee and Springer [1987] t_w relation are very low, however the qualitative trend also appears to agree well with the results.

It has been shown that the bonding predictions for the same temperature and pressure data can vary tremendously depending on the welding time, intimate contact model and the assumed viscosity of the material in the region of the bond interface. Three different sets of experimentally validated model parameters from the literature were applied to the model and found to give bond strength predictions that differed by more than a factor of five. It is likely that this is because the parameters in early work were adjusted as tuning factors to get the best fit to the experimental results, and it was assumed that the predicted temperature and pressure histories applied to those models were accurate. There will of course be differences in prepreg

material quality also which would predominantly effect the intimate contact development due to the initial surface topology. While such models were appropriate for investigating the response of a particular AFP head to various process parameters, it would appear that the models cannot be simply assumed to produce good predictions when applied to other AFP head designs. The more recent formulations of intimate contact models [Yang and Pitchumani, 2001a] use directly measurable parameters as inputs, thus are not required to be tuned to experimental data, providing more robust predictive capability. The published values of welding time differ by many orders of magnitude, and it was shown that the model predictions vary significantly depending on the values considered. Results suggest that BPS-1 and BPS-3 provide the best approximations of bond strength out of the parameters investigated. Those models assumed the viscosity of neat PEEK for the intimate contact model and the assumption of the welding times that are similar (in the case of BPS-3) or equivalent (in the case of BPS-1) to the stress relaxation time of the polymer. The results presented here also show that the non-isothermal formulations are able to predict bond strengths that correlate well with the experimental results under highly non-isothermal conditions.

4.5 Extended placement trials

Now that the experimental method has been proven to be able to differentiate between bond strengths, and the non-isothermal bonding models appear suitable for the laser tape placement process, further experimental trials were continued using the same methodology. The laser AFP placement head was updated from an experimental model to a production version. Extended placement trials were performed to further investigate the validity of the bonding models while simultaneously investigating the response of the process to changes in consolidation force and placement rate.

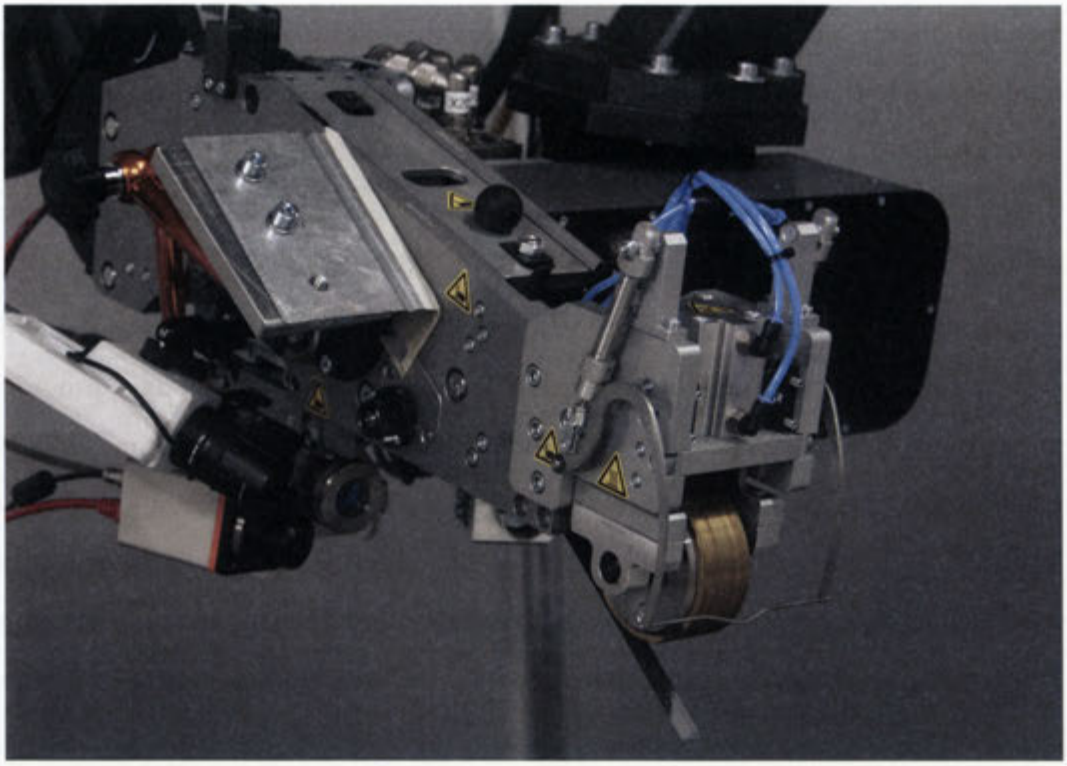


Figure 4.15 – The updated production model placement head used for the extended lap shear studies. The 80 mm brass consolidation roller is installed in this case.

4.5.1 Updated laser AFP head

In the extended placement trials, a new production version of the laser AFP head was used (Figure 4.15). The main differences are a change in the consolidation roller design, it was increased in diameter from 64 mm to 80 mm, and options of either a rigid brass roller or a conformable silicone roller were available. The pneumatic cylinders for the consolidation load application were replaced with a single 32 mm diameter version. The new control system for the placement head maintains a user-set pressure on the consolidation cylinders with an electronic pressure regulator. The temperature control system for the laser was also updated with new, compact long wave infra-red (LWIR) sensor arrays.

Table 4.6 – Process parameter sets for the extended lap shear trials. The process temperature was fixed at 450 °C.

Trial	Consolidation roller [Silicone/Brass]	Consolidation force [N]	Placement rate [mm/s]
ET-1	Silicone	150	100
ET-2	Silicone	150	200
ET-3	Silicone	150	333
ET-4	Silicone	500	100
ET-5	Silicone	500	200
ET-6	Silicone	500	333
ET-7	Brass	150	200
ET-8	Brass	500	200
ET-9	Brass	500	333

4.5.2 Process parameters

Process parameters for the extended placement trials are presented in Table 4.6. The process temperature was maintained at a constant value of 450 °C as this was shown to result in the highest strength in the preliminary trials. Parameters were selected to investigate the effects of consolidation pressure and placement rate on the bonding behaviour.

4.5.3 Temperature and pressure histories

Temperature measurements were performed using the same technique as in the preliminary lap shear study Section 4.3.1. The pressure measurement was modified in this case in order to measure the pressure directly during the process. This was achieved by placing a high temperature version of the 5051 sensor beneath the substrate Figure 4.16. The sensor was thermally isolated using a thin polyimide film combined with a layer of aluminium foil to provide protection from laser irradiation. Static pressure measurements yielded the same pressure distributions with and without the protective layers. It is expected that the material will plastically deform during the process which would result in slightly lower normal pressure under the substrate, however the substrate is only one ply thick and the viscosity of the material

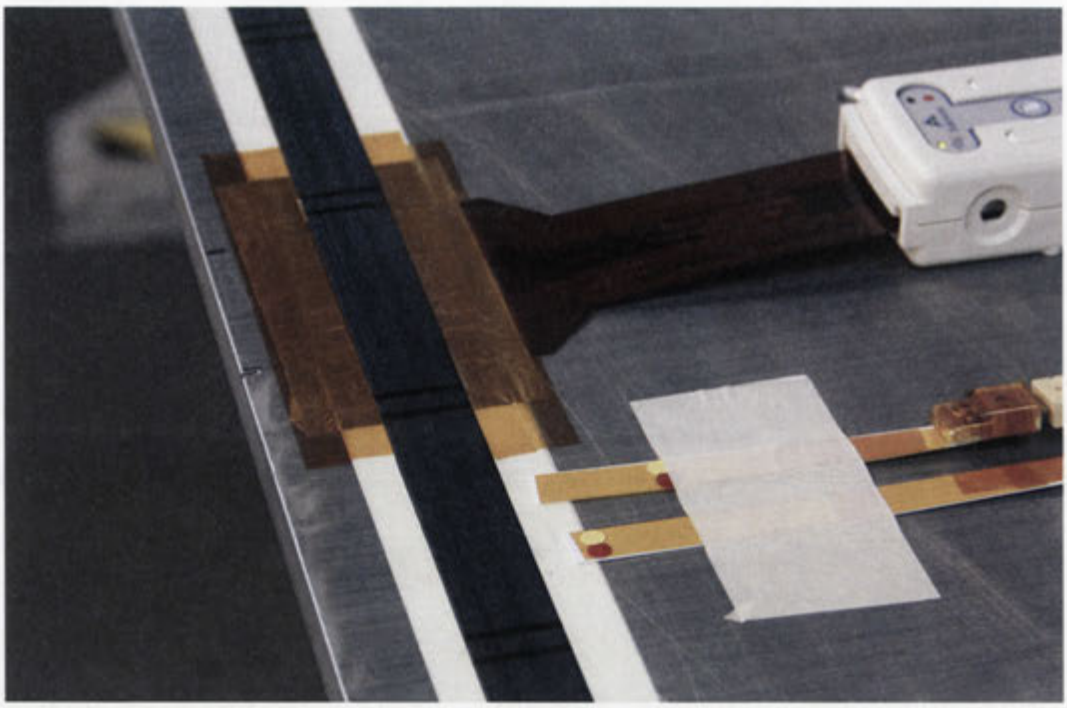


Figure 4.16 – Example of process instrumentation for the extended lap shear studies. A high temperature pressure sensor array placed under the substrate, insulated with polyimide film and protected from the laser with aluminium foil. Fine wire thermocouples can also be seen welded to the substrate.

is high. The scale of deformation is also low, therefore this measurement is assumed to be a reasonable approximation. A comparison of the static and dynamic pressure measurements revealed an insignificant difference in the pressure distribution, however a slight degree of asymmetry was found in the case of the conformable roller due to the back tension of the tape lifting the front edge of the roller.

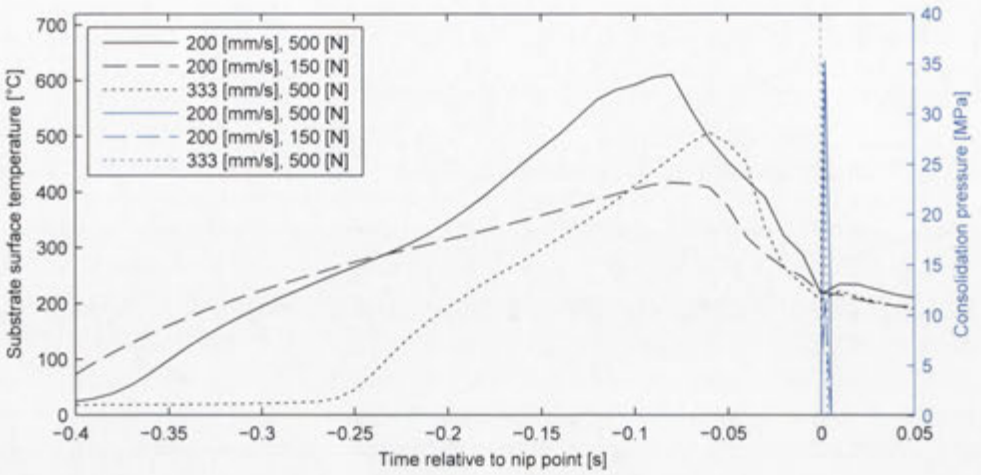
The results of the thermal model in Chapter 3 suggest that a shadow occurs in laser heating due to the positioning of the laser above the plane of placement. The results of the thermocouple measurements Figure 4.17 strongly support this hypothesis with clearly defined transitions in the temperature history caused by such a shadow. The approximate length of the shadows based on simple geometric calculations are shown in Table 4.7. The 80 mm brass roller does not deform, and therefore the corner radius is 40 mm which would result in a substrate shadow of approximately 96 and 48 ms for placement rates of 100 and 200 mm/s respectively. Inspection of the

Table 4.7 – Approximate length of shadows for various corner radii including the corresponding time periods for the shadows at various placement rates. Grey cells indicate shadow periods less than two samples of the thermocouple data acquisition module (< 20 ms).

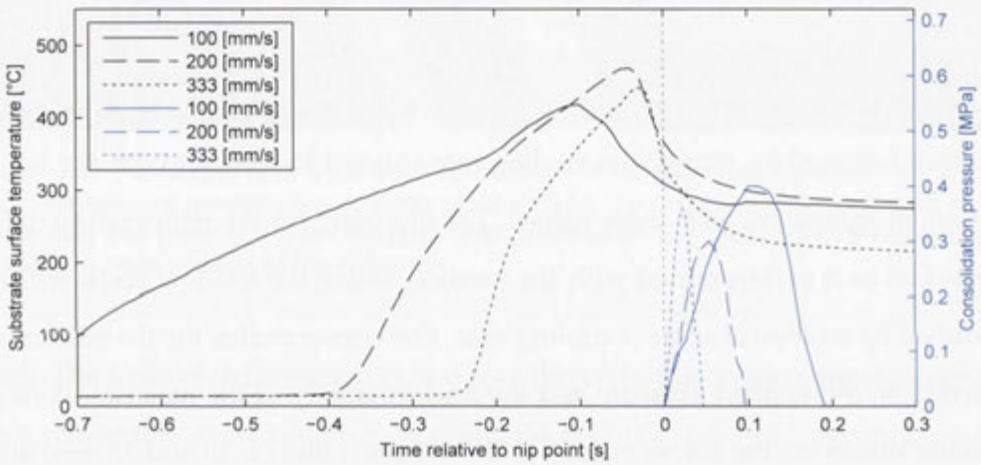
	Shadow Length		100 mm/s		200 mm/s		333 mm/s	
Radius [mm]	Substrate [mm]	Tape [mm]	Substrate [ms]	Tape [ms]	Substrate [ms]	Tape [ms]	Substrate [ms]	Tape [ms]
5	1.15	2.25	11.5	22.5	5.8	11.3	3.5	6.8
10	2.32	4.55	23.2	45.5	11.6	22.8	7.0	13.7
15	3.49	6.85	34.9	68.5	17.4	34.2	10.5	20.5
40	9.60	18.0	96.0	180.0	48.0	90.0	28.8	54.0

thermocouple measurements (Figure 4.17a) show corresponding decreases in temperature followed by changes in cooling rate (caused by contact with the hot tape) that are in agreement with these values. The nip point for the temperature data was aligned so as it corresponded with the location where the shadow ends, which was identified by sudden change of cooling rate. The corner radius for the silicone roller depends on the applied pressure and the conformability of the material. A range of possible values for the corner radius of the silicone roller (5, 10 and 15 mm) are also shown in Table 4.7. The thermocouple data acquisition module has a maximum sample rate of 100 Hz/channel which equates to one measurement every 10 ms. There must be at least two measurement points in order to identify a feature such as a shadow, therefore shadows of less than 20 ms (highlighted grey in Table 4.7) would not be positively identifiable.

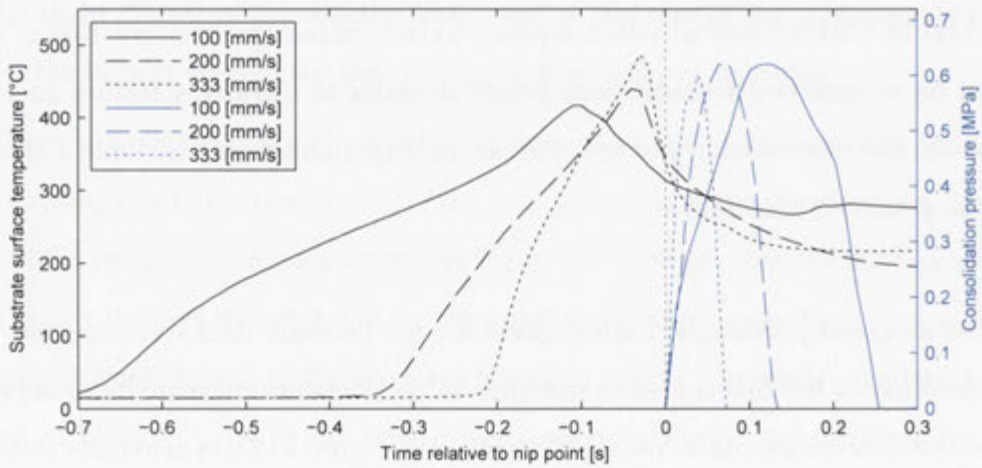
As assumed previously, the nip point for the pressure data was assumed to be the location of the first non-zero pressure value. Pressure measurements show the pressure distribution under the rigid brass roller (Figure 4.17a) is extremely short and very high pressures are experienced– two orders of magnitude higher than under the conformable silicone roller (Figures 4.17b and 4.17c).



(a) Rigid metallic roller.



(b) Silicone roller for consolidation force of 150 N.



(c) Silicone roller for consolidation force of 500 N.

Figure 4.17 – Experimentally measured temperature and pressure histories relative to the nip point for the extended lap shear placement trials.

4.5.4 Comparison of predicted and experimental strength

4.5.4.1 Rigid brass roller

In the case of all of the brass roller trial process measurements, the temperature during the heating phase greatly exceeded the melting point of the PEEK matrix (T_m = 343 °C), indicating that the crystalline phases would have been completely melted. The temperature history from the nip point forward was well below the melting point with temperatures in the range of 200-250 °C. Due to the extremely short cooling periods in the AFP process in which no significant re-crystallisation can occur, it was assumed in this study that the material remains amorphous and bond development can occur at temperatures as low as the glass transition point (T_g = 143 °C). The bonding behaviour is highly temperature dependent and it is possible that the rates of bonding will be insignificant at low temperatures. It was assumed that the properties of the amorphous PEEK at these temperatures can be extrapolated using Arrhenius relations. The re-crystallisation behaviour is highly dependent on the residence time spent at particular temperatures within the temperature range of 200-280 °C as seen in Table 4.2. While highly dependent on the particular temperature history, for time periods beyond 0.5 s it is most probable that crystallinity levels could begin to impede the healing behaviour. In such a case it would therefore be necessary to couple healing with crystallisation models to obtain more accurate predictions. In the case of the current work, at least 80 % of the total predicted healing development occurred before 0.5 s had elapsed for all of the predictions, therefore the amorphous assumption should provide valid approximations.

An example of the typical bond development history in the case of a brass roller is shown in Figure 4.18. Despite the low consolidation temperatures (<250 °C), it can be seen that the predicted degree of intimate contact and healing can in fact reach reasonable levels of approximately 40 and 50 % respectively. The resulting degree of bonding is predicted to be 22 %. It can also be seen that when considering the intimate contact development for the brass rollers, the pressure distribution is very

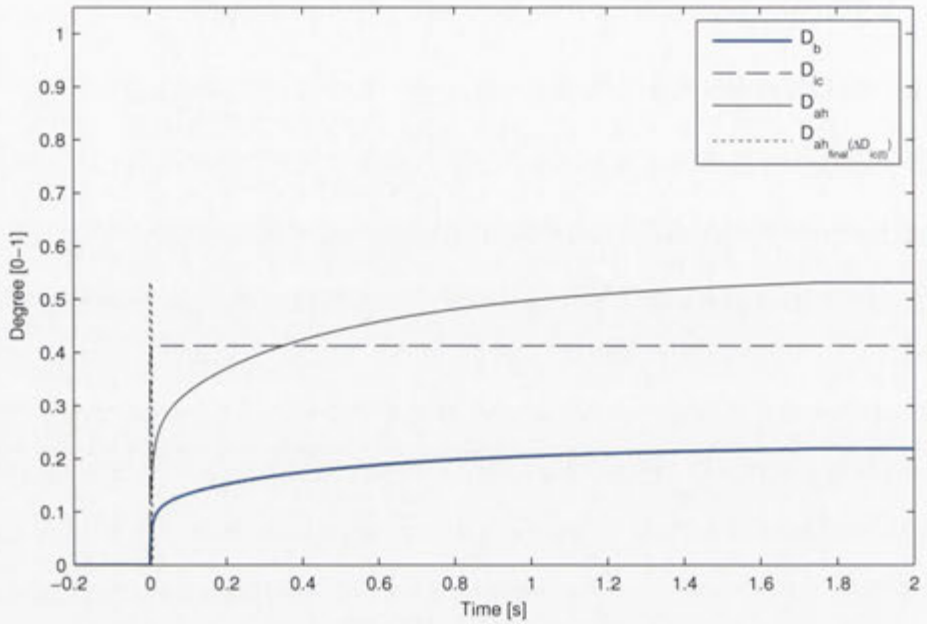


Figure 4.18 – Example bond development history (BPS-3, Table 4.4) for trials using an 80 mm rigid brass roller (ET-7).

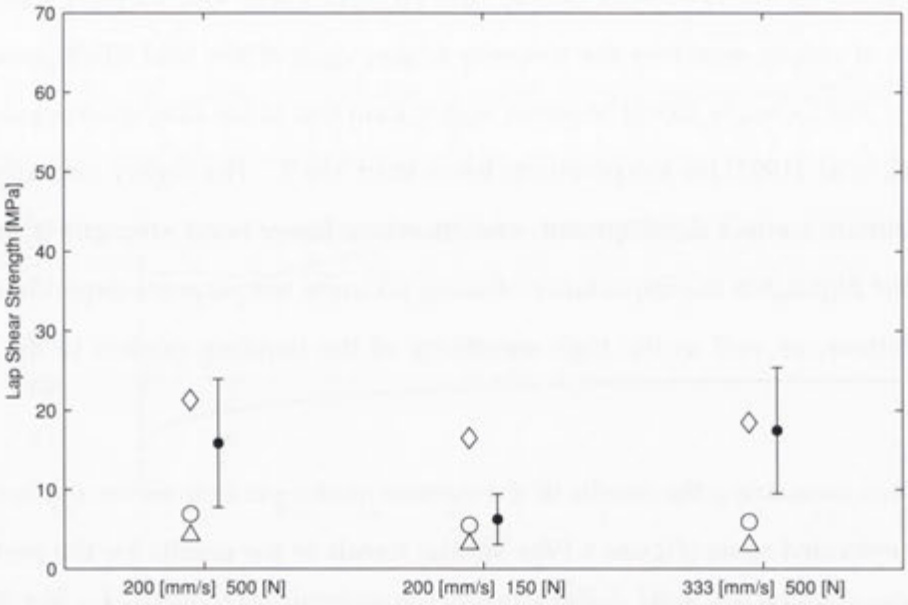
short, effectively an impulse compared with the much longer pressure application under a conformable roller. This results in extremely rapid intimate contact development. This suggests that the simplification of a step function for the intimate contact development in previous studies [Tierney and Gillespie, 2006] is a valid assumption, however only in the specific case of a rigid, non-conformable roller.

The characteristic behaviours of the different bonding models from both the literature and the currently proposed models as shown previously in Sections 4.4.3 and 4.4.4 were also observed in the predictions for the brass roller, therefore for the sake of brevity they are not presented here. The final predicted bond strengths are however presented, with predictions based on the literature and the currently proposed models shown in Figure 4.19. In the case of the predictions based on parameters from the literature (Figure 4.19a), the results for these placement trials are a bit different to those found for the preliminary studies with the parameters of Mantell et al. [1992] predicting higher strengths than Tierney and Gillespie [2006]; Khan et al. [2010]. The reason for this is the extended trials had lower interface temper-

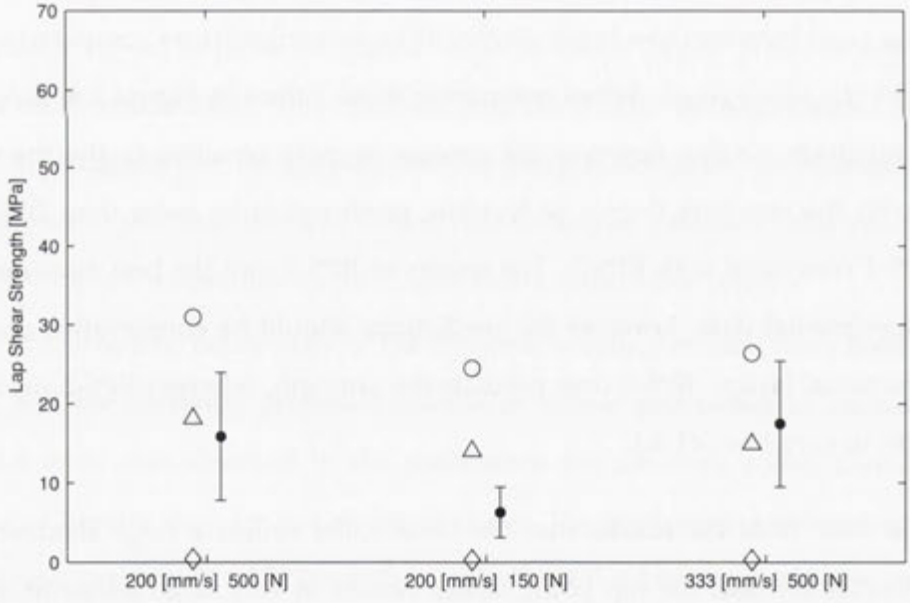
atures compared with the preliminary trials, and when comparing the temperature dependence of the viscosities ($\mu_{(\text{PEEK L\&S})}$, $\mu_{(\text{CFPEEK K,M\&S})}$ and $\mu_{(\text{CFPEEK M\&S})}$) in Figure 2.6, it can be seen that the viscosity ($\mu_{(\text{PEEK L\&S})}$) of the neat PEEK assumed by Tierney and Gillespie [2006] becomes higher than that of the fibre-matrix assumed by Mantell et al. [1992] for temperatures lower than 310 °C. The higher viscosity retards the intimate contact development, and therefore lower bond strength is predicted. This fact highlights the importance of using accurate temperature-dependent viscosity relations, as well as the high sensitivity of the bonding models to the thermal history.

When comparing the results of the current model predictions for the brass roller in the extended trials (Figure 4.19b), similar trends to the results for the preliminary studies are observed. The main difference here is the prediction for BPS-3 is now further separated from BPS-1. This is because the welding time assumed for BPS-3 ($t_{w\ (\text{PEEK S\&H})}$) increases to a larger degree at lower temperatures compared with that in BPS-1 ($t_{w\ (\text{PEEK K,M\&S})}$). When comparing these values in Figure 2.8, they appear to be relatively similar, however the process is quite sensitive to the the welding time with the resulting degree of bonding predicted to be more than 70 % higher for BPS-1 compared with BPS-3. The results of BPS-3 give the best agreement with the experimental data, however the predictions should be conservative due to the unidirectional layup. BPS-1 over-predicts the strength, whereas BPS-2 predicts the strength to very low (<1 %).

It is clear from the results that the brass roller causes a large shadow for the laser irradiation near the nip point, which results in very large temperature drops in excess of 180 °C as indicated by the thermocouple measurements in Figure 4.17a. Interestingly, despite this large temperature drop, the results of the placement trials for the brass roller strongly imply that bonding can definitely occur at temperatures well below the melting point of PEEK for consolidation temperatures in the range of 200-250 °C. Furthermore, the strength of the bond can be predicted with some degree



(a) Predictions based on parameters assumed in the literature (Table 4.3). Khan et al. [2010] (○), Mantell et al. [1992] (◇) and Tierney and Gillespie [2006] (△).



(b) Predictions based on the parameters assumed in the current work (Table 4.4). BPS-1 (○), BPS-2 (◇) and BPS-3 (△).

Figure 4.19 – Extended lap shear trials: comparison of experimental strengths (•) with bond strength predictions for trials using the 80 mm rigid brass roller. Error bars represent $\pm\sigma$.

of accuracy when considering the bonding parameter set BPS-3. The models are quite sensitive to the temperature-dependent viscosity and welding time relations, and measurement of their values at these low temperatures in the amorphous state is generally not experimentally feasible as the material will crystallise in a matter of seconds in this temperature range.

Prediction of this low temperature bonding for low final strengths may seem to be of limited value, however during the manufacture of laminates the interface is reheated to lower temperatures during the placement of subsequent layers, increasing the degree of bonding. The findings here suggest that as long as the material is in the amorphous state, low but significant levels of bonding can still develop at temperatures right down to the glass transition. It is therefore important to take this into consideration when performing strength predictions for the manufacture of laminates.

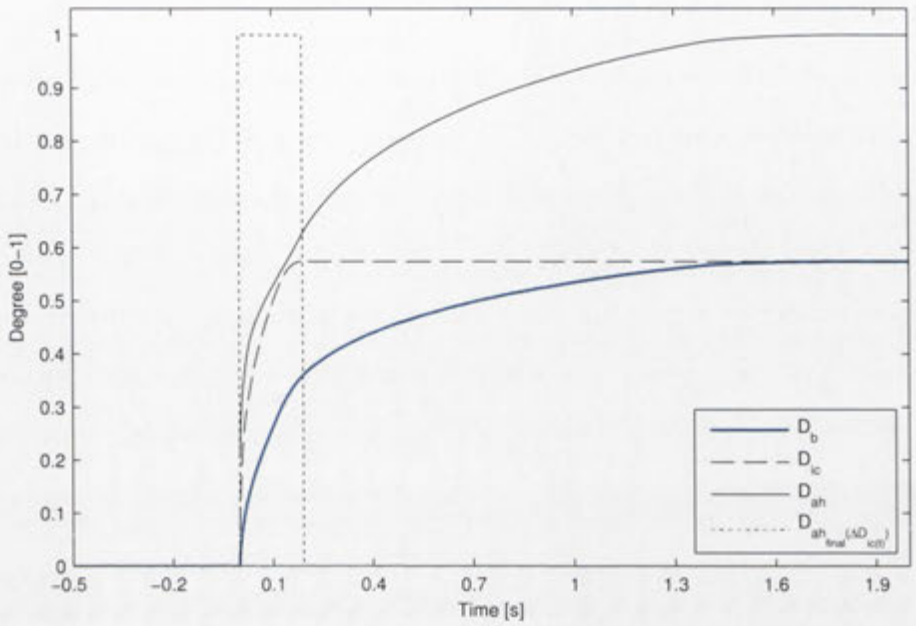
4.5.4.2 Conformable silicone roller

As with the brass roller, the temperature histories for the conformable silicone roller in the extended placement trials show that the pre-nip point temperature exceeded the melting point of the PEEK matrix ($T_m = 343\,^{\circ}C$), indicating that the matrix would be highly amorphous prior to the nip point. The consolidation temperatures were higher than the brass roller trials due to the smaller corner radius of the conformable silicone roller casting a much smaller shadow near the nip point. The initial consolidation temperatures were in the range of 300-350 °C as seen in Figures 4.17b and 4.17c. The temperatures are generally below the melting point of the PEEK matrix ($T_m = 343\,^{\circ}C$) for the majority of the consolidation period.

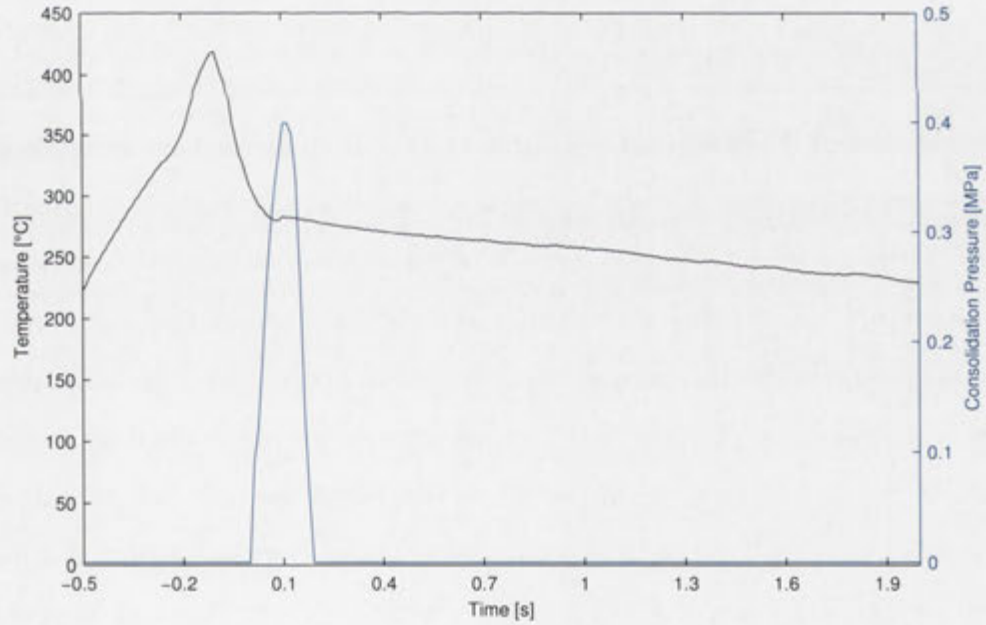
An example of the typical bond development history in the case of the 80 mm conformable silicone roller is shown in Figure 4.20a. Despite the low consolidation temperatures (<300 °C), it can be seen that the predicted degree of intimate contact is almost 60 % while healing reached completion. The resulting degree of bonding

is predicted to be 58 %. When examining the temperature history (Figure 4.20b) it can be seen that a significant period (1.5 s) is spent in the range of temperatures where the crystallisation rate is highest (210-270 °C). It is therefore likely that a significant amount of crystallisation could occur, inhibiting the healing. However 80 % of the healing is predicted to develop in under 0.5 s, therefore it is likely that the assumption of the material remaining amorphous would result in an overestimation of healing to the order of 20 %. This value is of course dependent on the particular welding time relation used, where shorter welding times would result in greater healing development in a shorter period of time.

The characteristic behaviours of the different bonding models from both the literature and the currently proposed models for the brass roller were also observed in the predictions for the 80 mm conformable silicone roller, therefore for the sake of brevity they are not presented here. The strength predictions based on the literature and the currently proposed models are however shown in Figure 4.21. In the case of the predictions based on parameters from the literature (Figure 4.21a), the strength prediction from Tierney and Gillespie [2006] is higher than that of Khan et al. [2010], which is the opposite of the case found for the brass roller (Figure 4.19a). Inspection of Figure 2.6 reveals that this because the temperature-dependent viscosity $\mu_{(\text{PEEK L\&S})}$ (assumed by Tierney and Gillespie [2006]) is lower than $\mu_{(\text{CFPEEK K,M\&S})}$ (assumed by Khan et al. [2010]) for temperatures greater than approximately 230 °C, leading to higher intimate contact development. Again it can be seen that the predictions of the various models can vary significantly depending on the particular input parameters. The strength predictions assuming the bonding model parameters from the literature show some agreement with the experimental values, with the general response of the models to the consolidation load showing good qualitative correlation with the experimental measurements. The strength predictions are consistently lower than the experimental measurements, but this is expected due to the crossed ply assumption of the intimate contact models. An anomaly is the prediction cor-



(a) Example bond development history (BPS-3, Table 4.4).



(b) The corresponding temperature and pressure history.

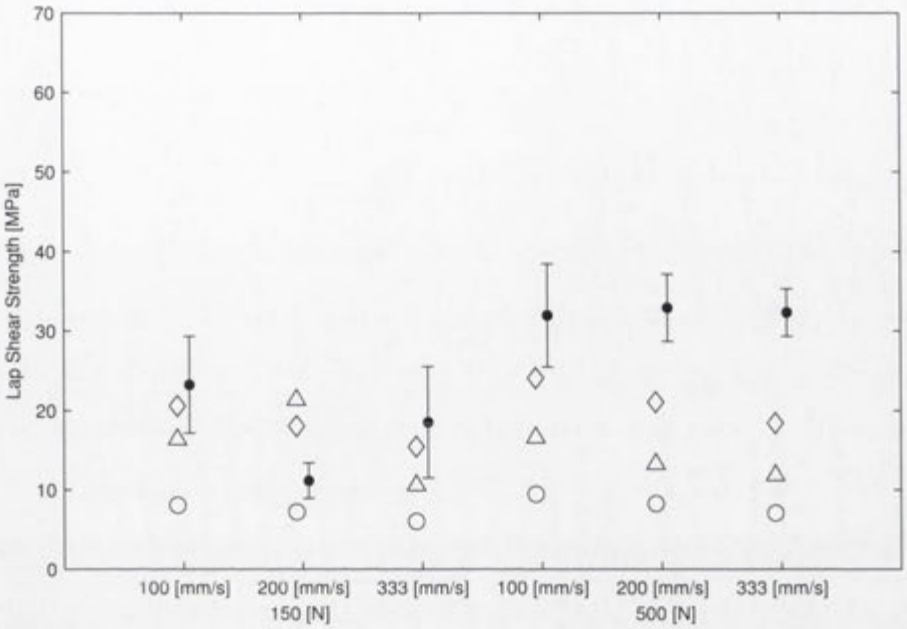
Figure 4.20 – Extended lap shear trials: Example bond development history for an 80 mm conformable silicone roller (ET-1).

responding to process parameters of 200 mm/s and 150 N shows a particularly low experimental strength, however the predicted strength is relatively high compared to the other predictions for a load of 150 N.

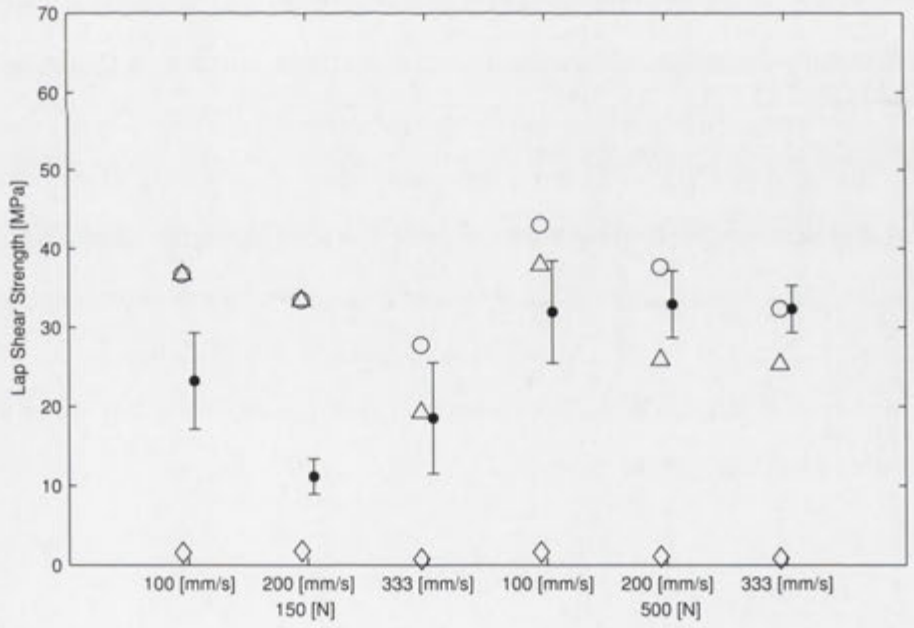
In the case of the currently assumed bonding model parameters (Figure 4.21b), similar qualitative agreements to the predictions based on the parameters from the literature were observed for BPS-1 and BPS-3, however the magnitude of the strength predictions agreed more closely with the experimental results. BPS-3 again showed the best agreement as was found to be the case for both the brass roller and also the preliminary placement trials. The strength predictions for BPS-2 were again found to be very low (<3 %) due to the long welding times determined by the $t_{w\,(\text{PEEK L\&S})}$ relation (Figure 2.8).

4.5.5 Effect of placement rate

When considering the response of the process to the placement rate, it can be seen that within the range of parameters studied, the lap shear strength was relatively independent of the placement rate for both the rigid brass and conformable silicone roller trials Figures 4.19 and 4.21. In fact there was no statistically significant difference in the strengths, and in the case of the silicone roller higher speeds actually resulted in less variability of the lap shear strengths. The bond strength predictions based on experimentally measured temperature and pressure histories also predicted a very similar outcome. This result is somewhat surprising as the time available for bonding to occur is inversely proportional to the placement rate. The intimate contact development is the limiting factor as it can only occur when pressure is applied to the interface. The healing is independent of pressure application and continues well after the pressure application has ceased. At higher placement rates, the time from the nip point to the point of maximum pressure application is reduced, therefore the intimate contact development occurs sooner compared with a lower placement velocity, and thus the material is also at a higher temperature as there has been less



(a) Predictions based on parameters assumed in the literature (Table 4.3). Khan et al. [2010] (○), Mantell et al. [1992] (◇) and Tierney and Gillespie [2006] (△).



(b) Predictions based on the parameters assumed in the current work (Table 4.4). BPS-1 (○), BPS-2 (◇) and BPS-3 (△).

Figure 4.21 – Extended lap shear trials: comparison of experimental strengths (•) with bond strength predictions for trials using the 80 mm conformable silicone roller. Error bars represent $\pm\sigma$.

time for it to cool. Therefore the decreased time period of pressure application at high speeds is partly compensated by higher temperatures, resulting in similar levels of intimate contact.

4.5.6 Effect of consolidation force

The effect of the consolidation force can be seen for the brass and silicone rollers in Figures 4.19 and 4.21 respectively. The process can be seen to respond favourably to increased consolidation force, a result of which would be expected as all of the placement trials in this case were predicted to be predominantly intimate contact limited. For the brass roller, increasing the consolidation force was found to increase the pressure, however length of the pressure distribution remained very short. Nonetheless, increasing the consolidation force increased the pressure resulting in higher levels of intimate contact, and the measured strength of the lap shear samples more than doubled when increasing the consolidation load from 150 N to 500 N. In the case of the conformable roller, an increase in consolidation force was found to increase the length of the pressure distribution by approximately 25 %. The conformability of the roller around the profile of the tape also resulted in a significant portion load being transferred to the tooling either side of the tape at higher pressures. As load was applied over a larger area, the maximum pressure in the consolidation zone was only found to increase by 80 % for a 333 % increase in consolidation force. This again leads to higher intimate contact development and the resulting lap shear strengths were found to increase by at least 50 %.

4.6 Conclusions

The purpose of this chapter was to investigate the suitability of the bonding models in literature for bond strength prediction in the laser AFP process. Another goal was to investigate whether bonding could occur at temperatures below the melting point of the polymer, as results from the previous chapter had suggested this was

occurring. The temperature and pressure histories were measured directly during the process using thermocouples and active pressure measurement sensor arrays. The results of which were fed into various bonding models that were implemented from the literature. Bonding predictions were made based on parameters from models in the literature that were experimentally validated, as well as parameters using more recent values for the particular composite under investigation.

It was necessary to select a bond characterisation test method to produce useful data points for validation of the bonding model predictions. Lap shear samples were manufactured with a single placement pass for a variety of processing conditions and consolidation rollers. A single placement pass ensured that the bond strength was not fully developed, which was necessary to generate data points to validate the bonding models. A technique for producing lap shear samples with consistent lap lengths in the in situ AFP process was developed, using polyimide tape to form precisely spaced breaks in the inter-laminar bond.

In situ temperature measurements were performed using fine wire thermocouples attached to the substrate. Trials were performed with rigid brass and also conformable silicone consolidation rollers. Using the knowledge gained in Chapter 3 for the thermal behaviour of the process, the position of the nip point in the temperature measurements could be determined. In the case of the brass roller, a large shadow was present resulting in very low nip point temperatures in the range of 200-250 °C. Nip point temperatures were in the range of 300-340 °C in the case of the conformable silicone rollers in the extended trials. The consolidation pressures were measured during the process with active pressure sensor arrays and it was found that the pressure distributions were almost identical to static measurements, however the distribution became slightly asymmetric due to the back tension of the feed tape.

Comparisons between the process temperature history and recently published data on the crystallisation behaviour of PEEK suggested that it would in fact remain highly amorphous during the consolidation phase, under the condition that

the temperature exceeded the melting point prior to the nip point. As the matrix remains in the amorphous state, it is possible for healing and intimate contact to develop right down to the glass transition temperature. Temperature measurements performed for placement trials using the brass roller strongly suggest that the consolidation temperature was low due to a large shadow before the nip point, and in the range of 200-250 °C. Lap shear tests of the samples showed that despite such low bonding temperatures, values could reach up to 25 % of the ultimate strength. For both the welding time and the viscosity it was assumed that the Arrhenius relations could be applied to determine the properties at these low temperatures in the amorphous state. Bonding predictions were found to correlate with the experimental results, with the currently proposed bonding parameter set 3 (BPS-3) providing the best agreement. Trials were also performed using a conformable silicone roller where the initial consolidation temperatures were in the range of 300-340 °C, just below the melting point of the polymer at 343 °C. Again, it was found that significant levels of bonding occurred with strengths up to 50 % of the ultimate lap shear strength. This is a significant finding as it strongly suggests bond development can occur in the laser tape placement process for temperatures lower than previously thought due to the extremely short time periods involved. As discussed in the literature review (Section 2.2.7), bonding of PEEK is generally considered to not be possible for temperatures below 290 °C as the PEEK will readily crystallise, strongly inhibiting the healing process. From this work it has been shown that the bond predictions for AFP processes must consider the crystalline state of the resin, which was likely to be amorphous for all of the trials in the current study. It is likely that the amorphous state will be achieved during subsequent passes and therefore higher bond strengths may be achieved that otherwise previously thought.

The bonding models were found to be sensitive to the welding time relations as well as the temperature-dependent viscosity. The relative magnitude of the strength predictions assuming bonding model parameters from the literature compared with

each other was found to be dependent on the particular temperature history, as the same viscosity relations assumed for the intimate contact models have a stronger temperature dependence than others, which would result in more rapid intimate contact development for high temperature yet much slower development at low temperatures relative to other models. The experimentally validated parameter sets from other studies in the literature predicted quite different strengths in all cases, highlighting the fact that models cannot simply be adopted for other processes. The models in the literature have generally used predicted temperature and pressure histories instead of true process data, and then the bonding model parameters have been adjusted as tuning factors to obtain satisfactory agreements with experimental data. The models are therefore strictly suitable for understanding the response of a particular placement system to which they are calibrated, however caution must be exercised when applying such models to other processes. In the current study, the intimate contact was assumed to be the deformation of neat PEEK polymer at the surface. Recent values for the viscosity of the particular grade of PEEK used in the composite prepreg were assumed, as well as the surface roughness parameters measured on the same prepreg. Three bonding parameters sets were formulated assuming different welding time relations. It was found that assuming the welding time from Lee and Springer [1987] (BPS-2) resulted in gross underestimations of the strength. The value assumed by Sonmez and Hahn [1997a] (BPS-3) agreed well with the experimental data in the vast majority of cases and provided the best estimates of strength out of all bonding model parameter sets studied. The welding time of Khan et al. [2010] (BPS-1) produced similar results, but predicted strengths were generally higher than found in the experiments.

Samples produced with the conformable silicone roller were found to produce superior strengths compared with the rigid brass roller. The measured temperature histories suggest that a large shadow formed by the large radius of the roller would cause much greater temperature drops before the nip point compared with

the silicone roller which has a much smaller shadow. The difference in strengths was therefore mostly attributed to the lower resulting temperatures in the consolidation zone rather than differences in the applied pressure distributions. The process was found to respond favourably to an increase in consolidation force from 150 N to 500 N, with the strength typically increasing by approximately 100 and 50 % for the brass and silicone rollers respectively. The maximum pressure under the silicone roller was found to only increase by 80 %, despite the 333 % increase in load. This was due to an increase in size of the contact patch, as well as a large portion of the load being supported by the tooling either side of the tape in the case where higher loads were applied. Interestingly, for the range of process settings studied, the bond strength was relatively independent of the placement rate, with no statistically significant difference between speeds in the case of a high consolidation load. This was explained by the fact the peak consolidation pressure would occur sooner after the nip point before the material has time to cool to the degree it would at a lower placement speed. The decreased time for pressure application was therefore partly compensated for by pressure application at slightly higher temperatures.

In this chapter, many thermocouple measurements, particularly those for the brass roller, strongly support the idea that there is significant shadow of the laser irradiation immediately prior to the nip point due to the positioning of the laser source above the plane of placement. The shadow causes significant decreases in temperature prior to the consolidation zone, adversely affecting the bond development process. It is clear that the interaction of the laser with the composite in the region near the nip point needs to be studied further. In the next chapters, optical characterisation and ray-tracing models will be used to further investigate the presence of the shadow in laser AFP. Such models can then be used to optimise the laser position to minimise the shadow.

Chapter 5

Optical characterisation

Abstract

The geometry of a nip point heating strategy in laser AFP results in a shadow before the nip point on both the tape and substrate, as strongly suggested by the findings in Chapters 3 and 4. The moderate laser angle leads to reflections in the cavity between the tape and substrate, potentially reducing the shadow. An optical model can provide valuable insight to the interaction of the laser with the composite, as well as detailed estimation of the irradiance distributions. This chapter describes the optical characterisation process and formulation of appropriate models to capture the composite surface and laser source behaviour, which are to be applied to a full optical model of the process in Chapter 6. First, the unique scattering behaviour of the composite is investigated and a model formulated to appropriately capture the macroscopic surface behaviour. As the laser is aimed at the composite from a substantial angle, the angular dependence of the composite is then characterised and suitable angular dependence relations determined. Finally, the laser beam profile and propagation are measured and suitable models constructed to provide an accurate representation of the source for later application to a full optical model of the laser AFP system.

5.1 Introduction

A well formulated 3D optical model can provide valuable insight into the laser's interaction with the cavity between the tape and substrate, as well as detailed estimation of the irradiance distributions. Such distributions can then be subsequently applied to a thermal model, allowing the influence of a shadow on the temperature profile to be understood, and accurate prediction of the temperature history. In this work a combined optical-thermal model is presented for carbon/PEEK NIR laser-assisted TP-ATP. The first step in formulating such a model is optical characterisation of the composite material and laser source, which is described in this chapter. Models for approximating the composite behaviour in terms of scattering and reflected power will be formulated. The laser beam profile and propagation will be measured and approximated.

5.2 Optical property characterisation

It is necessary to first understand the optical behaviour of the composite prior to formulating the optical model. As the configuration of the laser tape placement system forms a wedge shaped cavity between the substrate and tape, the scattering distribution of the reflected radiation is also important, as will be shown later. The properties need to be determined at the wavelengths of the multi-mode laser source, which emits at $\lambda = 940$ and 980 nm.

Initially, a *Suprem*™ *T* 55 % v/v AS4/PEEK-150 0.15 mm × 12 mm unidirectional prepreg tape was analysed at 50× magnification on a *Nikon* confocal microscope. A three dimensional reconstruction of the surface is shown in Figure 5.1. The PEEK appears to be transparent as the fibres can be clearly seen beneath the surface. The colouring in select regions is suggestive of thin film interference, implying a local resin thickness to the order of the wavelength of the light. The surface of the matrix is also not flat; it undulates predominantly in the transverse direction. The microscope

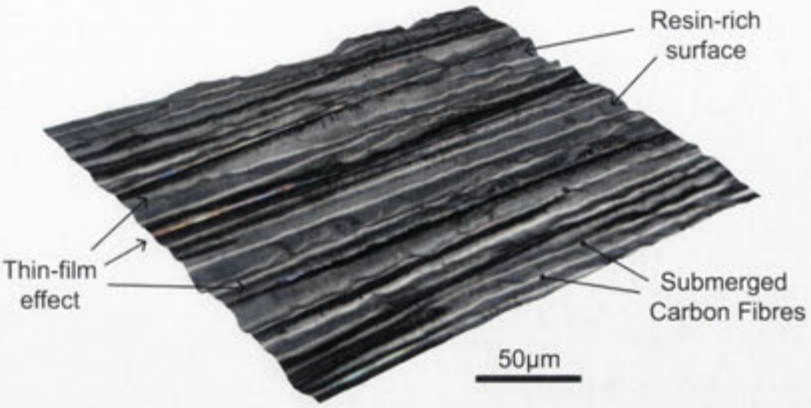


Figure 5.1 – 3D surface profile of the composite produced by a confocal microscope at 50x magnification.

image is from the visible wavelengths, however the following measurements show that the image should also be representative of the composite at the laser wavelength.

5.2.1 Optical properties of PEEK

Optical measurements were performed on a *Perkin Elmer Lambda 1050* UV/Vis/NIR spectrophotometer equipped with a 150 mm integrating sphere. The 100 % baseline was performed with a *NIST* traceable 99 % reflectance standard mounted in the reflectance port. The 0 % baseline was performed using the internal attenuator. Transmittance and reflectance measurements were first performed on 100 µm *Stabar K200* amorphous PEEK film. A semicrystalline (highly translucent) sample was also prepared by annealing the film at 250 °C for 3 h. From the transmittance (T) and reflectance (R) measurements, the level of absorptance (A) can be determined using the conservation of energy:

$$T + R + A = 1 \tag{5.1}$$

$$A = 1 - T - R \tag{5.2}$$

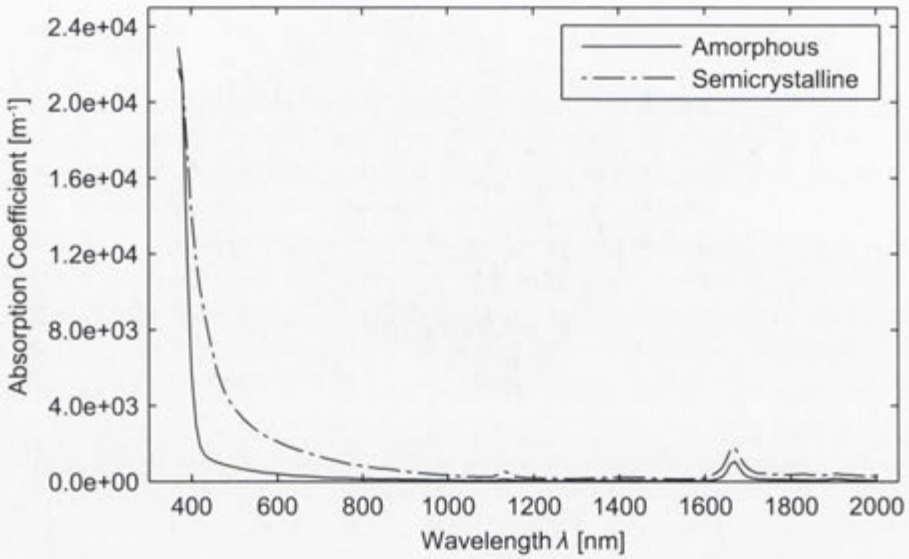


Figure 5.2 – Absorption coefficient vs. wavelength for amorphous and semicrystalline PEEK films.

Then using the measured thickness t of the film, the absorption coefficient α is determined:

$$\alpha = \frac{-\ln(1-A)}{t} \tag{5.3}$$

The absorption coefficient is relatively low except for shorter wavelengths, Figure 5.2. The crystalline phases in semicrystalline polymers are known to scatter light due to local variations of refractive index [Becker and Potente, 2002; Chen et al., 2011], thus the higher apparent absorption coefficient for the semicrystalline film is likely due to backscattering of the incident light during transmission measurements rather than increased absorption. To put the measurements into context, the transmitted intensity T can be related to the path length (t) by the Beer-Lambert Law [Swinehart, 1962]:

$$T = e^{-\alpha t} \tag{5.4}$$

The intensity vs. path length at the wavelengths of the laser (λ = 940 and 980 nm) is shown in Figure 5.3. Based on observations of the surface (Figure 5.1) the thickness of the matrix covering the fibres is expected to be no greater than 10 µm. The crystalline

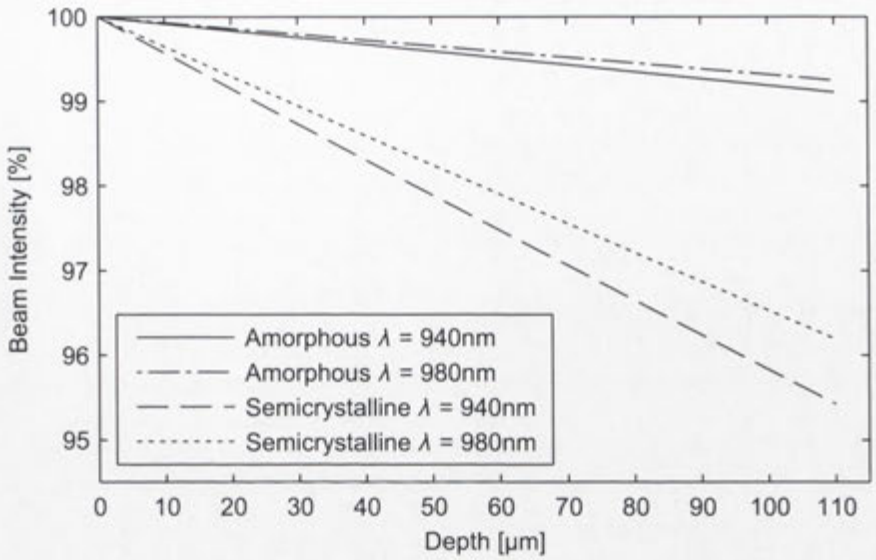


Figure 5.3 – Transmitted intensity vs. path length for amorphous and semicrystalline PEEK at the wavelength of the laser.

phases in semicrystalline polymers are known to scatter light which results in a thickness dependent transparency [Becker and Potente, 2002]. In the case of PEEK, spherulites range from 1-10 μm in size [Cogswell, 1992], suggesting a low number of scattering centres for the thickness of the PEEK covering the fibres on the surface of the composite. Therefore any crystalline phases present in this context are likely to have a mild scattering effect. Therefore, the PEEK is considered to be transparent.

The refractive index of the PEEK is also of interest as it can be used to determine the angular dependent reflectance. The reflectance measurements performed in the spectrometer are the result of the combined reflections from the air-to-PEEK interface and also the PEEK-to-air interface at the rear side of the sample. As it is known that the level of absorption is very low, the double reflectance equation was assumed to solve the reflectance (R) from only the air-PEEK interface:

$$R_{measurement} = \frac{2R}{1+R} \tag{5.5}$$

For a normal angle of incidence on a dielectric, the reflection is related to the refrac-

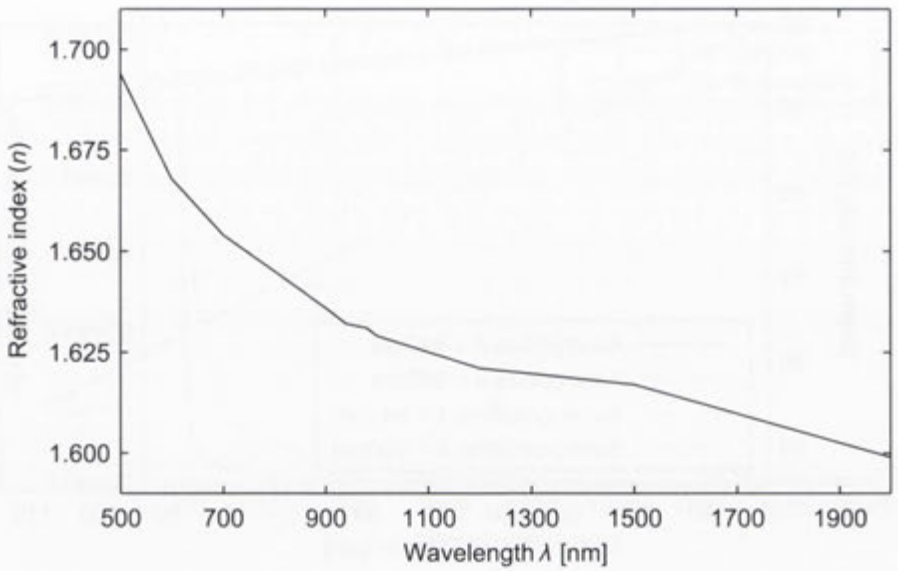


Figure 5.4 – Refractive index vs. wavelength for the amorphous PEEK film.

tive indices by:

$$R = \left(\frac{n_2 - n_1}{n_2 + n_1}\right)^2 \tag{5.6}$$

Since the reflection measurements were performed at a small angle of 8°, the above equation provides a good approximation of the refractive index (within 0.02 %). Assuming $n_1 = 1.0$ for air, the refractive index of the PEEK was determined and plotted in Figure 5.4. It can be seen that there is normal dispersion. Since there is minimal dispersion (in the context of reflected power level) and absorption for wavelengths λ = 500-1000 nm, the behaviour observed in the visible range should be representative of that at the wavelength of the NIR laser as there is no significant difference in optical properties.

5.2.2 Optical properties of AS4/PEEK composite

The scattering behaviour was observed qualitatively using the following approach, as illustrated in Figure 5.5. A low power red laser (λ = 670 nm) with a 2 mm spot diameter was aimed at the composite sample at a fixed angle of incidence of θ = 65°. The scattering pattern was observed on a white diffuse target placed behind

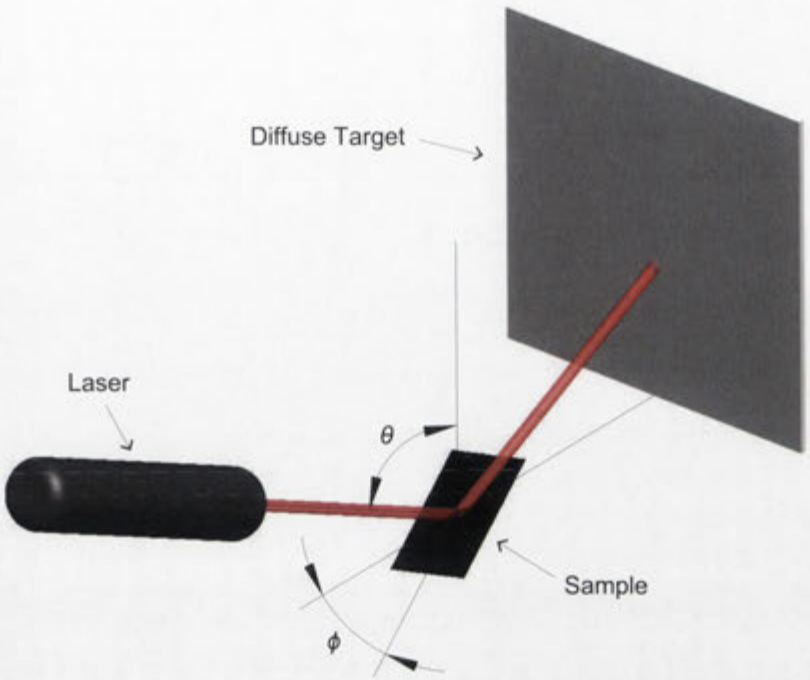


Figure 5.5 – Experimental setup for qualitative scattering observation.

the sample. The angle of the composite sample was varied from angles ranging from ϕ = 0-90°. Assuming that the diffuse target is Lambertian, then the radiance is proportional to the irradiance [Ramamoorthi and Hanrahan, 2001]. The observed distributions should therefore represent the relative irradiance. The scattering pattern was recorded with a digital SLR camera in RAW format and processed linearly, to enable equal comparison with the modelled irradiance distributions. The scattering behaviour for the unidirectional composite tape is shown in Figure 5.6.

It is anisotropic and changes quite drastically from a crescent shape when the beam is aligned with the fibres to a vertical line when the sample is positioned perpendicularly. Since the PEEK is effectively transparent, the scattering behaviour would be dominated by specular reflections from the individual carbon fibres. The crescent shape is formed by the specular ray being spread into a hollow cone-shaped distribution where the axis of the cone lies in the plane of the sample. The level of diffuse reflection was observed to be minimal with some scattering centred about the

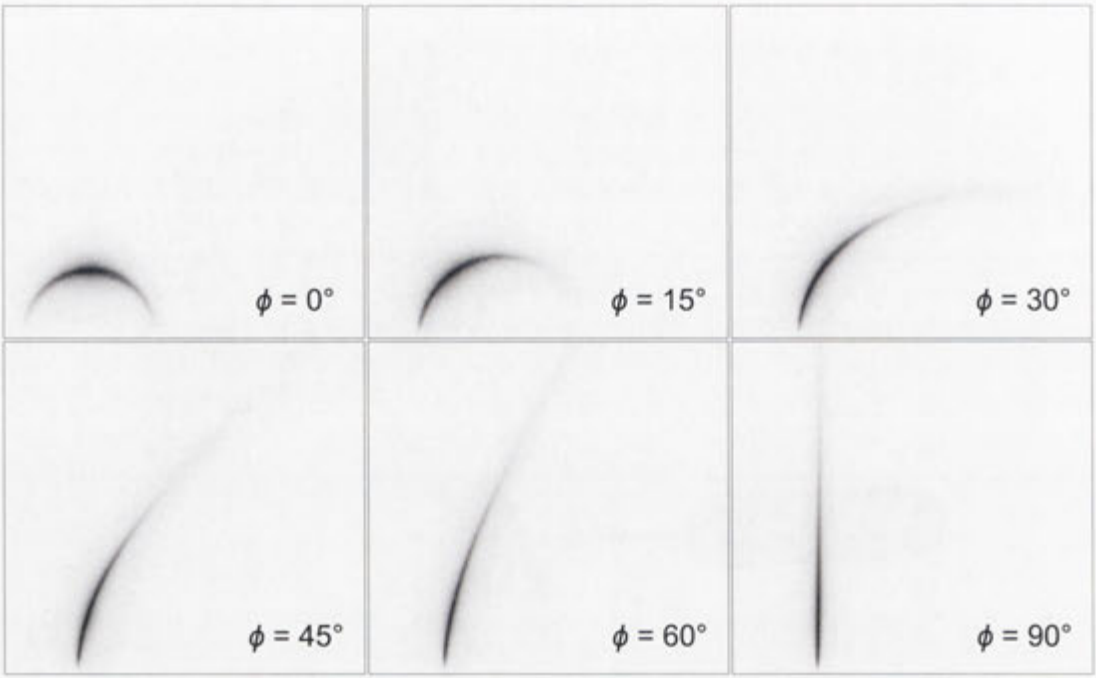


Figure 5.6 – Experimental observations of scattering patterns from the composite tape at various orientations.

crescent shaped distribution.

Transmittance and reflectance measurements were performed on five different AS4/PEEK samples in the spectrophotometer. The transmittance was found to be <0.1 % at all wavelengths, indicating strong absorption by the carbon fibres. As the transmittance is zero, the reflectance is the complement of the absorptance (Eq. (5.2)). As the composite displays significant scattering behaviour it is necessary to measure the total hemispherical reflectance with a device such as an integrating sphere. The angular dependent reflectance behaviour was measured using the central sample holder for the integrating sphere as shown in Figure 5.7.

Measurements were performed at incident angles ranging from 5-85° with the beam aligned to the fibre direction. The results in Figure 5.8 show that the reflectance increases with wavelength. This is attributed to anomalous dispersion from the carbon fibres, as published values for graphite show anomalous dispersion from λ = 500-2000 nm [Borghesi and Guizzetti, 1997; Stagg and Charalampopoulos, 1993]. This provides further evidence that the behaviour is dominated by reflections from

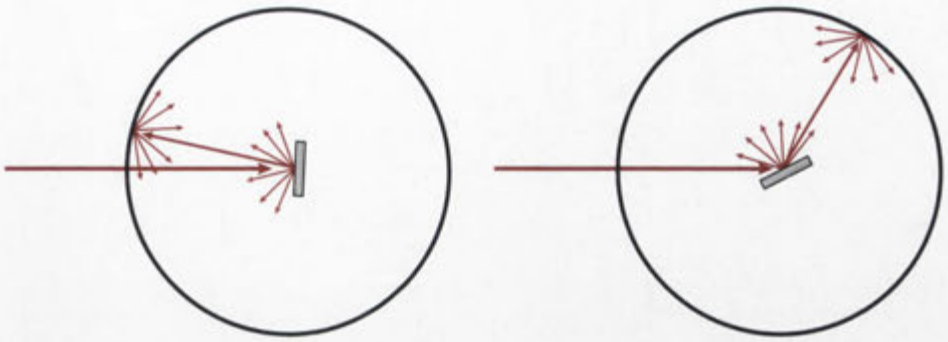


Figure 5.7 – Examples of measurements at 10° and 60° angles of incidence using integrating sphere centre mount.

the carbon fibres, rather than reflection off the surface of the matrix. For high angles of incidence, it is likely that the reflection would transition to being dominated by reflections from the PEEK due to higher Fresnel reflection. The difference between λ = 940 nm and λ = 980 nm is insignificant, therefore the proceeding optical analysis is assumed monochromatic.

For the laser TP-ATP process the composite surface can reach temperatures of 600 °C as shown in Chapter 4. Stagg and Charalampopoulos [1993] measured the effective refractive indices of pyrolytic graphite, amorphous carbon and soot at temperatures of 25-600 °C. The reflected power was calculated from this data and found to be independent of temperature within the measured range for the three forms of carbon. The structure of a high strength carbon fibre is between pyrolytic graphite and amorphous carbon, and hence the optical properties of the composite are assumed to be constant for the studied temperature range.

5.3 Optical model formulation

Non-sequential ray tracing software (*OptiCAD 10*) was used for the optical analysis. The ultimate goal of the optical model is to determine the irradiance/heat flux distribution on the composite due to the laser. It is therefore important to formulate a macroscopic model which efficiently captures:

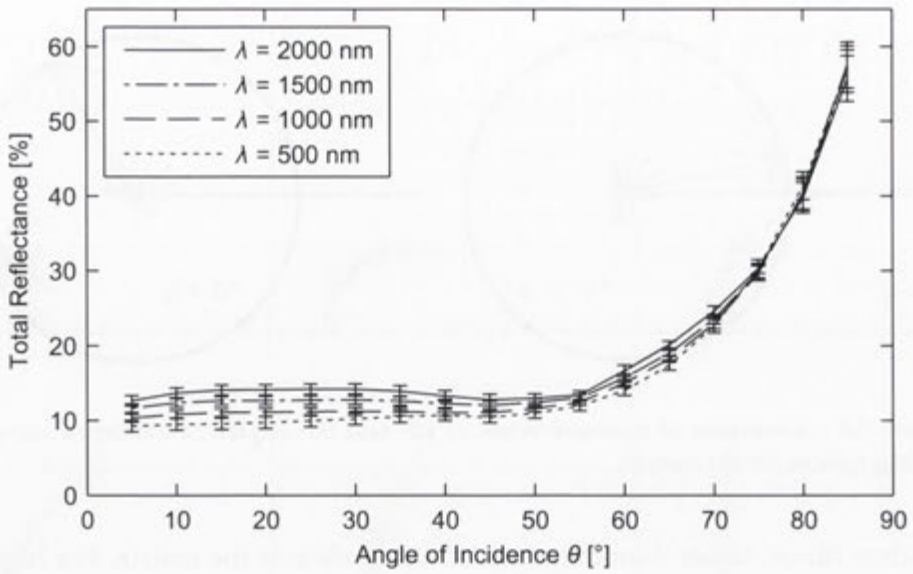


Figure 5.8 – AS4/PEEK reflectance vs. angle of incidence at various wavelengths. Error bars represent $\pm\sigma$.

1. The correct angular dependent reflection behaviour as the angle of incidence varies significantly, particularly for the tape on the consolidation roller where it ranges from approximately 50° up to 90° due to the curvature.

2. The scattering distribution of the reflected light as it is typically reflected onto the opposite side of the cavity formed by the tape and substrate.

3. The profile of the laser beam, and importantly the way in which it propagates as the laser is aimed at an inclined angle relative to the irradiated surfaces.

Ray tracing is valid where the objects are much larger than the wavelength of light as physical optical effects such as diffraction and interference are not captured. In this case the fibres are an order of magnitude larger than the wavelength of the laser, thus a ray tracing technique is justified. Furthermore, the confocal microscope images (Figure 5.1) show minimal areas exhibiting thin film effects and the thickness of the PEEK above the fibres is variable so any physical effects would be averaged on the macroscopic level.

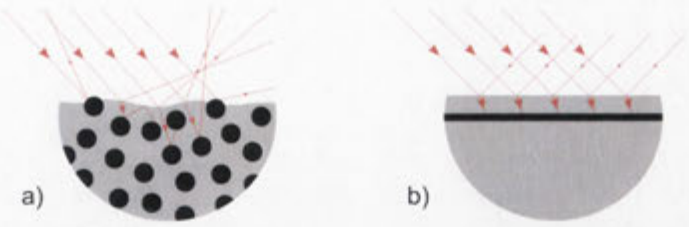


Figure 5.9 – a) Interaction of light with the composite b) Specular surface model with absorbing radiometric film behind surface

5.3.1 Scattering

The actual behaviour is a combination of reflection from both the surface of the matrix and the fibres beneath the surface, and possibly from any exposed fibres present at the surface. An illustration of this behaviour is shown in Figure 5.9a. Light incident on the carbon fibres is mostly absorbed and partially reflected whereas the light incident on the PEEK is partially reflected and mostly refracted. The light reflected off a submerged fibre may be totally internally reflected if it strikes the PEEK-air boundary at an angle of incidence greater than the critical angle, otherwise the light will escape the composite.

Modelling the composite with individual filaments is impractical for model formulation, computation and analysis. Since most of the power is absorbed by the fibres just beneath at the surface as suggested in Boley and Rubenchik [2013], it can safely assumed that the light is absorbed in a thin layer or film near the surface for the purposes of a macroscopic model. In ray tracing analyses, radiometric films are used to measure irradiance distributions. Using film alone as the composite surface will however result in total absorption of the incident light without reflections. The composite was therefore modelled as a transparent body with a fully absorbing radiometric film placed immediately beneath the surface (Figure 5.9b). This allows the correct reflection behaviour to be modelled at the surface of the composite as well as measurement of the irradiance distribution.

For most optical analyses a flat surface is assumed (Figure 5.9b) for the geometry and a scattering function is applied as required. The scattering functions available

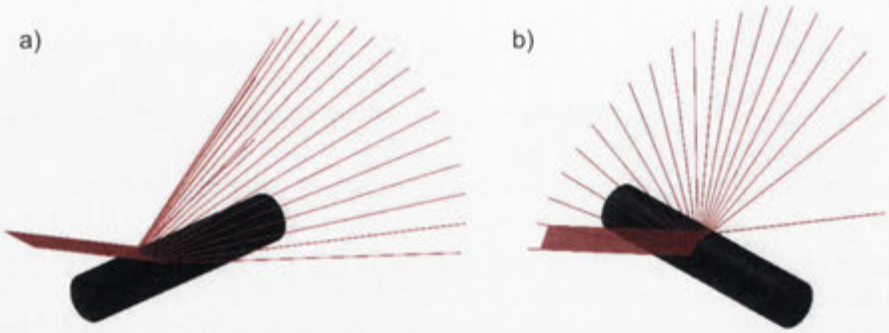


Figure 5.10 – Scattering from a cylindrical object for a) $\phi = 0°$, and b) $\phi = 90°$

in most optical packages assume isotropic scattering in the sense that the scattering function is independent of surface orientation. Measurements have shown the surface shows highly anisotropic scattering behaviour characteristic of a cylindrical element as demonstrated in Figure 5.10.

When a collimated beam of light strikes the cylinder along its axis, the light is scattered in a cone-shaped distribution about the axis of the cylinder (Figure 5.10a). In the case where the light is perpendicular to the cylinder axis, it is scattered in a disc shaped distribution that lies in a plane perpendicular to the cylinder (Figure 5.10b). The scattering distribution observed for the composite is in fact dominated by specular reflections occurring on subsurface carbon fibre filaments. This type of highly anisotropic reflectance behaviour is characteristic of brushed metal surfaces, hair and fabric [Poulin and Fournier, 1990; Ward, 1992] and has been modelled in the field of computer graphics rendering using both explicit geometric models and a wide range of bidirectional reflectance distribution functions (BRDFs) [Bosch et al., 2008; Kurt and Edwards, 2009; Schröder et al., 2012]. Many of the BRDFs can reproduce the appearance of the surface very well, however these models are not always energy conserving or available in optical CAD packages suitable for radiometric analysis. Poulin and Fournier [1990] modelled anisotropic reflectance by applying arrays of micro cylinders to the surface. Interestingly, it was found that the distribution produced by many small cylinders is equivalent to one larger cylinder and an accurate approximation holds as long as many cylinders cover the sampled region.

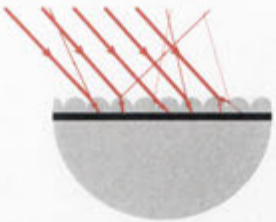


Figure 5.11 – MHC surface model with absorbing radiometric film behind surface.

Therefore, in this study an explicit geometric model is used whereby the surface is treated with an array of microscopic half cylinders (MHC) to account for the anisotropic scattering behaviour of the composite (Figure 5.11). This was realised by applying the cylindrical surface texture to the surfaces of the composite in a CAD model, and subsequently importing the model into *OptiCAD*. The diameter of the cylinders was assumed to be 10 µm, the same order of magnitude as the carbon fibres.

The experimental setup used to investigate the scattering behaviour (Figure 5.5) was recreated in *OptiCAD* to enable a qualitative comparison between the proposed MHC surface model and the earlier experimental results (Figure 5.6). The laser source was assumed to be a collimated beam with a Gaussian profile with a 2 mm waist. The results of the MHC surface model are shown in Figure 5.12.

The results correlate well with the experimental observations, giving a good approximation of the scattering behaviour. The observed distributions tend to be marginally wider for low angles of ϕ which can be attributed to waviness/undulation along the length of the fibres.

5.3.2 Angular dependent reflectance

When light passes the interface of two mediums of differing refractive indices, it is partially transmitted and reflected. The relative portions of reflection and transmission are dependent on the incident angle θ_i, polarisation of the light and the refractive indices of the two mediums n_1 and n_2. Fresnel's equations describe this behaviour and were therefore used for this model. For absorbing media, a complex refractive

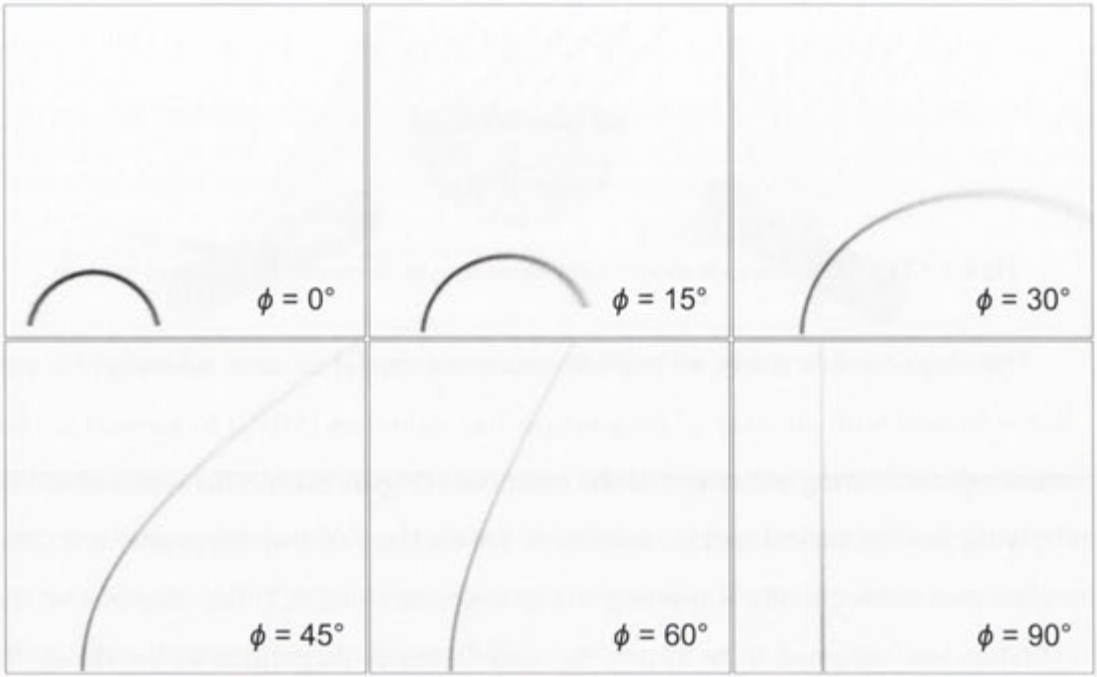


Figure 5.12 – Scattering patterns from the MHC surface model at a range of orientations.

index is typically defined where the imaginary part represents the absorption. In this work, an absorbing radiometric film is placed immediately behind the composite surface, and any light transmitted will be absorbed by the film and therefore a complex refractive index is not considered. The fractions of power reflected for the s- and p-polarised light from a smooth, planar surface are:

$$R_s = \left| \frac{n_1 \cos\theta_i - n_2 \cos\theta_t}{n_1 \cos\theta_i + n_2 \cos\theta_t} \right|^2 \qquad R_p = \left| \frac{n_1 \cos\theta_t - n_2 \cos\theta_i}{n_1 \cos\theta_t + n_2 \cos\theta_i} \right|^2 \tag{5.7}$$

Where θ_t is calculated using Snell's law:

$$\frac{\sin\theta_i}{\sin\theta_t} = \frac{n_2}{n_1} \tag{5.8}$$

The overall fraction of the reflected power assuming even portions of s- and p-polarised light incident on the surface is:

$$R = \frac{R_s + R_p}{2} \tag{5.9}$$

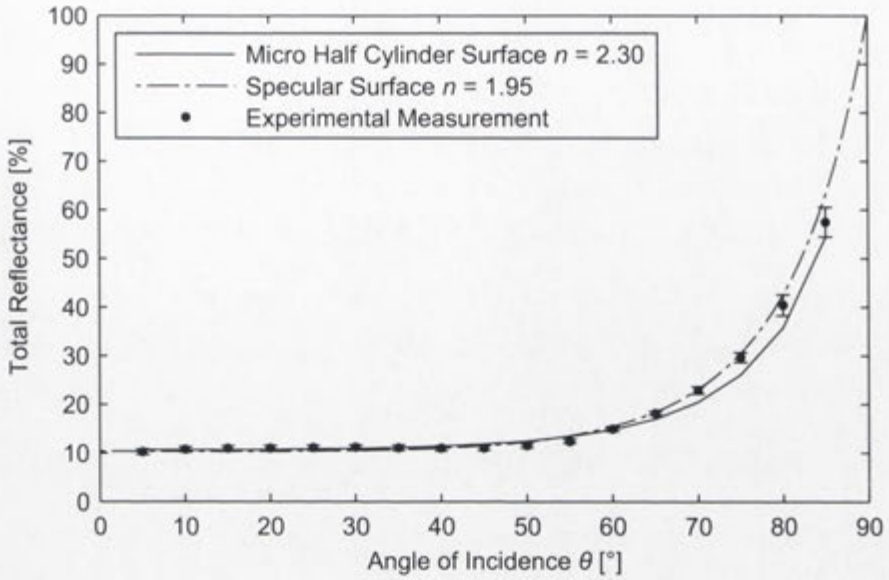


Figure 5.13 – Angular dependence of reflection for AS4/PEEK at $\lambda = 980$ nm compared with surface models.

The effective refractive index of the composite material needs to be determined for Eq. (5.7). This was achieved by a least squares curve fit of Eq. (5.9) to the reflectance measurements assuming a refractive index for air of $n_1 = 1.0$, resulting in an effective refractive index of $n_2 = 1.95$ (Figure 5.13). A test sample of the same refractive index was also modelled in *OptiCAD* and yielded the same result. The Fresnel equations assume a homogeneous flat surface, therefore this value only applies to a specular surface model.

In the case of the MHC surface model, the surface is not flat and therefore its effective refractive index must also be determined. A test sample with the MHC surface was modelled in *OptiCAD*. The total hemispherical reflectance was found to be lower than a specular surface of the same refractive index, most likely due to a light trapping effect between the cylindrical features. A least squares fit to the measured data resulted in a refractive index of $n_2 = 2.30$ for the MHC surface (Figure 5.13). This provides a good approximation of the angular dependent reflectance while preserving the scattering behaviour. It can be seen that for high angles of incidence the MHC surface model has slightly lower reflectance while the specular model has a

higher reflectance compared with the experimental measurements.

5.3.3 Laser source model

In this study, a 3 kW *Laserline GmbH. LDF* series diode laser source is located outside the placement cell. It contains 4 diode laser stacks which are first combined in pairs via polarisation coupling and then coupled by wavelength. The resulting beam is non-polarised and divided evenly between $\lambda = 940$ nm and $\lambda = 980$ nm. The beam is then coupled with a light cable which is attached to the placement head in the work cell.

For contemporary laser tape placement using a NIR laser with large rectangular spot sizes, the beam is delivered to optics on the placement head via a light cable. The optics in the current system comprise of 3 main elements. First the beam is collimated after entering from the light cable. The collimated beam then enters a homogeniser which is typically constructed using a series of crossed cylindrical micro-lens arrays which divide the beam into many discreet beamlets. A field lens then superimposes the beamlets on a plane at the lens' focal length. The result of the superposition of the beamlets results in a homogenous rectangular spot. Further details for such systems can be found in Köhler et al. [2007]; Homburg et al. [2008]. In this study the homogeniser and the field lens have focal lengths of 40 and 200 mm respectively, producing a rectangular spot 45 mm $\times$ 16 mm at a distance of 200 mm. The resulting spot size at the focal length is much larger than the 25 mm window that the beam emerges from, therefore the beam must have a reasonable level of divergence.

The efficiencies of a microlens optical system is typically >95 % [Köhler et al., 2007]. For every optical interface (2 per optical element) in the system there are losses due to Fresnel reflections. Anti-reflective coatings can greatly reduce reflective losses, however the cumulative loss can be at least a few percent. The laser source output can also vary. The power stability for the source in this study is specified as ± 2 % over 2 h. It is therefore expected that the power incident on the composite

could be at least 5 % lower than reported by the laser source.

Since the optics illuminate a wedge shaped cavity, rather than a plane normal to the beam, the irradiated area is not located precisely at the focal length of the optics. For the process parameters used in this study, the beam is incident on the composite at distances from 150 mm to 200 mm from the optics. Beam divergence will cause an inverse square-like behaviour for the beam irradiance vs. distance from the optics. It is therefore important to measure the divergence of the beam.

5.3.3.1 Beam profiling

The laser beam was profiled using a radiometric technique similar to that described in Baba et al. [1986]. The method involves aiming the beam at an absorbing film with a low transverse thermal diffusivity. The absorbed radiation heats the thin film uniformly through thickness, but the low transverse diffusivity restricts thermal conduction in the plane of the film. Furthermore, if the temperature rise is small $\sim$10 °C the rate of transverse conduction will be insignificant, in which case the local temperature rise is proportional to the local heat input, which corresponds to the relative irradiance given that the absorption is uniform:

$$\Delta T(x, y) \propto Q(x, y) \tag{5.10}$$

A *Xenics Gobi-640* long wave infra-red (LWIR) camera was used. It has a high sensitivity sensor capable of measuring temperature differences of 0.05 °C at 50 Hz, at a resolution of 640 × 480 pixels. A polyimide film was chosen as it has very low thermal diffusivity and good temperature resistance. *Kontakt Chemie Graphit 33* graphite spray was applied uniformly to the front surface, resulting in a highly absorbing diffuse coating. The coating also has high emissivity in the LWIR range, improving the temperature measurement. The camera was mounted beside the laser optics, and the temperature profile recorded while the film was briefly exposed to the laser at 100 W. The process was repeated at working distances of z = 100, 150, 200 and 250 mm. The

irradiance profile was taken as the first frame immediately after the laser was turned on. Typical maximum temperature rise of 10-15 °C was observed. The temperature profile was then scaled between the background temperature and the peak temperature rise, resulting in a relative irradiance profile. The distributions were then scaled using a steel ruler that was placed in the image as a reference. The measurement at z = 200 mm is shown in Figure 5.15a. The spot is close to a rectangular top-hat distribution, with relatively steep sides and slightly higher irradiance in the centre 20 mm. An artefact is present at y = +35 mm, which is also visible when the red pilot laser is on (Figure 5.15b). It is present at all working distances and attributed to imperfections in the optical system. This was however captured in the profiling, highlighting the sensitivity of the technique.

In order to understand the propagation of the beam, the dimensions of the profiles at relative irradiance levels of 5, 25, 50 and 75 % were measured and plotted (Figure 5.16) in terms of spot half width (hw). The percentage of the total power encircled within these irradiance levels was determined to be 99.8, 96.9, 90.4 and 77.8 % respectively. It can be seen that the beam has significant divergence, with the size of the 50 % irradiance level increasing by 22.6 and 24.5 % in the x- and y-axes respectively, when the working distance is increased from 150 mm to 200 mm. The divergence should therefore be captured by the source model.

5.3.3.2 Source model formulation

The divergence was modelled by performing a linear fit (Figure 5.16) of the 50 % irradiance (corresponding to 90 % of the encircled power) to working distances of 150 and 200 mm, the range used in the current setup. From the intercepts of the linear fit, the effective focal points on the z-axis were determined from where the rays would originate, −70.4 and −53.6 mm for the x- and y-axes respectively. As the origins for the x and y divergences are not co-located, rays cannot be launched from a point source. Instead, the source is modelled as collimated beam aimed though an

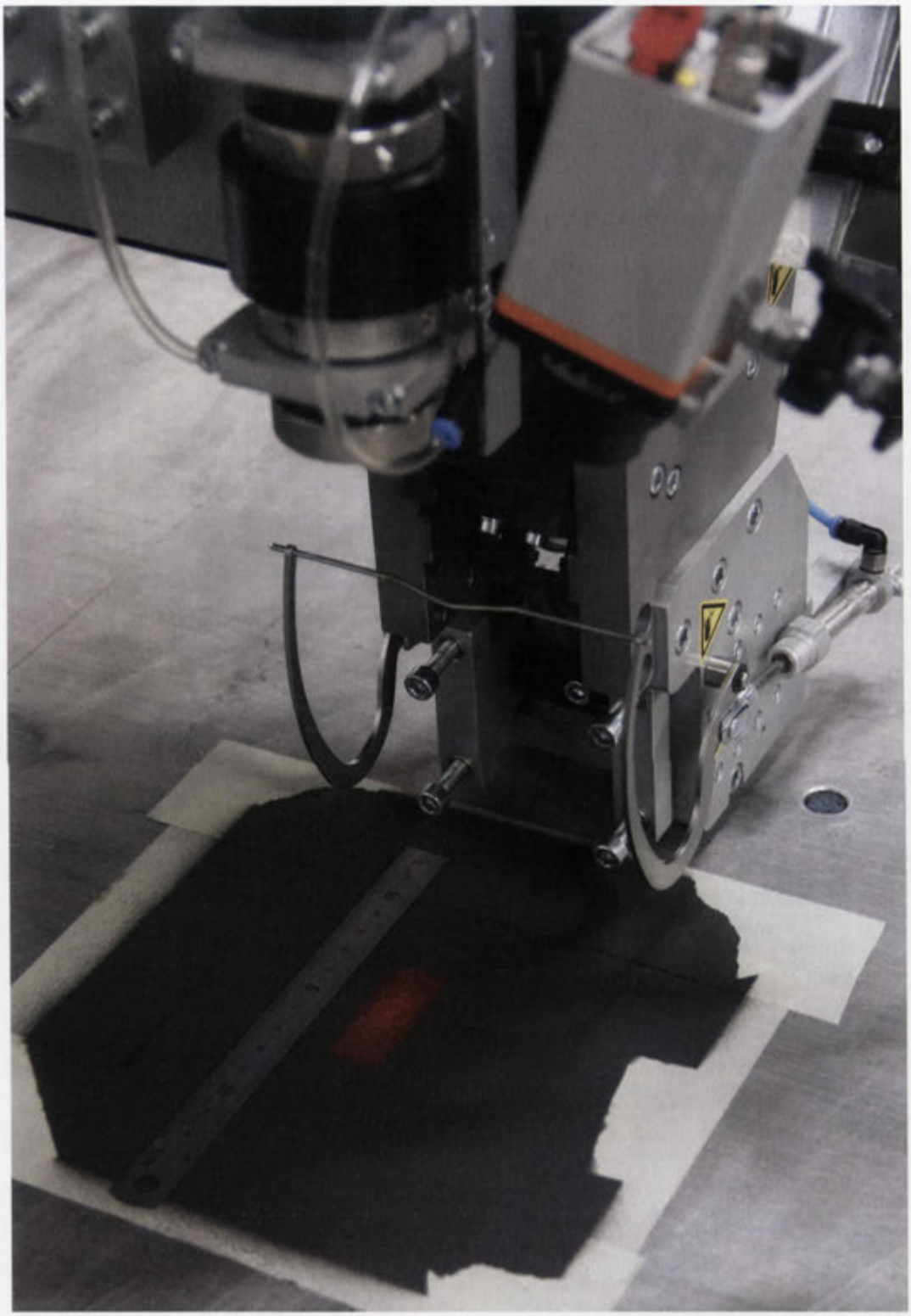
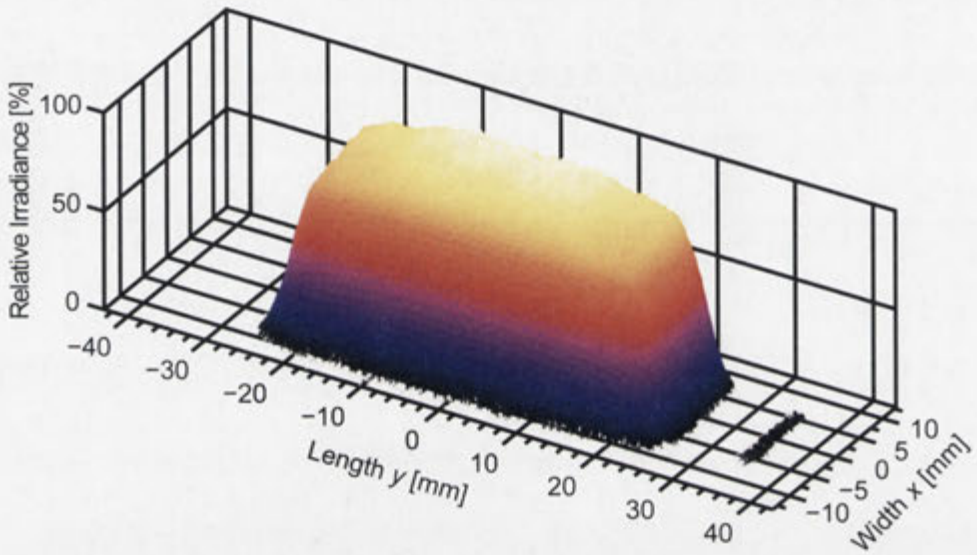
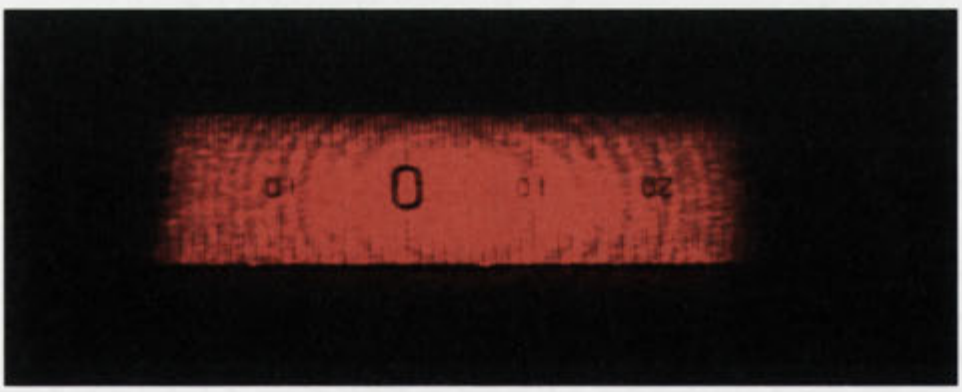


Figure 5.14 – Example of the irradiance profile measurement technique. The red pilot laser is activated showing the rectangular spot. The laser optics (top left) are positioned perpendicularly to the absorbing graphite-coated polyimide film target. The thermal camera (top right) mounted beside the optics records the temperature rise on the surface of the target. The consolidation roller was removed from the placement head while performing these measurements.



(a) Measurement of the relative irradiance at $z = 200\,\text{mm}$, artefact still present at $y = +35\,\text{mm}$ for $\lambda = 940$ & $980\,\text{nm}$.



(b) Photograph showing the red pilot laser spot with artefact on right-hand side.

Figure 5.15 – Measurements of the irradiance profile at $z = 200\,\text{mm}$.

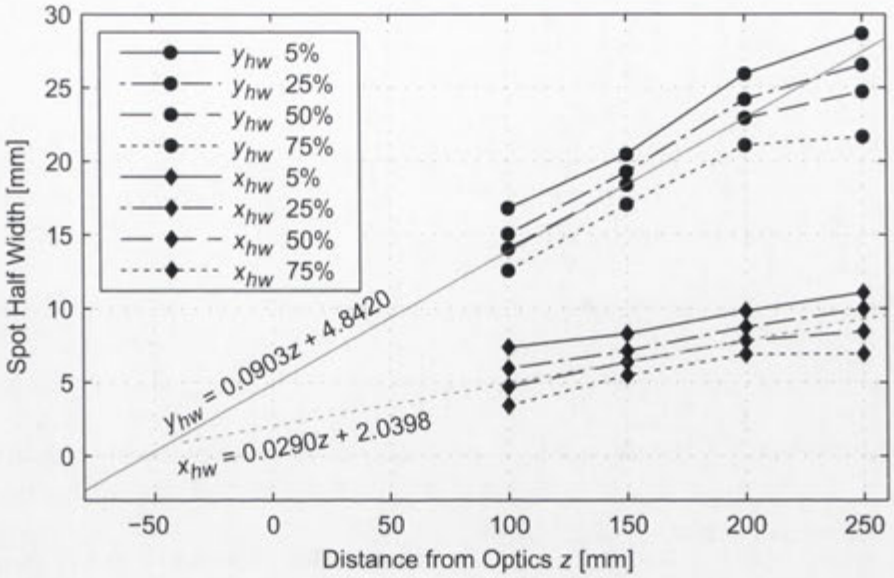


Figure 5.16 – Dimensions of irradiated spot vs. distance, measured at different irradiance levels. Linear fits to the 50% intensity measurements are shown, which are used for the approximation of the source divergence.

xy-paraxial lens placed at $z = 0$ mm with focal lengths of -70.4 and -53.6 mm. The profile of the collimated beam is generated using the $z = 200$ mm irradiance profile as a spatial emittance function (emf.). It is scaled, based on the divergence, so as to match the distribution $z = 0$ mm, the location of the paraxial lens. The resulting source is equivalent to the $z = 200$ mm irradiance profile propagating as if the rays originate from virtual points at $x_f = -70.4$ mm and $y_f = -53.6$ mm in the x- and y-axes respectively.

Comparison of the measurements (Figure 5.17a) with the modelled source (Figure 5.17b) shows good agreement for a distances of $z = 150$ and 200 mm. The profiles at $z = 100$ and 250 mm show some differences, however these are out of the working distance range for the current study. In reality, the rays originate from many points within the microlens arrays forming many overlayed images, with rays crossing each other as they propagate. This means that while the irradiance profiles agree, the radiance (incident angles of the rays) would be slightly different. However, as the aspect ratio of the studied working lengths to the spot size is reasonably large, geometric calculations based on ray origins from within the limits of the cover glass

Table 5.1 – Optical source models considered for the study.

Source Model Name	Beam Propagation	Beam Profile
Div. Emf.	Divergent $x_f = -70.4\,\text{mm}$ $y_f = -53.6\,\text{mm}$	Measured irradiance profile ($z = 200\,\text{mm}$) as spatial emittance function
Div. Top-hat	Divergent $x_f = -70.4\,\text{mm}$ $y_f = -53.6\,\text{mm}$	Rectangular top-hat $45\,\text{mm} \times 16\,\text{mm}$ at $z = 200\,\text{mm}$
Coll. Emf.	Collimated	Measured irradiance profile ($z = 200\,\text{mm}$) as spatial emittance function
Coll. Top-hat	Collimated	Rectangular top-hat $45\,\text{mm} \times 16\,\text{mm}$

of the optics show there would be a maximum difference of $\pm 2.5°$ in incident angle. Therefore it was concluded that this effect is likely to have an insignificant effect on the accuracy of the results.

In the next chapter, the impact of assuming various source simplifications will be studied. In addition to the divergent source using the irradiance profile as an emf., also considered was the simplification of a top-hat source with the same divergence (Figure 5.17c), producing a uniform spot $45\,\text{mm} \times 16\,\text{mm}$ at $z = 200\,\text{mm}$. In previous literature for modelling of a NIR laser-assisted TP-ATP process, a collimated beam was assumed [Grouve, 2012]; therefore such an assumption was also investigated with both an emf. and a $45\,\text{mm} \times 16\,\text{mm}$ top-hat beam profile (Figure 5.17d). The sources are summarised in Table 5.1, including short forms of the names used in the next chapter.

5.4 Conclusions

The optical behaviour of the composite and laser were characterised and approximated, providing the foundations necessary to develop a complete 3D ray tracing model for the NIR laser-assisted TP-ATP process. The scattering behaviour of the

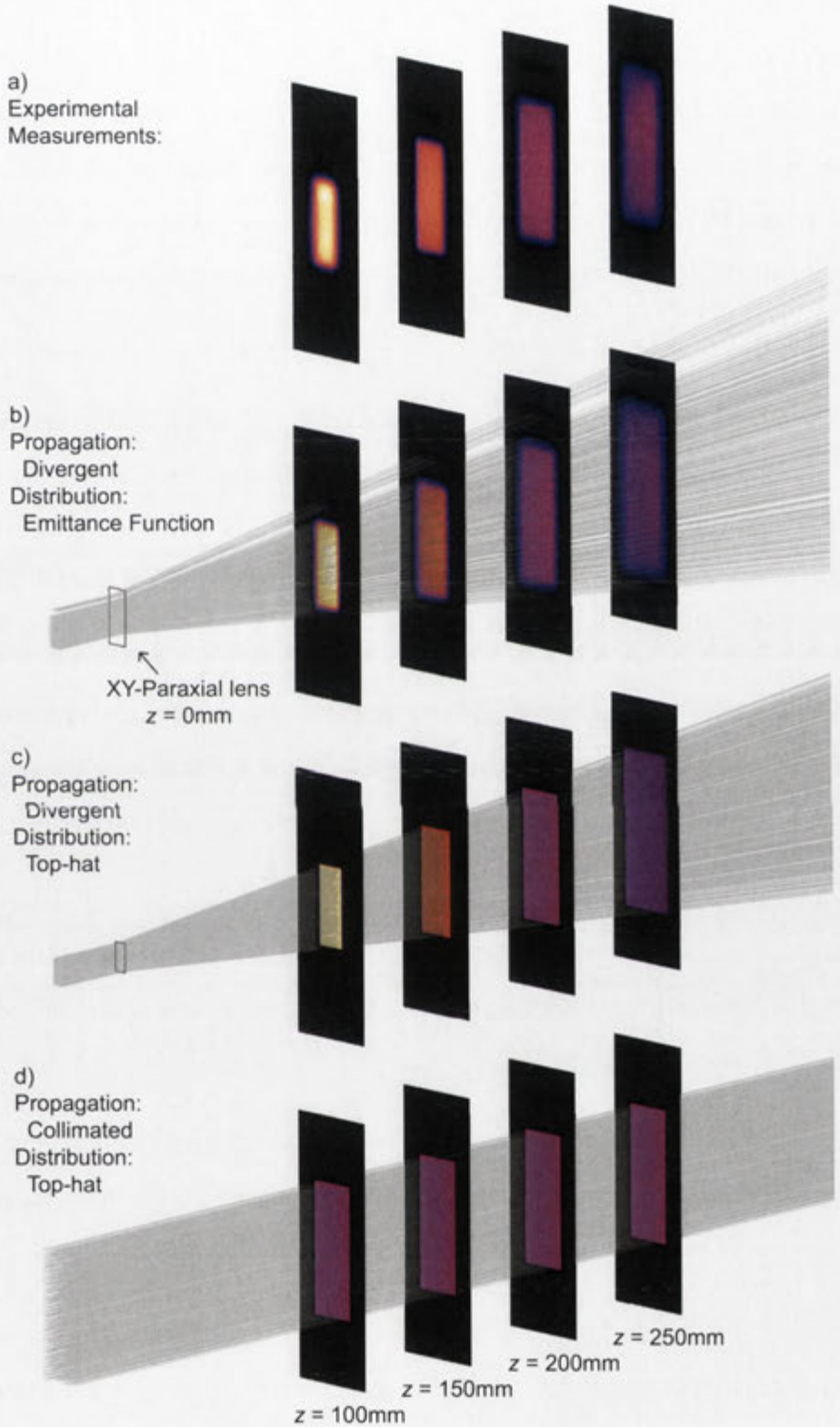


Figure 5.17 – Visualisation of beam propagation. a) Experimental measurements. b) Divergent source constructed with collimated emf. source and paraxial lens. c) Divergent source constructed with collimated top-hat source and paraxial lens. d) Collimated top-hat source.

composite was observed qualitatively using a low power laser source and camera. The scattering nature of the composite required the total hemispherical reflectance to be measured. This was achieved by performing measurements with a spectrophotometer equipped with an integrating sphere. The laser source profile and propagation were determined using a thermographic technique. Models for the composite material and the laser source were subsequently developed in a non-sequential ray tracing environment. The findings are summarised below:

- The PEEK thermoplastic matrix was characterised and found to be effectively transparent for the thickness on the surface of the composite over the range λ = 500-2000 nm. Crystalline phases are assumed to have only a minor scattering effect as the number of scattering centres will be low over the small thickness of PEEK covering the surface of the fibres.

- The scattering behaviour of the AS4/PEEK composite was found to be highly anisotropic, with measurements suggesting the behaviour is dominated by specular reflections from the surfaces of the embedded carbon fibres.

- Angular dependent reflectance measurements show increased reflection for higher wavelengths which is attributed to anomalous dispersion from the carbon fibres, further reinforcing the idea that the behaviour is dominated by reflections from the carbon fibres.

- A micro-half-cylinder (MHC) surface model was shown to give a good macroscopic approximation of the highly anisotropic scattering behaviour, without the complexity of modelling a three dimensional composite with individual fibres.

- Fresnel reflection equations provide a good approximation of the angular dependent reflectance. The refractive indices were determined to be $n = 2.30$ and $n = 1.95$ when considering MHC and specular surfaces respectively.

- The laser source was profiled and found to have a relatively uniform top-hat distribution. The propagation of the beam was also measured and shown to have significant divergence.

- The best approximation of the laser source was made using the $z = 200$ irradiance profile as a spatial emittance function (emf.) with the rays originating from points at $x_f = -70.4\,\text{mm}$ $y_f = -53.6\,\text{mm}$. This was achieved by launching collimated rays with an emf. through an xy-paraxial lens with focal lengths of $x_f = -70.4\,\text{mm}$ $y_f = -53.6\,\text{mm}$.

In the next chapter, the models developed for the composite surface and laser source will be applied to a 3D optical model of the laser tape placement head. The interaction of the laser is with the composite is investigated in detail and a combined optical-thermal model used to accurately predict the temperature history for near-infrared laser heating in a thermoplastic AFP process.

Chapter 6

Combined optical-thermal model

Abstract

A combined optical-thermal model is presented for near-infrared laser heating of carbon fibre reinforced thermoplastic composites in an automated fibre placement process. A three dimensional ray tracing model is presented for a near-infrared laser AFP process which captures the unique anisotropic scattering behaviour of the composite, using the models for an AS4/PEEK composite surface and near-infrared laser source that were developed in Chapter 5. Predicted irradiance distributions on the composite are subsequently applied to a 2D non-linear finite element thermal model that was formulated in Chapter 3. The presence of a shadow near the nip point is investigated and the resulting effect on bonding temperature will be studied.

6.1 Introduction

Thermoplastic AFP (TP-AFP) is a thermally driven process. It is therefore of particular importance to have a good understanding of the characteristic thermal behaviour. Such knowledge can then be used for both process optimisation and improvement of process control. Due to the rapid processing behaviour, it is difficult to measure the temperature distributions throughout the process, particularly in the bonding zone which is out of view. Current temperature control technologies for laser-assisted TP-AFP are based non-contact temperature measurements of the tape and substrate prior to the nip point. The correlation between the pre-nip point and consolidation temperature is not well understood, and previous work suggests that significant temperature drop would occur due to a shadows on the tape and substrate immediately prior to the nip point [Grouve, 2012; Stokes-Griffin et al., 2013]. A well formulated thermal model will give valuable insight into the process behaviour as well as a tool for optimisation of the thermal history. The thermal model predictions can only ever be as good as the bondary conditions applied to it, such as the laser heat flux distribution in this case. For these reasons, it was decided that a detailed optical model for predicting the interation of the laser with the composite was necessary to acheive more accurate temperature predictions as well as a better understanding of the process overall.

In this study a combined optical-thermal model is presented for carbon/PEEK NIR laser-assisted TP-AFP. Using the MHC composite surface approximation and laser source model developed in Chapter 5, a three dimensional optical model of the laser TP-AFP process will be constructed. Three dimensional ray tracing of the laser TP-AFP model will then used to predict the irradiance distributions on the composite, and subsequently applied to a non-linear finite element thermal model (developed in Chapter 3), providing a accurate predictions of the thermal history. Previous work suggests that there is a shadow which causes significant temperature drops immediately prior to consolidation [Grouve, 2012; Stokes-Griffin et al., 2013]. The

presence and significance of the shadow will be investigated. As the optical model captures the anisotropic scattering behaviour, the effect of substrate fibre orientation will be studied. The influence of various source and surface model simplifications on the temperature predictions will also be investigated.

6.2 Optical tape placement model

Non-sequential ray tracing software (*OptiCAD 10*) was used for the optical analysis. A model of the tape placement system was first created using CAD software; the geometry and dimensions are presented in Figure 6.1 and Table 6.1 respectively. Two different surface models are investigated, a specular surface and a MHC surface. Arrays of 10 µm half cylinders were therefore applied to the composite surfaces in the case of the MHC model. The models were subsequently imported into *OptiCAD* as IGES files. The refractive indices applied to the composite were $n = 1.95$ and $n = 2.30$ for the specular and MHC surface models respectively. The consolidation roller material was a translucent silicone elastomer. It was assumed to have a refractive index of $n = 1.43$ [Gu and Zhou, 1998], and volumetric scattering was applied to account for the translucency. The volumetric scattering model implemented in *OptiCAD* is based on the work of Wang et al. [1995]. The scattering, volumetric absorptance and anisotropy coefficients were approximated as 1.00/mm, 0.00/mm and 0.95 respectively. While the scattering properties of the roller are only approximate, they provide an understanding of how the consolidation roller interacts optically with the system and an estimate of the irradiance on the rear side of the tape.

Radiometric films with power bins 0.25 mm square are used to measure the irradiance distributions. They were placed immediately behind the surfaces of the composite as illustrated in Figures 5.9 and 5.11. The rays were launched using Sobol sampling and terminated when any one of the following three conditions was met:

1. The number of surfaces intercepted (min. depth) exceeds 100.

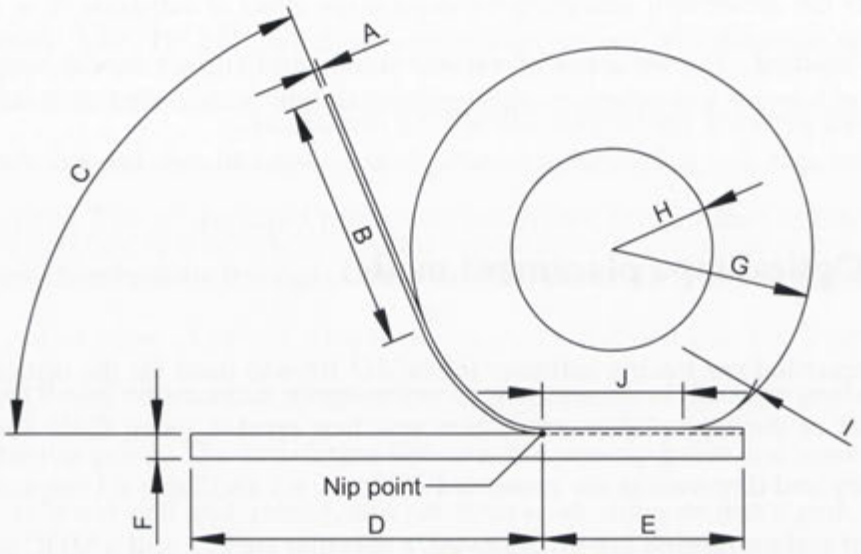


Figure 6.1 – Model geometry, refer to Table 6.1 for dimensions. Note: For the sake of clarity, tape and substrate thickness are not to scale.

Table 6.1 – Combined optical-thermal model geometry.

Parameter	Dimension	Value	Unit
Tape width		12.0	mm
Tape thickness	A	0.15	mm
Tape feed length (prior to roller)	B	50.0	mm
Tape feed angle (relative to substrate)	C	67.4	°
Substrate width		50.0	mm
Substrate length (pre-nip point)	D	70.0	mm
Substrate length (post-nip point)	E	40.0	mm
Substrate thickness	F	1.65	mm
Roller outside diameter	G	80.0	mm
Roller internal diameter	H	40.0	mm
Roller width		40.0	mm
Roller corner radius	I	16.0	mm
Roller contact length	J	28.0	mm
Laser optics (front face relative to nip point):			
[X, Y, Z] (left handed)		[0.0, 98.1, -171.6]	mm
[RX, RY, RZ] (left handed)		[-32.0, 0.0, 0.0]	°

2. The energy of a ray falls below 1 % of its initial value (min. transmission).

3. The number of times the ray has divided (max. ghost rays) has exceeded 100.

6.3 Thermal model

The thermal modelling approach applied here builds on the model developed in Chapter 3. A 2D non-linear finite element thermal model was implemented in *ANSYS 13.0 APDL* using an Eulerian frame of reference attached to the placement head. The geometry is meshed with *PLANE55* first order quadrilateral elements that are capable of mass transport heat for constant velocity fields. This is achieved by adding a velocity terms v_x and v_y to the left hand side of the heat transfer differential equation:

$$\rho c \left(\frac{\partial T}{\partial t} + v_x \frac{\partial T}{\partial x} + v_y \frac{\partial T}{\partial y} \right) = \ddot{q} + \frac{\partial}{\partial x} \left(K_x \frac{\partial T}{\partial x} \right) + \frac{\partial}{\partial y} \left(K_y \frac{\partial T}{\partial y} \right) \tag{6.1}$$

The velocity terms impose a size limit on the elements; they must be sufficiently small in the direction of the motion to prevent oscillations in the solution. The solution is valid when the Peclet number is less than unity [Gresho and Lee, 1981]:

$$Pe = \frac{vl}{2\alpha} < 1.0 \tag{6.2}$$

Thus the maximum element dimension (l) aligned with the velocity vector is dependent on the thermal diffusivity (α) of the material and the magnitude of velocity (v). The maximum element dimensions for the materials used in the current model were calculated and are shown in Table 6.2. The mesh therefore needs to be very fine in the direction of the mass flow, particularly for the roller due to the very low thermal diffusivity of the elastomer.

Table 6.2 – Maximum element dimensions in direction of flow for $v = 133\,\text{mm/s}$.

	Unit	AS4/PEEK 61 % v/v axial [Cogswell, 1992]	Roller Elastomer	Aluminium (Tooling)
Thermal Diffusivity	m^2/s	2.70×10^{-6}	1.15×10^{-7}	9.29×10^{-5}
Maximum element dimension	mm	5.40×10^{-2}	2.30×10^{-3}	1.86

6.3.1 Model geometry and meshing

The geometry and dimensions are the same as used in the optical model as shown earlier (Figure 6.1 with accompanying dimensions in Table 6.1). The only exception is the roller is modelled as a slender 1 mm strip near the contact boundary, which was previously found to be a suitable approximation Chapter 3. To minimise computational effort while meeting the requirements of Eq. (6.2), the elements for the roller are meshed with high aspect ratios in the areas away from the contact boundary of the roller and the tape.

6.3.2 Material properties boundary conditions

The non-linear thermal material properties are presented in Table 6.3.

Refering to Figure 6.2, the boundary conditions are described as follows:

The boundary S_0 is the base of the composite substrate in contact with an aluminium tooling plate. Due to the large thermal mass of the tool, a fixed temperature boundary condition was assumed where:

$$T = T_{tool} = 20\,^{\circ}\text{C} \quad \text{on } S_0 \tag{6.3}$$

The mass flow inlet boundaries S_1 and S_2 for the substrate and tape respectively were assumed to be at ambient temperature.

$$T = T_{amb} = 20\,^{\circ}\text{C} \quad \text{on } S_1 \text{ and } S_2 \tag{6.4}$$

Table 6.3 – Temperature dependent material properties.

Temperature °C	Specific Heat J/(kg · °C)	Density kg/m^3	Thermal Conductivity (Axial) W/(m · °C)	Thermal Conductivity (Transverse) W/(m · °C)
AS4/PEEK 61 % v/v composite tape [Cogswell, 1992]:				
0	800	1601	3.5	0.42
50	930	1598	4.6	0.52
100	1040	1593	5.1	0.6
150	1260	1586	5.9	0.7
200	1300	1575	5.9	0.7
250	1400	1563	6.1	0.7
300	1550	1551	6.7	0.75
350	1650	1537	6.8	0.68
400	1700	1524	7.0	0.65
Roller Elastomer:				
–	1255	1250	0.18	0.18
Aluminium Tooling:				
–	951	2689	237.5	237.5

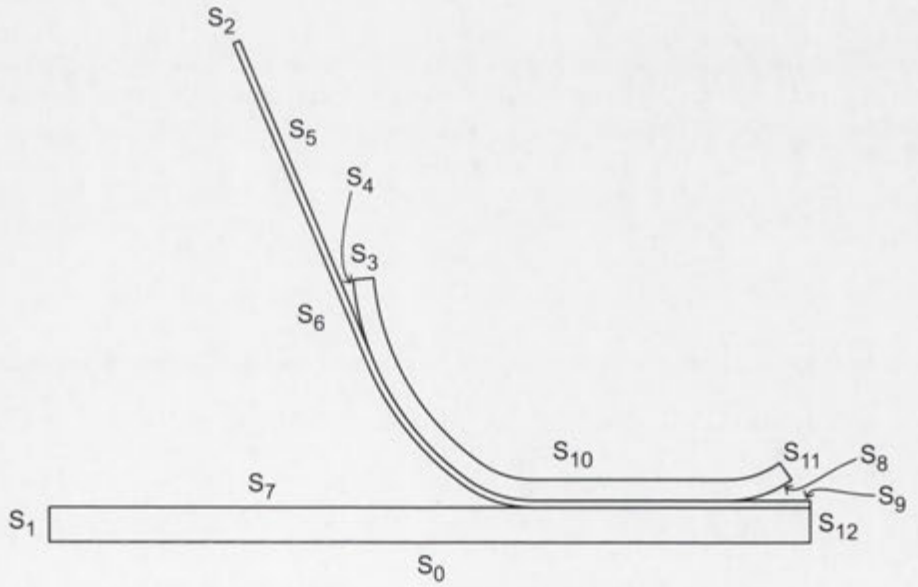


Figure 6.2 – Thermal model boundary locations.

The roller mass flow inlet boundary S_3 was assumed to be a fixed temperature boundary condition at 50 °C, approxmiated from LWIR camera images.

$$T = T_{roller} = 50\,^{\circ}\mathrm{C} \quad \text{on } S_3 \tag{6.5}$$

The boundaries exposed to the ambient environment (S_4–S_9) were assumed to have a convective heat transfer boundary condition.

$$k_t \frac{\partial T}{\partial y} = -h(T - T_{amb}) \quad \text{on } S_4\text{–}S_9 \tag{6.6}$$

Where k_t is the transverse thermal conductivity of the material and h is the convective heat transfer coefficient, the values of which were adapted from Chapter 3.

Select areas of the boundaries S_6 and S_7 are also irradiated by the laser. The optical model irradiance distributions were exported from *OptiCAD* as tabular data. Scripts were used to convert the data into a suitable format for import into *ANSYS 13.0 APDL* where the irradiance was then mapped onto the appropriate surfaces as a heat flux boundary condition. As the optical model is in 3D but the thermal model is 2D, the position dependent irradiance values $q_{(x)}$ were applied from the centre of the process width, corresponding with the location where experimental measurements were performed.

$$k_t \frac{\partial T}{\partial y} = -q_{(x)} \quad \text{on irradiated areas of } S_6 \text{ and } S_7 \tag{6.7}$$

The inside boundary of the roller S_{10} was assumed to have a zero temperature gradient (perfectly insulated) boundary condition as assumed previously in Chapter 3, as are the mass flow outlet boundaries S_{11} and S_{12}.

$$\frac{\partial T}{\partial x} = 0 \quad \text{on } S_{10}, S_{11} \text{ and } S_{12} \tag{6.8}$$

Perfect contact was assumed for the roller-to-composite interface, as the roller is

Table 6.4 – Process control settings.

Parameter	Value	Unit
Placement velocity	100	mm/s
Laser power (fixed)	1130	W
Laser angle	-3.0	°
Placement head angle	30.0	°
Consolidation roller extension	19.5	mm
Consolidation roller cylinder pressure	0.50	MPa

soft and conformable and the contact surfaces were both very smooth. The tape and substrate were assumed to be in perfect contact after the nip point, justified by the high surface quality of the prepreg used, the high surface temperatures and the pressure application from the conformable the roller.

6.4 Experimental

The tape placement experiments were performed at *AFPT GmbH*. The work cell consists of a placement head (type *STWHMA313011*) mounted on six axis robot. As performed in Chapters 3 and 4, the temperature on the substrate was measured by affixing 25 µm fine wire thermocouples to the centre of the substrate using shavings of PEEK and a clean soldering iron. Measurements were logged at 100 Hz using a *National Instruments cDAQ-9213* thermocouple module. A *Xenics Gobi-640* LWIR camera was used with a 100-650 °C calibration for process observation.

Initially a single 25 mm wide AS4/PEEK tape was attached to an aluminium substrate using a thin layer of high temperature adhesive to ensure consistent thermal contact. Ten layers of 12 mm AS4/PEEK tape were placed on top forming a 1200 mm long, 11 ply thick unidirectional substrate. Thermocouples were then attached and the temperature recorded while a final ply was placed on top. The process settings are presented in Table 6.4. Similar settings have been found to result in consolidation temperatures adequate for bonding of AS4/PEEK Chapter 4, with peak temperatures prior to the nip point in the order of 600 °C.

6.5 Results and discussion

6.5.1 Optical model

6.5.1.1 Laser interaction with the composite

Initial investigations focus on the interaction of the laser with the cavity formed by the substrate and the tape for the proposed MHC model. This was achieved by launching a linear array of ten evenly spaced beamlets centred within the laser source. To begin with, the first order reflections from the substrate (0° fibre orientation) cast onto the tape (Figure 6.3) were investiagted. For the beamlets incident on the substrate furthest from the nip point, only a small portion of the reflected radiation is incident on the tape, however for the reflections close to the nip point all of the reflected radiation is incident on the tape. Next investigated was the first order reflections from the tape cast onto the substrate (Figure 6.4). The behaviour is very similar to the previous case, however the curvature of the tape around the roller magnifies the reflections, broadening the spacing and also the width of the reflected beamlets. This effect was investigated in more detail by launching 40 beamlets, the irradiance maps in Figure 6.5 show the first order reflections on either side. It can be seen that reflections from the substrate onto the tape are spaced uniformly as the substrate is planar. The relative irradiance increases significantly for reflections near the nip point as most of the scattered distribution is captured by the tape. One might expect that reflections from curved section of the tape at high angles of incidence (higher Fresnel reflection) would lead to higher levels of reflected irradiance on the substrate compared with those on the tape. Interestingly, this is not the case due to the magnification effect of the curvature as the tape wraps around the roller. Furthermore, the curvature creates a larger shadow on the tape, and thus the reflected radiation from the tape cast onto the substrate is further from the nip point. The result is a diffuse-like reflection onto regions further away from the nip point, and specular-like behaviour close to the nip point. This unique behaviour is due to the

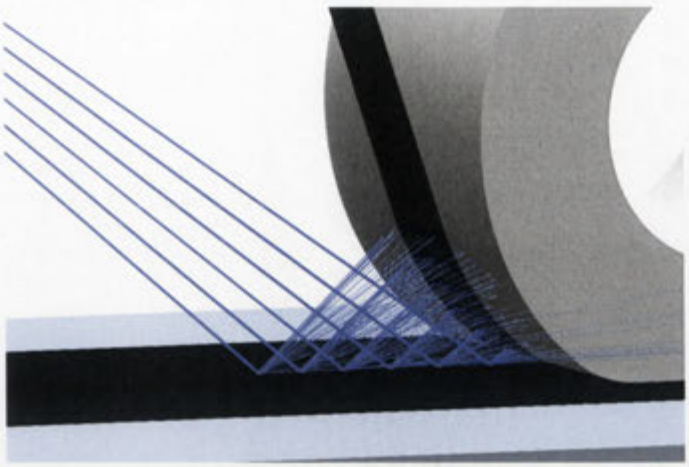


Figure 6.3 – A linear array of beamlets demonstrating first order reflections from the substrate onto the tape and roller.

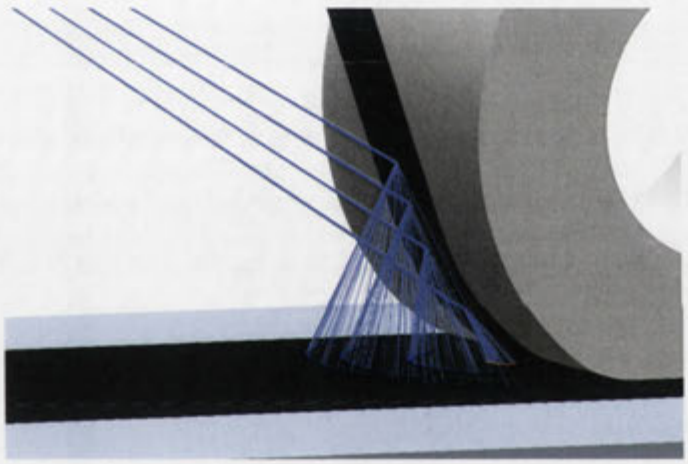


Figure 6.4 – A linear array of beamlets demonstrating first order reflections from the tape onto the substrate.

anisotropic scattering which is captured by the MHC surface model.

6.5.1.2 Analysis of full model

Due to the scattering nature of the cylindrical surface model a large number of rays were required to reach a converged solution for the areas receiving scattered radiation, in this case 10 million rays resulted in convergence within 2 % of the irradiance weighted bin values. The maximum percentages of total power truncated by depth, transmission and ghost criteria were 0.2, 0.6 and 0.0 % respectively. First, results

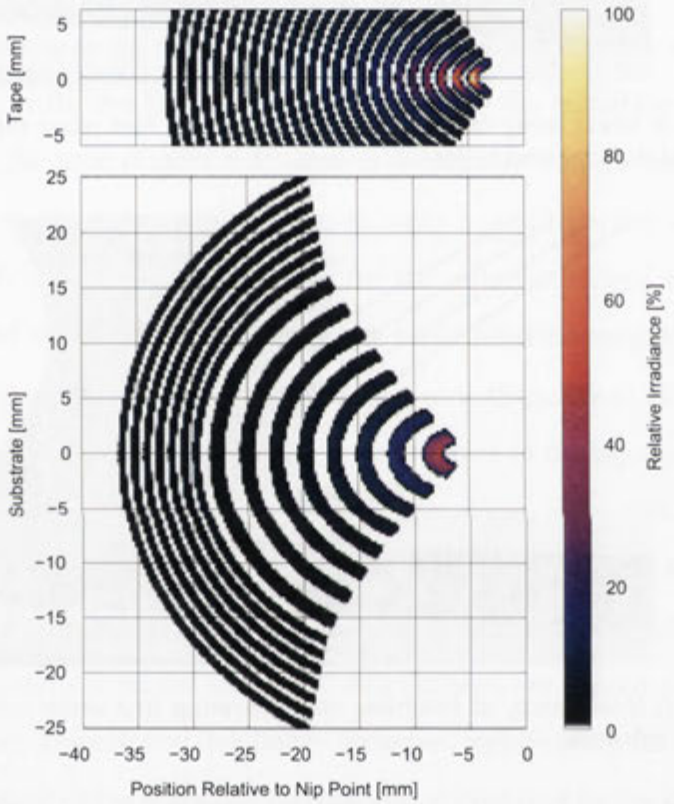


Figure 6.5 – Irradiance maps of first order reflections on tape and substrate from a linear array of 40 beamlets.

will be presented for the various surface models using a divergent top-hat source (Figure 6.6a-c). A top-hat source is used for the comparison as it demonstrates the behaviour more clearly.

As a reference case, a model with no reflections and yet Fresnel (angular dependent) absorption behaviour (Figure 6.6a) was initially investigated. The irradiance on the substrate decreases towards the nip point due to the divergence of the beam. Angle of incidence increases from approximately 52-60° and thus the absorption behaviour would be relatively constant at 87-84 % respectively according to Figure 5.13. Irradiance ceases 4.4 mm before the nip point due to the shadow cast by the tape/roller. Relatively uniform irradiance is observed on the tape feed (flat section before the roller) located at distances of −32-−44 mm from the nip point with angles of incidence from 49-51° resulting in uniform absorption of 88 %. As the tape curves around the roller to the nip point, the angle of incidence increases rapidly with absorption approaching 0 % at the edge of the shadow starting at −8.8 mm from the nip point. The result is a long gradient in irradiance as the tape approaches the nip point. The shadow cast on the tape is approximately twice the size of that on the substrate.

Next, the specular surface model with Fresnel reflections (of all orders) was considered. There is a strong specular reflection from the tape feed onto the substrate from −29-−37 mm (Figure 6.6b). The magnification effect due to the curvature of the tape around the roller reduces the intensity of the reflections markedly, however the reflections increase approaching the nip point due to the increased Fresnel reflection. The resulting irradiance is surprisingly uniform with the drop in irradiance due to the source divergence being evenly compensated by the increased reflection from the tape. Even considering specular reflections, the penetration of the beam into the substrate shaded region is limited in terms of both distance and irradiance. The reason being the rays must first reflect ($R \approx 15\,\%$) from the substrate onto the tape, and then from the tape back onto the substrate ($R \approx (15\,\% \times 15\,\%) \approx 2\,\%$).

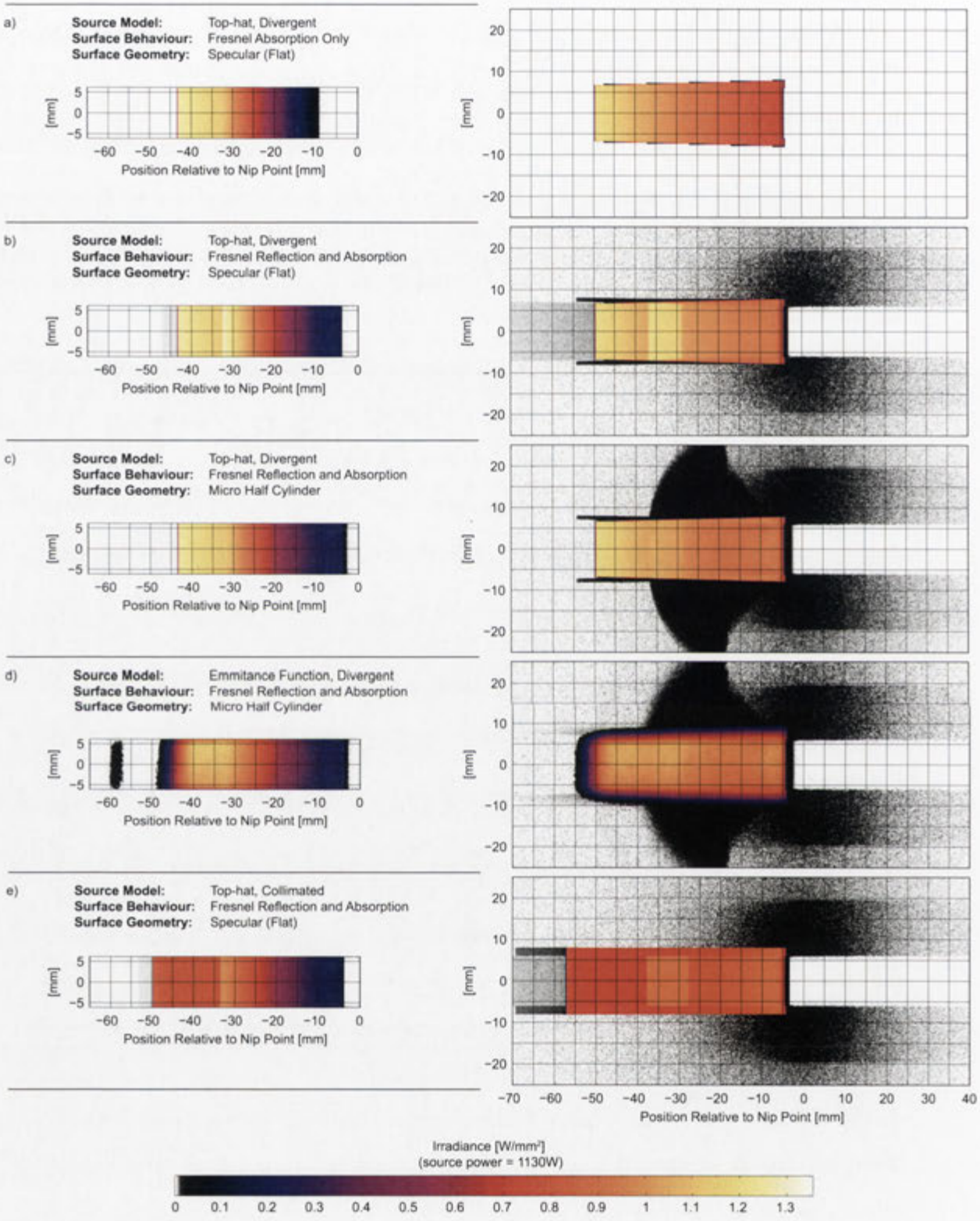


Figure 6.6 – Irradiance maps for various source and surface approximations. Tape and substrate distributions are shown in the left and right columns respectively.

The reflection from the substrate is relatively constant at 13-16 % and is cast onto the tape from −32.5-−3.9 mm from the nip point. Mild levels of radiation are reflected onto the shaded portion of the tape, halving the length of the shadow compared with Figure 6.6a. Specular reflections of the laser (that which overshoots the width of the tape) from the surface of the roller are observed on the substrate forming lines on the edge of the distribution extending back to −54 mm behind the nip point. The light which enters the roller is scattered, landing on the substrate and also the back side of the tape with insignificant levels of irradiance.

The results of the MHC surface model are presented in Figure 6.6c. The scattering behaviour spreads the reflected radiation outside of the processing width (centre 12 mm), particularly in locations further from the nip point. The result is lower irradiance within the processing width, however the behaviour close to the nip point is very similar to that of specular model for reasons explained in Section 6.5.1.1. As the light is scattered to angles lower than a specular reflection, the shadow is decreased on the tape and substrate to distances of −2.5 and −2.8 mm from the nip point respectively, however the levels of irradiance are of little significance. A reasonable portion of the light reflected from the substrate enters the roller (as in Figure 6.3), and thus slightly higher levels of scattered light hitting the rear of the tape and the substrate beneath the roller.

The next simulation (Figure 6.6d) uses the MHC surface model with the div. emf. source. The behaviour is identical however the emf. source has a slight bias towards the centre (Figure 5.15) leading to marginally higher irradiance closer to the nip point, resulting in uniform irradiance of the substrate in the process direction. This uniformity is however coincidental as the increasing reflections from the tape cancel the decrease due to divergence and is unlikely to be observed for different head configurations and laser source profiles. The emf. also shows much softer edges on the irradiance distributions which extend further than the top-hat assumption. The artefact observed earlier (Figure 5.15) can be seen on the tape at −59 mm, however

the irradiance is very low. Less than two percent of the system power lands on the rear of the tape due to the scattering from the roller.

Finally, a collimated source and a specular surface (Figure 6.6e), that has been assumed in other work [Grouve, 2012] was considered. The collimated beam intercepts the tape and composite further from the nip point. As a result the irradiated area is larger and the irradiance is lower. The irradiance on the substrate is relatively uniform with a strong specular reflection from the tape as with the divergent source, however it is larger and in a different location due to the difference in source propagation. The behaviour on the tape is similar to the divergent source, but again the size and position of the specular reflections have changed. When comparing this result with the best approximation (MHC surface model with the div. emf. source), it can be seen that there is a significant difference in terms of the irradiance distributions.

6.5.2 Thermal model

The composite shows highly specular reflection at LWIR wavelengths, and given the geometry involved, the apparent temperature on surfaces near the nip point are a combination of both the surface emittance and significant specular reflections of the opposing surfaces. As the reflected temperature is of a surface with strong temperature gradients, a standard ambient reflection compensation (that assumes totally diffuse reflection of a constant temperature) is not suitable. The apparent temperature of the surfaces near the nip point is therefore misleading and not considered.

For process observation, the emissivity in the LWIR camera software was calibrated using the thermocouple measurement with the surface at 100 °C. During processing when temperatures exceeded approximately 250 °C, the observed temperatures of the thermocouples became higher than that of the surrounding composite (Figure 6.7).

The thermocouple is welded to the composite using a sparing amount of shavings from the surface of the same material, therefore the emissivity of the attached

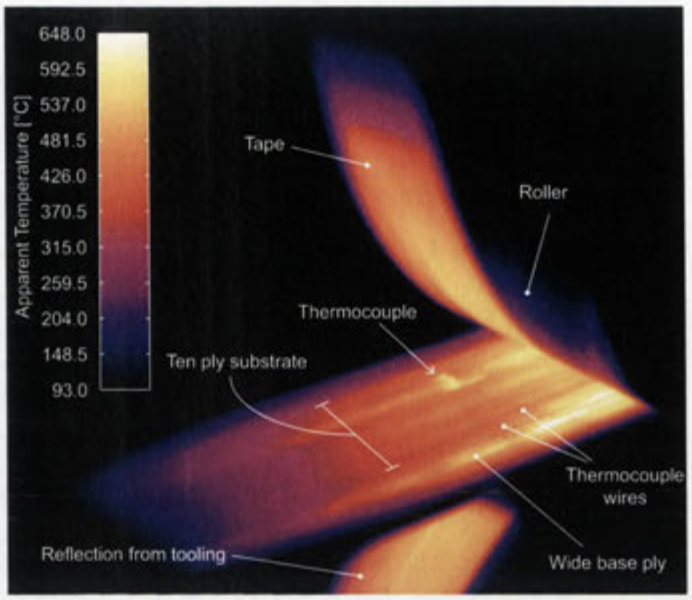


Figure 6.7 – LWIR image showing thermocouple at higher temperature.

thermocouple should be equivalent to the substrate, and this was observed to be the case at low temperatures. The thermocouple wire appears cooler than the substrate in the thermal image, suggesting lower emissivity for the embedded thermocouple. The increased temperature of the thermocouple during heating is thought to occur due to imperfect contact with the substrate. The fine wire thermocouples are very fragile so only light pressure can be applied during attachment. It is likely that air gaps and voids are present, which would expand at higher temperatures, decreasing thermal contact. As the thermocouple is subject to heating by the laser, it then increases in temperature above that of the substrate. This phenomenon was observed for a large number of experimental trials. The rise in thermocouple temperature was compensated for by first determining the relative temperature difference between the thermocouple and the average temperature of substrate at the same distance from the nip point.

$$\Delta T = T_{TC} - T_{substrate} \tag{6.9}$$

This is calculated for all frames of the LWIR video, when the thermocouple is

in view and the temperature value is below saturation (Figure 6.8). An exponential curve fit of the measurements was made so as the compensation can be extrapolated to points where the thermocouple is out of view. This assumption is justified by the fact the predictions show a relatively constant irradiance on the substrate. Since the thermocouple will no longer be heated by the laser from the shadow onwards, an exponential cooling function is applied to bring the compensation back to zero in the consolidation zone where the thermocouple temperature will have equalised to the surroundings. This monotonic compensation function is then applied to the thermocouple measurement to approximate the complete temperature profile on the surface of the substrate.

6.5.2.1 Experimental validation

The results of the combined thermo-optical model considering the best approximation (MHC surface model with the div. emf. source) are shown in Figure 6.8, along with the raw and compensated experimental temperature measurements. The tape temperature is shown on the left, and the substrate and post-nip point temperatures on the right.

The post-nip point temperature is between both the tape and substrate during consolidation. It can be seen that there is good agreement with the compensated measurement, however the peak temperature and consolidation temperature is predicted to be higher by 7 %. As discussed in Chapter 5, there are variations in the source power (± 2 %) and losses throughout the optical system (≈ 5 %) which would amount to this difference. The laser power was therefore reduced in the model to 1056 W, and it can be seen that there is an excellent agreement, with slightly higher temperatures predicted for the first half of the heating profile and a slightly lower temperatures towards the nip point. It is likely that part of the difference in profile is due to discrepancies between the actual geometry and that used in the model, leading to slight changes in the positioning of reflections in the irradiance distributions.

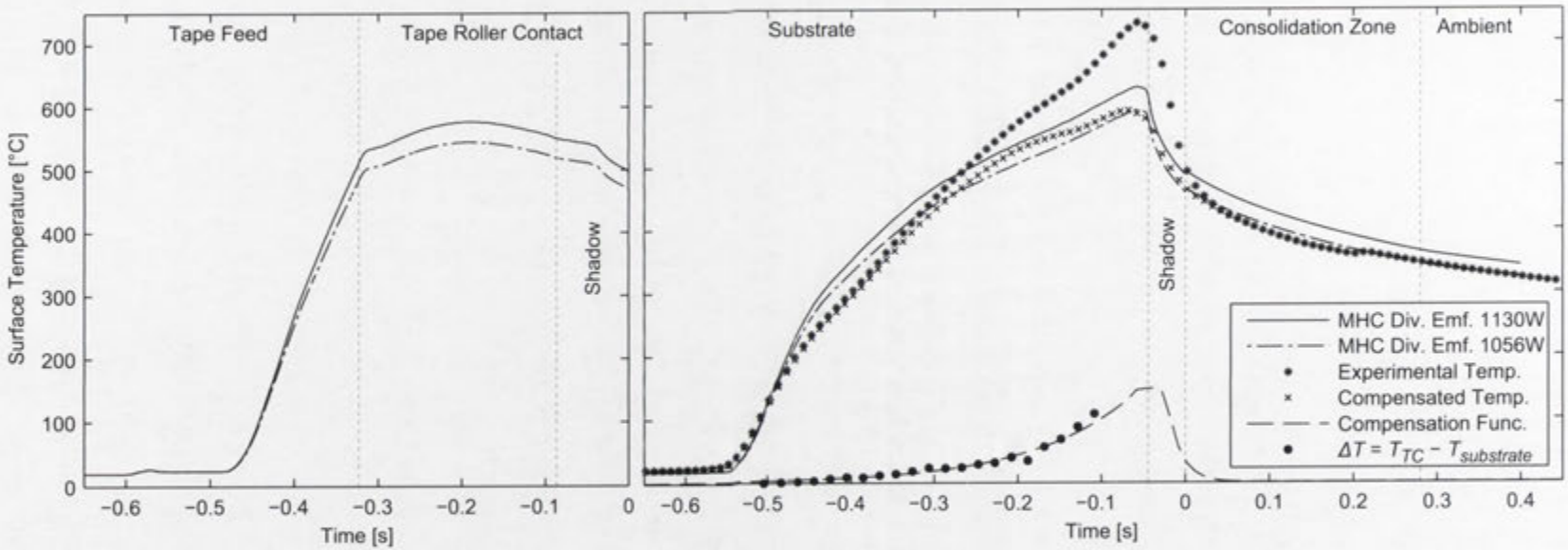


Figure 6.8 – Experimental measurements compared with the best approximation for laser powers of 1130 and 1056 W. Surface temperatures for the tape (left) and substrate (right) are presented relative to the nip point ($t = 0$).

For example, the shape of the tape around the deformed roller is assumed to be a perfect radius, however the deformed shape will be more complex. The timing of the onset of irradiation and the period of the shadow agree very well with the results. Most importantly, the temperature profile for the consolidation zone shows strong agreement.

While there is no direct validation of the tape temperature profile, comparison with the LWIR image (Figure 6.7) suggests good agreement as there is a relatively constant apparent tape temperature after a steep initial gradient. It can also be seen that there is some variability in the substrate temperature, attributed to local variations of fibre volume fraction. The peak temperature on the substrate reaches 590 °C yet drops by 130 °C in the shadow to a temperature of 460 °C at the nip point. This rapid drop is due to the heat sink effect of the substrate. As identified in Chapter 3, the tape accumulates heat through its thickness so despite the shadow, the temperature drop is much lower at only 40 °C. The accumulated heat in the tape also decreases the rate of cooling in the consolidation zone. The temperature in the consolidation zone varies from 460-340 °C. This explains why improved properties were found in Chapter 4 when the pre-nip point surface temperatures were in the range of 600 °C, as these higher input temperatures are required to achieve the consolidation temperatures required for high levels of bonding at the nip point and immediately behind; while under pressure.

In this work, it was shown that for a conformable roller with a relatively small corner radius of 16 mm produces a shadow of approximately 4 mm. When moving to larger radii, particularly for non-conformable rollers, this shadow would become much larger. This would result in even higher temperature drops before the nip point, adversely affecting bond strength. It should therefore be noted that observed temperatures on the tape and substrate do not necessarily represent the temperature experienced in the consolidation zone, thus it is likely that different results will be obtained for different placement head configurations given the same process control

temperature targets.

6.5.2.2 Effect of surface model

Figure 6.9 shows the effect of assuming various surface models. As a reference to the assumptions made in Chapter 3, a uniform irradiance assumption is shown. The uniform irradiance agrees surprisingly well for the substrate, however this is merely coincidental due to the configuration of the placement head as discussed in Section 6.5.1.2. It can be seen that this predicts quite a different profile for the tape with a much greater shadow effect. When considering the specular surface with only Fresnel absorption, the heating profile remains the same initially but the lack of reflections results in temperatures 70 and 40 °C lower on the tape and substrate respectively prior to the nip point compared with the reference case. The discontinuity in temperature at the nip point is due the consolidation zone temperature becoming close to the average of the tape and substrate temperatures. When considering a specular surface with reflections, an over-prediction of the temperature is observed, particularly on the tape. Compared with the best approximation, temperatures are higher by 25 and 15 °C on the tape and substrate prior to the nip point, and 20 °C higher post nip point.

6.5.2.3 Effect of source model

The effect of the source model is shown in Figure 6.10. When comparing the top-hat and emf. beam profiles, the only significant difference is at the beginning of the temperature profiles. The lack of irradiance outside of the top-hat is compensated for by slightly higher irradiance in the top-hat region (as the power is equivalent over a smaller area), resulting in little effect on the peak and consolidation temperatures compared with the emf. When comparing a collimated assumption it can be seen that the temperature profile is extended and the temperature predictions are lower by 50, 60 and 45 °C for the peak tape, substrate and consolidation temperatures re-

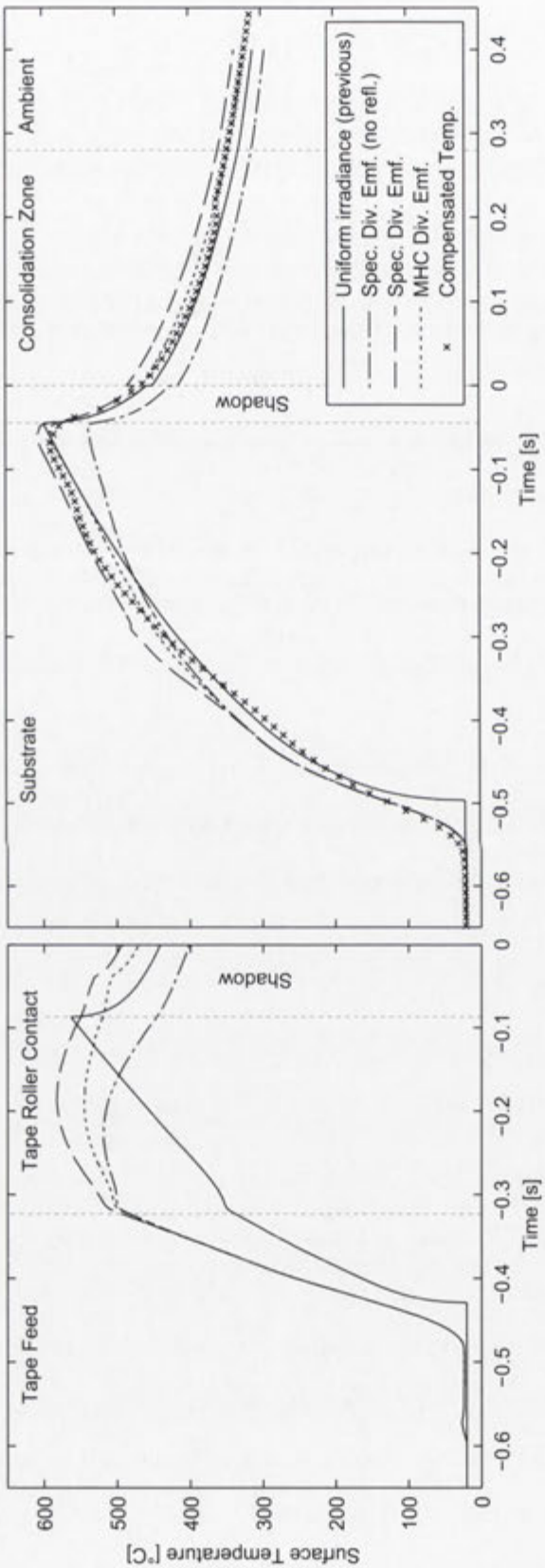


Figure 6.9 – Comparison of temperature profiles for different surface approximations in optical model.

spectively. Lastly, the assumptions from previous work [Grouve, 2012], a collimated top-hat source and a specular surface were applied to the model. The increased reflection from the specular surface brings the prediction closer to that of the best approximation, however the temperature profile does not agree with measurements and the peak temperatures are lower by 12, 45 and 30 °C for the tape, substrate and consolidation zone respectively.

6.5.2.4 Effect of fibre orientation

Since the proposed cylindrical surface model accounts for the anisotropic scattering behaviour of the composite, it is now possible to study the effect of the fibre orientation on the irradiance. As the feed tape is unidirectional and always has zero degree orientation, only the effect of changing the substrate fibre orientation is considered. The effect of changing the substrate orientation is shown in Figure 6.11. The temperature profiles are largely unaffected. As the tape is in the same orientation, the first order reflections onto the substrate remain constant, therefore the substrate irradiance should not change significantly. Slight variation is observed however due to a slight change in substrate absorption for the cylindrical surface model from 85-83.5 % when the fibre orientation is changed from 0-90°, given an angle of incidence of 60°. The distribution of first order reflections from the substrate onto the tape changes significantly with the substrate orientation. Interestingly, the relative difference is insignificant with less than 1 °C difference in peak tape temperature predicted for 0, 45 and 60° orientations. In the 90° orientation, there is a 10 °C higher peak tape temperature as the scattered distribution (Figure 5.10(b)) remains within the cavity between the tape and substrate, thus a spreading the scattered light along the length of the tape rather than escaping to the side into the ambient environment. Compared with the 0° orientation, the other orientations receive less irradiation on the shaded region of the tape, leading to pre-nip point temperatures 10 °C lower. In the consolidation zone, temperatures are from 8-11 °C lower.

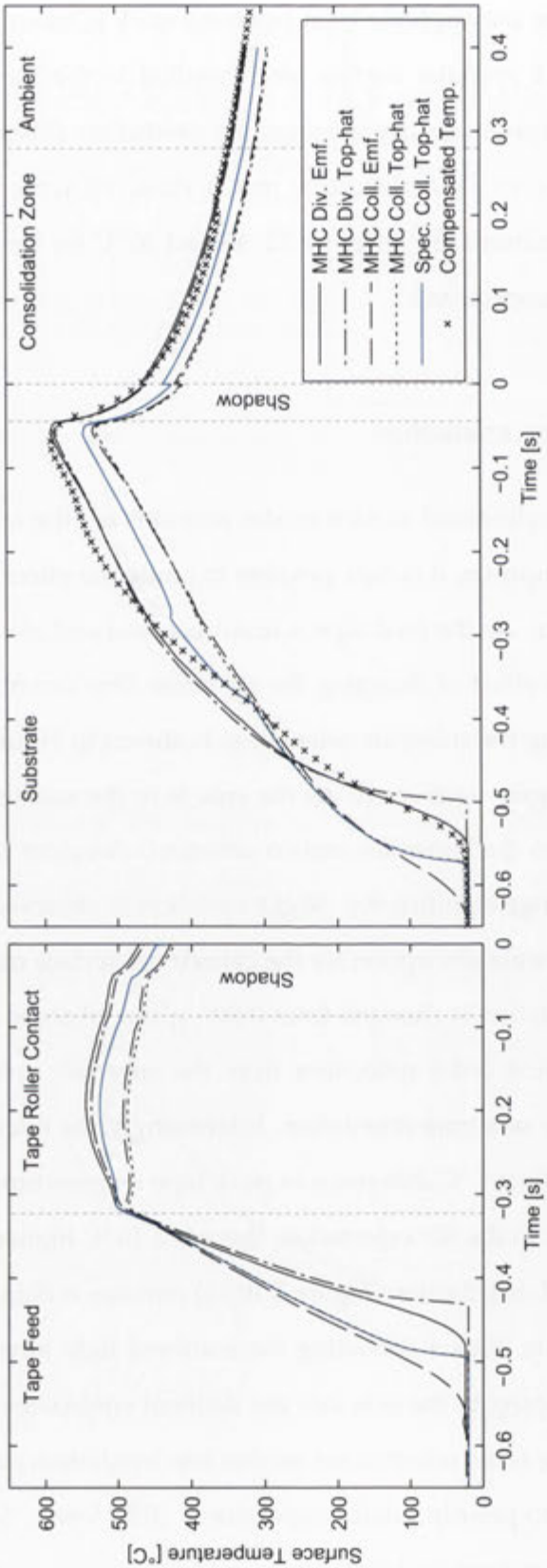


Figure 6.10 – Comparison of temperature profiles for different source approximations in optical model.

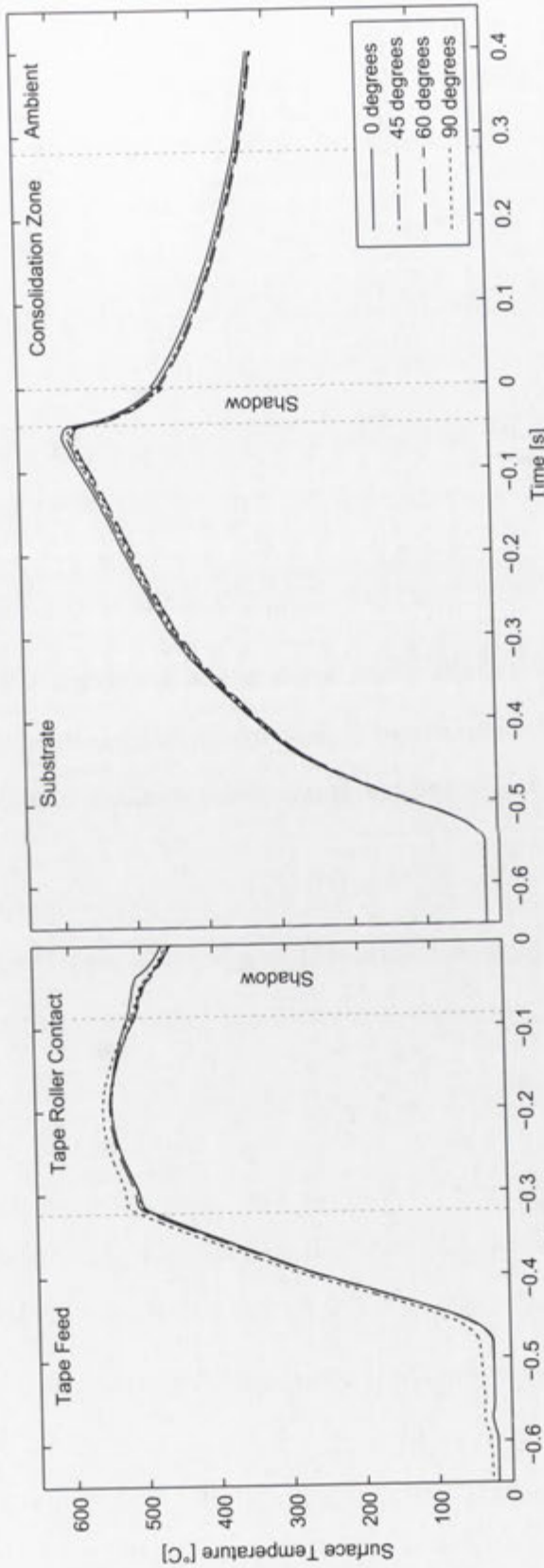


Figure 6.11 – The effect of the substrate fibre orientation on the surface temperature profiles.

6.6 Conclusions

A combined optical-thermal model was presented for carbon/PEEK near-infrared laser-assisted TP-AFP. Irradiance distributions on the composite were predicted using a 3D ray tracing model and subsequently applied to a 2D non-linear finite element thermal model. A good agreement was shown between the predicted thermal history and the experimental results. The main conclusions for this chapter are summarised below:

- It is important to model the anisotropic scattering behaviour of the composite as it leads to specular-like behaviour near the nip point, yet diffuse reflection behaviour away from the nip point. A specular surface assumption leads to over-prediction of irradiance. Omitting reflections leads to a significant decrease in temperature predictions.
- Due to the inclination of the laser source, it is important to model the beam propagation as well as the irradiance profile. Assuming collimated propagation leads to overestimation of the length of the temperature profile, and underestimation of the temperatures. It was found that a top-hat profile simplification leads to a shortening of the profile, however the peak temperatures and the rest of the profile remain mostly unchanged compared with a spatial emittance function (emf.)
- Even considering reflections, it was found that a significant shadow is still present. This has a strong impact on the temperature history, with a 130 and 40 °C drop in surface temperature before the nip point for the substrate and tape respectively. This effect will be greater for larger rollers/corner radii.
- Initial results of the thermal model using the reported process power (1130 W) overestimated the peak temperature by 7 %. The difference was attributed to losses in the optical system and source output variation. Temperature profiles agreed extremely well after an adjustment of the laser power to 1056 W.

- The effect of the substrate fibre orientation was found to have only a small influence on the temperature history. The micro-half-cylinder model is still required however for accurate prediction of the temperature history.

In the next chapter, this combined optical-thermal model is used to determine the bond interface temperature histories for samples produced under conditions that reflect those experienced during the manufacture of components. Bond strength predictions using the models and parameters from Chapter 4 will also be performed. Predictions of void content and crystallinity will also be included.

Chapter 7

Short beam strength: comparison of process simulator predictions with experimental results

Abstract

In this chapter the strength of laminates manufactured using the laser AFP process is investigated. Multi-layered samples were manufactured under conditions that reflect those experienced during practical manufacture of components. The additional quality development due to subsequent placement passes was therefore included. The inter-laminar bond strengths of the samples was characterised through short beam strength measurements. The temperature history predictions were made for the mid-plane bond interface of the SBS samples for the entire process history, using the combined optical-thermal model that was formulated in Chapter 6. The temperature history predictions were found to be in good agreement with experimental measurements for both the surface temperature during laser heating and also the through thickness history during the placement of subsequent layers. Bond strength predictions were performed by applying the full process history to the bonding model from Chapter 4. Experimentally validated crystallinity and void dynamics models from the literature were also implemented. Trials were performed to determine the response of the process to the process temperature. Experimental SBS results found that full bond strength can be acheived using laser AFP at placement rates of 100 mm/s without the use of heated tooling. When moving to a placement rate of 400 mm/s, values 98 % of the reported ultimate SBS in literature were achieved showing the superior properties achievable with the modern near infra-red laser AFP process. Furthermore, the crystallinity and void content predictions for such conditions were within recommended values. Predictions of the bond strength were found to be conservative compared with the experimental results.

7.1 Introduction

When making components with the laser AFP process, each bond interface undergoes multiple re-heating and pressure application cycles due to the subsequent passes of the placement head during placement of additional layers above. As discussed in the literature review (Section 2.3), these additional passes are known to help further develop bond strength and increase the levels of crystallinity. Depending on the specific processing conditions, the void content may either increase or decrease. The quality of the resulting laminate is dependent on the complete temperature and pressure history throughout the manufacturing process. In order to assess the ability of the laser AFP process to produce components of high strength, it is therefore necessary to consider a mechanical test method that characterises a bond interface that has experienced the subsequent passes that would occur in a practical manufacturing process. In this case the short beam strength (SBS) test method was selected as the resulting properties will reflect those achievable when manufacturing components with the laser AFP process. The SBS test has been widely utilised for inter-laminar bond strength characterisation in similar thermoplastic AFP studies [Mantell et al., 1992; Mazumdar and Hoa, 1995, 1996; Agarwal et al., 1996; Rosselli and Santare, 1997; Pistor et al., 1999; Tierney and Gillespie, 2006; Schledjewski and Miaris, 2009].

The processing temperature for carbon/PEEK composites reported in material data sheets is typically 370-390 °C. Such values apply to traditional manufacturing processes such as autoclave and press consolidation where typical process times are to the order of tens of minutes if not hours. When processing at temperatures just above these recommended values, the material is known to degrade in the form of cross-linking. As discussed in Section 1.3.2.5 and Section 2.2.5, the time periods over which the cross-linking process occurs is to the order of hours. The cross-linking process is slow and it has been suggested to be driven by diffusion of oxygen through the melt. When considering the extremely short periods over which the material is

exposed to high temperatures in the laser AFP process, it is likely that the material can be processed at much higher temperatures without incurring significant degradation or loss of properties. It has been suggested that PEEK can be exposed to temperatures of up to 600 °C for periods of up to 2 seconds (Table 1.1). The onset of thermal decomposition observed as rapid mass loss occurs when the temperature exceeds 575-580 °C in thermogravimetric analysis (TGA) performed relatively low heating rates 10 °C/min [Patel et al., 2010, 2011]. It is also possible that the high surface heat flux in the laser AFP process could lead to localised vaporisation/ablation resulting in removal of PEEK matrix from the surface. This phenomenon was observed by Rosselli et al. [1997] in a laser consolidation process, and no obvious char residue could be detected in photomicrographs. In such a case, little matrix would be available at the interface to form a bond, resulting in poor mechanical properties.

The bonding process is dependent on two highly temperature sensitive properties, the viscosity of the material at the bond interface which affects the intimate contact development rate, and also the characteristic welding time of the polymer which controls the rate of molecular diffusion/healing. Bonding can occur more quickly at higher temperatures, however degradation imposes an upper limit on the process temperature. Secondary quality effects such as void dynamics and crystallinity are also affected by the process temperature. For experimental placement trials in the literature (Section 2.1.1.1), it has been suggested that the best mechanical properties are achieved for process temperatures in the range of 600 °C. In this chapter, the effect of process temperature on the SBS, crystallinity and void content will be investigated. The predictive capability of the combined optical-thermal formulated in Chapter 6 coupled with the bonding models from Chapter 4 will be evaluated and compared with the experimental results. Experimentally validated crystallinity and void dynamics models from literature will be additionally implemented.

7.2 Process model implementation

7.2.1 Bonding model

The same bonding models and input parameters from Chapter 4 are also considered and implemented in this chapter. As suggested by the findings in Chapter 4, the temperature threshold for bonding calculations was assumed to be the glass transition of the polymer, under the condition that the matrix had first exceeded the melting point, erasing any crystalline phases present in the matrix.

7.2.2 Crystallisation

The following model for two stage crystallisation of PEEK originates from Velisaris and Seferis [1986]. Tierney and Gillespie [2004] investigated this model for highly non-isothermal conditions and good agreement was found with experimental results. It was also implemented for a thermoplastic tape placement simulation by Guan and Pitchumani [2004]. In this work, the implementation was performed following the work of Tierney and Gillespie [2004].

The crystalline volume fraction X_{vc} is detemined by:

$$X_{vc} = X_{vc\infty}(w_s F_{vc(s)} + w_e F_{vc(e)}) \tag{7.1}$$

Where $X_{vc\infty}$ is the equilibrium volume fraction crystallinity and w_s and w_e are the weight factors for the spherulitic and epitaxial crystal growth mechanisms respectively. They are subject to the constraint:

$$w_s + w_e = 1 \tag{7.2}$$

The normalised volume fraction of crystllinity for the spherulitic phase $F_{vc(s)}$ is de-

termined using the following relation:

$$\left[\ln\left(\frac{1}{1-F_{vc(s)}}\right)\right]^{1/n_s} = \left[\ln\left(\frac{1}{1-F_{vc(s)_0}}\right)\right]^{1/n_s} + \int_t^{t+\Delta t} [K_s(T(t))]^{1/n_s} dt \qquad (7.3)$$

Where $F_{vc(s)_0}$ is the normalised volume fraction crystallinity from the previous time step and n_s is the Avrami constant. Correspondingly, for the normalised volume fraction for the epitaxial phase $F_{vc(e)}$ is given by:

$$\left[\ln\left(\frac{1}{1-F_{vc(e)}}\right)\right]^{1/n_e} = \left[\ln\left(\frac{1}{1-F_{vc(e)_0}}\right)\right]^{1/n_e} + \int_t^{t+\Delta t} [K_e(T(t))]^{1/n_e} dt \qquad (7.4)$$

$K_s(T)$ and $K_e(T)$ are the crystallisation rate constants for the spherulitic and epitaxial phases respectively. The spherulitic constant is expressed as:

$$K_s(T) = C_{1(s)} T \exp\left[-\left(\frac{C_{2(s)}}{T - T_g + 51.6} + \frac{C_{3(s)}}{T(T_{m(s)} - T)^2}\right)\right] \qquad (7.5)$$

Where $C_{1(s)}$ is the temperature dependent pre-exponential factor, $C_{2(s)}$ is an empirical parameter related to the temperature dependence of viscosity and $C_{3(s)}$ is associated with the free energy of nucleation. Correspondingly, the epitaxial rate constant is calculated by:

$$K_e(T) = C_{1(e)} T \exp\left[-\left(\frac{C_{2(e)}}{T - T_g + 51.6} + \frac{C_{3(e)}}{T(T_{m(e)} - T)^2}\right)\right] \qquad (7.6)$$

Where T_g and T_m are the glass transition and melting points respectively. The complete non-isothermal expression for the normalised volume fraction crystallinity for the spherulitic growth mechanism with respect to time is given by:

$$F_{vc(s)}(t) = \left[1 - \exp\left(-C_{1(s)} \int_0^t T \exp\left[-\left(\frac{C_{2(s)}}{T - T_g + 51.6} + \frac{C_{3(s)}}{T(T_{m(s)} - T)^2}\right)\right] n_s t^{(n_s - 1)} dt\right)\right] \qquad (7.7)$$

And for the epitaxial growth mechanism:

$$F_{vc(e)}(t) = \left[1 - \exp\left(-C_{1(e)} \int_0^t T \exp\left[-\left(\frac{C_{2(e)}}{T - T_g + 51.6} + \frac{C_{3(e)}}{T(T_{m(e)} - T)^2}\right)\right] n_e t^{(n_e-1)} \mathrm{d}t\right)\right] \tag{7.8}$$

Thus the volume fraction of crystallinity can then be determined by applying Eqs. (7.7), (7.8) and (7.2) to Eq. (7.1) during the temperature interval over which crystallisation develops $T_g \leq T \leq T_m$. The time t in Eqs. (7.7) and (7.8) refers to the cumulative period of time for which crystallisation is occurring. When the temperature $T > T_m$, the crystalline phases are assumed to melt instantaneously in this implementation of the model. This is justified in this work by the fact that the temperature during thermoplastic tape placement often exceeds 400 °C. In the case where partial melting is significant, this assumption would lead to conservative approximation of the final crystalline volume fraction.

It is important to consider the parameters for a composite rather than that of neat resin as the carbon fibres are known to interact with the crystal nucleation behaviour. The parameters applied to the model in this case are adopted from Tierney and Gillespie [2004] which correspond to a carbon/PEEK composite. They are presented in Table 7.1.

7.2.3 Void dynamics

In this work, the microscopic void dynamics model of Ranganathan et al. [1995] is used to estimate the void content. The implementation of this model is as follows. The model considers a spherical void (of raduis r_v) that is encased by viscoelastic shell of resin (of raduis r_s) as depicted in Figure 7.1. The growth and collapse of the void is determined by the balance of the internal void pressure P_g and the pressure applied to the exterior of the shell P_f, the surface tension σ_v and the resin viscosity

Table 7.1 – Parameters applied to the crystallisation model for a carbon/PEEK composite [Tierney and Gillespie, 2004].

Symbol	Parameter	Value	Unit
X_{vc_i}	Initial volume fraction crystallinity	10.5	%
$X_{vc\infty}$	Equilibrium volume fraction crystallinity	37.0	%
T_g	Glass transition temperature	417	K
$T_{m(s)}$	Melting point (Spherulitic)	611	K
n_s	Avrami constant (Spherulitic)	2.5	-
w_s	Weight constant (Spherulitic)	0.61	-
$C_{1(s)}$	Constant coefficient of the temperature dependent pre-exponential factor	2.08×10^{10}	s^{-n}
$C_{2(s)}$	Empirical parameter, associated with the temperature dependence of viscosity	4050	K
$C_{3(s)}$	Parameter associated with the free energy of nucleation	1.80×10^{7}	K^3
$T_{m(e)}$	Melting point (Epitaxial)	611	K
n_e	Avrami constant (Epitaxial)	1.5	-
w_e	Weight constant (Epitaxial)	0.39	-
$C_{1(e)}$	Constant coefficient of the temperature dependent pre-exponential factor	2.08×10^{10}	s^{-n}
$C_{2(e)}$	Empirical parameter, associated with the temperature dependence of viscosity	7600	K
$C_{3(e)}$	Parameter associated with the free energy of nucleation	3.2×10^{6}	K^3
ρ_c	Density of fully crystalline PEEK	1400.6	kg/m^3
ρ_a	Density of amorphous PEEK	1262.6	kg/m^3

μ_s:

$$4\mu_s \left(\frac{r_v^3}{r_s^3} - 1 \right) \frac{\mathrm{d}r_v}{\mathrm{d}t} + \left(P_g - P_f \right) r_v - 2\sigma_v = 0 \tag{7.9}$$

The internal pressure P_g is determined by assuming the ideal gas law:

$$\frac{P_{g0} r_{v0}^3}{T_0} = \frac{P_g r_v^3}{T} \tag{7.10}$$

The viscous shell surrounding the void is assumed to be incompressible therefore the volume is conserved, with r_{v0}^3 and r_{s0}^3 corresponding to the initial void and shell radii:

$$r_s^3 - r_v^3 = r_{s0}^3 - r_{v0}^3 \tag{7.11}$$

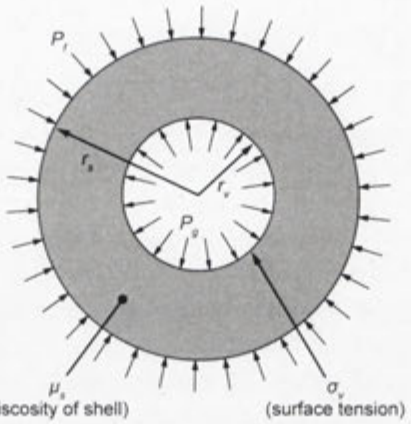


Figure 7.1 – Microscopic void model of Ranganathan et al. [1995]. The model assumes a spherical void encased by a viscoelastic shell. The rate of growth/collapse is determined by the balance of P_f and P_g, and the parameters σ and μ.

The radii are then expressed in non-dimensional form, determined by normalising by the initial radius:

$$r_v^* = \frac{r_v}{r_{v0}} \qquad r_s^* = \frac{r_s}{r_{v0}} \tag{7.12}$$

Substitution of Eqs. (7.10)–(7.12) in Eq. (7.9) yields:

$$4\left(\frac{r_v^{*3}}{r_{s0}^{*3} + r_v^{*3} - 1} - 1\right)\frac{\mathrm{d}r_v^*}{\mathrm{d}t} + \left(\frac{P_{g0}}{r_v^{*3}}\frac{T}{T_0} - P_f\right)\frac{r_v^*}{\mu_s} - \frac{2\sigma_v}{\mu_s r_{v0}} = 0 \tag{7.13}$$

Which can be re-arranged to give:

$$\frac{\mathrm{d}r_v^*}{\mathrm{d}t} = \frac{\frac{2\sigma_v}{\mu_s r_{v0}} - \left(\frac{P_{g0}}{r_v^{*3}}\frac{T}{T_0} - P_f\right)\frac{r_v^*}{\mu_s}}{4\left(\frac{r_v^{*3}}{r_{s0}^{*3} + r_v^{*3} - 1} - 1\right)} \tag{7.14}$$

By integrating Eq. (7.14) with respect to time, the non-dimensional void radius at a time t can be determined:

$$r_v^*(t) = \int_0^t \frac{\mathrm{d}r_v^*}{\mathrm{d}t}\mathrm{d}t \tag{7.15}$$

The void volume fraction v_v at time t is then calculated as follows:

$$v_v(t) = \frac{r_v^{*3}(t)}{r_{s0}^{*3} + r_v^{*3}(t) - 1} \tag{7.16}$$

The input parameters for the model are presented in Table 7.2. The initial shell radius

Table 7.2 – Parameters applied to the void dynamics model for a carbon/PEEK composite.

Symbol	Parameter	Value	Unit
P_{atm}	Atmospheric pressure	1.01×10^5	Pa
v_{v0}	Initial void content	3.1	%
r_{v0}	Initial void radius	10×10^{-6}	m
P_{g0}	Initial void pressure	1.23×10^5	Pa
T_{g0}	Initial void temperature	20	°C
σ	Surface tension	0.015	N/m
μ_s	Shell viscosity	$\mu_{\text{(CFPEEK K,M\&S-b)}}$	Pa · s

was determined from the definition of the void fraction:

$$\frac{\frac{4}{3}\pi r_{v0}^3}{\frac{4}{3}\pi r_{s0}^3} = v_v(0) \tag{7.17}$$

Which can be simplified and rearranged to give:

$$r_{s0} = \left(\frac{r_{v0}^3}{v_{v0}}\right)^{1/3} \tag{7.18}$$

The fluid pressure P_f (must be absolute due to the use of the ideal gas law) was evaluated as:

$$P_f = P_{app} + P_{atm} \tag{7.19}$$

Where P_{app} and P_{atm} are the applied and atmospheric pressures respectively.

7.2.4 Temperature history

The temperature history in this chapter was determined using the combined optical-thermal model. The SBS samples ideally fail in the mid-plane, therefore the bonding calculations were performed for the mid-plane bond interface which in this case corresponds with the surface of the 10^{th} ply, as 20 ply samples were manufactured. The geometric details of the laser placement head such as the positioning of the laser and consolidation roller extension were measured. The optical model was updated

accordingly. The best approximation of the laser source and the micro-half-cylinder (MHC) surface model was assumed for the heat flux predictions. Measurement of the complete through thickness temperature history for all process conditions was attempted but proven difficult, as the fine wire thermocouples are fragile and often broke during subsequent placement passes. In this case the temperature predictions were validated for a sample of placement trials where the measurements were made successfully. Predictions were found to be in good agreement in terms of the profile shape and timing, and peak temperatures typically predicted to within 10 % of the measured values. The surface temperature of the tape and substrate were successfully measured for all of the trials using the *Xenics Gobi-640* long wave infra-red (LWIR) camera. The emissivity of the camera was calibrated for the composite using a thermocouple attached to the surface. The observed temperatures were found to be in good agreement with the model predictions.

7.2.5 Pressure history

The consolidation pressure history applied to the bonding and void dynamics models were determined experimentally. The pressure distribution under the roller was measured using the *Tekscan I-Scan* system coupled with a type 5051 sensor employing the same technique as previously in Chapter 4. As found previously, when performing trials with a silicone roller, the pressure is applied over a large area and minimal plastic deformation occurs, the pressure measured under the substrate layer is very similar to that applied by the consolidation roller to the top side of the tape. For the current placement trials, a 20 ply unidirectional stack was manufactured. It is therefore assumed in this work that the pressure distribution at the interface on subsequent passes is equivalent to that measured for the placement of the 10^{th} layer, as little deformation occurs and the pressure is spread over a large area. In the case of a metallic roller where the pressure distribution is extremely localised to a line, this assumption would no longer be valid as the pressure field under the roller would

diffuse/radiate outwards from this small contact point, resulting in much greater changes in the pressure distribution with depth.

7.3 Experimental

7.3.1 Placement trials

Trials were performed at speeds of 100 and 400 mm/s. In previous trials it was found that the temperature control system can cause oscillations of the laser angle and laser power due to tuning of the control gains. In order to ensure consistency and also repeatability of the experiments, in this study the laser power and angle were fixed. The temperature control system is however required for more complex geometries and also control of the power during the transient start-stop conditions. In this case the geometry of the laminate is constant, and experiments are performed under tightly controlled conditions, therefore fixed power and angle are appropriate for this situation. Samples are taken from the centre of the laminate, avoiding the sub-optimal properties from the transient regions. The result was higher temperature stability, providing higher bond consistency and also making thermal model implementation of the process more straightforward.

In order to determine the appropriate laser powers and angles for the trials, experiments were first performed using the temperature control system with fixed process temperature control targets. The average laser power and laser angle were then noted. Trials were then repeated using these average values applied as fixed laser powers and laser angles.

Samples were prepared by placement of 1200 mm long strips of *Suprem*™ *T* 60 % v/v AS4/PEEK-150 0.15 mm × 12 mm prepreg across the length of an aluminium tool. The tool was not heated. A high performance double-sided technical adhesive tape was applied to the tooling, and the first ply was placed by performing a 'dry' run without laser power. 20 ply, single tape width, unidirectional laminates were then

Table 7.3 – Process parameter sets for the short beam shear trials. Note: the process temperature is based on non-contact process control measurements and may not be representative of the true temperature.

Placement rate [mm/s]	Process temperature [°C]	Consolidation force [N]	Laser power [W]	Laser angle [°]
100	400	500	745	-0.5
100	450	500	835	-0.5
100	500	500	920	-0.5
100	550	500	1000	-0.5
100	600	500	1090	-0.5
400	400	500	1515	0.5
400	450	500	1700	0.5
400	500	500	1880	0.5
400	550	500	2110	0.5
400	600	500	2335	0.5

manufactured based on the process parameters listed in Table 7.3. After each pass of the placement head, the resulting laminate was allowed to cool close to ambient temperature before placement of the subsequent layer. This was done so as to avoid heat build up which would otherwise change the resulting substrate temperature, given the use of fixed laser power and angle. This would also result in conditions that would more closely mimic the manufacture of a large component, where significant periods of time would pass prior to placement over the same given area of substrate. Due to the cooler substrate temperatures, the strengths would be lower than the case where heat build up is allowed to occur, thus this represents the worst case scenario. Thermocouples were applied to the surface of the 10^{th} ply after it was placed. Measurement of the 10^{th} ply interface temperature was then recorded until after the placement of the 20^{th} ply.

The 80 mm conformable silicone roller was selected over a rigid metallic roller for these trials as it was shown (in Chapter 4) to result in superior bond strength development. Also based on the findings in Chapter 4, the consolidation load was fixed at the highest practical value for the current placement head which was 500 N.

7.3.2 Short beam strength tests

Short beam strength tests were performed for inter-laminar bond strength characterisation. In this study, the *ASTM D 2344* standard was followed.

7.3.2.1 Sample preparation

Short beam strength samples were prepared using material taken from the centre of the 1200 mm placement length in the region where the process is most stable, avoiding any transient effects that occur at the start and finish of the placement pass. The samples were prepared for the SBS tests as follows. First, samples approximately 125 mm long were cut to the 5.5 mm test width using a 1 mm diamond slitting wheel installed in a surface grinding machine. This required the use of a customised fixture to hold the sample from the centre while the edges were cut parallel to each other. The surface grinder allows for superior control of the sample dimensions as the position can be adjusted in 1 µm increments. Only small amounts of material are removed on each pass, minimising heat input as well as undue stresses on the sample. The resulting cuts are very clean, straight, and high quality. The samples were then held by the freshly cut parallel sides in a precision vice and ground to a thickness of 2.75 mm using a diamond grinding wheel, removing equal amounts of material from the top and bottom sizes of the laminate. This resulted in samples approximately 125 mm long, with a highly accurate 2.75 mm × 5.5 mm cross-sections extracted from the centre of the laminate. A precision diamond saw was then used to cut the samples to length, which was six times the sample thickess at 16.5 mm. The finished dimensions of the samples were 2.75 mm × 5.5 mm × 16.5 mm, within the tight tolerances of the *ASTM D 2344* standard. The samples were then de-burred and labelled.

7.3.2.2 Test procedure

The samples were tested in a screw driven *Intron* universal testing machine. A 5 kN load cell was installed. The sample was placed on support pins 3 mm in diameter, separated by a span four times the sample thickness at 11 mm. The loading nose was 6 mm in diameter. Tests were performed with a 1 mm/min cross-feed rate. A typical example of the test is shown in Figure 7.2. A minimum of five samples were tested for each process setting. The short beam strength σ_{sbs} [MPa] was calculated as per the standard, using Eq. (7.20):

$$\sigma_{sbs} = 0.75 \times \left(\frac{F_{max}}{b \times h} \right) \tag{7.20}$$

Where F_{max} [N] is the maximum force observed during the test and b [mm] and h [mm] are the measured specimen width and thickness respectively.

7.4 Results and discussion

The following sections investigate the response of the process to increasing process temperature from 400-600 °C in terms of the degree of bonding, crystallinity and void dynamics. Trials were performed at speeds of both 100 and 400 mm/s. Predictions of the short beam strength are compared to the experimental results.

7.4.1 Temperature and pressure history

Examples of the combined temperature and pressure histories for the 10^{th} ply at a placement rate of 100 mm/s are plotted in Figure 7.3. For the periods when the temperature drops below the temperature threshold for bonding, void dynamics and crystallisation, which is assumed to be the glass transition (T_g) in this study, the history has no effect on the resulting quality and therefore the history from these periods of time was truncated. The plotted data was truncated equally on each data set to make back to back comparisons clearer.

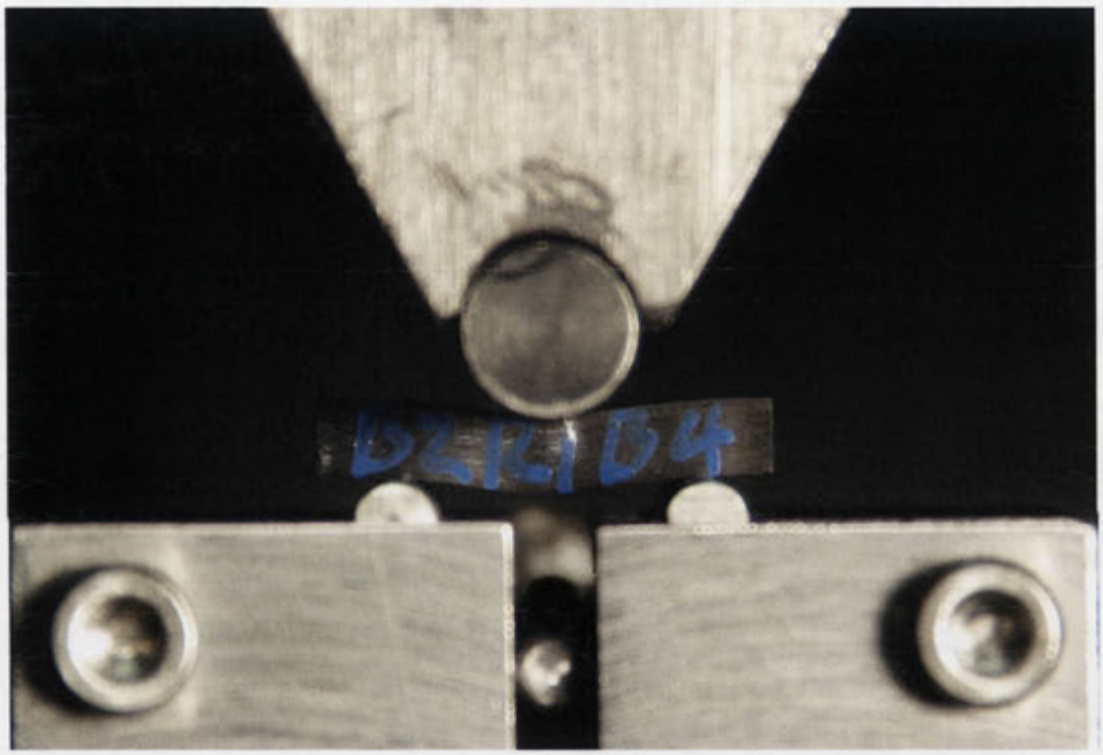


Figure 7.2 – Example showing the *ASTM D 2344* short beam strength test method performed on a sample. Sample dimensions are 2.75 mm × 5.5 mm × 16.5 mm. The span length between the 3 mm diameter support pins was four times the sample thickness at 11 mm.

When comparing the temperature histories for different process temperatures (Figures 7.3a–7.3c), it can be seen that the cooling rates increase for higher process temperatures, which is expected due to higher rates of conduction/thermal diffusion of heat through the thickness of the composite as the overall temperature gradients between the surface and bulk of the composite are greater. An interesting observation is that as the bond interface becomes deeper as additional plies are placed, the relative position of the peak temperature is delayed with respect to the application of pressure from the consolidation roller. This is because it takes longer periods of time for the heat to diffuse to the depth of the 10^{th} bond interface as it progressively becomes deeper in the laminate during subsequent placement passes. For a process temperature of 400 °C (Figure 7.3a), the interface temperature on the first subsequent pass (placement of the 11^{th} ply) reaches approximately 300 °C, which is below the melting point (343) of the PEEK matrix. At process temperatures of 500 and 600 °C (Figures 7.3b and 7.3c), the temperature during the first subsequent pass is above the melting point at 350 and 390 °C respectively, indicating that higher levels of further bond development will occur and also the crystalline phases will be re-melted.

When increasing the placement rate by a factor of four from 100 mm/s to 400 mm/s, it can be seen that the time period of pressure application and the laser irradiation is correspondingly decreased by one quarter (Figure 7.4. The result of the decreased period of laser irradiation, given the same process temperature, is reduced heat soak which in turn leads to higher rates of cooling in the consolidation zone. The thermal penetration is also reduced, with much lower temperatures experienced during the subsequent passes. Temperatures of 200, 240 and 280 °C occur on the first subsequent pass for process temperatures of 400, 500 and 600 °C (Figures 7.4a–7.4c) respectively, which is much lower than the 300, 350 and 390 °C experienced for a placement rate of 100 mm/s. This indicates that given the same process temperatures, there will be much lower levels of bond development on subsequent passes for a placement rate of 400 mm/s.

7.4.2 Bond Development

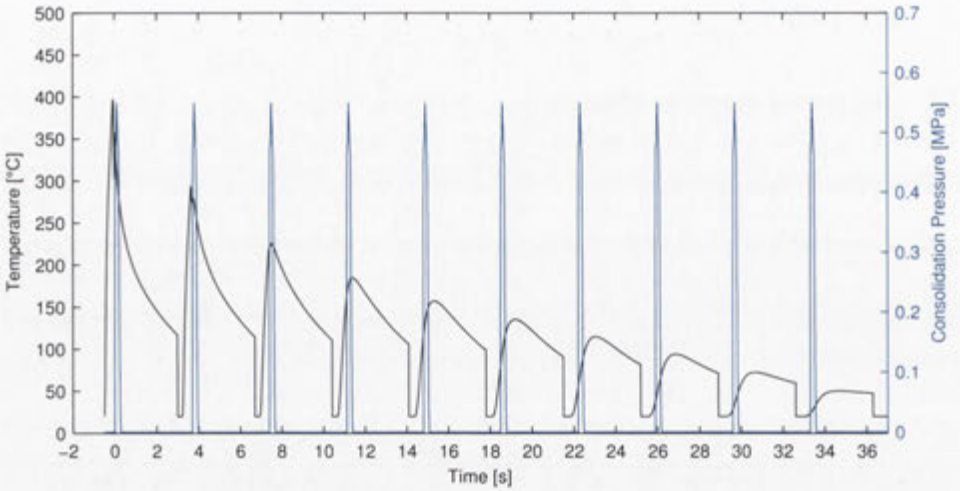
7.4.2.1 100 mm/s placement rate

The bond development history at different process temperatures for a placement rate of 100 mm/s is presented in Figure 7.5. The example predictions plotted are determined using Bonding Parameter Set 3 (BPS-3) that was shown (in Chapter 4) to provide the best agreement with experimental strength over a large range of process parameter settings. Predictions were also made based on the other bonding parameter sets from the literature and current work, however for the sake of brevity only the resulting bond strengths predictions will be presented in the next section.

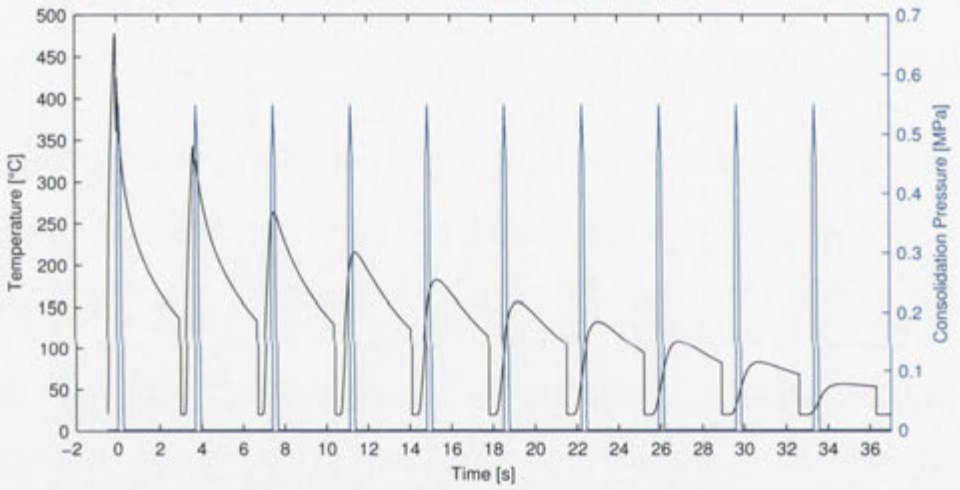
For a process temperature of 400 °C, the intimate contact is predicted to reach 74 % on the initial placement pass (Figure 7.5a). On the subsequent passes it progressively increases to values of 81, 83 and 84 %, with no further development after the 5th pass. The total degree of healing develops in a similar but more rapid fashion, with the final degree of healing for the areas in intimate contact reaching 98 %. As the healing is close to completion, the overall degree of bonding (82 %) closely follows the intimate contact, suggesting that the bonding in this case would be intimate contact limited.

When increasing the process temperature to 500 °C, the intimate contact develops more rapidly with values of 87, 94 and 98 % after the first, second and third consolidation passes respectively. Due to the elevated process temperature, the healing reaches values close to completion for the first to third consolidation passes. The healing for the increments of intimate contact developed during the 4th and 5th passes reach values of 75 and 58 % respectively as indicted by $D_{ah_{final}(\Delta D_{ic(t)})}$, however the relative portion of intimate contact developed for these passes is minimal, therefore the incomplete healing for these regions has a minimal effect on the overall degree of healing. The resulting degree of bonding is predicted to be very high at 98 %.

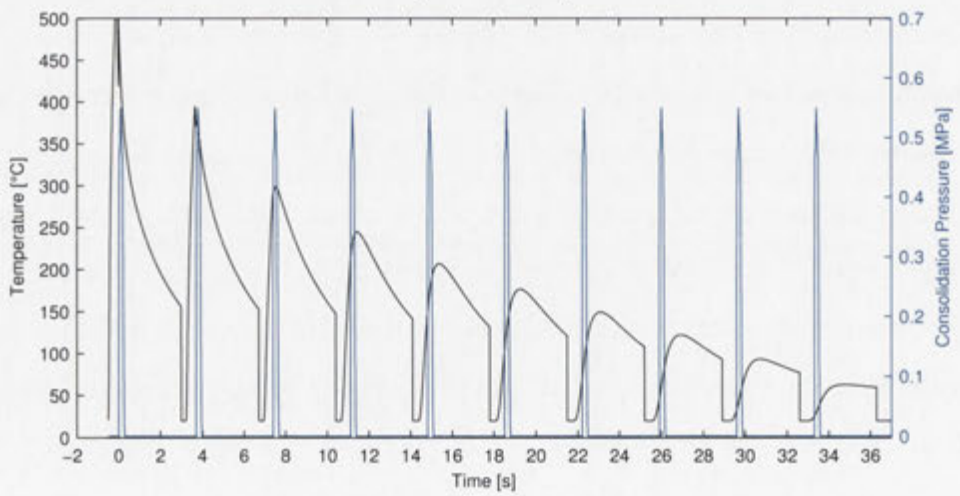
At a process temperature of 600 °C, the intimate contact development is extremely rapid with 99 % developed on the initial placement pass. The healing develops almost



(a) 400 °C process temperature.

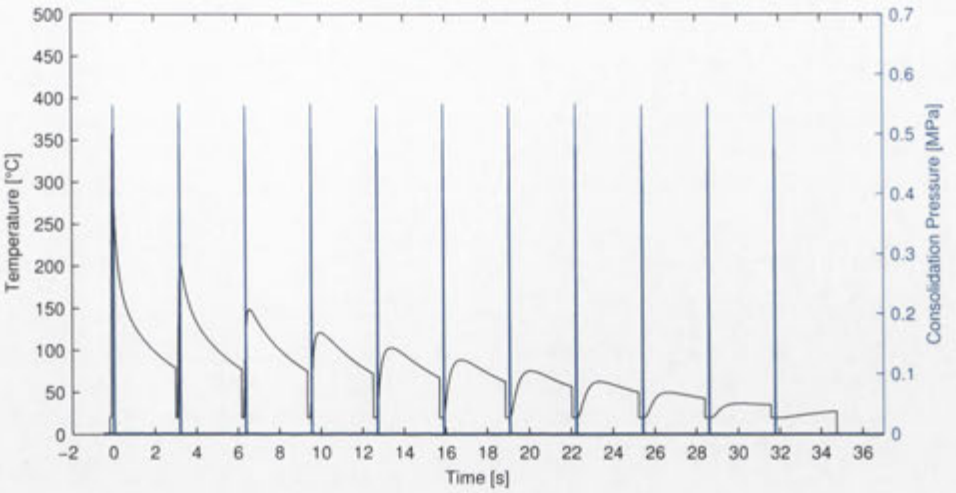


(b) 500 °C process temperature.

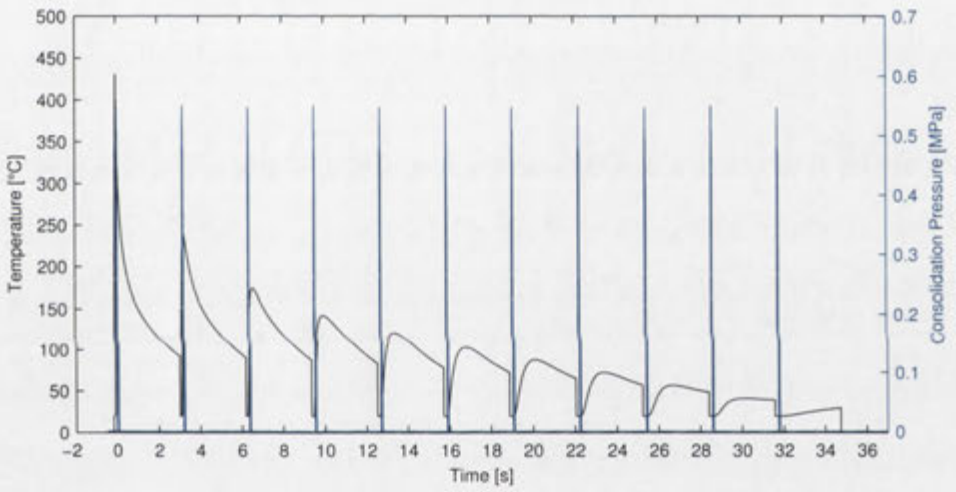


(c) 600 °C process temperature.

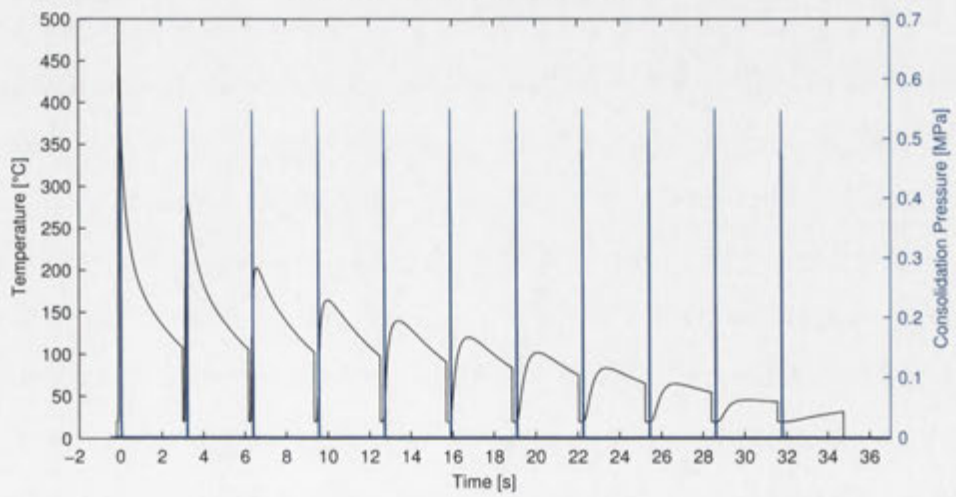
Figure 7.3 – Temperature and pressure histories (10^{th} ply) for different process temperatures at a placement rate of 100 mm/s. The time between placement passes has been truncated when the temperature is too low to affect bonding. Each pair of temperature and pressure peaks corresponds to a placement pass.



(a) 400 °C process temperature.



(b) 500 °C process temperature.



(c) 600 °C process temperature.

Figure 7.4 – Temperature and pressure histories (10^{th} ply) for different process temperatures at a placement rate of 400 mm/s. The time between placement passes has been truncated when the temperature is too low to affect bonding. Each pair of temperature and pressure peaks corresponds to a placement pass.

instantaneously due to the high interface temperatures. After the second placement pass, both the bonding and intimate contact have fully developed, resulting in 100 % strength prediction.

7.4.2.2 400 mm/s placement rate

Next, the bond development history was investigated for a placement rate of 400 mm/s (Figure 7.6a). Comparing the temperature and pressure histories for a process temperature of 400 °C for placement rates of 100 mm/s (Figure 7.3a) and 400 mm/s (Figure 7.4a), it can be seen that for the placement rate of 400 mm/s the cooling rate is much higher and the temperatures during the subsequent passes are much lower by almost 100 °C. The resulting impact on the bond development is significant, with the degree of intimate contact only developing over the first and second passes, and reaching a maximum value of 54 %. As mentioned in the previous section, the maximum temperature becomes delayed relative to the nip point for subsequent passes due to the time taken for the heat to diffuse through the thickness of the composite. At 400 mm/s the time period of pressure application is also reduced. This reduced time period combined with the delayed peak temperature results in pressure application before the interface reaches the temperatures required to develop intimate contact. This is particularly evident for the third pass onwards in the temperature and pressure plots (Figure 7.4), and also by the lack of intimate contact development for the third pass onwards in the bond development plots (Figure 7.6). Therefore it can be seen that when moving to higher placement velocities, not only are the cooling rates higher, the interface temperatures for subsequent passes lower, and the period of pressure application reduced, but also the peaks in temperature and pressure application become de-synchronised. This de-synchronisation effect still occurs at the lower placement rate of 100 mm/s, however the length of time for the pressure application is longer, and therefore the elevated temperatures and pressures still overlap up until the 5^{th} pass. The healing is predicted to be incomplete at 63 % and only seen

to develop over the first three passes. The process is therefore predicted to be equally limited by intimate contact and healing, with a resulting bond strength of only 35 %. The corresponding degree of bonding at 100 mm/s was 82 %, predicting a significant reduction in strength and therefore sensitivity of the process to placement rate.

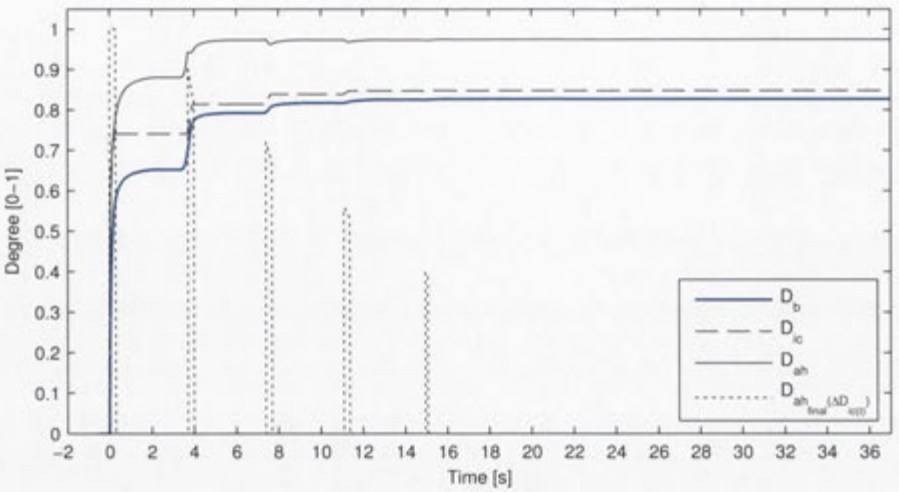
The intimate contact development for a process temperature of 500 °C (Figure 7.6b) is very similar to that at 400 °C, however the values are slightly higher with the final degree of intimate contact reaching 63 %. A minuscule amount of intimate contact development now occurs after the third placement pass. The degree of healing is much higher due to the increased time periods experienced at elevated temperatures with a final value of 87 %. The resulting level of bonding is mostly intimate contact limited with a value of 55 %. The results for a process temperature of 600 °C predict the intimate contact to reach 72 % on the initial consolidation pass and plateau at a value of 74 %. Due to the higher interface temperatures, healing rapidly develops to high levels greater than 99 %. Here the final degree of bonding reaches 74 % rather than 100 % as predicted for the lower placement rate of 100 mm/s.

In summary, the bond development process was found to respond positively to increases in process temperature. In the case of a 100 mm/s placement rate, 82 % bond strength was predicted for the lowest process temperature of 400 °C, while complete bonding was predicted for process temperatures greater than 500 °C. When moving to a higher placement rate of 400 mm/s, predictions suggest the bonding is relatively low for a process temperature of 400 °C at 35 %. Increasing the process temperature to 600 °C suggested 74 % strength would be achieved.

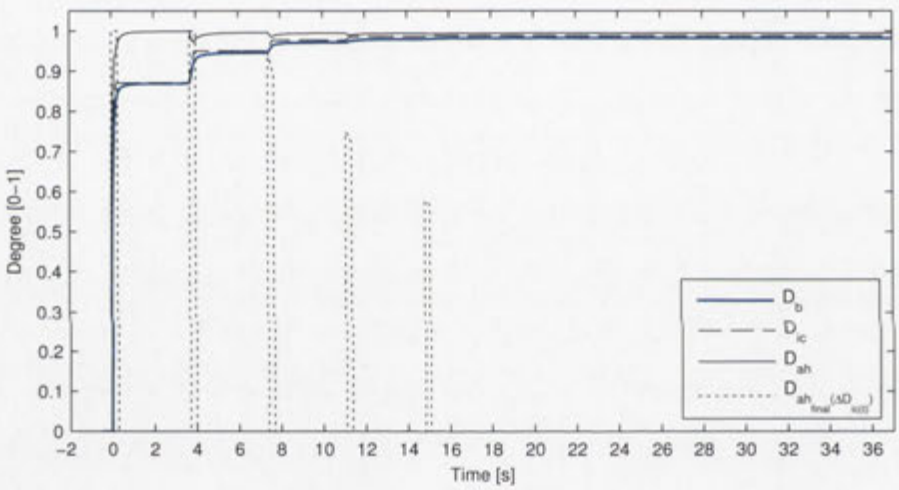
The reason for lower strengths at higher placement rates, given the same process temperature was explained by multiple phenomena:

- Increasing the placement rate decreases the effective time period of laser irradiation and consolidation pressure application.

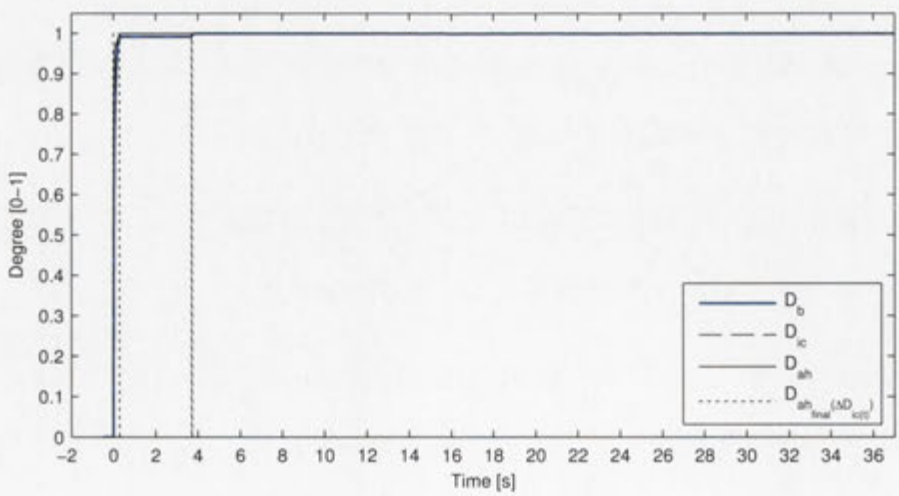
- For a fixed process temperature, the result is lower heat soak of the composite.



(a) 400 °C process temperature.

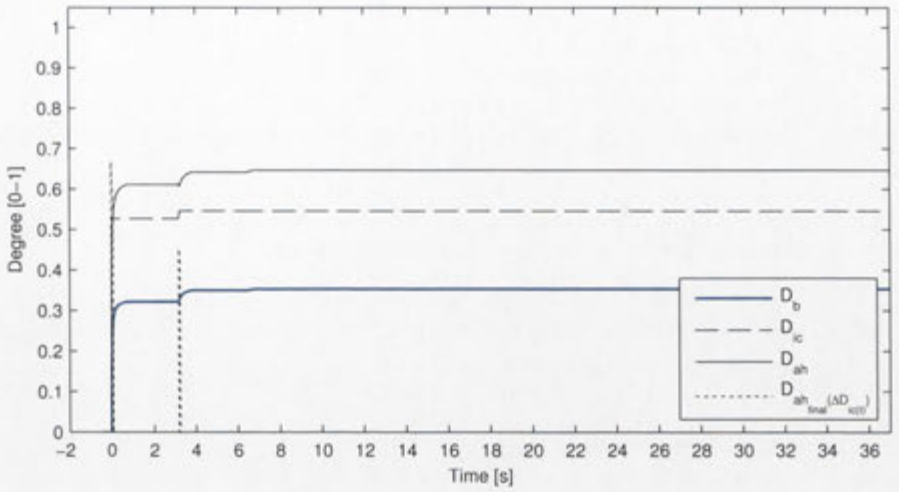


(b) 500 °C process temperature.

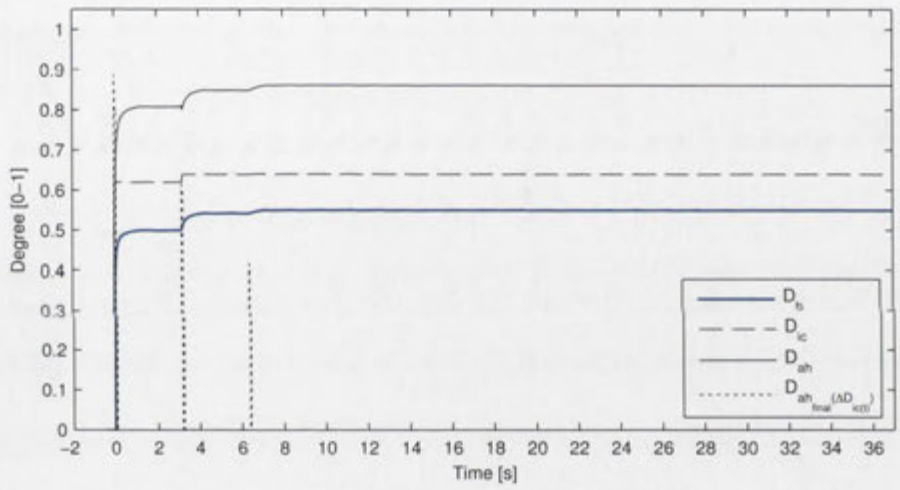


(c) 600 °C process temperature.

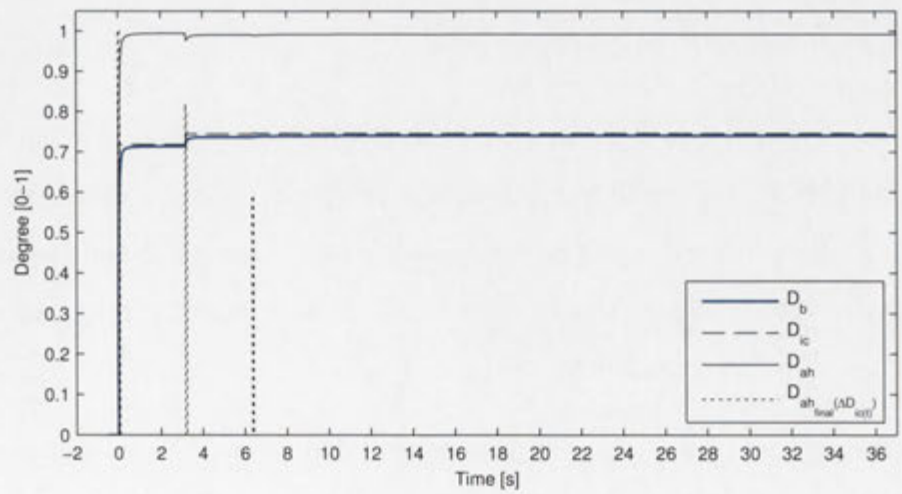
Figure 7.5 – Comparison of bonding predictions (based on BPS-3, Table 4.4) for different process temperatures at a placement rate of 100 mm/s.



(a) 400 °C process temperature.



(b) 500 °C process temperature.



(c) 600 °C process temperature.

Figure 7.6 – Comparison of bonding predictions (based on BPS-3, Table 4.4) for different process temperatures at a placement rate of 400 mm/s.

- The cooling rates are therefore higher, resulting in lower dwell times at high temperature at the bond interface.
- The thermal penetration through the thickness of the subsequently placed layers is also lower, resulting in lower temperatures and thus bond development during placement of the subsequent layers above.
- As the heat takes time to diffuse through the thickness, a delay in the peak temperature occurs for the subsequent passes which becomes larger as the thickness of the subsequently placed layers increases.
- This delay causes de-synchronisation of the high temperature and pressure application. The pressure application occurs prior to the interface experiencing elevated temperatures, thus greatly limiting intimate contact development on subsequent passes.
- Shorter pressure application periods reduce the intimate contact development.
- Furthermore, shorter pressure application increases the sensitivity of the process to the de-synchronisation as there is less overlap in the temperature and pressure peaks.

Based on the above findings, in order to maintain the bond strength while increasing placement rate:

- The length of the irradiated area should be increased, so as to maintain the same period of heat input in the time domain. Doing so will maintain the same level of heat soak, resulting in the same cooling rates and thermal penetration through the thickness for the subsequent passes. Doing so would be relatively easy to realise, however there must be a sufficient length of feed tape exposed between the feed mechanism and the nip point.
- Increase the length of the pressure distribution so as to maintain the pressure history in the time domain. The most obvious way to achieve this would be

to increase the diameter of the consolidation roller, however this would likely have an adverse effect of increasing the size of the shadow prior to the nip point, which would in turn decrease the consolidation temperature history. Other avenues include softer roller materials, design-based roller modifications or even a caterpillar style consolidation device for example.

7.4.3 Short beam strength: experimental vs. predictions

Short beam strength predictions were performed with the bonding models investigated in Chapter 4 using parameters from the literature and also from the current work. The results of the model predictions will then compared and contrasted with the results of the experimental placement trials. The SBS test was found to result in very low covariance, allowing for greatly increased differentiation between process settings as the statistical significance is higher, when compared with the results of the lap shear test method used in Chapter 4.

7.4.3.1 100 mm/s placement rate

First, the results for a placement rate of 100 mm/s are considered (Figure 7.7). The experimental SBS results indicate that the inter-laminar properties of the samples are fully developed, with values at if not above the ultimate SBS value reported in literature for the same particular *Suprem*™ *T* 60 % v/v AS4/PEEK-150 prepreg. The exception is the strength for a process temperature of 600 °C which was found to be only 87 % of the reference, the result of which is attributed to thermal degradation as PEEK is known to show rapid decomposition for temperatures in excess of 575 °C [Patel et al., 2010].

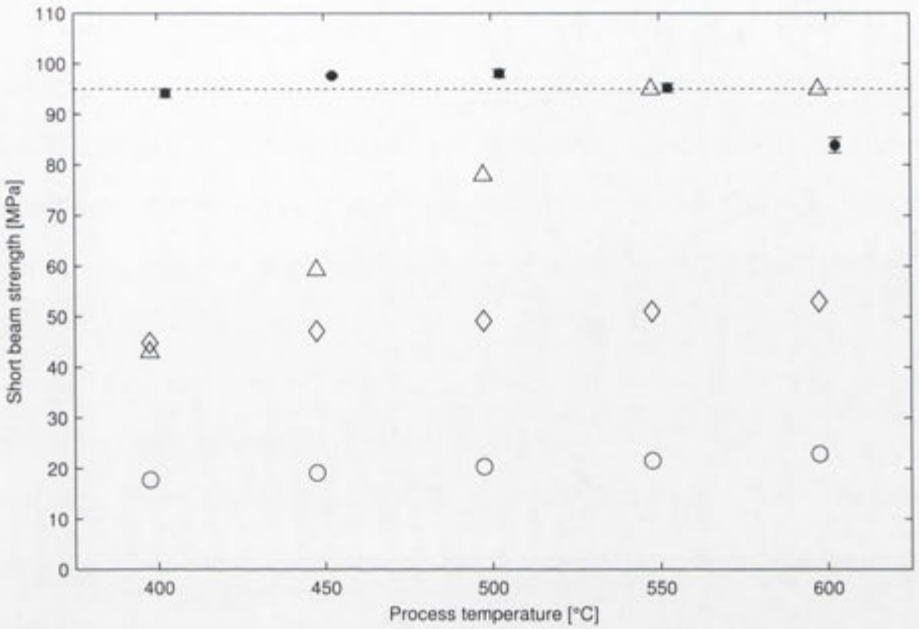
When considering the bonding model parameters from literature (Figure 7.7a) it can be seen that the predictions are only for approximately 25 % and 50 % strength for the parameters of Khan et al. [2010] and Mantell et al. [1992] respectively. These are very conservative predictions, however they are expected to be somewhat con-

servative as they represent the case of crossed rather than aligned plies that were manufactured in this case. The parameters of Tierney and Gillespie [2006] show a much stronger response to increasing process temperature, however the results do not agree well with the experimental data.

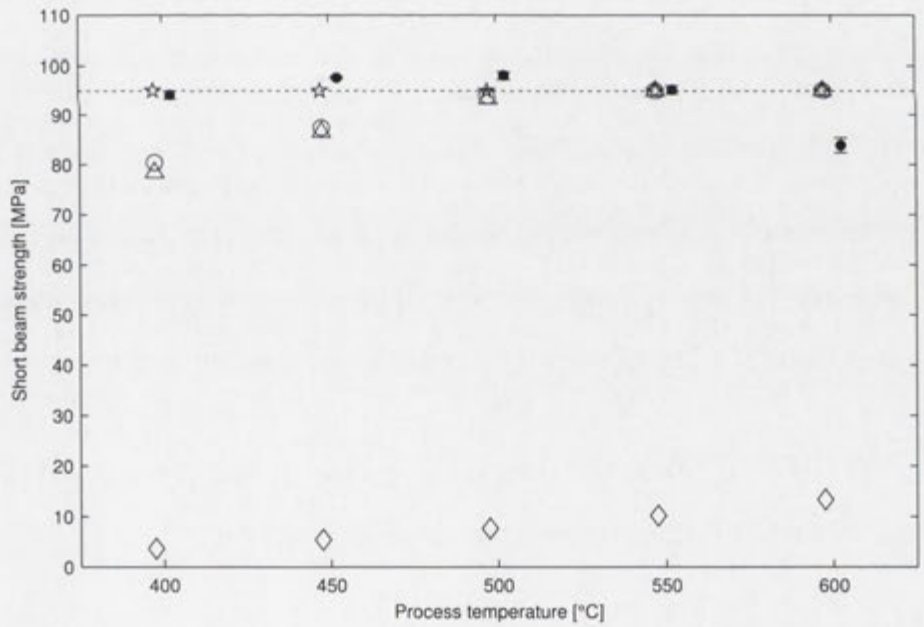
The results of the predictions based on the current parameters are presented in Figure 7.7b. It can be seen that there is much better agreement in the case of BPS-1 and BPS-3, however BPS-2 shows extremely conservative predictions as was found to also be the case in Chapter 4. As the bonding models do not take thermal degradation into consideration, the predictions at 600 °C are expected to predict full bond development. A fourth bond prediction was made assuming the same parameters as BPS-3, however the intimate contact is assumed to develop instantaneously. Under such an assumption, the bonding is predicted to be fully developed in all cases, which agrees with the data the best for all conditions.

7.4.3.2 400 mm/s placement rate

Now the bond predictions for a placement rate of 400 mm/s are investigated (Figure 7.8). The experimental strengths in this case suggest that bonding has not reached completion for temperatures of 400, 450 and 500 °C, however the strengths are still quite high at 80, 86 and 92 % of the reference SBS value. The experimental strengths for temperatures of 550 and 600 °C are both approximately 98 % of the reference value, with no statistically significant difference between the values. Furthermore, it would appear that no adverse degradation has occurred for the 600 °C process temperature at this higher placement rate. This is an extremely positive result, demonstrating that this modern form of NIR laser AFP can produce fully bonded laminates at much higher rates rates than previously reported in the literature. Furthermore, the current trials were performed with ambient temperature tooling, rather than heated tooling (280 °C) that was used for the highest previously reported strengths (68 MPa at 150 mm/s) found in a review of the literature Figure 2.1.



(a) Predictions based on parameters assumed in the literature (Table 4.3). Experimental result (•), Khan et al. [2010] (◯), Mantell et al. [1992] (◇) and Tierney and Gillespie [2006] (△).



(b) Predictions based on the parameters assumed in the current work (Table 4.4). Experimental result (•), BPS-1 (◯), BPS-2 (◇) and BPS-3 (△), ($D_{ic} = 1$, $t_{w\ (PEEK\ S\&H)}$) (⋆).

Figure 7.7 – Comparison of the experimental short beam strength with the model predictions for different process temperatures at placement rate of 100 mm/s. Error bars represent $\pm\sigma$. The ultimate SBS is represented by the dashed line.

The bond predictions based on the literature parameters (Figure 7.8a) show very similar results to those at 100 mm/s (Figure 7.7a). The predictions are lower at approximately 10 % and 30 % strength for the parameters of Khan et al. [2010] and Mantell et al. [1992] respectively. Again, the parameters of Tierney and Gillespie [2006] show a much stronger response to increasing process temperature, however the results do not agree well with the experimental data.

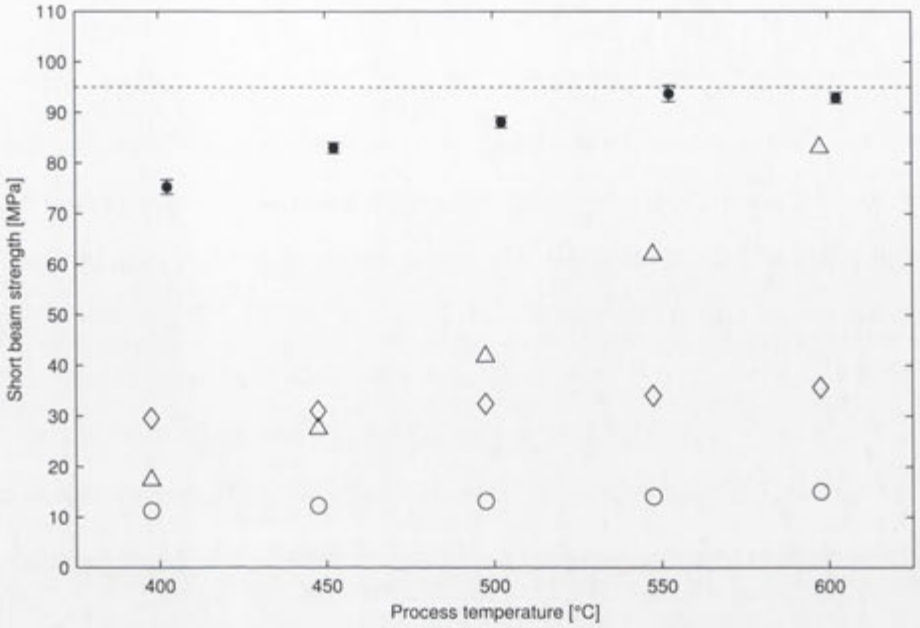
The predictions for the current parameters are shown in Figure 7.8b. Again, BPS-2 shows extremely conservative predictions. It can be seen that there is much better agreement in the case of BPS-1 and BPS-3, with BPS-1 showing the best correlation in this case. The fourth prediction assuming BPS-3 modified for instantaneous intimate contact development again provides the best correlation of all. This suggests that the intimate contact development is occurring much faster than the predictions, which would be somewhat expected as nesting of the fibres can occur when manufacturing unidirectional laminates resulting in more rapid intimate contact development.

7.4.4 Crystallinity and void content

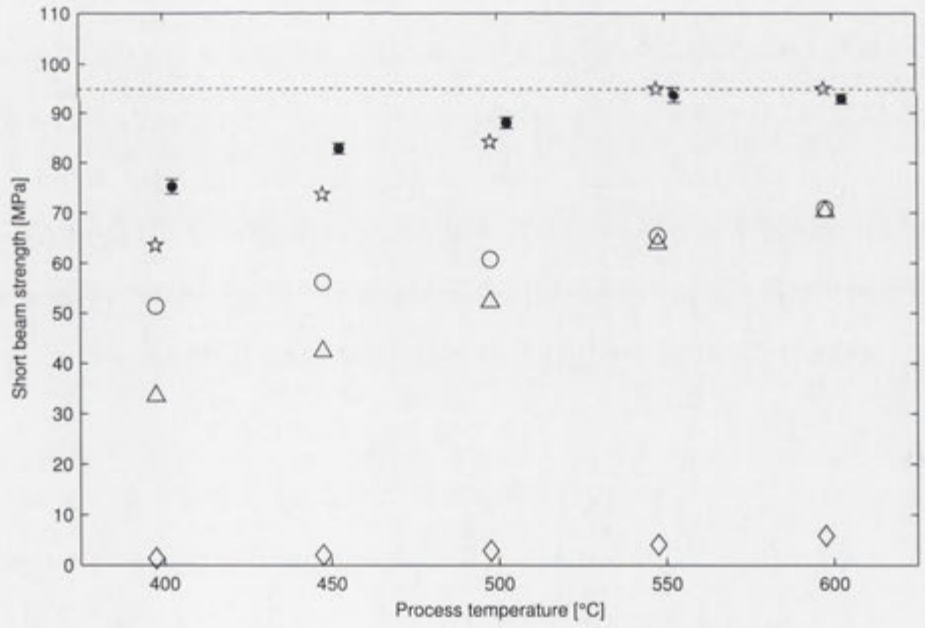
The bond strength of the samples produced with the NIR laser AFP process was shown to have developed to completion for multiple process parameter settings. While achieving full bond strength is the most important aspect of the process, other factors such as crystallinity and void dynamics also play an important role in the final resulting quality of the composite. This section investigates the predicted behaviours of the crystallinity and void dynamics during the process and how they might be affected by process temperature and placement rate.

7.4.4.1 100 mm/s placement rate

First, examples of the crystallinity and void dynamics predictions for a placement rate of 100 mm/s are plotted in Figure 7.9. The corresponding temperature and pressure plots were shown previously in Figure 7.3. Referring to the plot for a process



(a) Predictions based on parameters assumed in the literature (Table 4.3). Experimental result (•), Khan et al. [2010] (◯), Mantell et al. [1992] (◇) and Tierney and Gillespie [2006] (△).



(b) Predictions based on the parameters assumed in the current work (Table 4.4). Experimental result (•), BPS-1 (◯), BPS-2 (◇) and BPS-3 (△), ($D_{ic} = 1$, $t_{w\ (PEEK\ S\&H)}$) (⋆).

Figure 7.8 – Comparison of the experimental short beam strength with the model predictions for different process temperatures at placement rate of 400 mm/s. Error bars represent $\pm\sigma$. The ultimate SBS is represented by the dashed line.

temperature of 400 °C (Figure 7.9a), the void content of the tape can be seen to increase significantly during the laser heating phase, reaching a maximum value of approximately 8.5 % prior to the nip point. In the case of the substrate, the void content only increases from the initial 3.1 % to a value of 3.8 % during the heating phase. This difference between tape and substrate was mostly due to a bias of the laser towards the tape, resulting in higher tape temperatures. The tape does also become heat soaked and remains at a high temperature for a longer period compared with the substrate as found previously in the thermal modelling chapters, therefore leading to a greater degree of void expansion. After the application of consolidation pressure on the initial consolidation pass, the void content decreases due to compression of the voids. Due to the rapid cooling, the viscosity remains high and only a minimal amount of void compaction occurs prior to solidification. The second consolidation pass results in a minimal degree of further compaction as the temperature is too low for significant viscosity reduction. The final void contents are 7.1 and 3.3 % for the tape and substrate respectively.

When increasing the process temperature to 500 °C (Figure 7.9b), even greater levels of initial expansion occur during the heating phase. As the material remains hotter, the viscosity is lower allowing for much greater levels of void compaction, particularly for the tape. Further void compaction is observed for the first two subsequent passes. The final void content of the tape and substrate are 4.2 and 3.3 % respectively in this case.

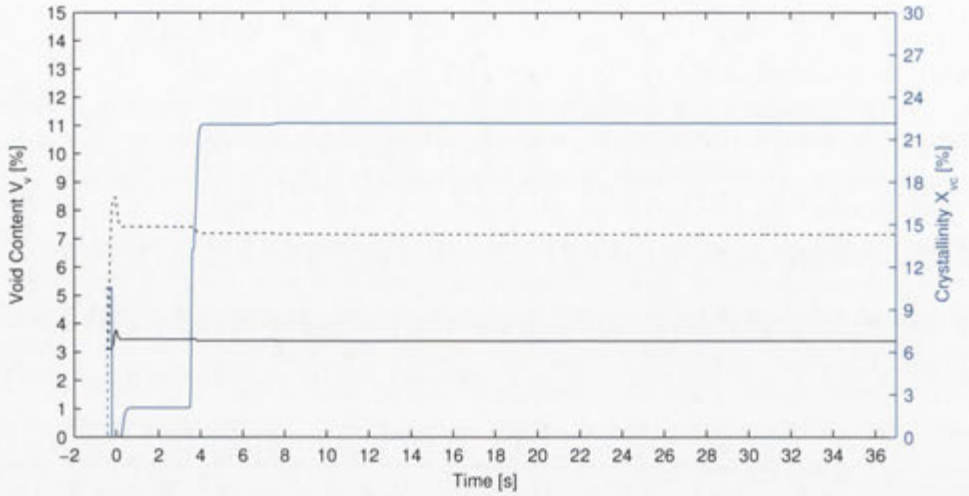
For a 600 °C process temperature (Figure 7.9c), the initial void content during heating reaches very high levels of 11 and 9.5 % for the tape and substrate respectively. Due to the high temperatures, very rapid compression occurs and the void content reaches a value as low as 1.8 % momentarily, but as the material is still soft and the internal gas temperature of the void is high, the void expands again to a value of 2.3 %. During the temperature excursion of the subsequent placement path, some further expansion occurs with the void content increasing to 3 %. This is quickly

compressed again by the consolidation roller, followed by a small rebound. The final void content is predicted to be 2.5 % for both the tape and substrate.

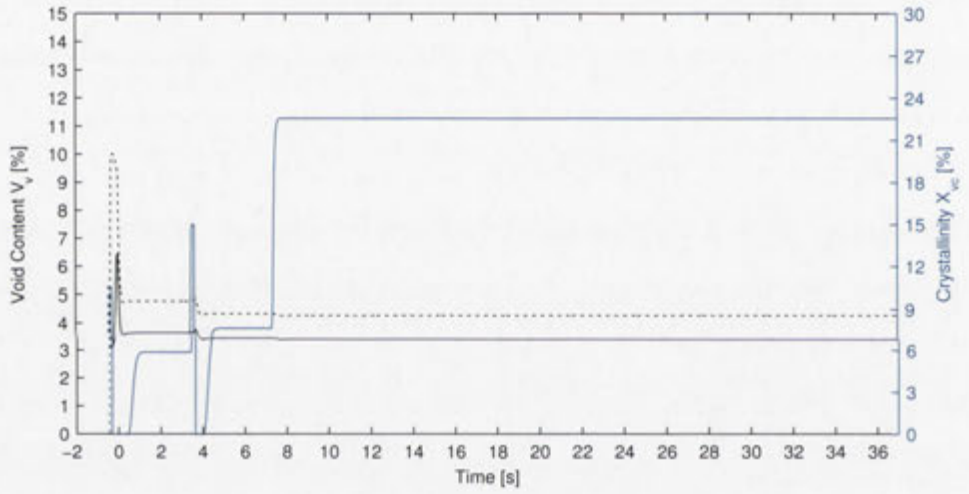
Referring back to the plot for a process temperature of 400 °C (Figure 7.9a), the crystallinity is completely erased during the heating phase as the temperature exceeds the melting point. As the temperature drops back below the melting point, the polymer starts to re-crystallise. During the cooling phase of the initial placement pass, the crystallinity develops to a low value of 2 %, as the temperature quickly passes through the peak crystallisation rate zone of approximately 210-280 °C. The temperature during the first subsequent pass peaks at a value of 300 °C, which is lower than the melting point. The crystallinity develops to a high degree due to the cumulative length of time experienced in peak crystallisation rate zone (210-280 °C). This crystalline development is predominantly spherulitic, as the epitaxial development occurs over much longer time scales. For process temperatures of 500 and 600 °C (Figures 7.9b and 7.9c), the temperature on the subsequent passes is above the melting point, resulting in multiple re-melting cycles. The final degree of crystallinity for all cases is approximately 22 %, which is in the recommended crystallinity range considered to give good mechanical properties with a balance of toughness and stiffness.

7.4.4.2 400 mm/s placement rate

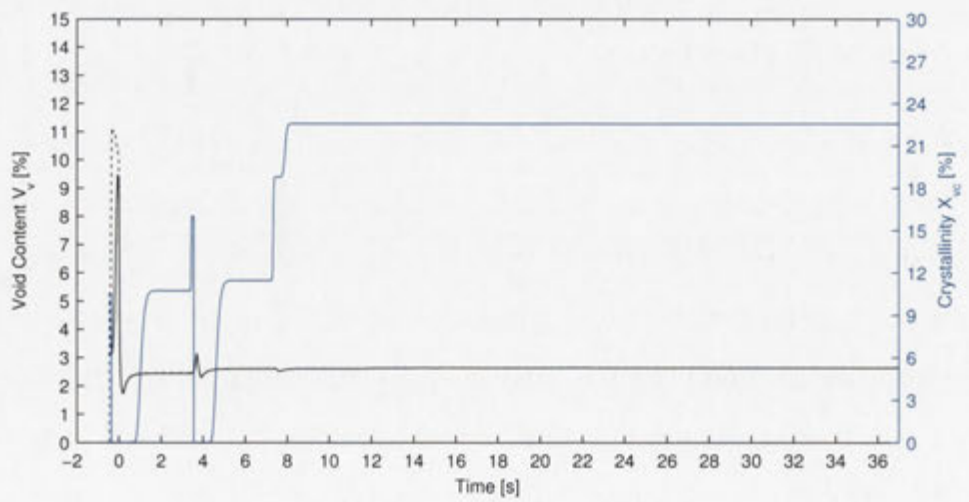
Now the void dynamics at a placement rate of 400 mm/s is investigated (Figure 7.10). In all cases the laser was biased towards the tape, resulting in higher tape temperatures compared with the substrate. Void expansion in the tape for a process temperature of 400 °C (Figure 7.10a) caused the void content to increase to a value of 5.9 %, however due to the short period of pressure application combined with the increased cooling rate, the degree of void compaction was minimal. No further activity occurs after the initial placement pass. The substrate void content remained unchanged, and the final void content for the tape was approximately 5.8 %.



(a) 400 °C process temperature.



(b) 500 °C process temperature.



(c) 600 °C process temperature.

Figure 7.9 – Comparison of the crystallinity and void content predictions for the substrate (solid) and tape (dashed) for different process temperatures, at a placement rate of 100 mm/s.

Moving to the 500 °C process temperature (Figure 7.10b), a very minimal amount of void expansion occurs for the substrate, however the tape experiences significant expansion to 9.5 %. The consolidation roller compresses the voids a small amount down to 8.5 %. Again the rapid cooling behaviour combined with the small period of pressure application has resulted in minimal void compaction.

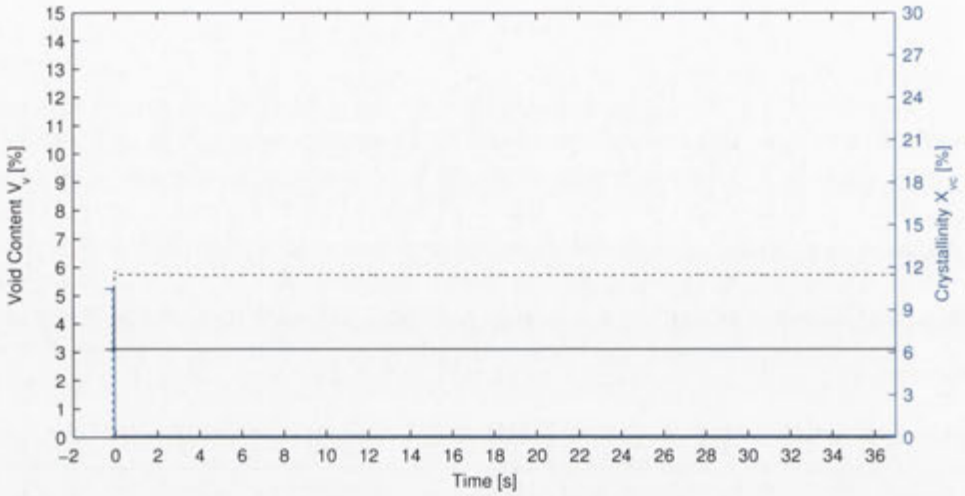
At a 600 °C process temperature (Figure 7.10c), the substrate underwent void expansion to a value of 3.9 %. Interestingly, the tape again has a significant increase in void content to 11 %, however the temperature remains higher under the consolidation roller, allowing for more significant compaction of the voids down to a value of 6 %. As in the other cases at this placement rate, no further behaviour is observed as the temperatures experienced during the subsequent passes are too low for void compression.

7.5 Conclusions

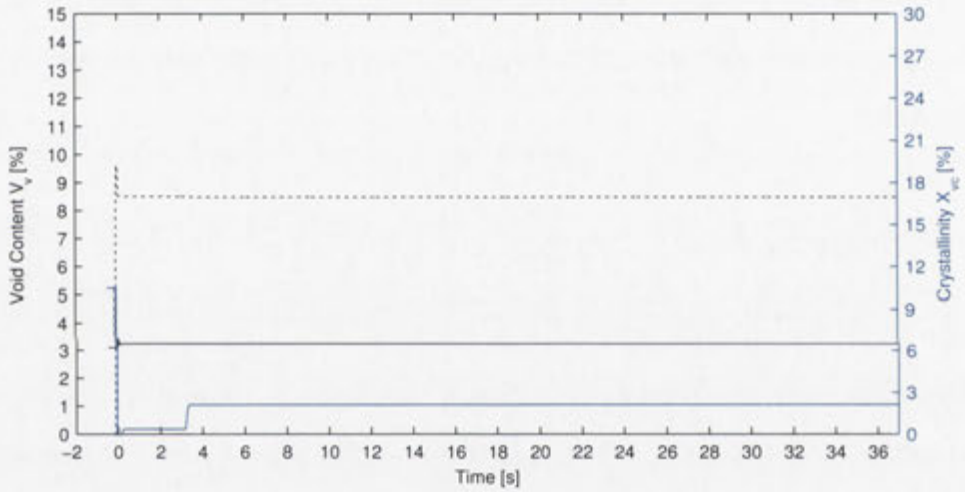
The capability of the laser AFP process for producing high strength laminates in an out-of-autoclave process was investigated. Multi-layered samples were manufactured under conditions that reflect those experienced during practical manufacture of components. The additional quality development due to subsequent placement passes was therefore included. The inter-laminar bond strengths of the resulting samples were characterised by short beam strength tests. The response of the process to increasing process temperature was investigated for temperatures from 400 °C to 600 °C, at placement rates of 100 mm/s and 400 mm/s.

A process simulator was formulated for the laser AFP process using the combined optical-thermal model that was developed over Chapters 3, 5 and 6. It was then coupled with the bonding model implemented in Chapter 4. Crystallinity and void dynamics models validated for AFP processes in the literature were also implemented.

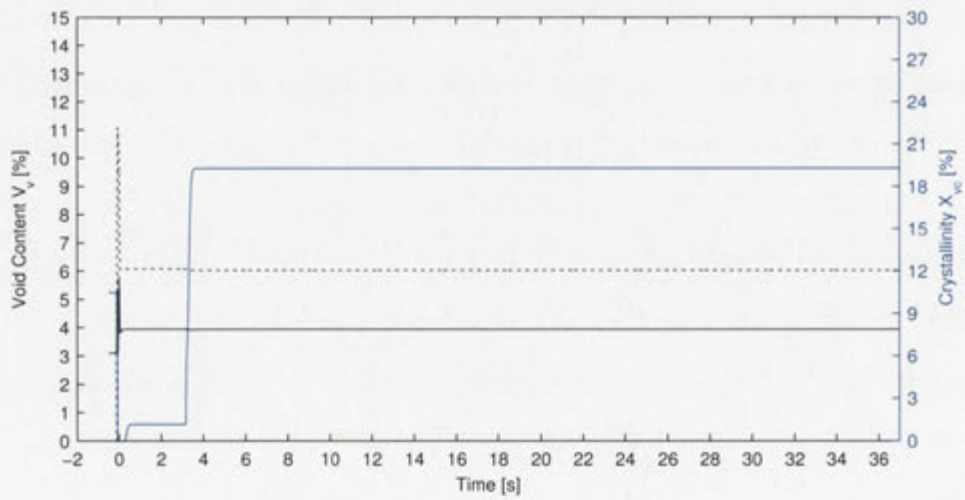
The temperature history predictions were made for the mid-plane bond inter-



(a) 400 °C process temperature.



(b) 500 °C process temperature.



(c) 600 °C process temperature.

Figure 7.10 – Comparison of the crystallinity and void content predictions for the substrate (solid) and tape (dashed) for different process temperatures, at a placement rate of 400 mm/s.

face of the SBS samples for the entire process history. The temperature history predictions were found to be in good agreement with experimental measurements for both the surface temperature during laser heating and also the through thickness history during the placement of subsequent layers. When comparing the temperature histories for placement rates of 100 mm/s and 400 mm/s, it was found that the higher placement rate resulted in reduced irradiation time, and for the same given process temperature, lower levels of heat soak were observed leading to higher cooling rates in the consolidation zone and reduced temperatures during subsequent passes of the placement head. Another important phenomenon observed was the desynchronisation of the temperature and pressure distributions on subsequent passes, caused by the delay of the heat diffusing through the thickness of the composite.

Experimental SBS results found that full bond strength can be achieved at placement rates of 100 mm/s for process temperatures as low as 400 °C without the use of heated tooling. When moving to a placement rate of 400 mm/s, values 98 % of the reported ultimate SBS in literature were achieved for process temperatures of 550 °C and 600 °C, illustrating the superior properties achievable with the modern NIR laser AFP process. No significant decrease in properties was observed for a process temperature of 600 °C at a placement rate of 400 mm/s, indicating no adverse degradation had occurred, however at placement rate of 100 mm/s a 10 % reduction in strength was observed, indicating that some form of degradation. Figure 7.11 provides a comparison of the best relative strength values from this work to those reported in experimental studies from literature. It can be seen that the current NIR laser AFP process using large rectangular laser spots produces far superior results compared with those previously reported, both in terms of strength, and particularly the placement rate.

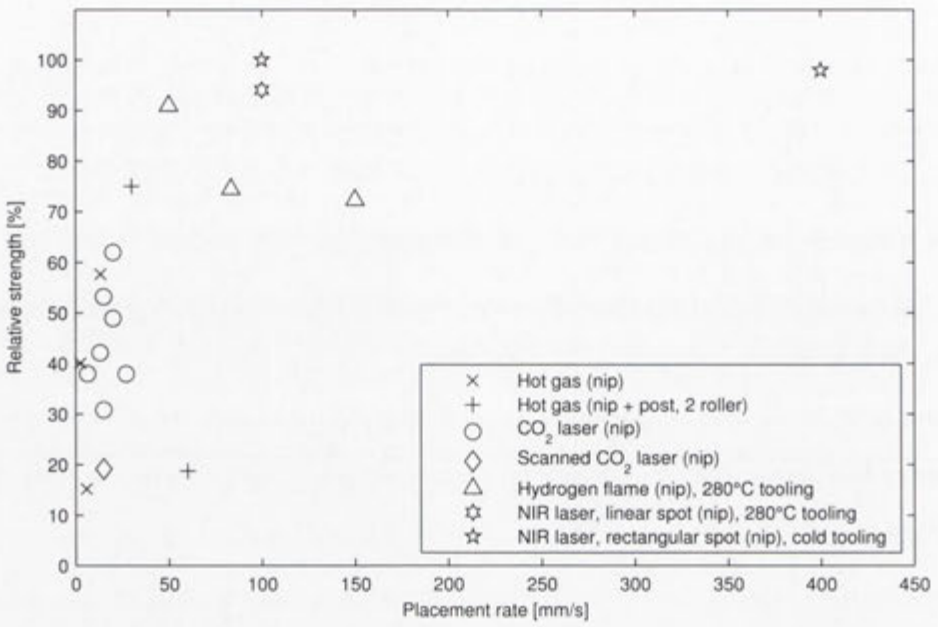


Figure 7.11 – NIR laser with rectangular spot from the current work compared with experimentally determined strengths reported for other AFP heat sources in the literature. Comparison of relative SBS vs. placement rate.

Predictions of the bond strength using the parameters from experimentally validated models in the literature were found to be overly conservative compared with the experimental results, with values typically in the range of 20-50 % of the experimental values. While the bonding models should provide conservative predictions due to the cross-ply assumption of the intimate models, this appears to be grossly conservative. Much better agreement was found using two of the bonding parameter sets (BPS) from the current work, BPS-1 and BPS-3. As found in Chapter 4, BPS-3 would appear to be the most robust parameter set as it shows good, although still conservative agreement with the experimental results across a wide range of process conditions. This also highlights the applicability of the bonding models for highly non-isothermal conditions.

Crystallisation model predictions indicate that the crystallinity of samples produced at 100 mm/s for all process temperatures lies within the recommended range of 20-35 %. For a 400 mm/s placement rate, the matrix is predicted to remain amor-

phous for process temperatures lower than 500 °C. At the highest process temperature of 600 °C the crystallinity is predicted to be just below 20 %, closely approaching the recommended range.

Void content predictions for a placement rate of 100 mm/s indicate that higher temperatures lead to lower void content, as greater levels of void compaction are achieved due to the decreased viscosity at elevated temperatures. The final void content is predicted to decrease from an initial value of 3.1 % to 2.5 % after placement for a process temperature of 600 °C. At a placement rate of 400 mm/s, the voids are predicted to expand significantly (to values in the range of 6 %) during the initial heating phase, particularly on the feed tape. The rapid cooling and the short pressure application results in minimal compaction. Furthermore the reduced temperature of the subsequent passes is insufficient for void compression. The resulting void content was predicted to be approximately 6 %.

Conclusion

8.1 Thermal Model

In Chapter 3 a 2D finite element thermal model incorporating the mass transport of heat was formulated for a laser assisted thermoplastic tape placement system using a conformable consolidation roller. It was found that the roller geometry could be significantly reduced due to a combination of the low thermal diffusivity of the roller elastomer and relatively fast mass flows.

In situ temperature measurements were performed with fine wire K-type thermocouples. The model was found to correlate reasonably well with the experimental measurements, particularly in terms of timing of the heated, shaded, consolidation and cooling regions with respect to each other, however experimental temperature measurements implied higher tape temperatures than modelled. The model predicted a relatively uniform temperature distribution through the thickness of the incoming tape, however a significant temperature gradient was present through the thickness of the substrate due to dissipation of the heat. The presence of the shaded region results in significant cooling of the surface prior to the nip point, particularly on the incoming tape.

The effects of roller temperature, corner radius and thermal contact were also studied. The temperature of the consolidation roller was found to have a significant impact on the cooling rate at the bond line and also on the temperature of the incoming tape. Increasing the thermal contact resistance was found to have a reasonable influence with the main effect of raising the incoming tape temperature due to a

decreased heat sink effect from the roller. Reducing the corner radius of the consolidation roller was found to slightly bias the heat towards the tape, as well as a small increase in the temperature at the nip point. The temperatures measured during the trials appeared to be too low for bonding as the temperature in the consolidation zone was lower than the melting point of PEEK ($T_m = 343\,^{\circ}\mathrm{C}$) at a value no greater than $330\,^{\circ}\mathrm{C}$. Despite the low consolidation temperature, the tape had bonded very well to the substrate. This prompted further investigation of the bonding behaviour, particularly for lower temperatures.

8.2 Bond Strength Development

Chapter 4 investigated whether bonding could occur at temperatures below the melting point of the polymer, as experimental results from Chapter 3 had suggested this was occurring. The suitability of the bonding models in literature for bond strength prediction in the laser AFP process was also investigated. The temperature and pressure histories were measured directly during the process using thermocouples and active pressure measurement sensor arrays. The results of which were fed into various bonding models that were implemented from the literature. Bonding predictions were made based on parameters from models in the literature that were experimentally validated, as well as parameters using more recent values for the particular composite under investigation.

It was necessary to select a bond characterisation test method to produce useful data points for validation of the bonding model predictions. Lap shear samples were manufactured with a single placement pass for a variety of processing conditions and consolidation rollers. A single placement pass ensured that the bond strength was not fully developed, which was necessary to generate data points to validate the bonding models. Trials were performed with rigid brass and also conformable silicone consolidation rollers. Using the knowledge gained in Chapter 3 for the thermal behaviour of the process, the position of the nip point in the temperature measure-

ments could be determined. In the case of the brass roller, a large shadow was present resulting in very low nip point temperatures in the range of 200-250 °C. Nip point temperatures were in the range of 300-340 °C in the case of the conformable silicone rollers in the extended trials.

Comparisons between the process temperature history and recently published data on the crystallisation behaviour of PEEK suggested that it would in fact remain highly amorphous during the consolidation phase, under the condition that the temperature exceeded the melting point prior to the nip point. As the matrix remains in the amorphous state, it is possible for healing and intimate contact to develop right down to the glass transition temperature. Temperature measurements performed for placement trials using the brass roller strongly suggest that the consolidation temperature was low due to a large shadow before the nip point, and in the range of 200-250 °C. Lap shear tests of the samples showed that despite such low bonding temperatures, values could reach up to 25 % of the ultimate strength. Bonding predictions were found to correlate with the experimental results, with the currently proposed bonding parameter set 3 (BPS-3) providing the best agreement. Trials were also performed using a conformable silicone roller where the initial consolidation temperatures were in the range of 300-340 °C, just below the melting point of the polymer at 343 °C. Again, it was found that significant levels of bonding occurred with strengths up to 50 % of the ultimate lap shear strength. This is a significant finding as it strongly suggests bond development can occur in the laser tape placement process for temperatures lower than previously thought due to the extremely short time periods involved. Bonding of PEEK is generally considered to not be possible for temperatures below 290 °C as the PEEK will readily crystallise, strongly inhibiting the healing process. From this work it has been shown that the bond predictions for AFP processes must consider the crystalline state of the resin. Higher bond strengths may be achieved that otherwise previously thought.

The bonding models were found to be sensitive to the welding time relations as

well as the temperature dependent viscosity. The relative magnitude of the strength predictions assuming bonding model parameters from the literature compared with each other was found to be dependent on the particular temperature history, as the same viscosity relations assumed for the intimate contact models have a stronger temperature dependence than others, which would result in more rapid intimate contact development for high temperature yet much slower development at low temperatures relative to other models. The experimentally validated parameter sets from other studies in the literature predicted quite different strengths in all cases, highlighting the fact that models cannot simply be adopted for other processes. The models in the literature have generally used predicted temperature and pressure histories instead of true process data, and then the bonding model parameters have been adjusted as tuning factors to obtain satisfactory agreements with experimental data. The models are therefore strictly suitable for understanding the response of a particular placement system to which they are calibrated, however caution must be exercised when applying such models to other processes. In the current study, the intimate contact was assumed to be the deformation of neat PEEK polymer at the surface. BPS-3 agreed well with the experimental data in the vast majority of cases and provided the best estimates of strength out of all bonding model parameter sets studied.

Samples produced with the conformable silicone roller were found to produce superior strengths compared with the rigid brass roller. The measured temperature histories suggest that a large shadow formed by the large radius of the roller would cause much greater temperature drops before the nip point compared with the silicone roller which has a much smaller shadow. The difference in strengths was therefore mostly attributed to the lower resulting temperatures in the consolidation zone rather than differences in the applied pressure distributions. The process was found to respond favourably to an increase in consolidation force from 150 N to 500 N, with the strength typically increasing by approximately 100 and 50 % for

the brass and silicone rollers respectively. The maximum pressure under the silicone roller was found to only increase by 80 %, despite the 333 % increase in load. This was due to an increase in size of the contact patch, as well as a large portion of the load being supported by the tooling either side of the tape in the case where higher loads were applied. Interestingly, for the range of process settings studied, the bond strength was relatively independent of the placement rate, with no statistically significant difference between speeds in the case of a high consolidation load. This was explained by the fact the peak consolidation pressure would occur sooner after the nip point before the material has time to cool to the degree it would at a lower placement speed. The decreased time for pressure application was therefore partly compensated for by pressure application at slightly higher temperatures.

8.3 Optical characterisation

The optical behaviour of the composite and laser were characterised and approximated in Chapter 5, providing the foundations necessary to develop a complete 3D ray tracing model for the NIR laser-assisted TP-ATP process. The scattering behaviour of the composite was observed qualitatively using a low power laser source and camera. The scattering nature of the composite required the total hemispherical reflectance to be measured. This was achieved by performing measurements with a spectrophotometer equipped with an integrating sphere. The laser source profile and propagation were determined using a thermographic technique. Models for the composite material and the laser source were subsequently developed in a non-sequential ray tracing environment.

The scattering behaviour of the AS4/PEEK composite was found to be highly anisotropic, with measurements suggesting the behaviour is dominated by specular reflections from the surfaces of the embedded carbon fibres. Angular dependent reflectance measurements show increased reflection for higher wavelengths which is attributed to anomalous dispersion from the carbon fibres, further reinforcing the

idea that the behaviour is dominated by reflections from the carbon fibres. A micro-half-cylinder (MHC) surface model was shown to give a good macroscopic approximation of the highly anisotropic scattering behaviour, without the complexity of modelling a three dimensional composite with individual fibres.Fresnel reflection equations provide a good approximation of the angular dependent reflectance. The refractive indices were determined to be $n = 2.30$ and $n = 1.95$ when considering MHC and specular surfaces respectively. The laser source was profiled and found to have a relatively uniform top-hat distribution. The propagation of the beam was also measured and shown to have significant divergence. The divergent source was modelled by launching collimated rays from a spatial emittance function through an xy-paraxial lens.

8.4 Combined optical-thermal model

In Chapter 6 a combined optical-thermal model was presented for carbon/PEEK near-infrared laser-assisted TP-AFP. Irradiance distributions on the composite were predicted using a 3D ray tracing model and subsequently applied to a 2D non-linear finite element thermal model. It was found that it is important to model the anisotropic scattering behaviour of the composite as it leads to specular-like behaviour near the nip point, yet diffuse reflection behaviour away from the nip point. A specular surface assumption leads to over-prediction of irradiance. Omitting reflections leads to a significant decrease in temperature predictions. Due to the inclination of the laser source, it is important to model the beam propagation as well as the irradiance profile. Assuming collimated propagation leads to overestimation of the length of the temperature profile, and underestimation of the temperatures. It was found that a top-hat profile simplification leads to a shortening of the profile, however the peak temperatures and the rest of the profile remain mostly unchanged compared with a spatial emittance function (emf.)

The results of the optical model irradiance predictions found that a significant

shadow is still present. This has a strong impact on the temperature history, with a 130 and 40 °C drop in surface temperature before the nip point for the substrate and tape respectively. This effect will be greater for larger rollers/corner radii. Initial results of the thermal model using the reported process power (1130 W) overestimated the peak temperature by 7 %. The difference was attributed to losses in the optical system and source output variation. Temperature profiles agreed extremely well after an adjustment of the laser power to 1056 W. The effect of the substrate fibre orientation was also studied and found to have only a small influence on the temperature history. Despite this fact, the micro-half-cylinder model is still required however for accurate prediction of the temperature history.

8.5 Process simulation and short beam strength

Chapter 7 investigated the capability of the laser AFP process for producing high strength laminates. Multi-layered samples were manufactured under conditions that reflect those experienced during practical manufacture of components. The additional quality development due to subsequent placement passes was therefore included. The inter-laminar bond strengths of the resulting samples were characterised by short beam strength tests. The response of the process to increasing process temperature was investigated for temperatures from 400 °C to 600 °C, at placement rates of 100 mm/s and 400 mm/s.

A process simulator was formulated for the laser AFP process using the combined optical-thermal model that was developed over Chapters 3, 5 and 6. It was then coupled with the bonding model implemented in Chapter 4. Crystallinity and void dynamics models validated for AFP processes in the literature were also implemented.

The temperature history predictions were made for the mid-plane bond interface of the SBS samples for the entire process history. The temperature history predictions were found to be in good agreement with experimental measurements for

both the surface temperature during laser heating and also the through thickness history during the placement of subsequent layers. When comparing the temperature histories for placement rates of 100 mm/s and 400 mm/s, it was found that the higher placement rate resulted in reduced irradiation time, and for the same given process temperature, lower levels of heat soak were observed leading to higher cooling rates in the consolidation zone and reduced temperatures during subsequent passes of the placement head. Another important phenomenon observed was the desynchronisation of the temperature and pressure distributions on subsequent passes, caused by the delay of the heat diffusing through the thickness of the composite.

Experimental SBS results found that full bond strength can be achieved at placement rates of 100 mm/s for process temperatures as low as 400 °C without the use of heated tooling. When moving to a placement rate of 400 mm/s, values 98 % of the reported ultimate SBS in literature were achieved for process temperatures of 550 °C and 600 °C, illustrating the superior properties achievable with the modern NIR laser AFP process. No significant decrease in properties was observed for a process temperature of 600 °C at a placement rate of 400 mm/s, indicating no adverse degradation had occurred, however at placement rate of 100 mm/s a 10 % reduction in strength was observed, indicating that some form of degradation.

Predictions of the bond strength using the parameters from experimentally validated models in the literature were found to be overly conservative compared with the experimental results, with values typically in the range of 20-50 % of the experimental values. While the bonding models should provide conservative predictions due to the cross-ply assumption of the intimate models, this appears to be grossly conservative. Much better agreement was found using two of the bonding parameter sets (BPS) from the current work, BPS-1 and BPS-3. As found in Chapter 4, BPS-3 would appear to be the most robust parameter set as it shows good, although still conservative agreement with the experimental results across a wide range of process conditions. This also highlights the applicability of the bonding models for highly

non-isothermal conditions.

Crystallisation model predictions indicate that the crystallinity of samples produced at 100 mm/s for all process temperatures lies within the recommended range of 20-35 %. For a 400 mm/s placement rate, the matrix is predicted to remain amorphous for process temperatures lower than 500 °C. At the highest process temperature of 600 °C the crystallinity is predicted to be just below 20 %, closely approaching the recommended range.

Void content predictions for a placement rate of 100 mm/s indicate that higher temperatures lead to lower void content, as greater levels of void compaction are achieved due to the decreased viscosity at elevated temperatures. The final void content is predicted to decrease from an initial value of 3.1 % to 2.5 % after placement for a process temperature of 600 °C. At a placement rate of 400 mm/s, the voids are predicted to expand significantly (to values in the range of 6 %) during the initial heating phase, particularly on the feed tape. The rapid cooling and the short pressure application results in minimal compaction. Furthermore the reduced temperature of the subsequent passes is insufficient for void compression. The resulting void content was predicted to be approximately 6 %.

The laser AFP process was found to be capable of producing laminates of full bond strength for placement rates as high as 400 mm/s when performing placement on non-heated tooling. Bonding models were found to provide conservative estimates of strength, suggesting that parametric studies in literature have underestimated the abilities of the process. Bonding was shown to be possible for temperatures below the melting point as the PEEK remains amorphous due to the high cooling rates experienced in the process.

8.6 Future Work

Further work includes validation of the crystallinity and void dynamics models that were implemented in this work. This would be achieved by performing DSC mea-

surements to determine the degree of crystallinity. Photomicrographs of the cross-sections could be used to determine the void content as well as observations of degradation at the bond interface. This work focused on the manufacture of unidirectional laminates where fibre nesting effects can potentially increase the rates of intimate contact development, enhancing the rate of bonding. Future studies should investigate the effects of bonding between plies with dissimilar orientation, for example in the manufacture of cross-ply or quasi-isotropic laminates.

In this work, it was found that a significant shadow is present in the process, which causes significant temperature drops prior to the consolidation zone, adversely effecting the bond strength. Optimisation of the laser position to reduce this shadow is an obvious avenue for future work. It is likely that reduction of the shadow would increase the bond strengths achievable for a given process speed.

Increasing the process speed was found to decrease the period of pressure application from the consolidation roller. It is likely that the process would greatly benefit from increased lengths of pressure application. The most obvious way of achieving such a goal would be to increase the consolidation roller diameter, however as it is also known from this work that the size of the laser shadow is proportional to the corner radius of the roller, thus a trade off must be made between the size of the shadow and the length of consolidation pressure application.

The ideal heat flux distribution to be applied to the surfaces of the composite could be determined by solving an inverse thermal model. This would involve applying fixed temperature profiles to the exposed surfaces of the composite prior to the nip point. Results of the thermal model would therefore provide the heat flux distributions that are required to achieve the applied temperature profiles. The heat input could then be optimised so as to maximise the heat soak while maintaining the surface temperature at temperatures below degradation, resulting in high levels of bonding while avoiding adverse thermal degradation.

Future applications for the combined optical-thermal model include related man-

ufacturing processes such as automated dry fibre placement and automated tape placement of thermosetting composites.

References

Agarwal, V.; Güçeri, S. I.; Mccullough, R. L.; and Schultz, J. M., 1992. Thermal characterization of the laser-assisted consolidation process. *Journal of Thermoplastic Composite Materials*, 5, 2 (Apr. 1992), 115–135. doi:10.1177/089270579200500203. (cited on pages 16, 17, 28, 42, 49, 82, 83, 84, 87, 88, 89, 100, 101, and 105)

Agarwal, V.; Mccullough, R. L.; and Schultz, J. M., 1996. The thermoplastic laser-assisted consolidation process-mechanical and microstructure characterization. *Journal of Thermoplastic Composite Materials*, 9, 4 (Oct. 1996), 365–380. doi:10.1177/089270579600900405. (cited on pages 15, 16, 17, 28, 42, 45, 48, 49, 87, and 226)

Aized, T. and Shirinzadeh, B., 2011. Robotic fiber placement process analysis and optimization using response surface method. *The International Journal of Advanced Manufacturing Technology*, 55, 1-4 (Jul. 2011), 393–404. doi:10.1007/s00170-010-3028-1. (cited on page 93)

August, Z.; Ostrander, G.; Michasiow, J.; and Hauber, D., 2014. Recent developments in automated fiber placement of thermoplastic composites. *SAMPE Journal*, 50, 2 (Mar. 2014), 30–37. (cited on page 4)

Baba, T.; Arai, T.; and Ono, A., 1986. Laser beam profile measurement by a thermographic technique. *Review of Scientific Instruments*, 57, 11 (Nov. 1986), 2739–2742. doi:10.1063/1.1139035. (cited on page 187)

Bastien, L. J. and Gillespie, J. W., 1991. A non-isothermal healing model for strength and toughness of fusion bonded joints of amorphous thermoplastics. *Polymer Engineering & Science*, 31, 24 (Dec. 1991), 1720–1730. doi:10.1002/pen.760312406. (cited on pages 67, 72, and 90)

Becker, F. and Potente, H., 2002. A step towards understanding the heating phase of laser transmission welding in polymers. *Polymer Engineering & Science*, 42, 2 (2002), 365–374. doi:10.1002/pen.10954. (cited on pages 174 and 175)

Beckwith, S. W., 2008. Filament winding vs. fiber placement manufacturing technologies. *SAMPE Journal*, 44, 2 (2008), 54–55. (cited on page 2)

Beyeler, E.; Phillips, W.; and Güçeri, S. I., 1988. Experimental investigation of laser-assisted thermoplastic tape consolidation. *Journal of Thermoplastic Composite Materials*, 1, 1 (Jan. 1988), 107–121. doi:10.1177/089270578800100109. (cited on pages 17, 24, and 87)

Beyeler, E. P. and Güçeri, S. I., 1988. Thermal analysis of laser-assisted thermoplastic-matrix composite tape consolidation. *Journal of Heat Transfer*, 110, 2 (May 1988), 424–430. doi:10.1115/1.3250502. (cited on pages 77, 82, 84, 88, 100, and 102)

Beziers, D.; Capdepuy, B.; and Chataignier, E., 1990. Electron beam curing of composites. In *Developments in the science and technology of composite materials*, vol. 4th, 73–78. Elsevier Applied Science, London and New York. (cited on page 2)

Beziers, D.; Perilleux, P.; and Grenie, Y., 1996. Composite structures obtained by ionization curing. *Radiation Physics and Chemistry*, 48, 2 (Aug. 1996), 171–177. doi:10.1016/0969-806X(95)00420-3. (cited on page 2)

Boey, F.; Rath, S. K.; Ng, A. K.; and Abadie, M. J. M., 2002. Cationic UV cure kinetics for multifunctional epoxies. *Journal of Applied Polymer Science*, 86, 2 (Oct. 2002), 518–525. doi:10.1002/app.11041. (cited on page 2)

Boley, C. D. and Rubenchik, A. M., 2013. Modeling of laser interactions with composite materials. *Applied Optics*, 52, 14 (May 2013), 3329–3337. doi:10.1364/AO.52.003329. (cited on page 181)

Borghesi, A. and Guizzetti, G., 1997. Graphite (C). In *Handbook of Optical Constants of Solids* (Ed. E. D. Palik), 449–460. Academic Press, Burlington. ISBN 978-0-12-544415-6. (cited on page 178)

Bosch, C.; Pueyo, X.; Mérillou, S.; and Ghazanfarpour, D., 2008. A resolution independent approach for the accurate rendering of grooved surfaces. *Computer Graphics Forum*, 27, 7 (2008), 1937–1944. doi:10.1111/j.1467-8659.2008.01342.x. (cited on page 182)

Burgess, J. W.; Wilenski, M. S.; Belvin, H. L.; Cano, R. J.; and Johnston, N. J., 2001. Development of a cure-on-the-fly automated tape placement machine for electron beam curable prepregs. In *International SAMPE Symposium and Exhibition (Proceedings)*, vol. 46 II, 2024–2036. (cited on page 2)

Butler, C. A.; Mccullough, R. L.; Pitchumani, R.; and Gillespie, J. W., 1998. An analysis of mechanisms governing fusion bonding of thermoplastic composites. *Journal of Thermoplastic Composite Materials*, 11, 4 (Jul. 1998), 338–363. doi:10.1177/089270579801100404. (cited on pages 10 and 72)

Bykanov, A. N.; Vorobyev, L. R.; Goodman, D. L.; Byrne, C. A.; Bykanova, L. G.; and Pond, T. W., 2001. Optimization of e-beam curing irradiation dose in ATP processing of epoxy resins. In *International SAMPE Technical Conference*, vol. 33, 269–282. (cited on page 2)

Cano, R. J.; Belvin, H. L.; Hulcher, A. B.; and Grenoble, R. W., 2001. Studies on automated manufacturing of high performance composites. Technical Report 20040086087, NASA Langley Research Center. (cited on page 2)

Chen, M.; Zak, G.; and Bates, P. J., 2011. Effect of carbon black on light transmission in laser welding of thermoplastics. *Journal of Materials Processing Technology*, 211, 1 (Jan. 2011), 43–47. doi:10.1016/j.jmatprotec.2010.08.017. (cited on page 174)

Choe, C. R. and Lee, K. H., 1989. Nonisothermal crystallization kinetics of poly(etheretherketone) (PEEK). *Polymer Engineering & Science*, 29, 12 (1989), 801–805. doi:10.1002/pen.760291208. (cited on pages 78, 91, and 92)

Cirri, G., 1993. Method for the production of manufactured articles of resin or composite material with a polymerizable resin matrix using electron beams. (cited on page 2)

Cogswell, F. N., 1992. *Thermoplastic aromatic polymer composites: a study of the structure, processing, and properties of carbon fibre reinforced polyetheretherketone and related materials*. Butterworth-Heinemann, Oxford. ISBN 978-0-750-61086-5. (cited on pages 11, 12, 15, 16, 103, 110, 175, 202, and 203)

Crivello, J. V., 1999a. The discovery and development of onium salt cationic photoinitiators. *Journal of Polymer Science Part A: Polymer Chemistry*, 37, 23 (Dec. 1999), 4241–4254. doi:10.1002/(SICI)1099-0518(19991201)37:23<4241::AID-POLA1>3.0.CO;2-R. (cited on page 2)

Crivello, J. V., 1999b. UV and electron beam-induced cationic polymerization. *Nuclear Instruments and Methods in Physics Research Section B: Beam Interactions with Materials and Atoms*, 151, 1–4 (May 1999), 8–21. doi:10.1016/S0168-583X(99)00109-3. (cited on page 2)

Crivello, J. V.; Walton, T. C.; and Malik, R., 1997. Fabrication of epoxy matrix composites by electron beam induced cationic polymerization. *Chemistry of Materials*, 9, 5 (1997), 1273–1284. (cited on page 2)

Dai, S.-C. and Ye, L., 2002a. Characteristics of CF/PEI tape winding process with on-line consolidation. *Composites Part A: Applied Science and Manufacturing*, 33, 9 (Sep. 2002), 1227–1238. doi:10.1016/S1359-835X(02)00083-0. (cited on pages 57 and 64)

Dai, S.-C. and Ye, L., 2002b. GF/PP tape winding with on-line consolidation. *Journal of Reinforced Plastics and Composites*, 21, 1 (Jan. 2002), 71–90. doi:10.1106/073168402024283. (cited on pages 57 and 64)

Dara, P. H. and Loos, A. C., 1985. Thermoplastic matrix composite processing model. Technical Report CCMS-85-10, VPI-E-85-21, Center for Composite Materials and Structures, Virginia Polytechnic Institute and State University, Blacksburg, Virginia. (cited on pages xix, 8, 50, 51, 52, 53, 55, 60, 66, and 68)

de Gennes, P. G., 1971. Reptation of a polymer chain in the presence of fixed obstacles. *The Journal of Chemical Physics*, 55, 2 (Jul. 1971), 572–579. doi:10.1063/1.1675789. (cited on pages 8 and 65)

Endruweit, A.; Johnson, M. S.; and Long, A. C., 2006. Curing of composite components by ultraviolet radiation: A review. *Polymer Composites*, 27, 2 (Apr. 2006), 119–128. doi:10.1002/pc.20166. (cited on page 2)

Endruweit, A.; Ruijter, W.; Johnson, M. S.; and Long, A. C., 2008. Transmission of ultraviolet light through reinforcement fabrics and its effect on ultraviolet curing of composite laminates. *Polymer Composites*, 29, 7 (Jul. 2008), 818–829. doi:10.1002/pc.20483. (cited on page 2)

Felderhoff, K. D. and Steiner, K. V., 1993. New compact robotic head for thermoplastic fiber placement. In *International SAMPE Symposium and Exhibition (Proceedings)*, vol. 38, 138–151. (cited on page 2)

Funck, R. and Neitzel, M., 1995. Improved thermoplastic tape winding using laser or direct-flame heating. *Composites Manufacturing*, 6, 3–4 (1995), 189–192. doi:10.1016/0956-7143(95)95010-V. (cited on pages 4, 16, 17, and 87)

Goodman, D. L.; Byrne, C. A.; Moulton, R.; Dixon, D.; Yen, A.; and Costen, R. C., 1999. Automated tape placement with in-situ electron beam cure. In *International SAMPE Symposium and Exhibition (Proceedings)*, vol. 44, I/. (cited on page 2)

Goodman, D. L.; Byrne, C. A.; Yen, A.; Moulton, R.; Dixon, D.; and Costen, R. C., 2000. Automated tape placement with in-situ electron beam cure. *SAMPE Journal*, 36, 2 (2000), 11–17. (cited on page 2)

Gresho, P. M. and Lee, R. L., 1981. Don't suppress the wiggles—they're telling you something! *Computers & Fluids*, 9, 2 (Jun. 1981), 223–253. doi:10.1016/0045-7930(81)90026-8. (cited on pages 103 and 201)

Grouve, W. J. B., 2012. *Weld strength of laser-assisted tape-placed thermoplastic composites*. PhD, University of Twente, Enschede, the Netherlands. (cited on pages 88, 105, 192, 198, 212, and 219)

Grouve, W. J. B.; Warnet, L.; Akkerman, R.; Wijskamp, S.; and Kok, J. S. M., 2010. Weld strength assessment for tape placement. *International Journal of Material Forming*, 3, 1 (Apr. 2010), 707–710. doi:10.1007/s12289-010-0868-z. (cited on page 4)

Grouve, W. J. B.; Warnet, L. L.; Rietman, B.; Visser, H. A.; and Akkerman, R., 2013. Optimization of the tape placement process parameters for carbon–PPS composites. *Composites Part A: Applied Science and Manufacturing*, 50 (Jul. 2013), 44–53. doi:10.1016/j.compositesa.2013.03.003. (cited on page 69)

Grove, S. M., 1988. Thermal modelling of tape laying with continuous carbon fibre-reinforced thermoplastic. *Composites*, 19, 5 (Sep. 1988), 367–375. doi:10.1016/0010-4361(88)90124-3. (cited on pages 82, 83, 84, 88, 100, 101, and 105)

Gruber, M. B.; Lamontia, M. A.; and Waibel, B. J., 2001. Automated fabrication processes for large composite aerospace structures: A trade study. In *International SAMPE Symposium and Exhibition (Proceedings)*, vol. 46 II, 1986–1997. (cited on page 2)

Gu, Q. G. and Zhou, Q. L., 1998. Preparation of high strength and optically transparent silicone rubber. *European Polymer Journal*, 34, 11 (Nov. 1998), 1727–1733. doi:10.1016/S0014-3057(97)00098-0. (cited on page 199)

Guan, X. and Pitchumani, R., 2004. Modeling of spherulitic crystallization in thermoplastic tow-placement process: heat transfer analysis. *Composites Science and Technology*, 64, 9 (Jul. 2004), 1123–1134. doi:10.1016/j.compscitech.2003.08.011. (cited on pages 4, 33, 78, 80, 81, and 228)

Han, Z.; Fu, Y.; Ma, Y.; and Fu, H., 2012. Modeling and analysis of heat transfer in fiber placement process of thermoplastic composites. In *2012 3rd International Conference on System Science, Engineering Design and Manufacturing Informatization (ICSEM)*, vol. 1, 282–286. doi:10.1109/ICSSEM.2012.6340728. (cited on pages 82, 83, and 84)

Hay, J. N. and Gara, P. O., 2006. Recent developments in thermoset curing methods. *Proceedings of the Institution of Mechanical Engineers*, 220, G3 (2006), 187. (cited on page 2)

Heider, D.; Piovoso, M. J.; and Gillespie Jr, J. W., 2003. A neural network model-based open-loop optimization for the automated thermoplastic composite tow-placement system. *Composites Part A: Applied Science and Manufacturing*, 34, 8 (Aug. 2003), 791–799. doi:10.1016/S1359-835X(03)00120-9. (cited on page 94)

Henninger, F.; Ye, L.; and Friedrich, K., 1998. Deconsolidation behaviour of glass fibre-polyamide 12 composite sheet material during post-processing. *Plastics, Rubber and Composites Processing and Applications*, 27, 6 (1998), 287–292. (cited on page 13)

Hinkley, J. A.; Marchello, J. M.; and Messier, B. C., 1996. Thermoplastic ribbon-ply bonding model. Technical Memorandum 110203, NASA Langley Research Center, Hampton, VA. (cited on page 58)

Holman, J. P., 2002. *Heat Transfer*. McGraw-Hill, New York, NY, USA, 9 edn. ISBN 978-0-07-240655-9. (cited on page 106)

Homburg, O.; Bayer, A.; Mitra, T.; Meinschien, J.; and Aschke, L., 2008. Beam shaping of high power diode lasers benefits from asymmetrical refractive micro-lens arrays. In *Proceedings of SPIE Conference Volume 6876*, vol. 6876, 68760B1–B7. San Jose. doi:10.1117/12.762892. (cited on page 186)

Khan, M. A.; Mitschang, P.; and Schledjewski, R., 2010. Identification of some optimal parameters to achieve higher laminate quality through tape placement process. *Advances in Polymer Technology*, 29, 2 (2010), 98–111. doi:10.1002/adv.20177. (cited on pages xx, 4, 16, 17, 40, 43, 45, 49, 60, 61, 62, 64, 69, 73, 76, 78, 83, 85, 87, 109, 123, 126, 127, 130, 131, 142, 144, 145, 158, 160, 162, 165, 169, 249, 251, 252, and 253)

Khan, M. A.; Mitschang, P.; and Schledjewski, R., 2013. Parametric study on processing parameters and resulting part quality through thermoplastic tape

placement process. *Journal of Composite Materials*, 47, 4 (Feb. 2013), 485–499. doi:10.1177/0021998312441810. (cited on pages xx, 61, 62, 78, 92, 131, 145, 146, and 147)

KHAN, M. A. AND SCHLEDJEWSKI, P. M. A. R., 2010. Tracing the void content development and identification of its effecting parameters during in situ consolidation of thermoplastic tape material. *Polymers & Polymer Composites*, 18, 1 (2010), 1–15. (cited on pages 16, 39, 40, 47, 75, 82, 84, 100, and 101)

KIM, H. J.; KIM, S. K.; AND LEE, W. I., 1996. A study on heat transfer during thermoplastic composite tape lay-up process. *Experimental Thermal and Fluid Science*, 13, 4 (Nov. 1996), 408–418. doi:10.1016/S0894-1777(96)00095-7. (cited on pages 82, 83, 84, 86, 100, and 102)

KIM, Y. H. AND WOOL, R. P., 1983. A theory of healing at a polymer-polymer interface. *Macromolecules*, 16, 7 (Jul. 1983), 1115–1120. doi:10.1021/ma00241a013. (cited on page 66)

KÖHLER, B.; NOESKE, A.; KINDERVATER, T.; WESSOLLEK, A.; BRAND, T.; AND BIESENBACH, J., 2007. 11-kW direct diode laser system with homogenized 55 × 20 mm^2 top-hat intensity distribution. In *Proceedings of SPIE Conference Volume 6456*, vol. 6456, 64560O1–O12. San Jose. doi:doi:10.1117/12.698837. (cited on page 186)

KURT, M. AND EDWARDS, D., 2009. A survey of BRDF models for computer graphics. *SIGGRAPH Comput. Graph.*, 43, 2 (May 2009), 41–47. doi:10.1145/1629216.1629222. (cited on page 182)

LAMÈTHE, J.; BEAUCHÊNE, P.; AND LÉGER, L., 2005. Polymer dynamics applied to PEEK matrix composite welding. *Aerospace Science and Technology*, 9, 3 (Apr. 2005), 233–240. doi:10.1016/j.ast.2005.01.008. (cited on pages 42 and 79)

LAMONTIA, M. A.; GRUBER, M. B.; FUNCK, S. B.; WAIBEL, B. J.; COPE, R. D.; AND BRUCE HULCHER, A., 2003. Developing a contoured deposition head for in situ tape laying and fiber placement. In *International SAMPE Symposium and Exhibition (Proceedings)*, vol. 48 II, 2062–2076. (cited on page 18)

LEE, W. I. AND SPRINGER, G. S., 1987. A model of the manufacturing process of thermoplastic matrix composites. *Journal of Composite Materials*, 21, 11 (Nov. 1987), 1017–1055. doi:10.1177/002199838702101103. (cited on pages xix, xx, 52, 53, 54, 55, 58, 60, 61, 62, 68, 69, 146, 148, 150, and 169)

LEMARCHAND, F., 2008. *Étude de l'apparition des contraintes résiduelles dans le procédé d'empilement par soudage et consolidation en continu de composites thermoplastiques*. Ph.D. thesis, Arts et Métiers ParisTech. (cited on pages 57 and 67)

LEMARCHAND, F.; BEAUCHÊNE, P.; LAINE, B.; AND CHINESTA, F., 2007. A multi-scale method to predict residual stress appearance in the process of on-line consolidation of thermoplastic composites. *International Journal of Forming Processes*, 10, 4 (Dec. 2007), 471–498. doi:10.3166/ijfp.10.471-498. (cited on page 14)

Levy, A.; Corre, S. L.; and Poitou, A., 2014a. Ultrasonic welding of thermoplastic composites: a numerical analysis at the mesoscopic scale relating processing parameters, flow of polymer and quality of adhesion. *International Journal of Material Forming*, 7, 1 (Mar. 2014), 39–51. doi:10.1007/s12289-012-1107-6. (cited on page 69)

Levy, A.; Heider, D.; Tierney, J.; and Gillespie, J. W., 2014b. Inter-layer thermal contact resistance evolution with the degree of intimate contact in the processing of thermoplastic composite laminates. *Journal of Composite Materials*, 48, 4 (Feb. 2014), 491–503. doi:10.1177/0021998313476318. (cited on pages 85 and 109)

Lopata, V. J.; Saunders, C. B.; Singh, A.; Janke, C. J.; Wrenn, G. E.; and Havens, S. J., 1999. Electron-beam-curable epoxy resins for the manufacture of high-performance composites. *Radiation Physics and Chemistry*, 56, 4 (Oct. 1999), 405–415. doi:10.1016/S0969-806X(99)00330-8. (cited on page 2)

Mantell, S. C. and Springer, G. S., 1992. Manufacturing process models for thermoplastic composites. *Journal of Composite Materials*, 26, 16 (Jan. 1992), 2348–2377. doi:10.1177/002199839202601602. (cited on pages 24, 54, 55, 57, 58, 60, 62, 72, 90, 91, 94, 125, and 126)

Mantell, S. C.; Wang, Q.; and Springer, G. S., 1992. Processing thermoplastic composites in a press and by tape laying–experimental results. *Journal of Composite Materials*, 26, 16 (Jan. 1992), 2378–2401. doi:10.1177/002199839202601603. (cited on pages xx, 16, 24, 34, 42, 45, 55, 57, 71, 72, 83, 84, 94, 123, 124, 130, 131, 132, 140, 141, 145, 158, 159, 160, 165, 226, 249, 251, 252, and 253)

Mazumdar, S. K. and Hoa, S. V., 1995. Application of taguchi method for process enhancement of on-line consolidation technique. *Composites*, 26, 9 (Sep. 1995), 669–673. doi:10.1016/0010-4361(95)98916-9. (cited on pages 26, 45, 93, and 226)

Mazumdar, S. K. and Hoa, S. V., 1996. Determination of manufacturing conditions for hot-gas-aided thermoplastic tape winding. *Journal of Thermoplastic Composite Materials*, 9, 1 (Jan. 1996), 35–53. doi:10.1177/089270579600900104. (cited on pages 16, 26, 43, 45, 48, 85, and 226)

McAfee, A. P., 1990. *On the appropriate level of automation for advanced structural composites manufacturing for commercial aerospace applications*. Thesis, Massachusetts Institute of Technology. Thesis (M.S.)–Massachusetts Institute of Technology, Dept. of Mechanical Engineering, 1990 and, Thesis (M.S.)–Massachusetts Institute of Technology, Sloan School of Management, 1990. (cited on page 2)

Nam, J.-D. and Seferis, J. C., 1992. Generalized composite degradation kinetics for polymeric systems under isothermal and nonisothermal conditions. *Journal of Polymer Science Part B: Polymer Physics*, 30, 5 (1992), 455–463. doi:10.1002/polb.1992.090300505. (cited on pages 77, 90, and 91)

Narnhofer, M.; Schledjewski, R.; Mitschang, P.; and Perko, L., 2013. Simulation of the tape-laying process for thermoplastic matrix composites. *Advances in Polymer Technology*, 32, S1 (2013), E705–E713. doi:10.1002/adv.21312. (cited on page 64)

Nejhad, M. N. G., 1993. Issues related to processability during the manufacture of thermoplastic composites using on-line consolidation techniques. *Journal of Thermoplastic Composite Materials*, 6, 2 (Apr. 1993), 130–146. doi:10.1177/089270579300600204. (cited on pages 77, 82, 84, 86, and 88)

Nejhad, M. N. G.; Cope, R. D.; and Güceri, S. I., 1991. Thermal analysis of in-situ thermoplastic composite tape laying. *Journal of Thermoplastic Composite Materials*, 4, 1 (Jan. 1991), 20–45. doi:10.1177/089270579100400102. (cited on pages 77, 82, 84, 88, 91, and 101)

Nicodeau, C., 2005. *Modélisation du soudage en continu de composites à matrice thermoplastique*. Ph.D. thesis, Arts et Métiers ParisTech. (cited on page 68)

Nicodeau, C.; Cinquin, J.; Regnier, G.; and Verdu, J., 2006. In-situ consolidation process optimization for thermoplastic matrix composites. In *International SAMPE Symposium and Exhibition (Proceedings)*, vol. 51. (cited on pages 77, 78, and 92)

Parihar, S. K. and Wright, N. T., 1997. Thermal contact resistance at elastomer to metal interfaces. *International Communications in Heat and Mass Transfer*, 24, 8 (Dec. 1997), 1083–1092. doi:10.1016/S0735-1933(97)00102-4. (cited on page 118)

Patel, P.; Hull, T. R.; Lyon, R. E.; Stoliarov, S. I.; Walters, R. N.; Crowley, S.; and Safronava, N., 2011. Investigation of the thermal decomposition and flammability of PEEK and its carbon and glass-fibre composites. *Polymer Degradation and Stability*, 96, 1 (Jan. 2011), 12–22. doi:10.1016/j.polymdegradstab.2010.11.009. (cited on page 227)

Patel, P.; Hull, T. R.; Mccabe, R. W.; Flath, D.; Grasmeder, J.; and Percy, M., 2010. Mechanism of thermal decomposition of poly(ether ether ketone) (PEEK) from a review of decomposition studies. (2010). (cited on pages 15, 227, and 249)

Pimenta, S. and Pinho, S. T., 2011. Recycling carbon fibre reinforced polymers for structural applications: Technology review and market outlook. *Waste Management*, 31, 2 (Feb. 2011), 378–392. doi:10.1016/j.wasman.2010.09.019. (cited on page 3)

Pistor, C. M. and Güçeri, S. I., 1999. Crystallinity of on-line consolidated thermoplastic composites. *Journal of Composite Materials*, 33, 4 (Feb. 1999), 306–324. doi:10.1177/002199839903300401. (cited on pages 16, 17, 33, 48, 49, 86, and 87)

Pistor, C. M.; Yardimci, M. A.; and Güçeri, S. I., 1999. On-line consolidation of thermoplastic composites using laser scanning. *Composites Part A: Applied Science and Manufacturing*, 30, 10 (Oct. 1999), 1149–1157. doi:10.1016/S1359-835X(99)00030-5. (cited on pages 16, 17, 31, 87, and 226)

Pitchumani, R.; Gillespie, J. W.; and Lamontia, M. A., 1997. Design and optimization of a thermoplastic tow-placement process with in-situ consolidation. *Journal of Composite Materials*, 31, 3 (Feb. 1997), 244–275. doi:10.1177/002199839703100302. (cited on pages 57, 67, 77, 82, 84, 90, 94, and 124)

Pitchumani, R.; Ranganathan, S.; Don, R. C.; Gillespie Jr., J. W.; and Lamontia, M. A., 1996. Analysis of transport phenomena governing interfacial bonding and void dynamics during thermoplastic tow-placement. *International Journal of Heat and Mass Transfer*, 39, 9 (Jun. 1996), 1883–1897. doi:10.1016/0017-9310(95)00271-5. (cited on pages 57, 67, 72, 73, 82, 84, 86, 90, and 146)

Plummer, C. J. G.; Bourban, P.-E.; Zanetto, J.-E.; Smith, G. D.; and Månson, J.-A. E., 2003. Nonisothermal fusion bonding in semicrystalline thermoplastics. *Journal of Applied Polymer Science*, 87, 8 (Feb. 2003), 1267–1276. doi:10.1002/app.11528. (cited on page 71)

Poulin, P. and Fournier, A., 1990. A model for anisotropic reflection. *SIGGRAPH Comput. Graph.*, 24, 4 (Sep. 1990), 273–282. doi:10.1145/97880.97909. (cited on page 182)

Quinlan, E.; Khoun, L.; Hubert, P.; Hojjati, M.; Chen, J.; and Yousefpour, A., 2010. Thermal and crystallinity analysis of thermoplastic composite parts manufactured by automated fibre placement. In *International SAMPE Technical Conference*. (cited on page 80)

Ramamoorthi, R. and Hanrahan, P., 2001. On the relationship between radiance and irradiance: Determining the illumination from images of a convex Lambertian object. *Journal of the Optical Society of America A: Optics and Image Science, and Vision*, 18, 10 (2001), 2448–2459. (cited on page 177)

Ranganathan, S.; Advani, S. G.; and Lamontia, M. A., 1995. A non-isothermal process model for consolidation and void reduction during in-situ tow placement of thermoplastic composites. *Journal of Composite Materials*, 29, 8 (May 1995), 1040–1062. doi:10.1177/002199839502900803. (cited on pages xix, xxi, 13, 73, 74, 75, 76, 90, 230, and 232)

Regnier, G.; Nicodeau, C.; Verdu, J.; Cinquin, J.; and Chinesta, F., 2007. A multiphysic and multi-scale approach to model the continuous welding of thermoplastic matrix composites. In *ICCM International Conferences on Composite Materials*. (cited on page 78)

Rosselli, F. and Santare, M. H., 1997. Comparison of the short beam shear (SBS) and interlaminar shear device (ISD) tests. *Composites Part A: Applied Science and Manufacturing*, 28, 6 (1997), 587–594. doi:10.1016/S1359-835X(97)00009-2. (cited on pages 29, 30, 45, 78, and 226)

Rosselli, F.; Santare, M. H.; and Güçeri, S. I., 1997. Effects of processing on laser assisted thermoplastic tape consolidation. *Composites Part A: Applied Science and Manufacturing*, 28, 12 (1997), 1023–1033. doi:10.1016/S1359-835X(97)00072-9. (cited on pages 15, 16, 17, 30, 33, 49, 87, and 227)

Sakota, Z. G.; Thomas Hahn, H.; Lackman, L.; and Bullen, G. N., 2006. Out of autoclave curing of composites. In *International SAMPE Symposium and Exhibition (Proceedings)*, vol. 51. Long Beach, CA. (cited on page 2)

Sarrazin, H. and Springer, G. S., 1995. Thermochemical and mechanical aspects of composite tape laying. *Journal of Composite Materials*, 29, 14 (Sep. 1995), 1908–1943. doi:10.1177/002199839502901407. (cited on pages 82, 83, 86, and 102)

Schell, J. S. U.; Guilleminot, J.; Binetruy, C.; and Krawczak, P., 2009. Computational and experimental analysis of fusion bonding in thermoplastic composites: Influence of process parameters. *Journal of Materials Processing Technology*, 209, 11 (Jun. 2009), 5211–5219. doi:10.1016/j.jmatprotec.2009.03.008. (cited on pages 57, 64, 67, and 124)

Schledjewski, R. and Latrille, M., 2003. Processing of unidirectional fiber reinforced tapes—fundamentals on the way to a process simulation tool (ProSim-FRT). *Composites Science and Technology*, 63, 14 (Nov. 2003), 2111–2118. doi:10.1016/S0266-3538(03)00108-8. (cited on pages 57, 74, 82, 84, 86, and 92)

Schledjewski, R. and Miaris, A., 2009. Thermoplastic tape placement by means of diode laser heating. In *International SAMPE Symposium and Exhibition (Proceedings)*, vol. 54. (cited on pages 38, 41, 45, and 226)

Schröder, K.; Zhao, S.; and Zinke, A., 2012. Recent advances in physically-based appearance modeling of cloth. In *Proceedings SIGGRAPH Asia 2012 Courses*, SA '12, 12:1–12:52. ACM, New York. doi:10.1145/2407783.2407795. (cited on page 182)

Seferis, J. C.; Ahlstrom, C.; and Dillman, S. H., 1987. Cooling rate and annealing as processing parameters for semicrystalline thermoplastic-based composites. 1467–1471. (cited on page 78)

Simacek, P.; Advani, S. G.; Gruber, M.; and Jensen, B., 2013. A non-local void filling model to describe its dynamics during processing thermoplastic composites. *Composites Part A: Applied Science and Manufacturing*, 46 (Mar. 2013), 154–165. doi:10.1016/j.compositesa.2012.10.015. (cited on pages 13 and 76)

Smith, G. D.; Plummer, C. J. G.; Bourban, P.-E.; and Månson, J.-A. E., 2001. Non-isothermal fusion bonding of polypropylene. *Polymer*, 42, 14 (Jun. 2001), 6247–6257. doi:10.1016/S0032-3861(01)00060-X. (cited on page 69)

Sonmez, F. O. and Akbulut, M., 2007. Process optimization of tape placement for thermoplastic composites. *Composites Part A: Applied Science and Manufacturing*, 38, 9 (Sep. 2007), 2013–2023. doi:10.1016/j.compositesa.2007.05.003. (cited on pages 57, 67, 77, 82, and 94)

Sonmez, F. O. and Hahn, H. T., 1997a. Analysis of the on-line consolidation process in thermoplastic composite tape placement. *Journal of Thermoplastic Composite Materials*, 10, 6 (Nov. 1997), 543–572. doi:10.1177/089270579701000604. (cited on pages xx, 57, 67, 69, 73, 77, 82, 83, 84, 88, 91, 94, 124, 146, 149, and 169)

Sonmez, F. O. and Hahn, H. T., 1997b. Modeling of heat transfer and crystallization in thermoplastic composite tape placement process. *Journal of Thermoplastic Composite Materials*, 10, 3 (May 1997), 198–240. doi:10.1177/089270579701000301. (cited on pages 15, 77, 78, 80, 81, 82, 83, 84, 88, 91, 100, and 101)

Sonmez, F. O.; Hahn, H. T.; and Akbulut, M., 2002. Analysis of process-induced residual stresses in tape placement. *Journal of Thermoplastic Composite Materials*, 15, 6 (Nov. 2002), 525–544. doi:10.1177/0892705702015006207. (cited on pages 14 and 82)

Stagg, B. J. and Charalampopoulos, T. T., 1993. Refractive indices of pyrolytic graphite, amorphous carbon, and flame soot in the temperature range 25° to 600°C. *Combustion and Flame*, 94, 4 (Sep. 1993), 381–396. doi:10.1016/0010-2180(93)90121-I. (cited on pages 178 and 179)

Steiner, K. V.; Bauer, B. M.; Pitchumani, R.; and Gillespie, J. W. J., 1995. Experimental verification of modeling and control for thermoplastic tow placement. *40th International SAMPE Symposium*, (1995), 1550–1559. Cited By (since 1996):8 Export Date: 10 August 2014. (cited on page 57)

Stokes-Griffin, C. M.; Compston, P.; Matuszyk, T. I.; and Cardew-Hall, M. J., 2013. Thermal modelling of the laser-assisted thermoplastic tape placement process. *Journal of Thermoplastic Composite Materials*, Article in press (Nov. 2013), DOI: 10.1177/0892705713513285. doi:10.1177/0892705713513285. (cited on pages 88 and 198)

Sun, W.-C.; Mantell, S. C.; and Stelson, K. A., 2001. Demonstration of bond quality improvement for closed loop control of thermoplastic tape-laying. *Journal of Composite Materials*, 35, 1 (Jan. 2001), 57–76. doi:10.1177/002199801772661867. (cited on pages 33, 57, 58, and 72)

Swinehart, D. F., 1962. The Beer-Lambert law. *Journal of Chemical Education*, 39, 7 (Jul. 1962), 333. doi:10.1021/ed039p333. (cited on page 174)

Tardif, X.; Pignon, B.; Boyard, N.; Schmelzer, J. W. P.; Sobotka, V.; Delaunay, D.; and Schick, C., 2014. Experimental study of crystallization of polyetheretherketone (PEEK) over a large temperature range using a nano-calorimeter. *Polymer Testing*, 36 (Jun. 2014), 10–19. doi:10.1016/j.polymertesting.2014.03.013. (cited on pages 12, 80, 81, 123, and 131)

Tierney, J. and Gillespie, J. W., 2003. Modeling of heat transfer and void dynamics for the thermoplastic composite tow-placement process. *Journal of Composite Materials*, 37, 19 (Oct. 2003), 1745–1768. doi:10.1177/002199803035188. (cited on pages 4, 16, 35, 37, 38, 47, 73, 75, 82, 83, 84, 85, 86, 100, 101, and 124)

Tierney, J. and Gillespie, J. W., 2006. Modeling of in situ strength development for the thermoplastic composite tow placement process. *Journal of Composite Materials*, 40, 16 (Aug. 2006), 1487–1506. doi:10.1177/0021998306060162. (cited on pages xx, 37, 45, 49, 57, 58, 64, 72, 82, 84, 123, 126, 130, 131, 139, 140, 142, 143, 145, 158, 159, 160, 162, 165, 226, 250, 251, 252, and 253)

Tierney, J. J. and Gillespie, J. W. J., 2004. Crystallization kinetics behavior of PEEK based composites exposed to high heating and cooling rates. *Composites Part A: Applied Science and Manufacturing*, 35, 5 (May 2004), 547–558. doi:10.1016/j.compositesa.2003.12.004. (cited on pages 12, 78, 228, 230, and 231)

Toso, Y. M. P.; Ermanni, P.; and Poulikakos, D., 2004. Thermal phenomena in fiber-reinforced thermoplastic tape winding process: Computational simulations and experimental validations. *Journal of Composite Materials*, 38, 2 (Jan. 2004), 107–135. doi:10.1177/0021998304038651. (cited on pages 84 and 86)

Tumkor, S.; Turkmen, N.; Chassapis, C.; and Manoochehri, S., 2001. Modeling of heat transfer in thermoplastic composite tape lay-up manufacturing. *International Communications in Heat and Mass Transfer*, 28, 1 (Jan. 2001), 49–58. doi:10.1016/S0735-1933(01)00212-3. (cited on pages 82, 83, 84, 86, and 100)

Velisaris, C. N. and Seferis, J. C., 1986. Crystallization kinetics of polyetheretherketone (PEEK) matrices. *Polymer Engineering & Science*, 26, 22 (Dec. 1986), 1574–1581. doi:10.1002/pen.760262208. (cited on pages 12, 78, and 228)

Vincent, D., 2009. In situ manufacturing system for large unitized composite space structures. In *AIAA SPACE 2009 Conference & Exposition*, 2009–6450. American Institute of Aeronautics and Astronautics, Pasadena, California. doi:10.2514/MSPACE09. (cited on page 1)

Wang, L.; Jacques, S. L.; and Zheng, L., 1995. MCML—Monte Carlo modeling of light transport in multi-layered tissues. *Computer Methods and Programs in Biomedicine*, 47, 2 (Jul. 1995), 131–146. doi:10.1016/0169-2607(95)01640-F. (cited on page 199)

Ward, G. J., 1992. Measuring and modeling anisotropic reflection. *SIGGRAPH Comput. Graph.*, 26, 2 (Jul. 1992), 265–272. doi:10.1145/142920.134078. (cited on page 182)

Wool, R. P., 1984. Molecular aspects of tack. *Rubber Chemistry and Technology*, 57, 2 (May 1984), 307–319. doi:10.5254/1.3536010. (cited on page 66)

Wool, R. P. and O'Connor, K. M., 1981. A theory crack healing in polymers. *Journal of Applied Physics*, 52, 10 (Oct. 1981), 5953–5963. doi:10.1063/1.328526. (cited on page 66)

Yang, F. and Pitchumani, R., 2001a. A fractal Cantor set based description of interlaminar contact evolution during thermoplastic composites processing. *Journal of Materials Science*, 36, 19 (Oct. 2001), 4661–4671. doi:10.1023/A:1017950215945. (cited on pages xix, 58, 59, 60, 61, 64, 73, 74, 92, 125, 126, 127, 129, and 151)

Yang, F. and Pitchumani, R., 2001b. Fractal description of interlaminar contact development during thermoplastic composites processing. *Journal of Reinforced Plastics and Composites*, 20, 7 (May 2001), 536–546. doi:10.1177/073168401772678580. (cited on pages 60, 61, and 64)

Yang, F. and Pitchumani, R., 2002a. Healing of thermoplastic polymers at an interface under nonisothermal conditions. *Macromolecules*, 35, 8 (Apr. 2002), 3213–3224. doi:10.1021/ma010858o. (cited on pages 67, 68, 72, 73, 90, 92, and 132)

YANG, F. AND PITCHUMANI, R., 2002b. Interlaminar contact development during thermoplastic fusion bonding. *Polymer Engineering & Science*, 42, 2 (Feb. 2002), 424–438. doi:10.1002/pen.10960. (cited on pages 60, 64, 124, and 129)

YANG, F. AND PITCHUMANI, R., 2003. Nonisothermal healing and interlaminar bond strength evolution during thermoplastic matrix composites processing. *Polymer Composites*, 24, 2 (Apr. 2003), 263–278. doi:10.1002/pc.10027. (cited on pages 61, 68, and 124)

YE, L.; LU, M.; AND MAI, Y.-W., 2002. Thermal de-consolidation of thermoplastic matrix composites—I. growth of voids. *Composites Science and Technology*, 62, 16 (Dec. 2002), 2121–2130. doi:10.1016/S0266-3538(02)00144-6. (cited on page 13)

YOUSEFPOUR, A. AND NEJHAD, M. N. G., 2001. Experimental and computational study of APC-2/AS4 thermoplastic composite c-rings. *Journal of Thermoplastic Composite Materials*, 14, 2 (Mar. 2001), 129–145. doi:10.1106/1RQV-317Q-36K0-1E6P. (cited on page 34)

ZANETTO, J.-E.; PLUMMER, C. J. G.; BOURBAN, P.-E.; AND MÅNSON, J.-A. E., 2001. Fusion bonding of polyamide 12. *Polymer Engineering & Science*, 41, 5 (May 2001), 890–897. doi:10.1002/pen.10787. (cited on page 71)